Understanding the Characteristics of Droughts over Eastern Africa in Past and Future Climates

Mariam Melikizedeki Nguvava

Thesis presented for the Degree of

DOCTOR OF PHYLOSOPHY

In the Department of Environmental and Geographical Science

University of Cape Town

Supervisor: Associate Professor Babatunde J. Abiodun

February 2020

Declaration I

I know the meaning of plagiarism and declare that all the work in the thesis, except for that which is properly acknowledged, is my own.

Signed by candidate

Mariam Melikizedeki Nguvava

Declaration II

Some Sections of this thesis have been published. The text of this thesis includes material from the paper Nguvava, M., Abiodun, B.J. and Otieno, F., 2019. Projecting drought characteristics over East African basins at specific global warming levels. *Atmospheric Research, 228*, pp.41-54.

Abstract

Drought poses a threat to socio-economic activities across eastern Africa and its river basins. While there are indications that global warming may continue to enhance evaporation and intensify droughts at all scales, most drought projections over eastern Africa are based on rainfall alone and are limited to meteorological droughts. The present study combines rainfall and Potential Evapotranspiration (PET) to examine the characteristics of meteorological and hydrological droughts in present and future climates at the regional and river basin scales. To accomplish that we have applied five objectives; i) Study the temporal and spatial characteristics of eastern Africa droughts modes, ii) Investigate how some atmospheric teleconnections influence the characteristics of the Africa droughts modes, iii) Examine the influence of 1.5°C and 2°C global warming levels on drought modes in eastern Africa under two future climate scenarios, RCP 4.5 and RCP8.5 iv) Assess how increases in global warming will influence drought characteristics over eastern African river basins. v) Examine the potential impacts of climate change and land use change on water availability in the Rufiji River basin (RRB), Tanzania, with an emphasis of hydrological droughts in this basin.

Different types of datasets, including gridded and station observation datasets, regional climate model simulations (CORDEX: Coordinated Regional Climate Downscaling Experiment) and hydrological simulations (SWAT: Soil and Water Assessment Tool), were analysed for the study. The meteorological drought were characterised using two indices (i.e. Standardized Precipitation Evapotranspiration Index, SPEI; Standardized Precipitation Index, SPI) at 3- and 12-month scales, while the hydrological droughts were characterised using four indices (i.e. soil water index, SWI; Surface Runoff Index, RFI; Water Yield Index, WYI; and Stream Flow index, SFI). The study combined principal component analysis (PCA) with wavelet analysis to identify the spatio-temporal structure of four dominant drought modes over the region. It also used wavelet coherence to quantify the influence of four atmospheric teleconnections (i.e. El Niño Southern Oscillation, ENSO; Indian Ocean Dipole, IOD; Tropical Atlantic

Dipole Index, TADI; and Quasi-Biennial Oscillation, QBO) on the drought modes. The study also projects the characteristics of future droughts over eastern Africa and its major river basins at different global warming levels (GWLs). Series of hydrological simulations were used to assess the sensitivity of future droughts to four land use change scenarios (i.e. increase in forestry, shrubs, cropland and agriculture) over the Rufiji River Basin (RRB), a prominent river basin in eastern Africa. Although eastern Africa have been documented with several drought studies, the application of a combination of PCA, Wavelet analysis, wavelet coherence and Self Organizing Maps provides more comprehensive representation of droughts in the region using SPEI/SPI derived from both models and observations

The results of the study show that the four drought modes, which have their core areas over different parts of eastern Africa, account for more than 45% of drought variability in the region. All the drought modes are strongly coupled with either ENSO or IOD indices (or both); but, in addition, one of the modes is also strongly coupled with the TADI. CORDEX models give a realistic simulation of the relevant climate variables for calculating drought indices over eastern Africa and the river basins. However, the ensemble mean struggles to reproduce the spatial distribution and frequency of drought intensity in the region. The CORDEX simulations project no changes in the spatial structure of the drought modes but suggest an increase in SPEI drought intensity and frequency over the hotspots of the drought modes and elsewhere in the region. The magnitude of the increase, which varies over the drought mode hotspots, increases with increasing GWLs. The projections also show that the increase in intensity and frequency of drought can be attributed more to increased PET than to reduced precipitation. In contrast to the SPEI projection, the SPI projection shows a weak change in intensity and frequency of droughts, and the magnitude of the increase does not vary with the GWLs. Over the river basins, the SPEI projections are more robust than the SPI projections. Over the RRB, the future projections of some hydrological drought indices (i.e. RFI and SFI) follow the change in the SPEI projections, while others (i.e. SWI and WYI) follow that of SPI. Among the four land use scenarios considered, only forestry and shrubs show a substantial change in the hydrological drought indices. The results of the study thus give valuable insight

into the characteristics of future droughts in eastern Africa and provide a useful guide to the effectiveness of using land cover to reduce the severity of hydrological droughts over river basins in the region. However, resolution of CORDEX dataset (50km, i.e. 0.44deg) could be among the potential limitation as it is too low to capture the influence of local-scale processes (e.g. sea breeze, mountain induced circulations) on drought over the region.

Acknowledgements

I would like to give my sincere thanks to my Supervisor, Associate Prof. Babatunde J. Abiodun, for believing in me and for giving me the chance to be one of his students. For the course of five years, I have learned abundantly through his guidance. I would like to extend my gratitude to Tanzanian Government through Sokoine University of Agriculture for granting me a study leave to spend time in South Africa during the PhD study. I thank the Applied Centre for Climate and Earth System Science (ACCESS) and Shlumberger Faculty for the Future Fellowship for their financial support.

My sincere thanks to Mr. Phillip Mukwenha for his support regarding computer technicalities. Also, thanks to my office mates Roland, Sawadogo and Shakirudeen for their support in scripting.

I am deeply grateful to my husband Mr. Msafiri for his support and calmness while I was far from home. To my parents Zuhura and Mohammed for their endless prayers and true love. I also thank my son Samiji.

I thank God for everything.

Dedication

To my Mother: Zuhura Selemani Chillo

Table of Contents

List of Figures

List of Tables

List of Abbreviations

20CR	20th Century Reanalysis
AGCM	atmospheric general circulation model
ANN	Artificial neural network
BMI	Bhalme–Mooley Index
CET	Channel evapotranspiration
CGCMs	Coupled general circulation models
CORDEX	Coordinated Regional Climate Downscaling Experiment
CMIP3	Phase 3 of the Coupled Model Intercomparison Project
CMIP5	Phase 5 of the Coupled Model Intercomparison Project
CRU	Climate Research Unit
CWB	Climate water balance
DEM	Digital Elevation Model
DM	Drought mode
ENSO	El Niño Southern Oscillation
ERSST	Extended Reconstructed Sea Surface Temperature version 4
ET	Evapotranspiration
FAO	Food and Agriculture Organization of the United Nations
FLOWOUT	Flow out
GCM	Global Climate Model
GDP	Gross Domestic Product
GIS	Geographical information system
GMFD	Global Meteorological Forcing Dataset
GPCP	Global Precipitation Climatology Project
GWL	Global warming levels
HRU	Hydrological Response Unit
IOD	Indian Ocean Dipole
IPCC	Intergovernmental Panel on Climate Change
ISRIC	International Soils Reference and Information Center
ITCZ	Inter-tropical Convergence Zone
LSU	Landscape unit

LULC	Land Use and Land Cover?
NAO	North Atlantic Oscillation
NCEP	National Centers for Environmental Prediction
NCAR	National Centers for Atmospheric Research
NDMC	National Drought Mitigation Center
NOAA	National Centres for Environmental Information
NSE	Nash-Sutcliffe Efficiency
PBIAS	Percent bias
PCA	Principal Component Analysis
PDSI	Palmer Drought Severity Index
PER	Percolation
PET	Potential Evapotranspiration
PRE	Precipitation
PSD	Physical Sciences Division
QBO	Quasi-Biennial Oscillation
QDM	Quantile Delta Mapping
RBWB	Rufiji Basin Water Board
RCM	Regional Climate Model
RCMRD	Regional Centre for Mapping of Resources for Development
RCP	Representative Concentration Pathway
RRB	Rufiji river basin
RFI	Surface runoff index
SF	Surface runoff
SFI	Stream Flow Index
SLR	Solar radiation
SOM	Self-organizing map
SOTER	Soil and Terrain
SPEI	Standardized Precipitation Evapotranspiration Index
SPI	Standardized Precipitation Index
SRB	Surface Radiation Budget
SRTM	Shuttle Radar Topography Mission
SW	Soil water
SWAT	Soil and Water Assessment Tool
SWI	Soil water index

TADI	Tropical Atlantic Dipole Index
TMA	Tanzanian Meteorological Agency
TMAX	Maximum temperature
TMIN	Minimum temperature
TRMM	Tropical Rainfall Measuring Mission
UNFCCC	United Nations Framework Convention on Climate Change
USDA-ARS	United States Department of Agriculture Research Service
WCRP	World Climate Research Programme
WYI	Water Yield Index
WMO	World Meteorological Organization
WRBWO	Wami/Ruvu Basin Water Office
WYLD	Water yield

Chapter 1

Introduction

1.1 Background

Eastern Africa consists of ten developing countries (i.e. Tanzania, Eritrea, Djibouti, Ethiopia, Somalia, Kenya, Uganda, Burundi, Rwanda, and South Sudan) located in the easterly part of sub-Saharan Africa (Fig 1.1). The eastern African region, which covers an area of about 5.9 million km^2, accommodates more than 150 million people, and is characterised by striking highlands (e.g. the Ethiopian highlands and the East African highlands), the continent's tallest mountains (Mount Kilimanjaro in Tanzania, Mount Kenya in Kenya and Mount Rwenzori in Uganda), the African Great Lakes (e.g. Lake Victoria and Lake Tanganyika), numerous rivers (e.g. the Nile River, the Rufiji River and the Tana River), and the world's greatest rift valley (Eastern Great Rift), where earthquakes and volcanic eruptions are common. This region features various climatic zones, from desert conditions in the east (arid zones of >500mm/year) to more humid conditions (>2000mm/year) in the west. It also has a large diversity of species and ecosystems. A wealth of cultural diversity and overflowing potentials for agriculture, mining, energy, and technology investment opportunities make this region unique and an attractive place for tourism.

Nevertheless, the populations dwelling in eastern Africa are among the poorest in the world. More than 80% of the eastern African population is living below the poverty line, which is attributed to several factors. These include high population density, environmental degradation, water shortages, poor infrastructure, inadequate access to information, and poor government policies, all of which have held back the development of the region. In addition, political instabilities that have resulted in wars and conflicts have led to refugee movements, increased migration, and unsettled societies, all of which hamper development planning. The spread of diseases such as HIV/AIDS and the prevalence of inadequate health systems also increase the severity of poverty. However, climate variability and change, which induce or intensify extreme events like heat waves, flooding and droughts, are considered to pose the biggest challenge to the development of the region. This is mainly because this region relies on

rain fed agriculture (~60%) and livestock production (~20%) for food and income generation. These climate extremes thus pose a significant threat to agriculture, food security and socio-economic activities in eastern Africa. To reduce poverty in this region, there is a need for studies on understanding the characteristics of these extreme events. The present thesis focuses on drought, which is the most notorious, most subtle and most prolonged of these extreme events.

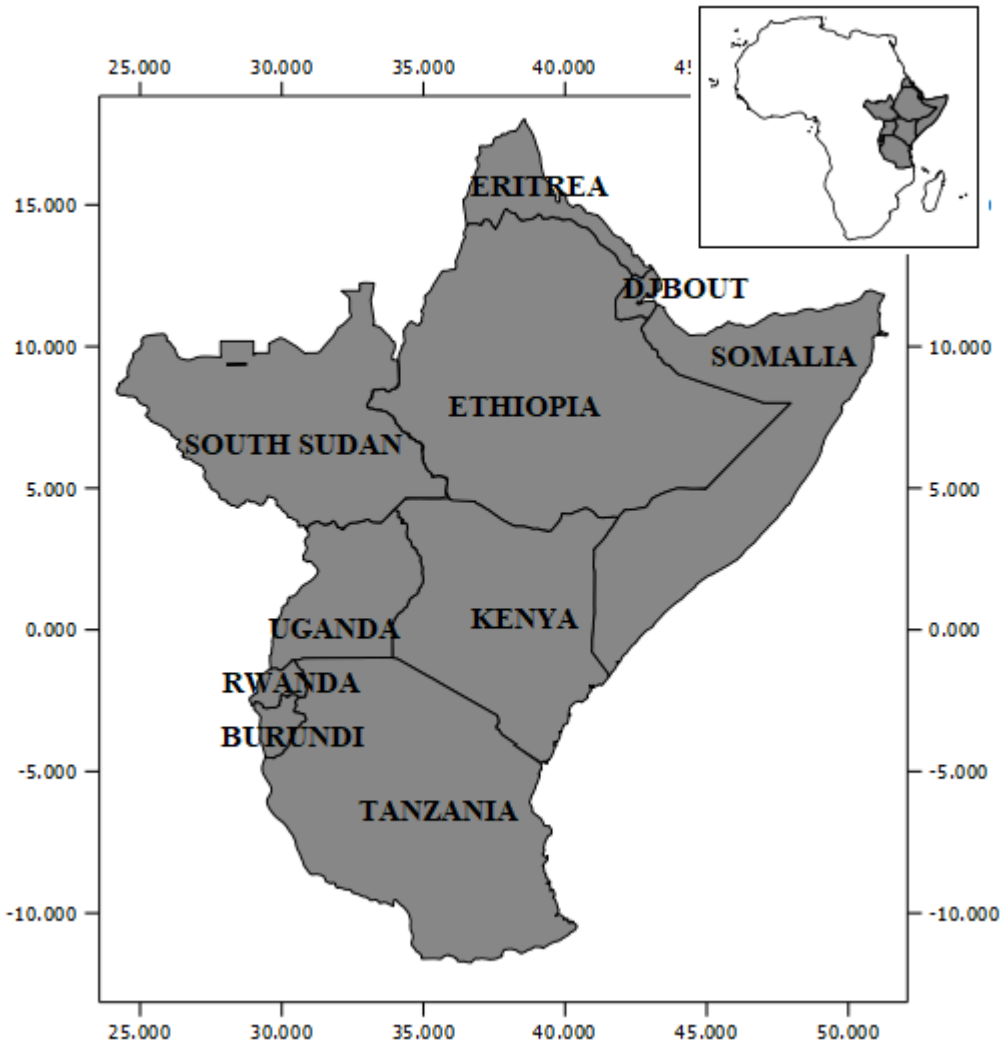

Figure 1.1: *Map of the Eastern African region.*

Eastern African river basins play a significant role in sustaining the wellbeing of the people. They provide fresh water for riparian communities and maintain life-supporting ecosystems. In addition, most agricultural activities in eastern Africa take place within the catchment areas of the basins. In recent years, the decreasing crop production due

to drying conditions over most eastern African river basins has been a cause for concern (Mbaga, 2015; McCartney et al., 2008; Mwakalila, 2011). Although the drying of the basin has been attributed to overpopulation and the overharvesting of forest resources, the impact of global warming has also been identified as a major driver. For example, Nauman et al. (2014) reported severe drought intensity over the eastern Nile basin, attributing this to enhanced evapotranspiration induced by higher temperatures. Githui (2009) also attributed the observed reduction in run-off over the Nzoia catchment to higher evapotranspiration due to higher temperatures. Given the magnitude of projected climate changes, there is a need to understand how climate change may affect the intensity and frequency of droughts in some river basins of East Africa, where the majority of the population is concentrated in order to access resources. That is also the focus of the present study.

1.2 What is a drought?

While drought is a well-known and widely accepted term in most societies globally, there is in fact no quantitative definition of drought that is acceptable to everyone. Several drought definitions have already been proposed (Wilhite & Glantz, 1985), and more definitions are still emerging. The most common definitions are given in Table 1.1.

Table 1.1: *Definitions of drought*

Drought definition	Reference
"Drought is the percentage of years when crops fail from the lack of moisture".	FAO, 1983
"Droughts originate from a deficiency of precipitation, resulting in water shortage for some activity or for some group, and its severity may be aggravated by other meteorological elements".	AMS, 1997
"Drought means the naturally occurring phenomenon that exists when precipitation has been significantly below normal recorded levels, causing serious hydrological imbalances that adversely affect land resource production systems".	General, 1994
"Drought means a sustained, extended deficiency in precipitation."	WMO, 1986
"Drought is an extended period – a season, a year, or several years – of deficient rainfall relative to the statistical multi-year mean for a region."	Schneider, 1996
"Drought is a significant deviation from the normal hydrologic conditions of an area".	Palmer, 1965

As can be seen from the above, different drought definitions could lead to different conclusions regarding the conditions of drought. For example, if the focus is on drought as defined by precipitation level, it is possible to conclude a no-drought condition for a certain season, even though the same condition would not be suitable for plant growth and production. Similarly, a good year for crop production might not omit the deficiencies in stream flow, dams and subsurface water storages. It is therefore important to note that drought affects different sectors of society differently, and that therefore the drought definition needs to be chosen carefully by focusing on the particular problem under study. In the current study we have based mostly on Palmer drought definition

1.3 Classification of droughts

Drought can be grouped into four major categories: meteorological, agricultural, hydrological, and socio-economic (Mishra & Singh, 2010; Wilhite & Glantz, 1985) (see Fig. 1.3).

1.3.1 Meteorological drought

Meteorological drought is the climatic condition that occurs when there is a deficit in precipitation compared to the long-term average (Dai, 2011). This definition is however not consistent over different regions, because atmospheric conditions vary in different areas. Therefore, the precipitation thresholds should be region-specific. Such a decrease in precipitation will also result in decreased cloudiness and relative humidity, as well as increased temperature, evapotranspiration, and radiation. The main causes of meteorological drought are the changes in large-scale atmospheric circulation patterns, which are often triggered by the variability of tropical sea surface temperatures (SSTs) or other remote conditions (Giannini et al., 2003; Hoerling et al., 2006).

1.3.2 Agricultural drought

Agricultural drought is a period of soil moisture deficits that results from below-average precipitation, above-normal evaporation, increased temperature, and persistent wind (Mishra & Singh, 2010). As a result, plant growth is affected, and crop production decreased. Because different plants have different demands for water, therefore, this concept varies in relation to each plant. Normally, this type of drought occurs after meteorological drought and before hydrological drought.

1.3.3 Hydrological drought

Hydrological drought occurs when the river stream flow and water storages in aquifers, lakes, or reservoirs decrease below long-term mean levels (Dai, 2011). Hydrological drought normally develops more slowly and lags the occurrence of meteorological and agricultural droughts. Climate fluctuations often trigger hydrological droughts, but other factors such as land use change, land degradation and poor water management, also enhance these types of droughts. For example, overgrazing and increased agriculture activities in the Ihefu basin of Tanzania threatened the ecosystem of Ruaha

National Park due to the increased dry period of the Great Ruaha River (Mwakalila, 2011).

1.3.4 Socio-economic drought

Socio-economic drought occurs when the demand for water resources in the community is higher than the supply (Wilhite, 2000). Such shortages in water supply that depend on weather will interfere with several activities, like industries and agriculture, which then affects human communities. For example, in Ethiopia in 2002-2003, drought resulted in agriculture failures, which placed increasing demand on crop products, such as cereals. In Tanzania, during 2011, drought resulted in a severely reduced electricity supply because the country's main sources of power were hydroelectric plants, which are water-based and thus affected significantly by decreased precipitation. This in turn placed increasing demands on industrial products that require a reliable power supply for production processes.

The emphasis of the present study is on the first three types of drought, namely: meteorological, agricultural, and hydrological droughts, which are easier to quantify than socio-economic drought.

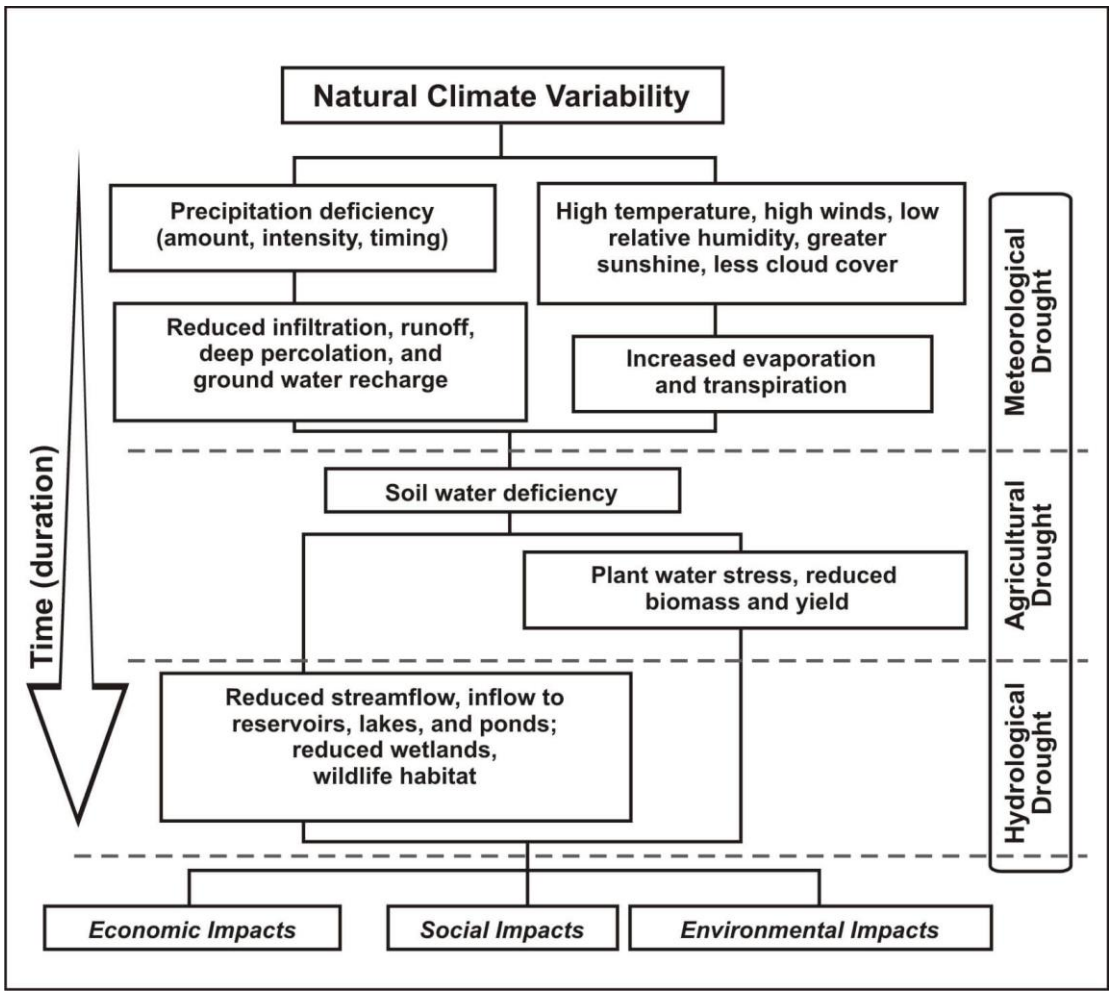

Figure 1.3: *Types of droughts and how they develop. Source: National Drought Mitigation Center (NDMC), University of Nebraska-Lincoln*

1.4 Essential characteristics of droughts

The environmental and socio-economic impacts of drought are determined by four main drought characteristics (Fig. 1.4): intensity, frequency, spatial coverage and duration. Intensity of drought denotes the degree of precipitation, soil moisture, or water storage deficit in each area over a specified period. Based on the most common drought models, such as the Palmer Drought Severity Index (PDSI) (Palmer, 1965), drought intensity can be classified as mild, moderate, severe or extreme. Frequency of drought is the recurrence interval between drought episodes in a given region. Spatial coverage denotes the geographical extent affected by a specific drought event. A moderate drought occurs over a small region, but extreme ones can cover a continent. Duration of drought refers to the length of time that a given drought episode lasts. Mild drought can last for several months and up to a few years, but extreme drought can persevere

for several years. In this thesis, all these drought characteristics are studied over the study domain.

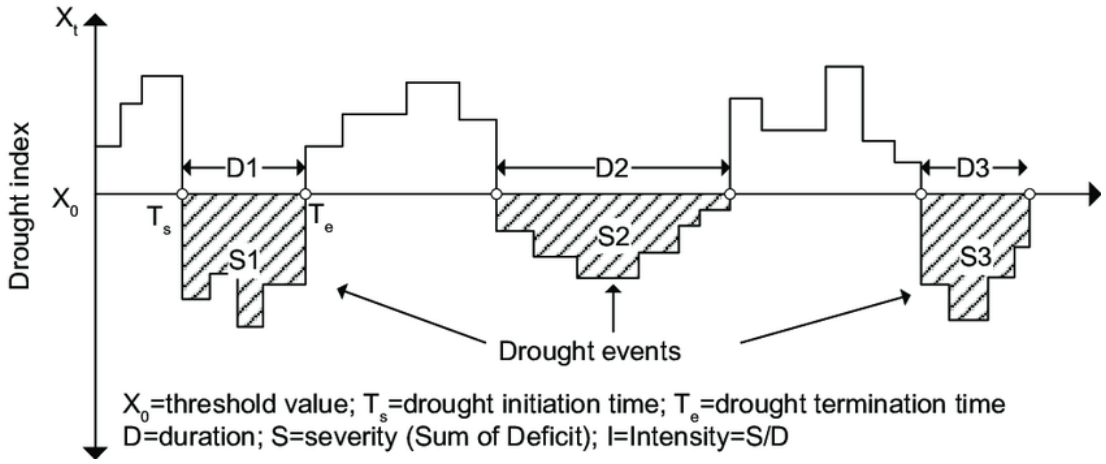

Figure 1.4: *Identification of drought characteristics (Source: Yevjevich, 1967).*

1.5 Quantification of drought

Choosing the most suitable index to characterise or quantify droughts is a major challenge in drought monitoring research (Ujeneza & Abiodun, 2014). As a result, different drought indicators have been introduced and used to characterise the different kinds of drought (e.g. meteorological, agricultural, and hydrological), and the performance of those indices differs across different regions (Heim, 2002; Mishra & Singh, 2010). Examples of such drought indices are the Palmer Drought Severity Index (PDSI) (Palmer, 1965), the Standardized Precipitation Index (SPI) (McKee et al., 1993), the Bhalme–Mooley Index (BMI) (Bhalme & Mooley, 1979) and the Standardized Precipitation Evapotranspiration Index (SPEI) (Vicente-Serrano et al., 2010a). These drought indices are essential tools for explaining drought events.

SPI, the most recommended drought indicator globally, has been used frequently for drought monitoring over eastern Africa (Degefu & Bewket, 2014; Ntale & Gan, 2003; Viste et al., 2013). It is also recommended by the World Meteorological Organization (WMO) for monitoring meteorological drought (Hayes et al., 2011). Positive and negative values of SPI indicate wet and dry periods, respectively, and reflect the drought intensity. SPI values between -0.1 and -1.0 refer to moderate droughts, values between -1.1 and -2.0 refer to severe droughts, and values below -2.1 indicate extreme

droughts (McKee et al., 1993). Ntale and Gan (2003) proposed the use of SPI in studying drought over eastern Africa in comparison to PDSI and BMI. The SPI was found to better represent the drought characteristics of the region. Also, the concept of SPI can be applied to other variables, such as soil moisture, agricultural drought, and hydrological drought monitoring (Belayneh et al., 2014; Bernard et al., 2013; Degefu & Bewket, 2014; Vicente-Serrano et al., 2012b); whereas SPI_3 (i.e. 3 months SPI) can be used as a meteorological drought index, SPI_6 (i.e. 6 months SPI) is highly correlated with an agricultural drought index, and SPI_12 (i.e. 12 months SPI) and SPI_24 (i.e. 24 months SPI) can detect hydrological droughts. Therefore, SPI is widely used in drought studies because it is multiscalar, flexible and simple to use (McKee et al., 1993). Its main drawback, however, is that its calculation is based on precipitation data only. The index does not consider other variables that can influence droughts, such as wind speed, evapotranspiration, temperature, and soil water holding capacity.

Drought is a complex phenomenon. Although it primarily originates from sustained precipitation deficits (e.g. Diasso & Abiodun, 2015; Marshall et al., 2012; Meque & Abiodun, 2015; Patricola & Cook, 2011; Shongwe et al., 2011; Vicente-Serrano et al., 2010b), one single indicator (i.e. precipitation) may be insufficient for describing all drought features. Nonetheless, in eastern Africa, most studies have characterised droughts using mostly precipitation (e.g. Dutra et al., 2013; Elagib, 2013; Elagib & Elhag, 2011; Viste et al., 2013). While some have used the precipitation index, such as the SPI (Belayneh et al., 2014; Degefu & Bewket, 2015; Dutra et al., 2013; Edossa et al., 2010; Elkollaly et al., 2017; Khadr, 2016), several studies have analysed the changes in rainfall itself by looking at the quantity, timing, intensity or duration of rainfall (Githui, 2009; Mtalo et al., 2005; Yanda & Munishi, 2007). The integration of different drought-related variables is essential for efficient drought analysis (Dai 2011; Sheffield et al., 2012; Vicente-Serrano et al., 2010b; Wilhite, 2005). For example, evapotranspiration is observed to have a significant influence on drought conditions, especially given ongoing global warming trends (Abramopoulos et al., 1988; Marshall et al., 2012), as it coincides with increases in maximum temperature. Evapotranspiration contributes significantly to drought variability in eastern Africa (Patricola & Cook, 2011; Shongwe et al., 2011; Ghebrezgarbher et al. 2016). Over most parts of southern Africa, ENSO is better correlated with temperature than with rainfall (Meque & Abiodun, 2015). Hence, using only precipitation to characterise eastern

African droughts might underestimate the drought intensity and misrepresent the influence of atmospheric teleconnections. The inclusion of evapotranspiration in characterising droughts would also account for the influence of other variables, like temperature, solar radiation, relative humidity and wind speed. Therefore, using both precipitation and evapotranspiration in quantifying droughts would result in more realistic drought characteristics than using only precipitation (Vicente-Serrano et al., 2012a).

To improve the accuracy of SPI, SPEI was developed by incorporating the variable of evapotranspiration (which allows drought conditions to be analysed based on variations in the water balance). Similar to SPI, SPEI quantifies the dry and wet conditions at different time scales. SPEI is more complex than SPI because it includes several other variables, such as temperature, solar radiation, relative humidity, and wind speed. Generally, the category and value of the SPEI are the same as those of the SPI. SPEI has been applied widely in several studies around the globe. For instance, the SPEI index is the best in computing drought responses on hydrological, agricultural and ecological variables (Vicente-Serrano et al. (2012b). Paulo et al. (2012) studied climate trends and the behaviour of drought indices using precipitation and evapotranspiration in Portugal. Among the indices applied, SPEI was found to be useful for identifying severe and extreme droughts at appropriate temporal and spatial distributions. The index was also found to be useful in reproducing the drought events in China (Yu et al., 2014) and in southern Africa (Ujeneza & Abiodun, 2014). However, only limited studies have applied SPEI to characterise the droughts over eastern Africa (e.g. Hassanein et al., 2013; Masih et al., 2014; Naumann et al., 2014; Ghebrezgarbher et al. 2016). Hence, the current thesis applies SPEI to identify the large-scale drought systems over the bigger domain of Eastern Africa which most studies have not presented. Also, it incorporates SPEI to analyse hydrological drought conditions in the region as it becomes more severe with increasing climate change.

1.6 Impacts of droughts on socio-economic activities in Eastern Africa

Droughts usually have devastating impacts on environments, agriculture, water resources, and socio-economic activities, and so too in eastern Africa. It causes land

degradation, damages crops, kills animals, initiates diseases and epidemics, affects human lives, and reduces the agricultural production (Haile et al. 2019) on which the Gross Domestic Product (GDP) of many eastern African countries is based (Dutra et al., 2013; Mishra & Singh, 2010). Since 1950, this region has witnessed recurrent severe droughts (Anyah & Qiu 2012; Cook & Vizy 2012; Damberg & Aghakouchak 2014; Lyon & DeWitt, 2012; Haile et al. 2019). For instance, in 1983-1984, droughts triggered a famine that led to more than 100,000 fatalities in Sudan and northwest Ethiopia (Degefu, 1987). The 1999-2001 drought led to a loss of more than 2.3 billion dollars in the economy of Kenya (UNDP, 2008). In 1998-2005, a persistent drought destroyed crops and livestock and caused a major food shortage in Tanzania (Kijazi & Reason, 2009), inducing widespread diseases and malnutrition, especially among children, women and elderly people (Funk et al., 2014). This necessitated an emergency appeal to support more than 70 000 people affected by the drought (Kijazi & Reason, 2009). The drought of 2002-2003 affected about 2.9 million people in Ethiopia (Degefu & Bewket, 2014). It caused a 12% decrease in agricultural outputs and led to a drop of about 3.8% in the GDP of the country. The drought of 2010-2011 plunged eastern Africa into the worst food security crisis in the last two decades (Earth Observatory, 2011), affecting more than 8 million people (ACTED, 2011; Funk, 2011). It was the worst drought in the past 60 years (ACTED, 2011; Funk, 2011).

As drought reduces the water volume in dams, it reduces hydroelectric power generation, thereby affecting non-agricultural economic sectors too (Kaunda & Mtalo, 2013). For instance, the drought in 2002-2003 over Ethiopia led to power interruptions that lasted for about 4 months, with complete interruptions occurring one day per week throughout the country (Degefu & Bewket, 2014). Drought is a major source of conflict among eastern African communities, as they fight for available scarce resources (Fjelde & Von Uexkull, 2012; Ide et al., 2014). Hence, directly and indirectly, droughts lead to human suffering and human death. Drought also depletes groundwater reservoirs and reduces freshwater availability. It forces people to use water from unsafe sources. As a result, people suffer from diseases like cholera, diarrhoea, and dysentery (Ujeneza & Abiodun, 2015). Other diseases like fever can also emerge (Chretien et al., 2007). For instance, the drier conditions in 1998 caused the outbreak of chikungunya fever along the coast of eastern Africa (Chretien et al., 2007). Other impacts of droughts in this region include mass migration of people and their animals, insect infestations and

degradation of biodiversity (Degefu & Bewket, 2014; Dutra et al., 2013). Therefore, reliable early warning systems on droughts could help to reduce the devastating impacts of droughts in this region, but the development of such systems requires good knowledge of the characteristics and drivers of eastern African climate and droughts.

1.7 Climate of eastern Africa

The climate of eastern Africa is complex, mainly because of the influence of the maritime and terrestrial interactions on the climate (Lyon, 2014; Yang et al., 2015). The region generally has a semi-arid climate and experiences small variations in temperature throughout the year but exhibits a high degree of spatio-temporal variability in rainfall (Yuan et al., 2013). This causes rainfall to be a key climatic factor in eastern Africa. The main control of rainfall over most of the region is the movement of the Inter-Tropical Convergence Zone (ITCZ), in combination with Hadley cell atmospheric circulations (Anyah & Qiu, 2012; Hastenrath, 2001). Topographical features also play an important role in low-level atmospheric circulation and moisture transport (Kinuthia, 1992), which causes the patterns of rainfall to change over short distances (Nicholson, 1996). However, compared to other regions along the same latitude, eastern Africa receives a low amount of mean annual rainfall (Yuan et al., 2013).

Eastern Africa is characterised by two major rainfall regimes: the bimodal regime rains in March–May (MAM) and October–December (OND), and the unimodal regime rains in June–September (JJAS) and December–March (DJFM) (Dutra et al., 2013; Lyon & DeWitt, 2012; Nicholson, 2017; Yang et al., 2015) (Fig. 1.5). The bimodal rains are strongly linked to the latitudinal migration of the ITCZ (Nicholson, 1996; Nicholson, 2017) (Fig. 1.6). When the ITCZ moves to the northern hemisphere, because of the bigger land mass in the north, it becomes much broader and moves much more slowly. This northward movement causes larger amounts of rainfall that are received during the longer season. Conversely, when the ITCZ shifts to the southern hemisphere, because of the smaller land mass in the south, it moves rapidly, particularly over the transition regions like the eastern part of East Africa. This slow movement creates less rain that does not last long (McGregor & Nieuwolt, 1998).

The north-eastern and central equatorial parts of eastern Africa are characterised by a bimodal rainfall distribution, which has been strongly affected by drought in recent years, for instance in 2010-2011 (Dutra et al., 2013). The unimodal JJAS pattern is dominant in the Ethiopian highlands and in the north-western regions of eastern Africa. The southern part of eastern Africa, in contrast, exhibits a unimodal rainfall pattern (DJFM) (Yang et al., 2015). MAM is referred to as the long rainfall season (more abundant rainfall), and is dominated by local factors rather than large-scale factors in the modulation of its patterns over the region (Indeje et al., 2000; Mutemi, 2003; Nyakwada et al., 2009). The corresponding OND rainfall period is regarded as the short rainfall season and tends to have stronger inter-annual variability and stronger spatial coherence, being substantially influenced by tropical and extratropical atmospheric circulations, such as the El Niño Southern Oscillation (ENSO) and the Indian Ocean dipole (IOD) (Hastenrath et al., 1993; Indeje et al., 2000; Nicholson & Kim, 1997; Nyakwada et al., 2009; Ogallo, 1989; Saji et al., 1999).

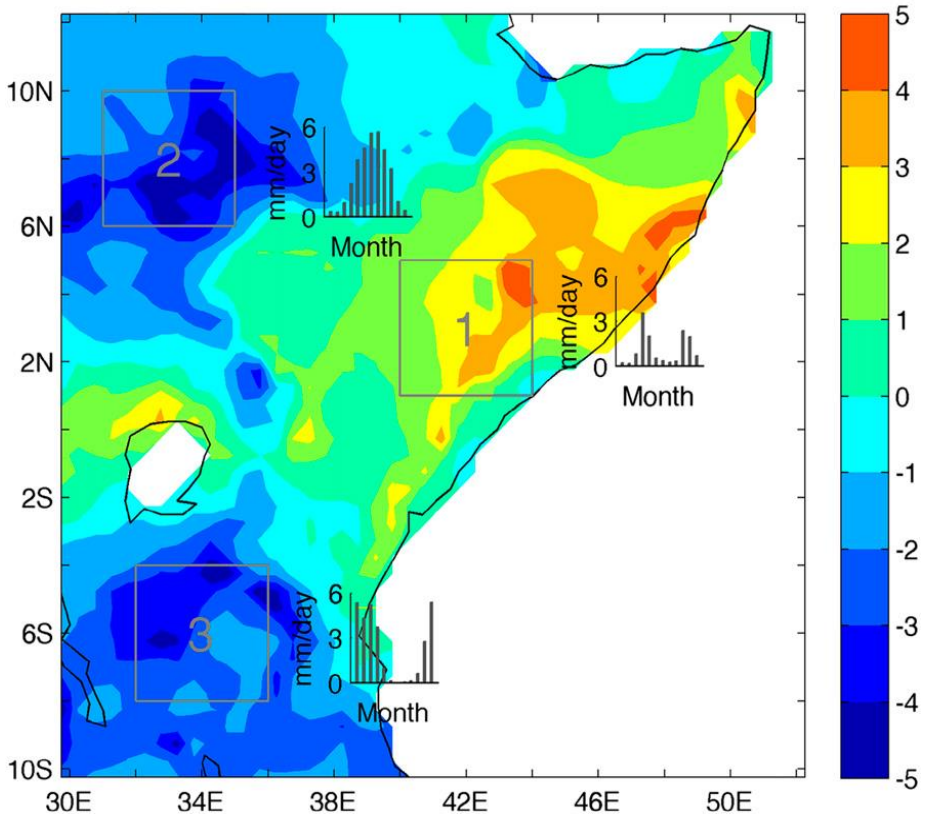

Figure 1.5: *Distribution of precipitation patterns over eastern Africa generated from GPCC data for the period 1901-2010. Bar graphs present the annual cycle of precipitation averaged by month. (Adapted from Yang et al., 2015).*

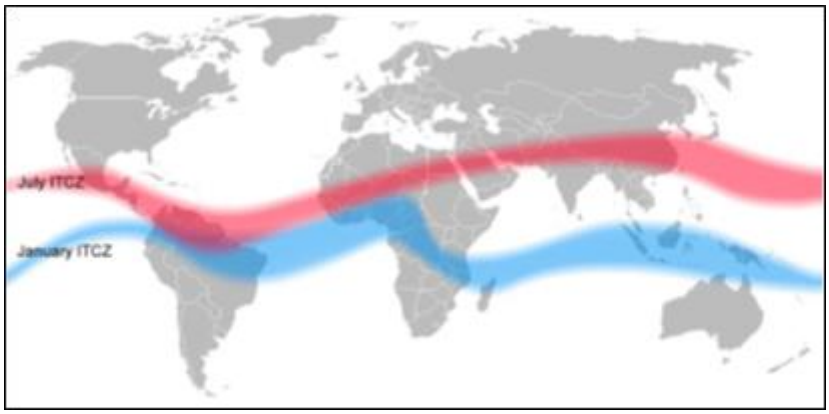

Figure 1.6: *The maximum positioning of the ITCZ during the northern hemisphere summer (July ITCZ) and the southern hemisphere summer (January ITCZ) (Source: Dommenget, 2018).*

1.8 The role of teleconnections over eastern Africa drought

Eastern African droughts have a large spatial-temporal variability because the climate of the region is controlled by complex interactions between large-scale atmospheric circulations and local-scale features induced by coasts, high altitudes, and major lakes (Cook & Vizy, 2013; Daron, 2014; Lyon, 2014; Yang et al., 2015). The major teleconnections that modulate drought in the region are: the El Niño–Southern Oscillation (ENSO) (e.g. Indeje et al., 2000; Russell & Johnson, 2007; Trenberth et al., 2014; Yuan et al., 2013), Tropical Indian Ocean SSTs (Black, 2005; Yamagata et al., 2004), the Indian Ocean Dipole (IOD) (Hastenrath et al., 2007; Saji et al., 1999; Tierney et al., 2013; Ummenhofer et al., 2009), the Atlantic Ocean SSTs (Nicholson, 1996), and the Quasi-Biennial Oscillation (QBO) (Indeje & Semazzi, 2000; Jury et al., 1994; Ng'ongolo & Smyshlyaev, 2010).

1.8.1 El Niño Southern Oscillation

El Niño is referred to as the anomalous warming of the eastern tropical Pacific Ocean. The reverse is called La Niña. The collective of El Niño and La Niña conditions forms the El Niño Southern Oscillation (ENSO). ENSO has the strongest signal in controlling drought over the eastern Africa region (Indeje et al., 2000; Russell & Johnson, 2007; Trenberth et al., 2000; Yuan et al., 2013) especially at inter-annual time scales. The

increase in the SSTs in the eastern tropical Pacific Ocean results in the weakening of the easterly trade winds. This alters the Walker circulation and the convection zone in the tropics, thus affecting the climate in the mid-latitudes, including the East African region, through Rossby wave trains. There is a greater chance of drought over eastern Africa during the cold phase of ENSO (La Niña) years than during the El Niño years. For instance, the strong La Niña conditions in the tropical Pacific were the main cause of the 200-2011 drought over the Horn of Africa (Dutra et al., 2013; Lott et al., 2013; Tierney et al., 2013). Also, the La Niña conditions were the major factor behind the 1999-2000 drought over eastern Africa (Anyamba et al., 2002). However, it is also known that some parts of eastern Africa, i.e. the North-western region, South Sudan and central-western Ethiopia, do experience drought during the warm phase of ENSO (El Niño) (e.g. Lyon, 2014; Zeleke et al. 2017). In addition, the influence of ENSO on the climate of eastern Africa is the result of an indirect forcing by ENSO on the Indian Ocean (Black, 2005; Latif et al., 1999). During ENSO cycles, anomalies from the tropical Pacific Ocean modulate Indian Ocean variability through changes to the atmospheric Walker circulation and in the ocean through the Indonesian Throughflow (Black et al., 2003; Meyers, 1996).

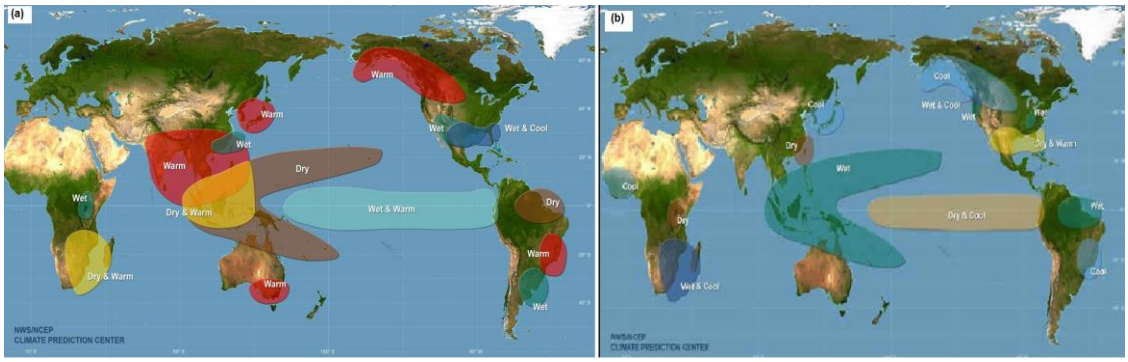

Figure 1.7: *The impact of (a) El Niño and (b) La Niña conditions globally during the December - February season (Source: NOAA).*

1.8.2 Indian Ocean Sea Surface Temperature

The tropical Indian Ocean SSTs have a strong influence on the climate of their near-by surroundings (Black et al., 2003; Cai & Cowan, 2013). Goddard and Graham (1999) observed a strong correlation between Indian Ocean SSTs and the variability of precipitation over eastern Africa using atmospheric general circulation model (AGCM)

experiments. Indian Ocean SSTs are found to drive the variability by altering (weakening/strengthening) the local Walker circulation. The AGCM simulations by Goddard and Graham (1999) showed that the convergent westerly flow, which results from cool SSTs anomalies in the western tropical Indian Ocean, reduces the moisture flux over eastern Africa, whereas the divergent easterly flow (from warm SST anomalies in the western tropical Indian Ocean) enhances the moisture flux over the region. Tierney et al. (2013) suggested that the changes in Indian Ocean SSTs or its gradient are the dominant influence on the eastern Africa precipitation variability at multi-decadal and longer time scales.

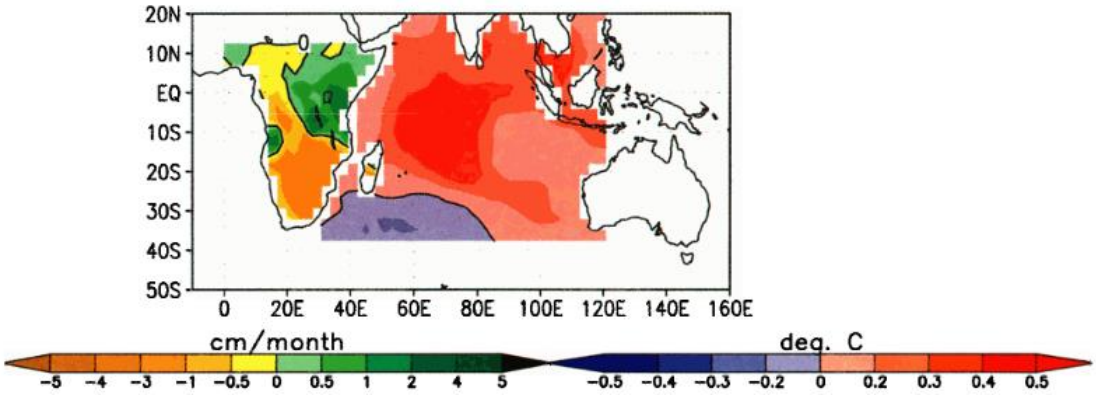

Figure 1.8: *The relationship between the tropical Indian Ocean and eastern Africa rainfall as shown with precipitation and SST dominant patterns for November-December-January during 1970-1992 (Source: Goddard & Graham, 1999).*

1.8.3 Indian Ocean Dipole

The Indian Ocean Dipole (IOD) mode is characterised by irregular fluctuations of SSTs in the Indian Ocean (Saji et al., 1999). It occurs inter-annually in the tropical Indian Ocean (Guo et al., 2015; Saji et al., 1999; Webster et al., 1999). The majority of IOD events emerge from SST anomalies near the Java coast in response to the surface wind anomalies (Behera et al., 2006; Saji & Yamagata, 2003; Saji et al., 1999). These surface wind anomalies result from the variability of the Indian Monsoon or remote forcing from ENSO (Annamalai et al., 2003; Behera et al., 2005). The negative phase of IOD (which is recognised with anomalous strong south-easterly winds) is shown to decrease convective activities over eastern Africa and to cause droughts (Clark et al., 2003; Meyers et al., 2007). The strong negative phase of the IOD during 1964, 1971, 1975,

and 1996 was documented to create low precipitation over eastern Africa (Saji & Yamagata, 2003). The positive phase of the IOD (which is recognised with anomalous strong north-westerly winds) causes droughts over regions of Burma, Thailand, Philippines, Malaysia, Indonesia, Singapore, Papua New Guinea and northern Australia and rainfall over eastern Africa. IOD can also modulate eastern African droughts during El Niño and in the year following El Niño events (Guo et al., 2015; Saji & Yamagata, 2003).

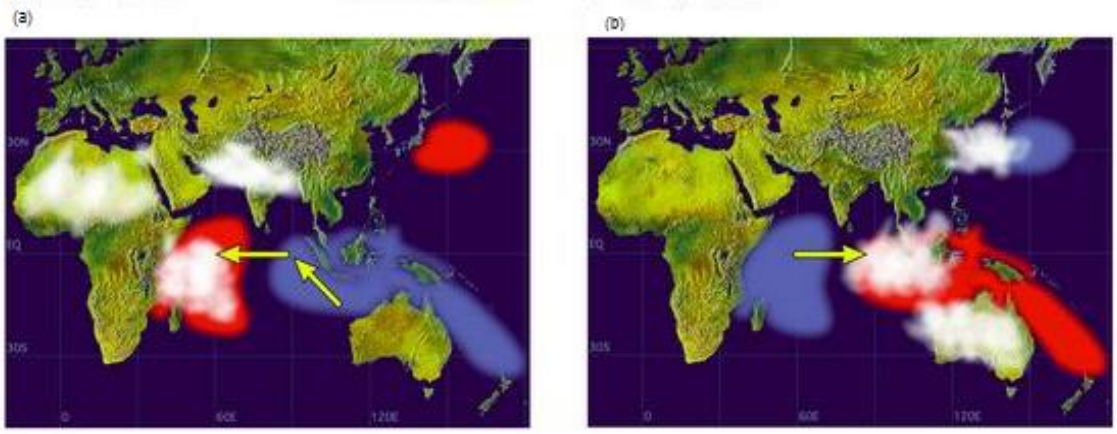

Figure 1.9: *IOD Schematic anomalies (a) Positive phase (b) Negative phase. Colour red is for warm anomalies, colour blue is for cold anomalies, and white clouds indicate active convective processes. The arrows show the direction of wind during IOD events (Source: http://www.jamstec.go.jp/aplinfo/sintexf/e/iod/about_iod.html.).*

1.8.4 Atlantic Ocean Sea Surface Temperature

The Atlantic Ocean affects the climate of eastern Africa through westerly flow winds (McHugh & Rogers, 2001). The strength of the westerly flow depends on fluctuations in the location and intensity of the Inter-tropical Convergence Zone (ITCZ). McHugh and Rogers (2001) demonstrated that a decrease in precipitation is pronounced over eastern Africa during the negative phase of the North Atlantic Oscillation (NAO). This phase develops when there are episodes of weak westerly flow (strong easterly flow). McHugh and Rogers (2001) also documented that, during the positive phase of NAO, precipitation increases over eastern Africa, with local factors modulating the precipitation sequence in some areas. These positive phases are shown to be associated with strong westerly flow episodes (weak easterly flow). Zeleke et al. (2017) showed the increasing drought of 1980 to 2014 over southern Ethiopia is linked to Atlantic

Ocean Warming. However, Lyon (2014) found a weak correlation between the Tropical Atlantic Ocean and eastern African seasonal drought.

1.8.5 Quasi-Biennial Oscillation

The Quasi-Biennial Oscillation (QBO) is a quasi-periodic oscillation in stratospheric and tropospheric zonal wind between westerly and easterly modes (Indeje & Semazzi, 2000), and has also been shown to play a significant role in modulating eastern African droughts. Jury et al. (1994) linked the weak phase of the QBO to a decrease in convection activities over south-eastern Africa, but Indeje and Semazzi (2000) associated the strong phase of QBO with a weakening of the Walker cell and the occurrence of droughts over eastern Africa. The current study examined the relationship between these teleconnections and drought over eastern Africa through application of drought indexes.

1.9 Major River Basins studied

The eastern African region is the main study domain for this thesis. This region is defined as the area lying within 28^0E and 52^0E longitudes, and 12^0S and 12^0N latitudes (Fig. 1). East Africa is characterised by four major river basins (the Rufiji, Tana, Juba and Upper-Nile basins). These four basins were used in achieving Objective IV of the study, while the RRB was used in attaining Objective V. This section will focus on descriptions of these four river basins since a detailed description of other physical features of eastern Africa (e.g. topography, climate, etc.) have already been given in Chapter 1.

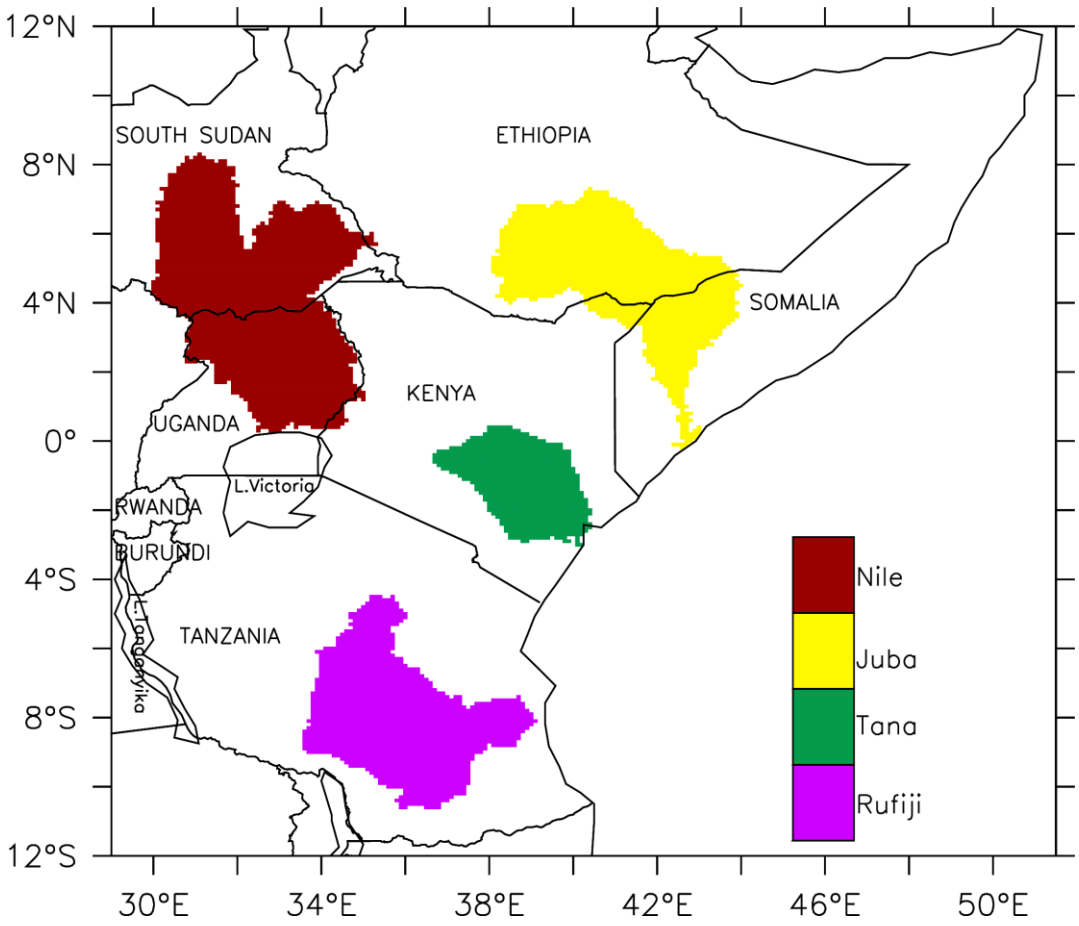

Figure 1.10: *The location of selected eastern African river basins used in the study.*

1.9.1 The Rufiji River Basin

The Rufiji River basin (RRB) is located entirely within Tanzania (Fig. 3.1). It lies between the latitudes of 5.7°S and 10.5°S and the longitudes of 33.5°E and 39°E. The whole catchment covers approximately 177,420 km^2, an estimated 20% of Tanzania's landmass (Mwalyosi, 1990). The RRB is made up of four major sub-basins: the Great Ruaha, Kilombero, Luwegu, and Rufiji (Mwalyosi, 1990; Temple & Sundborg, 1972), and occupies 47%, 23%, 15% and 15% respectively of the total basin area (Mwalyosi, 1990). The Kilombero sub-basin, which contributes more than 60% of the total RRB water, is the main source of water throughout the year (Mwalyosi, 1990). It also provides the largest freshwater catchment at low elevation (<300m a.s.l.) in East Africa (Burghof et al., 2018). The main Rufiji River collects its water from its tributaries across different landscapes, and discharges into the Indian Ocean (at a location called the Mafia Channel). The topography of the RRB ranges from relatively flat land

downstream to the east, to mountainous areas up to 3,000 m above sea level in the west (Fig. 3.2 (a)). Its climate varies from tropical humid along the cost to temperate in the south-western highlands (Mwalyosi, 1990). The movement of the Inter-Tropical Convergence Zone (ITCZ) also contributes to the climate of the basin. The large part of the basin experiences a unimodal rainfall season: the rainy season (NDJFM) and the dry period (JJAS). However, the north-eastern parts of the RRB mostly have a bimodal pattern (short rainy season: OND; long rainy season: MAM; dry period: JJA). The crop production is mostly concentrated during the rainfall season, because of the high relative humidity, low diurnal temperatures, and minimum sunshine. The annual rainfall over most parts of the catchment varies from 250 to 1,800 mm/year, with higher rains over the high-altitude basin areas (Temple & Sundborg, 1972). In most parts of the basin, the annual PET, which ranges between 1,400 and 2,400 mm/year, exceeds the annual precipitation (Temple & Sundborg, 1972).

The RRB plays a crucial role in socio-economic developments in Tanzania, because it is an important source of freshwater. It provides much of the country's water resources for agriculture, fisheries, livestock, mining, forest products, tourism, and minerals (Bernacsek, 1981; Mwalyosi, 1990). The presence of many permanent rivers in the basin makes it attractive for hydroelectric power generation. Thus, it currently accommodates the Kidatu, Kihansi and Mtera hydropower plants and provides more than 50% of hydropower energy in the country (Kichonge et al., 2016). It is also a key feature in the Greater Selous Ecosystem (the Selous-Kilombero seasonal wildlife migrations), which is a World Heritage Site; recently, approximately 7,600 km^2 of the catchment area has been labelled a Ramsar site (Ramsar Bulletin Board, 2002). Additionally, the RRB's delta contains the biggest mangrove forest in eastern Africa. However, in recent times the RRB hydrological system has been severely affected by the expansion of agricultural land, deforestation, over-harvesting of forest resources, increasing water abstraction and land degradation (Kashaigili, 2008; Mtalo et al., 2005; Mwakalila, 2011). All of these make the RRB the best candidate for the present study.

1.9.2 The Tana River Basin

The Tana River basin (Fig. 3.1) covers an area of approximately 120,000 km^2 and has the longest river system in Kenya (Kitheka et al., 2005), which flows for ~1100km from source to mouth. The Tana River basin is found in the tropical region and is largely

dominated by a semi-arid climate. The pattern of annual rainfall follows the monsoon and is highly seasonal. The main season (i.e. long rainy season) occurs in April-June and the low season (short rainy season) occurs in November–December. The spatial distribution of rainfall varies enormously, from ~1800 mm/yr in the upper catchment to ~300 mm/yr in the lower catchment (Leauthaud et al., 2013). Five hydroelectric power dams are located within the basin. As it has bigger dams, more intense irrigation schemes, higher evaporation rates and channel losses, the lower part of the Tana basin also has less water flow during the dry season (Maingi & Marsh, 2002). Apart from the direct economic importance of this basin to the community, the Tana basin also has a high conservation value. It is characterised by the presence of numerous endemic species of plants (Luke et al., 2005), primates (Hamerlynck et al., 2012), and endemic fish species (Nyingi et al., 2011; Seegers et al., 2003). The Tana basin is also a suitable habitat for migratory water birds (Bennun & Njoroge, 1999). The drought in this river basin is mostly associated with intense irrigation schemes, high evapotranspiration rates and high channel losses (Maingi & Marsh, 2002).

1.9.3 The Juba River Basin

The Juba River basin is a transboundary basin shared by Somalia, Ethiopia and Kenya (Fig. 3.1). The riverine populations of Ethiopia, and to a much smaller degree Somalia, depend on this river for the supply of water resources and irrigation for agricultural purposes, as well as for recharging regional groundwater. The approximate area of the basin is 218,114 km^2 (Basnyat, 2007), with more than 75% of the basin area located in Ethiopia, 20% in Somalia, and only 5% in Kenya (Kameer, 1989). The Juba River originates from the Bale mountain ranges in Ethiopia at an altitude of about 4,230 meters, and it enters the Indian Ocean in southern Somalia. The climatic conditions of the Juba basin are mainly arid and semi-arid, influenced by the north-easterly and south-easterly wind flows of the ITCZ (Artan et al., 2007). Rainfall intensity varies considerably over the basin. In the Bale mountain ranges, the annual mean rainfall reaches 1,600 mm/year, decreasing dramatically to around 300–600 mm/year downstream. There are two distinct annual rainfall seasons in the basin: the long rains (locally known as 'Gu' season) from April to June and the short rains (locally known as 'Deyr' season) from October to November (Artan et al., 2007). PET is also variable, ranging from ~1500 mm/year in the high-altitude areas to ~2000

mm/year in the lowlands (Houghton-Carr et al., 2011). Drought is a recurrent event over most parts of the basin (Mutua & Balint, 2011).

1.9.4 The Nile River Basin

The Nile River basin is the largest in Africa, covering an area of ~2.7 million km^2 (more than 10% of Africa's landmass). This river basin is home to almost 20% of Africa's population, with 11 countries, viz. Egypt, Eritrea, Sudan, South Sudan, Ethiopia, Uganda, Democratic Republic of Congo, Rwanda, Burundi, Tanzania and Kenya, relying on the basin as the main source of freshwater. The basin has two major river tributaries, i.e. the Blue Nile from Lake Tana, and the White Nile from Lake Victoria. In the current study, we are working on the sub-basins that contribute to the flow of the White Nile River, extending from 0° to 8°N (referred to as the Upper-Nile (Fig. 3.1). This part of the Nile basin is made up of the Victoria, Bahr El Jebel, and Bahr El-Ghazal sub-basins (Di Baldassarre et al., 2011). These basins contribute about 20 to 25% of the total flow of the Nile River, while ~60-70% comes from the Blue Nile River (Di Baldassarre et al., 2011). The Nile basin has experienced high population growth rates in the past, and it is projected that the population will double by 2025 (El-Fadel et al. 2003). Such continuing population growth will increase demand for natural resources among the riparian countries of the Nile River. In addition, the potential effects of climate change on the Nile River basin have been given much more attention in recent years (e.g. Conway et al., 2007; Yates & Strzepek, 1998a, b), showing that the water resources of the basin are critically sensitive to climate change. Georgakakos (2007) also show a decreasing trend of resource production in the Nile basin, which is mostly associated with mismanagement.

1.10 The aim and objectives

The aim of this study is to understand the characteristics of meteorological and hydrological droughts in present and future climates over the eastern African region. This aim is accomplished by meeting the following set of objectives:

i. To study the temporal and spatial characteristics of eastern Africa droughts modes
ii. To investigate how some atmospheric teleconnections influence the characteristics of the Africa droughts modes

iii. To examine the influence of 1.5°C and 2.0°C global warming levels on drought modes in eastern Africa under two future climate scenarios (RCP 4.5 and RCP8.5).
iv. To assess how increases in global warming levels can influence drought characteristics over eastern African river basins at four specific global warming levels (1.5°C, 2.0°C, .5°C and 3.0°C) under one future climate scenario (RCP 8.5).
v. To examine the potential impacts of climate change and land use change on water availability in the Rufiji River basin (RRB), Tanzania, with an emphasis of hydrological droughts in this basin.

Hence, the main scientific question addressed in the thesis are:

i. What are the characteristics of regionally extensive drought (i.e. drought modes) over eastern Africa and how are they influenced by atmospheric teleconnections?
ii. What are the potential impacts of the ongoing global warming on drought modes in eastern Africa?
iii. How can increases in global warming level affect drought characteristics over the major river basins in the eastern Africa?
iv. What are the potential impacts of climate change and land use change on water availability in the Rufiji River basin (RRB) in Tanzania?

1.11 Thesis outline

The present thesis is organised into 8 chapters, as follows:

Chapter 1 introduced the concept of drought, its classification, attribution, and quantification. It also introduced the impacts of droughts over eastern Africa. The chapter also described the climate of the region, major teleconnections that influence drought in eastern Africa, major river basins studied and the motivation for this study.

Chapter 2 provides an overview of the main studies that have documented droughts in Africa and eastern Africa, both in the past and in the future. It also reviews the impact of land use and climate change on hydrological drought in river basins. Various climate

and hydrological modelling techniques at global and regional scales are also discussed in this chapter.

Chapter 3 describes the datasets as well as the methodology used in order to achieve the different objectives of the study, as set out in Section 1.9 above. About eight different climate datasets are described, and it is explained which objective each of the datasets is used for. In addition, hydrological and GIS datasets are explained. About the methodology, the drought indices of SPEI and SPI are discussed in detail. Principal Component Analysis, Wavelet Analysis and Self-Organising Maps tools are also focused on. Finally, the hydrological model known as the Soil and Water Assessment Tool (SWAT) is introduced, and details are given on how it is applied in the current study.

Chapter 4 presents and discusses the results of the analysis on the characteristics and drivers of four dominant drought modes in eastern Africa. It describes the spatial and temporal characteristics of these drought modes and investigates the link between the drought modes and four atmospheric teleconnections. This section combines objective (i) and (ii).

Chapter 5 discusses the impact of global warming at 1.5°C and 2.0°C levels on the characteristics of the four major drought modes discussed in the previous chapter. It starts by examining the capability of the Coordinated Regional Climate Downscaling Experiment (CORDEX) models in simulating the drought models, and then considers the impacts of global warming levels on the major drought modes under two future climate forcing scenarios, namely Representative Concentration Pathway 4.5 (RCP 4.5) and RCP8.5.

Chapter 6 presents the projected future changes in meteorological drought over four river basins (i.e. Rufiji, Tana, Juba and Upper-Nile) in eastern Africa, as simulated by the CORDEX models. Before presenting these projections, the chapter discusses the capability of the climate simulations in representing the climatology over eastern Africa in general and over the basins more specifically.

Chapter 7 discusses the potential impacts of climate change and land use change on water availability in the RRB, Tanzania, with an emphasis of hydrological droughts over the basin. This chapter thus contributes information for water resource planning and management in this particular river basin.

Chapter 8 summarises the findings of the study. It also presents the conclusions and makes some recommendations on how to improve the study and the way forward.

Chapter 2

Literature Review

This chapter provides an overview of the main studies that have documented droughts in eastern Africa both in the past and in the future. It also reviews the impact of land use and climate change on hydrological drought over river basins in that region. Various climate and hydrological modelling techniques at global and regional scales are also reviewed.

2.1 Regionally extensive droughts in eastern Africa

Historical studies have shown that eastern Africa has experienced several regionally extensive droughts in the past (i.e. Bessems et al., 2008; Verschuren et al., 2000). For example, Verschuren et al. (2000) investigated droughts over the period AD 900 to 2000 based on sediment analysis of Lake Naivasha, in eastern Africa, finding that the period AD 1000 to 1270 was the driest period over the last 1100 years (Verschuren et al., 2000). Bessems et al. (2008) also documented extreme droughts in eastern Africa about 150 years ago, based on the sediment analysis of three lakes, namely, Chibwera, Kanyamukali and Baringo. Moreover, according to the cultural history of eastern Africa, it appeared that droughts observed in the above studies covered a wide area with devastating effects (Verschuren et al., 2000). However, no study has investigated the characteristics of these regionally extensive droughts. Most drought characteristics studies have focused on understanding the characteristics and mechanisms of specific drought cases in small areas of the region (i.e. Dutra et al., 2013; Hastenrath et al., 2007; Kijazi & Reason, 2009; Zeleke et al. 2017). Meanwhile, understanding the characteristics and drivers of regionally extensive drought is important for several reasons. For instance, when a regionally extensive drought occurs, it is difficult to even know where to transport food and other important resources from, since the effect of the drought will cover the whole region. The difference between local and regional scale droughts can also be found in their patterns and characteristics. Regionally extensive droughts could better show the influence of large-scale factors, e.g. ENSO effects, than could local-scale drought. Therefore, the present study sets out to improve

knowledge of the characteristics and drivers of regional scale droughts in eastern Africa (see Chapter 4).

2.2 Future projection of drought over eastern Africa

Several studies have reported an increase in the intensity and frequency of droughts in eastern Africa over the past decades, particularly in Somalia, Ethiopia and Kenya (Damberg & Aghakouchak, 2014; Elagib & Elhag, 2011; Shongwe et al., 2011; Viste et al., 2013). Some of these studies have projected that this increase may continue into the future, due to ongoing global warming (Anyah & Qiu, 2012; Cook & Vizy, 2013; Dai, 2011; IPCC, 2014; Shongwe et al., 2011). For example, by using regional climate models, Patricola and Cook (2011) simulated large precipitation reductions at the end of the 21st century over parts of eastern Africa, especially during August and September. Similarly, a recent study by Cook and Vizy (2012) projected that the future increase in temperature over eastern Africa would be accompanied by an increase in potential evapotranspiration and a decrease in precipitation, hence leading to more frequent and more severe droughts. Wang et al. (2009) showed that climate change has caused a 30% decrease in runoff in the Bai River basin, while Githui et al. (2009) documented that climate change accounted for more than a 35% decrease in runoff over the Nzoia River basin in Kenya. Adhikari et al. (2017) projected a decreased water supply for agriculture in Tanzania especially in dry seasons, under the business-as-usual climate scenario (i.e. RCP 8.5). However, most of these studies have only used rainfall to characterise drought. Instead, drought is influenced by both rainfall and evapotranspiration, and various studies (e.g. Cook & Vizy, 2012; Nguvava et al., 2019) have shown that ongoing global warming may increase evapotranspiration in the future. Hence, using only rainfall to characterise drought may lead to underestimating the intensity of droughts in the future. The present study will thus use a drought index that incorporates both rainfall and potential evapotranspiration (PET) to quantify the future impact of climate change on droughts in eastern Africa.

As part of efforts to minimise the impacts of global warming, the 21st Conference of the Parties to the United Nations Framework Convention on Climate Change (UNFCCC) resolved to limit the increase in global mean average temperature to well below 2°C above pre-industrial levels, and in fact to pursue efforts to limit the

temperature increase to 1.5°C, because some studies have shown that an increase of 2°C above pre-industrial levels is not safe (UNFCCC, 2015). Understanding the differences in the regional impacts of the various GWLs is thus essential and has been the topic of investigation by several studies. For example, King et al. (2017) reported that limiting warming to 1.5°C rather than 2°C would reduce the frequency of extreme heat events and heat in the Coral Sea region off the Australian coast by 26% and 22% respectively. Su et al. (2017) documented a lower evapotranspiration rate for 1.5°C relative to a warming of 2°C over the Tarim River basin, China. They furthermore projected that regional warming of 1.5°C would occur later than the global average, whereas regional warming of 2°C would occur earlier than the global average. Ying et al. (2017) found that, relative to the pre-industrial era, the mean temperature over Asia would increase by 2.3°C and 3.0°C, at global warming targets of 1.5°C and 2°C respectively. However, only few studies have reported the impacts of the various GWLs on the East African climate (e.g. Osima et al., 2018). Most future projection studies have focused on specific time periods using certain emission scenarios (Adhikari et al., 2015; Niang et al., 2014; Otieno & Anyah, 2013b; Souverijns et al., 2016). Therefore, the current study analysed drought projections using both specific time periods as well as the various GWLs at certain emission scenarios.

There has been much controversy on the capability of some models to represent the climatic variables over eastern Africa faithfully. For instance, Otieno and Anyah (2013b) used the Phase 5 of the Coupled Model Intercomparison Project (CMIP5) to project climate variability over eastern Africa under the effect of greenhouse gas increases (representative concentration pathway 4.5 and 8.5). Their results projected an increase in precipitation over the region. Meehl et al. (2007) also suggested that increasing atmospheric greenhouse gas concentrations would lead to increases in eastern African precipitation during the boreal winter. Their output was generated through coupled general circulation models (CGCMs) from the World Climate Research Programme's Phase 3 of the Coupled Model Intercomparison Project (CMIP3) multimodel dataset (IPCC) (Solomon et al., 2007). Conversely, Shongwe et al. (2011) analysed a multimodel ensemble of CMIP3 CGCMs and reported that these models project overall increasing trends in precipitation rates and intense rainfall events in the 21st century, with a decreased propensity for drought, and that therefore the CGCMs do not generally produce an accurate representation of the eastern African

climate. Endris et al. (2015) examined the ability of the Coordinated Regional Climate Downscaling Experiment (CORDEX) (Samuelsson et al., 2011) models, with lateral and surface boundary conditions derived from the same Coupled Global Climate Models (CGCMs), to simulate the teleconnections between tropical SSTs and rainfall over eastern Africa. They found that Regional Climate Models (RCMs) driven by CGCMs poorly represent teleconnections over time and space. Otieno and Anyah (2013a) examined the ability of CMIP5 models to simulate the precipitation and temperature conditions over the region. In comparison to the gridded satellite-derived observations, some models produced the mean seasonal cycle correctly, while others did not. Determining the future patterns of eastern Africa drought conditions requires a careful examination of the ability of models to simulate realistic natural variability and forced changes (Mwangi et al., 2014). Therefore, the present study will evaluate and quantify the capability of regional climate models in simulating the characteristics of eastern African droughts.

2.3 Impact of climate change on hydrological drought over eastern African basins

Several studies have identified climate change as a driver of hydrological droughts over various regions in the world (e.g. IPCC, 2007; Schulze, 2000; Wang et al. 2011). They show that climate change can alter the spatial and temporal distribution of precipitation and increase the trend of the frequency and severity of extreme climate events (e.g. meteorological droughts and heat waves), thereby altering regional hydrological cycles and inducing hydrological droughts (Dai, 2013; Sheffield et al., 2012; Trenberth et al., 2014). For instance, Nguvava et al. (2019) projected that global warming would intensify drought in East African basins mostly due to associated increases in PET. Kingston and Taylor (2010) found a decrease in annual flow and groundwater discharge in the Upper-Nile River at a 4°C increase in global mean air temperature. Wang et al. (2009) showed that the climate change has caused a 30% decrease in runoff in the Bai River basin, while Githui et al. (2009) documented that climate change accounted for a more than 35% decrease in runoff over the Nzoia River basin in Kenya. Adhikari et al. (2017) projected a decreased water supply for agriculture in Tanzania, especially in dry seasons, under the business-as-usual climate scenario (i.e. RCP 8.5). However, none of these studies has investigated the projected impact of climate change on hydrological

drought over the RRB. The only study that has investigated the impacts of climate change on drought over this basin has limited it to meteorological drought, without considering the impact on hydrological drought, which is more relevant to the socio-economic activities of the community living in that basin. Given the different responses of river basins to climate change effects (URT, 2003), the impact of climate change on the hydrological cycle and on hydrological droughts cannot not be generalised to other river basins. The present study is thus envisaged to improve knowledge on the impacts of climate change specifically on the RRB.

2.4 Impact of land cover change on hydrological drought over eastern African basins

Land cover changes have also been identified as a driver of droughts. Land cover changes (such as afforestation, deforestation, overgrazing and urban construction) can in fact induce hydrological droughts by changing surface flow, groundwater recharge, infiltration, and evaporation systems, and consequently change the amount of water available in space and time (e.g. Brown et al., 2005; Sajikumar & Remya, 2015; Yang et al., 2012). For instance, Croke et al. (2004) and Strauch et al. (2013) show that, in the tropics, deforestation decreased the retention of water in the soil, increased the surface runoff, decreased the recharge of the aquifers, and eliminated low flows. Yang et al. (2012) found that land cover changes (from human activities in China) decreased the stream flow in the Laohahe Basin by 90%. Wang et al. (2009) also attributed ~70 % of the decrease in runoff in the Chaobai River basin to human activities. Baker and Miller (2013) found that a reduction in the forested area decreased the groundwater recharge by 7%, while it enhanced the peak runoff by 9%. They also reported a decrease in evapotranspiration due to reduction in forest cover. Tadele and Fo¨rch (2007) reported an increase in the mean monthly discharge for wet months by 12.5%, while in the dry season, a decrease of up to 30.5% was found in the Hare river watershed (Ethiopia), following a conversion of forest cover to farmlands and settlements. Githui et al. (2009) revealed that land cover changes account for a difference of about 55–68% in runoff. Näschen et al. (2018) shows that increasing agricultural land, between 1970 and 2014, over the Kilombero floodplain has caused tremendous shifts in the water balance components, i.e. decreasing evapotranspiration and groundwater. Mango et al. (2011) attributed the reduced dry season flows and the increased peak flow (which led

to greater water scarcity at critical times of the year in the Mara basin) to the clearing of natural forest for agricultural expansion. Natkhin et al. (2015) reported that changing land use and land cover (LULC) affects surface run-off and increases floods in the Ngerengere catchment area. Nevertheless, most of the studies on future projections in respect of hydro-climate variables over the RRB have only focused on the impact of climate change, neglecting the potential impacts of ongoing land cover changes in the basin. Consequently, the present study will also analyse the contribution of land cover changes to future drought projections in the RRB.

2.5 Climate modelling

Several studies have established that climate models, which are developed from physical laws, are the most viable tools to represent and study the climate systems (IPCC, 2007). These models can simulate both historical and/or future climatic variables, e.g. temperature, precipitation, wind, etc. The most used dynamic models for climate studies in literature are Global Climate Models (GCM) and Regional Climate Models (RCM) (IPCC, 2007; IPCC, 2014). GCMs have been found to be useful in advancing the understanding of the dynamic mechanisms governing climatic variability (Cook & Vizy, 2012; Endris et al., 2015; Mishra & Singh, 2009; Schubert et al., 2009; Shongwe et al., 2011). Studies have shown that the GCMs can reproduce observed or expected patterns of drought with high fidelity (Endris et al., 2015; Mishra & Singh, 2009; Ujeneza & Abiodun 2014). They also show that results from GCMs can be independently compared and verified against observational data sets and empirical studies. However, some studies (e.g. Rummukainen, 2010; Wang et al., 2004) have argued that the coarse resolution of GCMs (grid-cells with dimensions 200-300 km or greater) limit GCMs from capturing the effects of local forcing, like terrain and vegetation effects, and land-sea contrasts that modulate the climate signal at finer scales. In addition, some studies (e.g. Endris et al., 2015) found that extreme events, such as heavy precipitation, are often not captured or their intensity is unrealistically low at coarse resolutions. The formulation of adaptation policies in response to climate change impacts for regional and national assessments requires information at finer spatial scales than the one provided by these GCMs. Nevertheless, to overcome the drawbacks of GCMs in regional climate studies, several studies have downscaled GCM simulations to higher resolution (e.g. Anyah & Semazzi, 2007; Endris et al., 2013;

Nguvava et al., 2019). The present study thus also downscaled all the GCM simulations used over eastern Africa.

Two techniques have been reported with about the downscaling of GCM simulations for regional scale studies, namely, statistical and dynamical techniques. Statistical downscaling is based on the relationship between the large-scale climatic state, and regional and/or local physiographic features, such as land-sea distribution and topography (Von Storch, 1995). The large-scale feature is generally derived from a GCM, while the small-scale feature comes from a specific grid point or meteorological station. The first approach is to create a statistical model that describes the relationship of large-scale climate variables, "predictors", to regional/local variables, "predictands". Then, output from the large-scale model is fed into the established statistical model, and the estimation of regional/local climatic variables can be made. Statistical downscaling techniques are popular due to their relative simplicity and low computational cost compared to dynamical downscaling. The major weakness of this method, however, is that the statistical relationships developed for the historical climate will not change for the projected future climate. Wilby and Wigley (1997) present a detailed comparison between some statistical downscaling methods. However, the current data were not generated using this tool.

The dynamic downscaling technique requires a nesting of a high-resolution RCM within a coarse resolution GCM simulation (Giorgi & Mearns, 1999). The RCM simulates the climate over a region by receiving boundary data from GCM forcings (Wang et al., 2004). The high horizontal resolution of RCMs (typically less than 50 km) is appropriate for incorporating small-scale features, such as topography and land use, that have a potential influence on climatological variables, such as precipitation and wind. Because of the complexity of topography over eastern Africa, Herrmann and Mohr (2011) argued that higher resolution simulations are the best approach to any future projection over the region. Hence, climate model data used in the present study were generated through dynamical downscaling technique.

2.6 The Coordinated Regional Climate Downscaling Experiment (CORDEX)

In the current decades, enormous efforts have been made to provide regional and accurate climate information through the dynamical downscaling approach. Among many projects, the CORDEX (Giorgi et al., 2009) was developed. CORDEX is a World Climate Research Programme (WCRP) aimed at downscaling climate projections and producing a detailed analysis of regional climate change information that is made accessible to stakeholders from different parts of the world, including Africa. The project also aimed at improving the impact and adaptation studies (Giorgi et al., 2009). Africa has been the focus of a multi-model downscaling project for the first time through CORDEX. CORDEX-Africa incorporates experts from the East African, Southern African, and West African regions, with the objective of evaluating the performance of multi-model ensembles of regional climate projections (CORDEX, 2015). There are several studies in eastern Africa that have used the CORDEX ensemble to investigate the ability of the models to capture the spatial and temporal variability of climate as well as to project future climatic conditions over the region. For instance, Endris et al. (2013) show that most CORDEX RCMs create a realistic simulation of eastern African rainfall characteristics. Thiery et al. (2014) showed that the models performed well when comparing the results with *in situ* and satellite observations in reproducing the eastern African Great Lakes climate. Nguvava et al. (2019) found a good agreement between the simulations of the CORDEX models and the Climate Research Unit's (CRU) observations regarding the frequency of SPI and SPEI drought in eastern Africa. As for climate projection, Osima et al. (2018) showed an increase of mean surface temperature by ~1°C and 1.5°C for GWL1.5 and 2.0 respectively over most parts of eastern Africa, using a 25 RCM ensemble from CORDEX. Nguvava et al. (2019) analysed a 19 RCM ensemble from CORDEX and projected an increase in the SPEI drought intensity and frequency over the northern and south-western parts of eastern Africa. In the same study, they also showed that, with SPI drought, the wetter condition is especially projected around the coastal parts of the region. Therefore, the existence of the CORDEX project will continue to enable regional climate analysis in Africa and other parts of the word to improve where it surfaces. In the present study, the CORDEX dataset was further analysed over the entire eastern Africa and over major river basins.

2.7 Hydrological modelling

Past studies have used many approaches to quantify the effects of climate change and human activities on hydrological regime (e.g. Brown et al., 2005; Legesse et al., 2003; Yang et al., 2012). These approaches can be classified into paired catchment approach (comparative tests methods), statistical approach (time series analysis) and hydrological modelling approach (e.g. Krause, 2002; Li et al., 2009; Natkhin et al., 2015). The paired catchment approach involves the use of two neighbouring catchments (one as a control and another as a treatment). These two catchments must have climate inputs, geology, soil conditions, and other variables, such as slope and vegetation that are homogeneous. The paired catchments approach is often considered as the best method in small experimental watersheds (i.e. ≤ 100 km^2). However, it is difficult to apply this to paired catchments that are larger in size, because it is not practical to find two similar medium- or large-sized watersheds. Lørup et al. (1998) argued that even the smaller watersheds may change greatly at different stages. Several literatures have documented the success of applying this method, especially in the analysis of the impact of land use change on annual flow, flood peaks, low flows and base flow (e.g., Andréassian, 2004; Bosch and Hewlett 1982; Ssegane et al., 2013). Statistical analysis is simply based on the analysis of hydro-climatic trends identified by monitoring stations in the study area. And for that reason, this method lacks the physical mechanism of the watershed (Li et al., 2009). Physically based and spatially distributed hydrological modelling is the most widely accepted method, as it is based on the relationship between land use, climate, soil and hydrological processes. Distributed hydrological models relate model parameters directly to physically observable land surface characteristics (Legesse et al., 2003), which means they can easily assess past and possible future impacts (using different land use scenarios and different warming levels); moreover, it is possible to simulate large areas (Jung & Kim, 2017). Such models have increasingly become a crucial tool in investigating the hydrological impacts caused by climate change and Land Use and Land Cover (LULC) modifications (Ren et al., 2012; Suliman et al., 2015; Yang et al., 2012). One of the comprehensive hydrological models of this type is the Soil and Water Assessment Tool (SWAT) model (Arnold et al., 1998), which is used in the present research to analyse Objective (iv), as set out in Section 1.9 (see Chapter 7).

The SWAT model is designed to simulate hydrology and water quality in basins of almost any size and complexity for a long-term and continuous process. The model is freely available, it has a user-friendly interface and is efficient in data handling, which are the main reasons for its popularity in the hydrology field (Hurkmans et al., 2009). It has been widely used to simulate and predict the impact of land use changes on catchment hydrology globally (e.g. Cao et al., 2009 (New Zealand); Franczyk & Chang, 2009 (USA); Guo et al., 2008 (China); Palamuleni et al., 2011 (Malawi); Saadati et al., 2006 (Iran); Setegn et al., 2010 (Ethiopia)). In Tanzania, few studies have applied the SWAT model to hydrology analysis (e.g. Adhikari et al., 2017; Dessu & Malesse, 2012; Mulungu & Munishi, 2007; Natkhin et al., 2013; Ndomba et al., 2008). However, none of them addressed the hydrological impact caused by climate change and LULC modifications using SWAT in the entire RRB.

Chapter 3

Methodology

This chapter describes the datasets analysed for the study and the methods used in analysing various datasets to achieve the objectives of the thesis. In some cases, different methods were applied to the same datasets, or the same methods were applied to different datasets, to achieve more than one objective. In other cases, a method and the datasets are unique to an objective.

3.2 Data

Different datasets were analysed for this thesis, consisting of climate, hydrology and geographical information system (GIS) data. The climate and hydrology datasets are observation (station and gridded), reanalysis (gridded) and simulation (gridded) datasets. Detailed information about the datasets is given below. This information includes the dataset source, its resolution (if applicable), the variable(s) used, the period analysed in the thesis, and the thesis objectives for which the dataset was analysed. All the datasets were re-gridded to 0.5° × 0.5° grid resolution.

3.2.1 Climate datasets

3.2.1.1 Station meteorological datasets

Climate datasets from the Tanzanian Meteorological Agency (TMA) and Rufiji Basin Water Board (RBWB) stations were analysed. The datasets consist of monthly precipitation data from 15 stations for a period of 10 years (1981-1990). The information about the stations is given in Table 3.1 and Fig. 3.2 (c). In order to achieve Objective (v), these datasets were used to assess the capability of a reanalysis dataset in reproducing the rainfall, temperature and wind characteristics over the RRB. The results of the assessment are reported in Chapter 7.

Table 3.1: *Name and location of the RRB climate stations considered in this study.*

Station Name	Longitude	Latitude	Elevation
IFUPIRA	35.430	-8.500	1765
IGAWA	34.380	-8.770	1113
IRINGA MTERA	36.000	-7.100	731
IRINGA OUTOMET	35.699	-7.780	1629
IRINGA MET STATION	35.770	-7.630	1369
IZAZI	35.730	-7.170	702
KIMANI	34.160	-8.830	1091
LIVALONGE	35.200	-8.700	1861
LUMEMO	36.620	-8.630	627
MADIBIRA	34.810	-8.230	1170
MAFINGA BOMANI	35.330	-8.250	1883
MATAMBA	34.016	-8.930	2035
MBEYA MET STATION	33.470	-8.930	1715
MOROGORO MET STATION	37.900	-6.800	503
MSEMBE FERRY	34.900	-7.750	899
MTANDIKA	36.430	-7.420	647

3.2.1.2 The CRU Datasets

The Climate Research Unit (CRU v.3.22) dataset was obtained from the University of East Anglia, United Kingdom (Harris et al., 2014; http://badc.nerc.ac.uk/data/cru/). The CRU datasets are gridded (0.5° × 0.5° global grid resolution) and consist of monthly

climate variable data compiled from meteorological station data over the period 1901-2014 (Harris et al., 2014). The choice of this data is based on its long time series (~110 years) and among the gridded datasets. CRU reproduces well the climate of the region (Endris et al. 2013). Moreover, CRU has all the climate variables needed for the study. Most other observation dataset either have rainfall or temperature alone, but CRU has the variables, in addition to other eight climate variables. In addressing Objectives (iii) and (iv), precipitation and temperature (i.e. maximum, minimum, and mean) data for the period 1940-2014 were analysed. The results of this analysis are reported in Chapters 5 and 6.

3.2.1.3 The SPEI Datasets

The SPEI data (at 3- and 12-month scales) were obtained from the SPEI database (http://hdl.handle.net/10261/128892; Beguería et al., 2014). According to Beguería et al. (2014), the SPEI data were calculated using observed monthly mean precipitation and potential evapotranspiration (PET) data from CRU (version 3.22; Harris et al., 2014). The CRU PET data were calculated using the Penman–Monteith approach (Allen, 1986; Beguería et al., 2014; Burke et al., 2006), utilising air temperature, solar radiation, relative humidity, and wind data. It should be noted that, while SPEI drought at the 3-month scale is regarded as meteorological drought, in the 12-month scale it is denoted as agricultural drought. The SPEI data cover a period of 75 years (1940–2014). The SPEI data were analysed towards the fulfilment of Objectives (i) and (ii) of this thesis, and the results of this analysis are discussed in Chapter 4.

3.2.1.4 The ERSST dataset

The Sea Surface Temperature (SST) dataset was obtained from the National Climate Data Centre's Extended Reconstructed Sea Surface Temperature version 4 (ERSST.v4) (Huang et al., 2015; Liu et al., 2014). The SST data were used to generate the climate indices data, including ENSO (Niño 3.4 regions), IOD, and Tropical Atlantic Dipole Index (TADI). The definitions used in generating these indices are specified in Table 3.2. SST data was also used to analyse the relationship between the eastern African drought and the global ocean. ERSST data has long time data which covers the period of our analysis (1940 to 2014). The results of the analysis performed with the dataset contribute towards Objectives (i) and (ii) and are reported in Chapter 4.

Table 3.2: *Climate indices and calculation methods*

Climate indices	Method	Reference
Indian Ocean Dipole (IOD)	The difference between SST anomalies in the western (50°E - 70°E, 10°S - 10°N) and south eastern (90°E – 110°E, 10°S - 0°S) equatorial Indian Ocean.	Saji et al., 1999
ENSO (Niño 3.4)	Average SST anomalies in Pacific region of 170°W-120°W, 5°N-5°S	Trenberth, 1997
Tropical Atlantic Dipole Index (TADI)	The difference between North (55°–15°W; 5°–25°N) and South 25°S–10°N, 55°–95°E Atlantic Ocean SST Anomalies	Endris et al., 2016
Quasi-biennial Oscillation (QBO)	Data downloaded from NOAA Physical Sciences Division (PSD)	http://www.esrl.noaa.gov/psd/data/ climateindices/list/

3.2.1.5 The NOAA dataset

The data for the Quasi-Biennial Oscillation (QBO) index was obtained from the Physical Sciences Division (PSD) of the National Centres for Environmental Information (NOAA) (http://www.esrl.noaa.gov/psd/data/Climate indices/list/) (Table 3.2). The QBO data from NOAA 20CR cover 1948-2014, which is the longest period acquired as compared to other QBO data sources. The dataset contributed to achieving Objectives (i) and (ii) of this thesis, the results of which are discussed in Chapter 4.

3.2.1.6 The 20th Century Reanalysis dataset

The reanalysis dataset from the 20th Century Reanalysis (20CR) (Compo et al., 2011) was also analysed in respect of Objective (ii). This dataset contains various upper-air atmospheric variables, but only temperature, wind, and specific humidity data were analysed in this study. The 20CR dataset covers a period of 75 years (1940–2014).

3.2.1.7 The Global Meteorological Forcing Dataset

The Global Meteorological Forcing Dataset (GMFD) (Hirabayashi et al. 2008) is another reanalysis data used in the study. The GMFD is a land gridded precipitation database that has a long record (1948-2010) and high spatial resolution (1° lat-lon; plus 0.5° X 0.5° and 0.25° X 0.25), and provides 3-hourly, daily, and monthly time steps. The spatial coverage is between 90°S and 90°N, and between 180°E and 180°W. The GMFD dataset was compiled by combining the National Centers for Environmental Prediction/National Centers for Atmospheric Research (NCEP/NCAR) reanalysis data (Kalnay et al., 1996) with observations. The observations come from the Climate Research Unit (CRU TS3.0) (Mitchell & Jones, 2005), the Global Precipitation Climatology Project (GPCP) (Huffman et al., 2001), the Tropical Rainfall Measuring Mission (TRMM) (Huffman et al., 2007), and the NASA Langley Surface Radiation Budget (LSRB) (Stackhouse et al., 2004). The GMFD dataset is freely available from the Terrestrial Hydrology Research Group at Princeton University (http://hydrology.princeton.edu/data.pgf.php). The GMFD data for the period 1951-2000 were analysed to contribute to Objective (v) of the thesis, and the results are discussed in Chapter 7.

3.2.1.8 CORDEX datasets

Twenty regional climate model (RCM) simulations from the CORDEX were analysed in the thesis (Nikulin et al., 2018). As part of CORDEX, the twenty simulations were generated by dynamically downscaling twelve global climate model (GCM) simulations with eight RCMs at 0.44^{o} grid resolution over Africa. The GCM simulations are from 5th phase of the Coupled Model Intercomparison Project (CMIP5) (Taylor et al., 2012). The names of the GCMs and RCMs that contributed to the simulations used in this thesis are given in Table 3.3. The monthly precipitation and temperature (i.e. maximum, minimum, and mean) from the CORDEX datasets were

used towards achieving Objectives (iii) and (iv) and the results are presented in Chapters 5 and 6.

In Table 3.3 below, the corresponding 30-year periods for various global warming levels (1.5 °C, 2 °C, 2.5°C and 3.0° C) are indicated. Where applicable, the corresponding periods for the RCP4.5 scenario are given in brackets. More detailed information on the GCMs, RCMs and method for calculating the periods is presented in Déqué et al. (2017).

***Table 3.3**: Names of GCMs and downscaling RCMs for simulations under the RCP8.5 scenario.*

GCMs	Period of the global warming levels				Downscaling RCMs
	1.5°C	**2°C**	**2.5°C**	**3°C**	
CanESM2[a]	1999 – 2028 (2002–2031)	2012 – 2041 (2017 – 2046)	2024 - 2053	2034 – 2063	RCA4[5]
CNRM-CM5[b]	2015 – 2044 (2021–2050)	2029 – 2058 (2042 – 2071)	2041 - 2070	2052 – 2081	RCA4[5], CCLM[2], ALADIN[1]
CSIRO-Mk3[c]	2018 – 2047 (2020 –2049)	2030 – 2059 (2033 – 2062)	2040 - 2069	2050 - 2079	RCA4[5]
EC-EARTH-r1[d]	2003 – 2032 (2006 – 2035)	2021 – 2050 (2028 – 2057)	2035 – 2064	2046 -2075	RACMO[4]
EC-EARTH-r3[e]	2006 – 2035 (2009 – 2038)	2023 – 2052 (2030 – 2059)	2036 - 2065	2047 -2076	HIRHAM[3]
EC-EARTH-r12[f]	2005 – 2034 (2010 – 2039)	2021 – 2050 (2031-2060)	2034 - 2063	2047 -2076	RCA4[5], CCLM[2]
GFDL-ESM2M[g]	2020 – 2049 (–)	2037 – 2066 (–)	2052 - 2081	2066 - 2095	RCA4[5]
HadGEM2-ES[h]	2010 – 2039 (2016 – 2045)	2023 – 2052 (2032 – 2061)	2033 - 2062	2042 - 2071	RCA4[5], CCLM[2], RACMO[4]
IPSL-CM5AMR[i]	2002 – 2031 (2002 – 2031)	2016 – 2045 (2020 – 2049)	2027 - 2056	2036 - 2065	RCA4[5]
MIROC5[j]	2019 – 2048 (2026 – 2055)	2034 – 2063 (2059 – 2088)	2047 - 2076	2058 - 2087	RCA4[5]
MPI-ESM-LR[k]	2004 – 2033 (2006 -2035)	2021 – 2050 (2029 – 2058)	2034 - 2063	2046 - 2075	RCA4[5], CCLM[2], REMO[6]
NorESM1-M[l]	2019 – 2048 (2027-2056)	2034 – 2063 (2062 – 2091)	2047 - 2076	2059 - 2088	RCA4[5], WRF[7]

The letters (a - l) and numbers (1 - 7) in brackets of the GCMs and RCMs (respectively) are used as tags to represent the simulations (e.g. a5 represents CanESM2_RCA4 simulation).

3.2.2 Hydrological datasets

The river flow dataset from the Rufiji gauging station was analysed in the thesis. The location of the station is found at the main basin outlet (Fig. 3.2 (d)). The dataset was obtained from the Rufiji Basin Water Board (RBWB). The dataset, which extends from 1970 to 2005, was used to calibrate and evaluate the hydrological model used in achieving Objective (v) of the thesis, and the results are presented in Chapter 7.

3.2.3 GIS datasets

Three major GIS datasets were required in the hydrological model (SWAT) used by the thesis: (a) the spatial input data for land topography, i.e. the Digital Elevation Model (DEM), (b) the land use or land cover (LULC) dataset, and (c) the soil characteristic dataset.

3.2.3.1 DEM

The DEM is a digital estimation of surface elevation, often stored in a fixed grid. The DEM is an essential input in the SWAT model; it is needed to delineate the watershed and subwatershed and to analyse the drainage patterns of the land surface terrain. It enables the generation of slope, which then gives the rate of movement and flow direction information, which are an essential basis for hydrological studies (Yang et al. 2014). The DEM used in this study is shown in Fig. 3.2 (a). This DEM is a product of the Shuttle Radar Topography Mission (SRTM); the post-processed version 4.1 was obtained from the CGIAR Consortium for Spatial Information's website (CGIAR-CSI; http://srtm.csi.cgiar.org/) at a resolution of 90 m X 90 m.

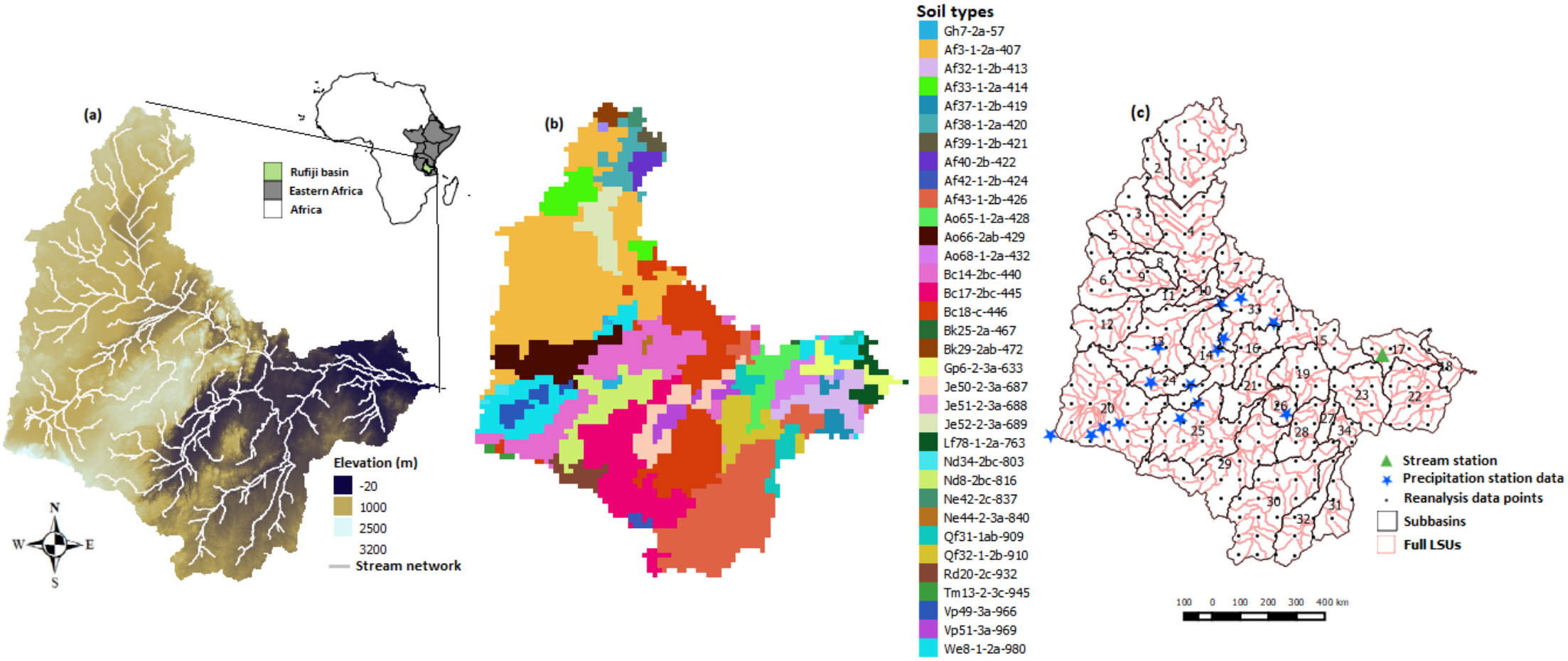

Figure 3.2. *The RRB domain, showing (a) the Digital Elevation Model (DEM) and stream networks, (b) Soil types, and (c) Sub-basins, precipitation stations, gauging stations and reanalysis data points used in this study*

3.2.3.2 Land use data

Land cover and management is an essential feature affecting different processes in the river basin, such as evapotranspiration, surface runoff, and erosion. The land cover data were acquired from the Tanzania Land Cover 2000 and 2010 Schemes generated by the Regional Centre for Mapping of Resources for Development in Eastern and Southern Africa (RCMRD) (geoportal.rcmrd.org) (Fig. 3.3 (a), (b)). Some of the RCMRD land cover classifications do not correspond with the appropriate land cover groupings within the SWAT internal database. Therefore, we had to reclassify these to match them to SWAT (Table 3.4). The land cover for 2000 was only used to justify the change of land use to 2010. We thus used the land cover of 2010 for our entire analysis. The basin is predominantly covered by forest (~28%) in the mountainous areas, consisting of natural as well as planted forest. Large areas of the RRB are covered by savanna (26%), shrubs (18%) and agriculture (13%), especially at low elevations. The major LULC changes in the RRB for the period from 2000 to 2010 were the steady expansion of cultivation land and shrubs, and the decline of savanna and dry land.

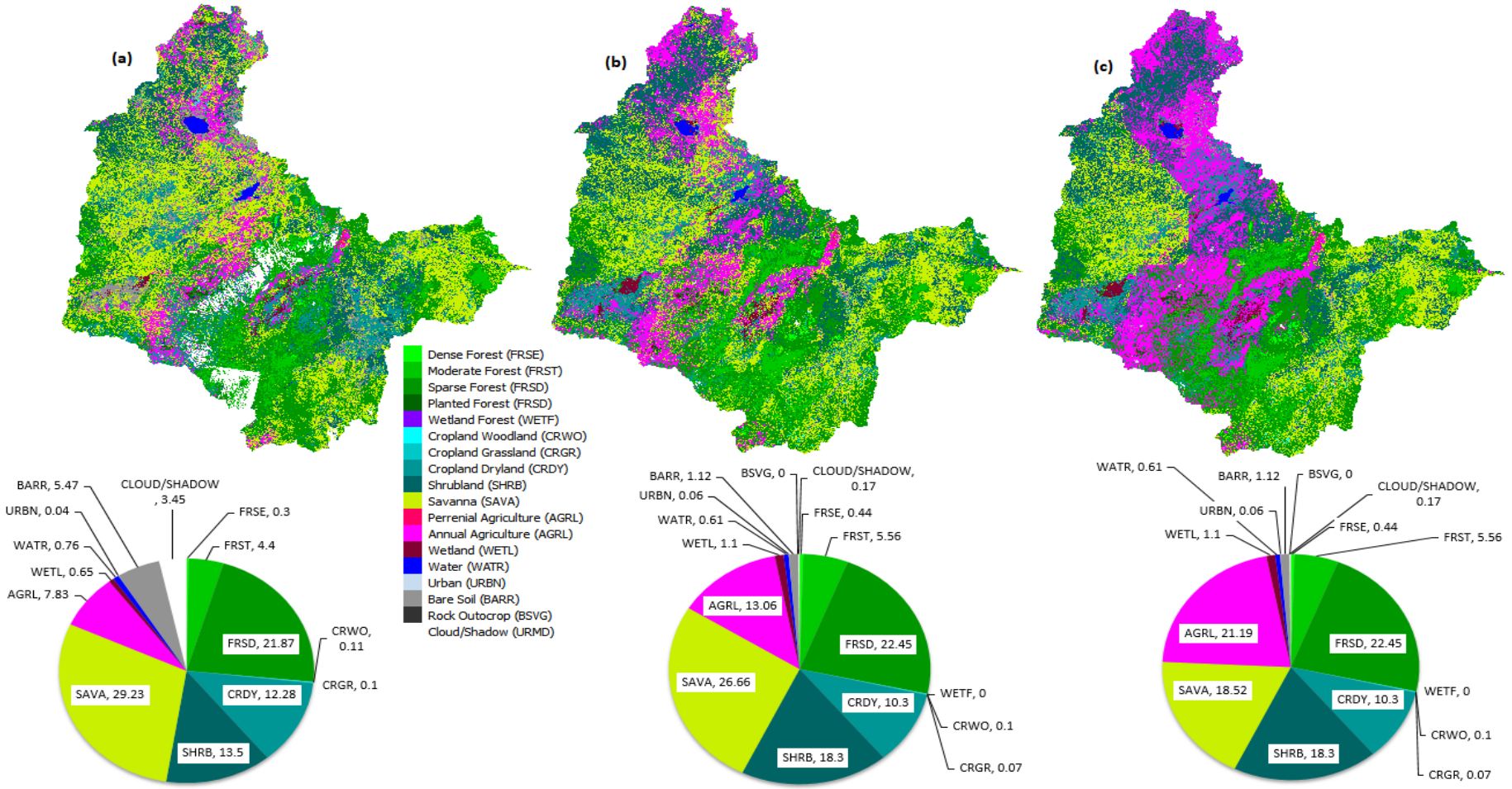

Figure 3.3. *RRB land use patterns (past and future scenarios) used in the study. Panels (a) and (b) show the past land use patterns (for 2000 and 2010, respectively). Panels (c), (d), (e) and (f) show the land use patterns under future scenarios (namely: "increased agriculture", forests, cropland dry land and shrub). The corresponding pie chart indicates the percentage contributions of the various land use types in each pattern.*

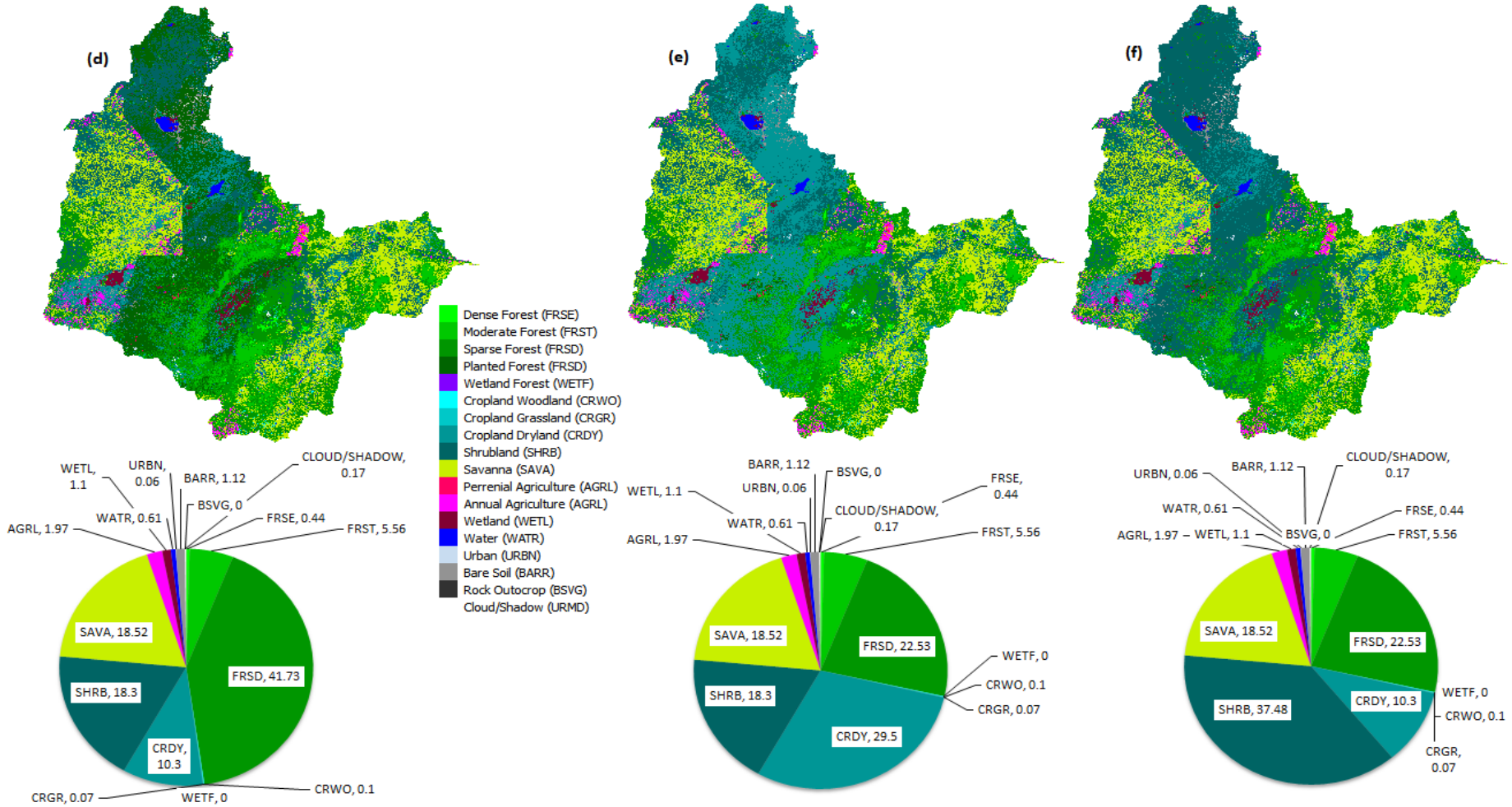

***Figure 3.3**. (Continues)*

Table 3.4: *Reclassification of existing land uses in the RRB to match the SWAT database*

RRB land use	SWAT land use	Model code
DENSE FOREST	EVERGREEN FOREST	FRSE
MODERATE FOREST	MIXED FOREST	FRST
SPARSE FOREST	DECIDUOUS FOREST	FRSD
PLANTED FOREST	DECIDUOUS FOREST	FRSD
MANGROVE FOREST	WETLAND FOREST	WETF
WOODLANDS	CROPLAND WOODLAND	CRWO
CLOSED GRASSLAND	CROPLAND GRASSLAND	CRGR
CLOSED BUSHLAND	SHRUB LAND	SHRB
OPEN GRASSLAND	CROPLAND DRYLAND PASTURE	CRDY
OPEN BUSHLAND	SAVANNA	SAVA
PERENIAL CROPLAND	AGRICULTURE LAND	AGRL
ANNUAL CROPLAND	AGRICULTURE LAND	AGRL
WETLAND	WETLAND	WETL
WATER BODY	WATER	WATR
SETTLEMENT	URBAN	URBN
BARE SOIL	BARE SOIL	BARR

3.2.3.3 Soil data

The reaction of a river basin to a particular weather event depends on the nature and conditions of its soils (Shrestha et al., 2008). The processing of the SWAT model requires the basin's physical and chemical properties of the soil, such as texture, porosity, available moisture content, bulk density, hydraulic conductivity, and organic carbon content for each of the soil types and at each layer (Setegn et al., 2010). The soil

data were obtained from the new 1:2 million scale Soil and Terrain (SOTER) database developed for Southern Africa by the Food and Agriculture Organization (FAO) of the United Nations and the International Soils Reference and Information Center (ISRIC) (Batjes, 2004). The spatial distribution of soil classes for RRB is shown in Fig. 3.2 (b). The major soil classes in the studied area were 20.5 % Sandy-Clay-Loam, 18.8 % Loam, and 11.6 % Sandy-Loam.

3.3 Methods

In this subsection, the drought indices SPEI and SPI are discussed in detail. Principal Component Analysis, Wavelet Analysis and Self-Organising Maps tools are also explained.

3.3.1 Drought indices

This study applies the SPI (McKee et al., 1993) and the SPEI (Beguería et al., 2014; Vicente-Serrano et al., 2010a) to characterise drought. The SPI has been used frequently for drought monitoring over eastern Africa (Belayneh et al., 2014; Bernard et al., 2013; Degefu & Bewket, 2014; Ntale & Gan, 2003; Viste et al., 2013). It is also recommended by the World Meteorological Organization (WMO) for monitoring meteorological drought (Hayes et al., 2011). As for SPEI, not many studies have used this index over the region (e.g. Vicente-Serrano et al., 2012a), although it is well documented in other regions (and shown to give a better representation of droughts), such as Portugal (e.g. Paulo et al., 2012), South Africa (e.g. Ujeneza & Abiodun, 2015), West Africa (e.g. Diasso & Abiodun) and China (e.g. Yu et al., 2014). The difference between the two indices is that SPEI is the product of climate water balance (CWB), i.e. Precipitation (P) minus potential evapotranspiration (PET), whereas SPI is solely a precipitation product. Our estimation of PET is based on the Hargreaves (Hg) equation (Hargreaves & Samani, 1985) for objective three, four and five. The Hg equation requires monthly temperatures (maximum and minimum), monthly mean precipitation and the latitudinal position of the site. Beguería et al. (2014) showed that the use of the Hg method is the best option, especially in regions with limited data. Objective one drought indices data were obtained from http://hdl.handle.net/10261/128892 (Begueria et al. 2014) and the PET computed using Penman-Monteith (PM) method. According to Allen et al. (1998), the two methods i.e Hg and PM, produce drought signals which do not differ much.

Begueria et al. (2014) also documented strong correlation (r>0.90) on drought computed using these methods for station and gridded data. In the present study, SPEI and SPI were used to characterise 3-month and 12-month droughts, which affect both agriculture and surface hydrological systems, especially reservoirs and streams.

3.3.2 Principal component analysis

To identify dominant drought modes over eastern Africa, we applied Principal Component Analysis (PCA) (Jolliffe, 2003), also described as empirical orthogonal function (EOF) analysis. PCA is a widely used statistical technique for reducing the dimensionality of multivariate data and for uncovering hidden structures in the data. It is commonly used in climate research for defining the leading spatial and temporal patterns of climate variability (Richman, 1986). For the PCA, we calculated the covariance matrix from standardised normalised variables, calculated the matrix's eigenvectors and eigenvalues, and ordered the eigenvectors according to the magnitude of eigenvalues. The eigenvector with the highest eigenvalue represents the first principal factor and the mode with the largest variability in the dataset. PCA has been used for the regionalisation of drought at different spatial and temporal scales globally (e.g. Bärring, 1988a, b; Indeje et al., 2000; Ogallo, 1989; Santos et al., 2010; Ujeneza & Abiodun, 2014). In eastern Africa, several studies used PCA to investigate spatial and temporal variation in climate variables (e.g., Bärring, 1988a, b; Indeje et al., 2000; Ogallo 1989). Here, we applied PCA with a varimax rotated option, because previous studies (e.g. Jolliffe et al., 2003) showed that varimax rotation enhances the physical application and understanding of PCA results. The PCA was applied to the SPEI and SPI of each dataset (observations and RCM simulations), and the first four principal factors of the PCA were retained as the most significant drought modes (DM1, DM2, DM3 and DM4) in the dataset. This method however has one major limitation. For example, the outcome of PCA analysis is sensitive to the selected domain for the analysis (Manatsa and Mukwada 2019)

3.3.3 Wavelet analysis and wavelet coherence

To study the temporal variability of drought modes, we applied the wavelet analysis to the PCA score and, to study the influence of some atmospheric teleconnections on the drought modes, we used correlation and wavelet coherence analysis on the PCA scores of the climate indices. Wavelet analysis, which unmasks the temporal characteristics of

periodic cycles in a time-series, is a common tool in climate analysis (i.e. Lau & Weng 1995). It has been used to study the annual variation in SST (i.e. Rao et al., 2002), to study ENSO variability (Torrence & Compo, 1998), to examine the influence of IOD and ENSO on precipitation (Manatsa & Matarira, 2009), and to study characteristics of drought modes over western and southern Africa (Diasso and Abiodun 2015; Ujeneza & Abiodun, 2014). Here, the correlation and wavelet coherence were used to quantify how the drought modes (PCA scores) are linked with some atmospheric teleconnection (IOD, ENSO, TADI and QBO, depicted with the climate index), which have been reported to influence the climate variability of eastern Africa (Daron, 2014; Goddard & Graham, 1999; Lyon, 2014; Saji et al., 1999). This predominant statistical analysis does not mean causality

3.3.4 Self-organizing maps

The additional analysis of our data was conducted by using an artificial neural network (ANN) tool. The ANN used in this study was the self-organizing map (SOM) that was originally proposed by Kohonen (1990). SOMs are useful for pattern recognition, clustering, classification, estimation and prediction (Kohonen, 2013) in multivariate data sets. The patterns captured from SOMs present continuity in the data space, which is not the case in other clustering techniques, such as the partitioning algorithm of k means (Fereday et al., 2008). SOMs have been applied in various research problems with notable success (Michaelides et al., 2001; Oja et al., 2003). It has been recently used for hydrology analysis (Chang et al., 2007), oceanographic studies (Leloup et al., 2007; Liu et al., 2006), and for climate and meteorology research (Hewitson & Crane, 2002; Malmgren & Winter, 1999; Reusch et al., 2007). In our case, the SOM was supposed to identify significant features to characterise the projected drought at different GWLs over the eastern African study area.

In this study, we thus applied the SOM analysis on two datasets, i.e. drought intensity and severe drought frequency, using the 12(4X3) neuron classification. The first dataset consists of all the projected changes in SPI and SPEI intensity at each GWL (GWL1.5, GWL2.0, GWL2.5, and GWL3.0) and for all simulations. The second dataset looks at severe drought frequency in terms of SPI and SPEI (i.e. 12-month drought with intensity <-1.5) at each GWL and for all simulations. The SOM package used for this

analysis is SOM_PAK 3.2 (Kohonen, 1999), which was freely available from the Helsinki University of Technology (http://www.cis.hut.fi/research/som_pak/).

3.3.5 Evaluation of climate model simulations

The performances of the climate model simulations over the study region were evaluated by comparing the simulations with the observations for the period 1971–2000 (referred to as the reference period). This reference period "1971–2000" was chosen because it is the most commonly used control period in climate impact application studies and in several previous research on GWL over Africa (e.g. Nikulin et al., 2018; Osima et al., 2018; Pinto et al., 2018). Therefore, it is used here to ensure that the results of the present study are consistent with other previous studies. In addition, using a climatological period starting beyond 1971 might cause the results to overlap with the GWL climatological projections. The variables used were minimum temperature (TMIN), maximum temperature (TMAX), precipitation (PRE), the standardized precipitation evapotranspiration index (SPEI), the standardized precipitation index (SPI), Solar radiation (SLR), potential evapotranspiration (PET), evapotranspiration (ET), soil water (SW), percolation (PER), surface runoff (SF), water yield (WYLD), and flow out (FLOWOUT).

The projected change in drought for 1.5°C, 2°C, 2.5°C and 3.0°C global warming (hereafter referred to as GWL1.5, GWL2.0, GWL2.5, and GWL3.0 respectively) were analysed using the 30-year period during which the GCM simulation reaches 1.5°C, 2°C, 2.5°C and 3.0°C warming for Representative Concentration Pathway (RCP8.5). For RCP4.5 simulations only 1.5°C and 2°C were analysed because most simulations do not show a warming level beyond 2°C. RCP 8.5 has a large number of ensemble members and reaches all the global warming levels needed for the study. In addition, it gives the most realistic global warming trend in the current decades, in comparison to RCP4.5 or RCP2.6 (Nikulin et al., 2018). To understand the impact of climate change, we calculated the differences between the simulation reference period (1971-2000) and the GWL period. The periods of the GWL do not necessary coincide for the different simulations (as shown in Table 3.3). This is because the GWL is defined based on 30-year climatology, at which the simulations project a higher global mean temperature than during the pre-industrial reference period (1861-1890) under a specific global warming value, i.e. 1.5°C, 2.0°C, 2.5°C, or 3.0°C (Nikulin et al., 2018). Details of how

the 30-year periods of warming levels were calculated can be obtained from Déqué et al. (2017) and Vautard et al. (2014). Objective III was analysed using both RCP 4.5 and 8.5 but only for warming level 1.5 and 2.0. Objective IV was dedicated to the high emission scenario RCP 8.5 and with warming levels 1.5°C, 2°C, 2.5°C and 3.0°C. However, in order to show the sensitivity of our results (in respect of Objective IV) to the various global warming scenarios, some of the results are also compared with those from the available RCM4.5 scenario data.

Hydrological drought projection was obtained using 7 global climate projections from CMIP5, downscaled by the latest version of the CORDEX Rossby Centre's Regional Climate Model RCA4 at 0.44 resolution (Samuelsson et al., 2011) and RCP 8.5 (Table 3.3). Each of the climate projections includes all of the SWAT input climate data (i.e. precipitation, maximum temperature, minimum temperature, solar radiation, wind, and relative humidity) in daily time steps for the period from 1950 through 2005 ("Baseline Run") and from 2006 to 2100 ("Projection Run"). The projected changes in hydrological drought for 1.5°C, 2°C, 2.5°C and 3.0°C global warming were analysed using the 30-year period that the GCM simulation reaches 1.5°C, 2°C, 2.5°C and 3.0°C warming for RCP8.5 (Vautard et al., 2014). Also, the Bias-Correction method, Quantile Delta Mapping (QDM) (Cannon et al., 2015) was applied to each of the seven RCA4 climate datasets, using the GMFD historical data. For precipitation, QDM accounts for uncertainties when the dry-day frequency of the historical observations is less than the climate model output (dry-day frequency). In addition, the QDM method corrects for future extreme climate values that do not occur in the historical observations (new extremes).

3.3.6 Analysing climate change robustness

The robustness of the projected climate change was quantified based on two criteria: 1) At least 80% of the simulations must agree on the sign of the change, and 2) At least 80% of the simulations must indicate that their climate change is statistically significant (at 99% confidence level, using a t-test). When both conditions are met, then the climate change signal is considered to be important. Several studies have applied these two conditions to check for the robustness of climate change projections in different parts of the world (e.g., Klutse et al., 2018 over West Africa; Nikulin et al., 2018 over Africa; Osima et al., 2018 over East Africa; and Máure et al., 2018 over Southern Africa).

3.4 Hydrological modelling

The hydrological model known as the Soil and Water Assessment Tool (SWAT) is introduced and details are given on how it is applied in the current study.

3.4.1 SWAT

The SWAT model was used to analyse hydrological drought in terms of Objective IV (Chapter 7). SWAT is a physically based, spatially distributed and watershed scale model operating continuously on a daily time step. It is applicable in ungauged river basins (Gassman et al., 2007), which is useful when studying watersheds with limited data like RRB. The model is also computationally efficient and therefore able to run simulations over very large basins, or basins with complex management practices, without consuming large amounts of time. SWAT was established by the United States Department of Agriculture Research Service (USDA-ARS) to assess the effects of climate, soil, changes in land use, and land management practices on the hydrology, sediment, and build-up of agriculture pollutants in large water basins (Arnold et al., 2012; Neitsch et al., 2005). The SWAT model is made up of several components with major ones including weather, hydrology, soil temperature and properties, plant growth, nutrients, pesticides, bacteria and pathogens, and land management (Arnold et al., 2012). The energy source that drives all SWAT components is based on the water balance equation (Neitsch et al., 2005) (Eq. (1)).

$$SW_t = SW_0 + \sum_{i=1}^{t} \left(R_{day} - Q_{surf} - E_a - W_{seep} - Q_{gw}\right) \qquad (1)$$

Where t is time in days, SW_t is the final moisture content of the soil, SW_0 is the initial moisture content of soil on day i, and R_{day}, Q_{surf}, E_a, W_{seep}, and Q_{gw} are daily amounts (mm) of rainfall, surface runoff, evapotranspiration, water transferred from the soil profile into the gas zone, and the return flow respectively. The water balance has direct impacts on plant growth and the movement of nutrients and sediments in the soil basin. Based on the nature of this study, we are mostly concentrating on the climate, hydrology, and vegetation components of the SWAT model. The current research applies the latest version of the model called SWAT+ (Bieger et al., 2017), which is

more flexible than the previous versions when it comes to watershed discretisation and configuration.

3.4.2 SWAT model setup, calibration and validation

The RRB was divided into 35 sub-basins and 386 landscape units (LSUs). The sub-basins were delineated with a ≥300 sq.km channel threshold and those with less than 18% mean area coverage were merged. Following slope classification criteria by EMBRAPA (1979), five slope classes were introduced. Slopes of 0-3% present flat surface, 3-8% soft wavy, 8-20% wavy, 20-45% strong wavy and >45% mountains. The land surfaces that occupy <2% of the watershed were exempted during the hydrological response unit (HRU) generating process so as to ascertain their effect regardless of their reduced coverage. This includes evergreen forest (0.44%), cropland woodland (0.10%), cropland grassland (0.07%), wetland (1.10%), water (0.61%), and urban (0.06%). Also, an exclusion approach (filter) of land use, soil and slope was adopted, and the sub-basin threshold was set to minimum limits of 5% for land use, soil types and slope degrees. Following this set-up, 9658 HRUs were generated over RRB. After HRU generation, the SWAT model was simulated by inputting the climate parameters (i.e. precipitation, air temperature, relative humidity, wind speed, and solar radiation).

The monthly calibration and validation of the SWAT model for streamflow were performed using manual calibration method. Ten years, i.e. 1976-1980 and 1995-1999, were used for calibration and validation respectively. The SWAT parameters used for calibration and validation are presented in Table 3.5.

***Table 3.5**: SWAT parameters used for calibration*

Parameters	Input file	Description	Change type	Change value
Cn2	hru	SCS runoff curve number for moisture condition II	abschg	-40
esco	hru	Soil evaporation compensation factor	abschg	-2
slope	hru	Average slope length	abschg	1

To assess the qualitative and quantitative performance of the model results compared to the observed data, three model evaluation statistics tools were applied: coefficient of determination (R^2) (Eq. (2)), Nash-Sutcliffe Efficiency (NSE) (Eq. (3)), and Percent bias (PBIAS) (Eq. (4)). These statistical tools are the most widely used tests to show the goodness of fit of the simulations during calibration and validation of hydrological models.

$$R^2 = \frac{\left[\sum_{i=1}^{n}(O_i-\bar{O})(P_i-\bar{P})\right]^2}{\sum_{i=1}^{n}(O_i-\bar{O})^2\sum_{i=1}^{n}(P_i-\bar{P})^2} \quad (2)$$

$$NSE = \frac{\sum_{i=1}^{n}(O_i-\bar{O})^2-\sum_{i=1}^{n}(P_i-O_i)^2}{\sum(O_i-\bar{O})^2} \quad (3)$$

$$PBIAS = \left(\frac{\sum_{i=1}^{n}(O_i-P_i)}{\sum_{i=1}^{n}O_i}\right)*100 \quad (4)$$

Where $\bar{O}$ is the mean of the observed values, O_i is the i^{th} observed value, P_i is the i^{th} simulated value, $\bar{P}$ is the mean of the simulated values and n is the total count of the sample pairs. The variables in Eq. (3), and Eq. (4) have similar meanings to those in Eq. (2).

NSE is a normalised statistic that determines the relative magnitude of the residual variance compared to the measured data variance during the modeling period (Nash & Sutcliffe, 1970). It is used to evaluate the simulation effect of hydrological models on streamflow. The NSE is dimensionless, and its values range from negative infinity to 1, in which NSE = 1 is considered a best value, as it corresponds to a perfect match of observed streamflow to simulated streamflow. Based on Moriasi et al. (2007), the range of $0.75 < NSE \geq 1$ means that the model results are very good; $0.65 < NSE \geq 0.75$ means that the model results are good; $0.5 < NSE \geq 0.65$ means that they are satisfactory; and finally, $NSE < 0.5$ means that the model results are unsatisfactory. An NSE value ≤ 0 suggests that the observed average is a better predictor than the model simulation. R^2 is used to measure the correlation between variables. The range of R^2 is 0-1. If $R^2 = 0$, there is no correlation between two variables. If $R^2 = 1$, the two variables are linearly related. R^2 should be greater than 0.60 for the model simulation to be considered good (Santhi et al., 2001). The PBIAS measures the deviation between variables by comparing the average tendency of the simulated data to the corresponding observed data (Gupta et al., 1999). It is an easy method to quantify water balance errors and indicate model performance. The optimal value of PBIAS is 0.0, with low-magnitude values showing a correct model simulation. A positive value indicates a model underestimation bias, and a negative value indicates a model overestimation bias (Gupta et al., 1999). PBIAS should range between ± 25% for the model simulation to be considered good (Moriasi et al., 2007). The statistical indicators and visual comparison of the time series plots between observed stream flow and simulated for calibration and validation are presented in Chapter 7.

3.5 Land use land cover change sensitivity experiment

Figs. 3.3(a) and 3.3(b) show the percentage changes among the LULC classes from 2000 to 2010 respectively. Among the LULC, agricultural land increased sharply by about 5.3%, while shrub land increased by 5% and forest (a combination of deciduous, evergreen and mixed forest) increased only by 2.2%. The LULCs that show a large decrease are savanna (~3%) and cropland dry land (~2%). Other studies have also reported an increase in agricultural land over some parts of the RRB (e.g. Mombo et al., 2011; Näschen et al., 2018). As for the forest (evergreen forest), Näschen et al. (2018) also reported an increase over the Kilombero catchment during the period 2004

to 2014. The catchment is part of the RRB. The increase in agriculture is mostly concentrated over certain areas of the basin, e.g. over the wetland of Kilombero, in the northeastern and central parts of the basin. Because of the tremendous increase in agriculture and the decrease in savanna, the projected LULC changes were considered first by increasing agricultural land through decreasing savanna in those specific zones that are prone to an increase in agricultural land (Fig. 3.3 (c)). Then, in order to demonstrate how other land use changes might affect the hydrology of the RRB, we also considered a further three experiments, in which agricultural land in Fig. 3.3 (c) was converted to forestry (planted forestry: Fig. 3.3 (d)), then again converted to cropland dry land (Fig. 3.3 (e)), and lastly converted to shrubs (Fig. 3.3 (f)). Based on these scenarios, our study analysed the impact of different LULC changes on hydrology variables and hydrological drought in the RRB.

Therefore, the analysis of the sensitivity experiment is divided into three major experiments: (1) Modelling to simulate hydrological components for the historical climate (1970-2000) for reanalysis and ensemble models, with a land use map of 2010; (2) Modelling to simulate hydrological components with changing global warming levels (1.5, 2.0, 2.5 and 3.0) but keeping the land use constant and not changing it (in other words, using the land use map of 2010); and (3) Modelling to simulate hydrological components for GWL2.0 with land use change, i.e. (a) Savanna converted to agricultural land, (b) agricultural land converted to crop land dry land, (c) agricultural land converted to forestry, and (d) agricultural land converted to shrubs.

Chapter 4

Characteristics and Drivers of Drought Modes in Eastern

This chapter presents and discusses the results of the analysis on the characteristics and drivers of four dominant drought modes in eastern Africa. It describes the spatial and temporal characteristics of these drought modes and investigates link between them and four atmospheric teleconnections. The correlation between each drought mode and the global SST is presented, and the chapter also discusses the atmospheric conditions associated with the drought modes in all the seasons. Both objectives (i) and (ii) are covered in this chapter.

4.1 The spatial and temporal structure of drought modes over eastern Africa

Figs. 4.1 and 4.2 present the spatial-temporal structure of the first four principal factors from the PCA (for the 3- and 12-month SPEI, respectively) over eastern Africa, depicting the four dominant drought modes (hereafter, DM1, DM2, DM3 and DM4) over the sub-region. The four modes explain 46.5% and 49.6% of the variation in the 3- and 12-month datasets, respectively. This implies that these four drought modes account for more than 45% of drought variability over eastern Africa; moreover, each drought mode (DM) has unique spatial-temporal characteristics.

The first drought mode (DM1) explains about 13.6% (3-month SPEI) and 15.9% (12-month SPEI) of the drought variability; it features the maximum positive loadings (≈ 0.8) in northeast Kenya and south Somalia (hereafter, the DM1 region), and the maximum negative loading over northern Ethiopia and Sudan. As expected, there is a good correlation between the DM1 scores and the SPEI over the DM1 region ($r > 0.7$). The 12-month SPEI for the DM1 region reveals that this drought mode has experienced two decades of drought conditions (1940–1960), followed by a decade of wet conditions (in the 1960s), and four decades of alternating dry and wet conditions (1970s–2010s; Fig. 4.2). In general, the DM1 score has a positive trend over the study period (1940–2014; Table 4.1), suggesting a wet condition in this drought mode. For instance, the frequency of the 3-month drought (i.e. 3-month SPEI < -1) in the DM1

mode decreases from about 30 months decade^{-1} in the 1940s to less than 8 months decade^{-1} in the 2000s (Fig. 4.3 (a)), while that of the 12-month drought (12-month SPEI < -1) falls from about 45 months decade^{-1} in the 1940s to less than 9 months decade^{-1} in the 2000s (Fig. 4.3 (b)). However, the wavelet analysis (Fig. 4.4 (a)) indicates that this drought mode is modulated at seasonal, inter-annual, and quasi-decadal scales. The global wavelet plot shows that the peak cycles in DM1 variability occur at 1-2 years and 4-10 years. While the 1-2 year cycle exhibits intermittent but significant variance throughout the study period (1940–2014), the 4-10 year cycle only features significant power after 1980 (Fig. 4.4 (a)).

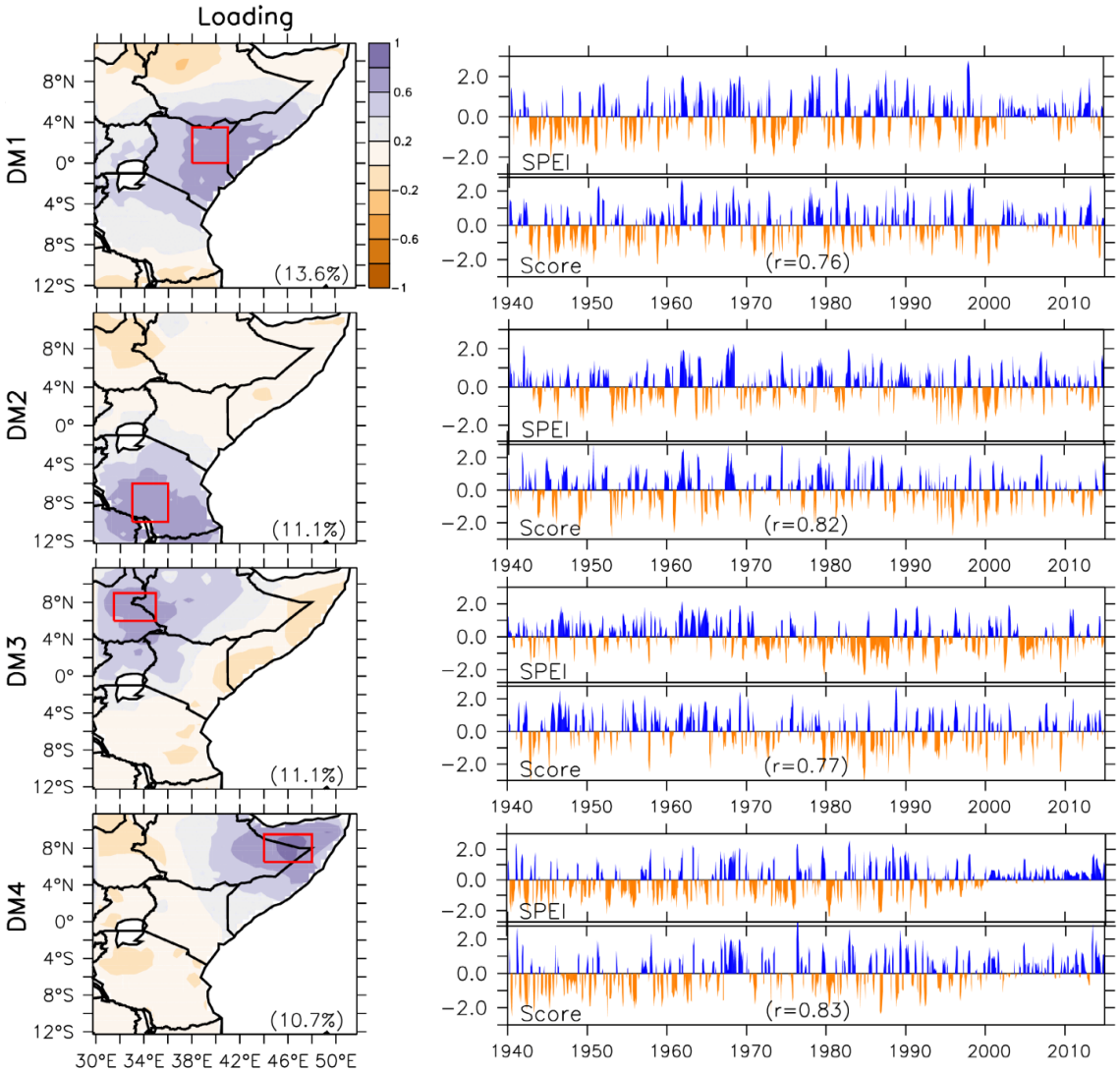

Figure 4.1: *The spatial and temporal variability of SPEI drought intensity at the 3-month scale in eastern Africa. The panels on the left represent the rotated PCA loading of SPEI drought with the variance for each drought mode (hereafter DM1, DM2, DM3, DM4) presented in the brackets. The time series panels on the right represent the DMs score and the SPEI drought averaged over the red box areas. The correlations (r) between the scores and the SPEI drought series are written in the brackets. In the time series plot, a positive value represents wet conditions, while a negative value represents dry conditions.*

The second drought mode (DM2), which explains 11% (3-month SPEI) and 12.6% (12-month SPEI) of the SPEI variance, features its highest positive loadings (≈ 0.8) over Tanzania (hereafter, DM2 region), where the correlation between the SPEI and DM2 is very high (r = 0.8). Its lowest negative loadings is located over northern South Sudan. The SPEI features alternating wet and dry conditions throughout the study period (1940–2014), and the DM2 score also shows no significant trend over the same period (Table 4.1). Nevertheless, the DM2 features its maximum 3-month and 12-month drought frequency (15 months decade^{-1} and 22 months decade^{-1}, respectively; Fig. 4.3) in the 1940s, when the DM2 has the most intensive 12-month drought episode (SPEI ≈ -2.0; Fig. 4.2). This drought episode has been extensively analysed by Ntale and Gan (2003), who used other drought indices to characterise it as an extreme drought (SPI <= -2; PDSI = -4). However, the wavelet analysis of the DM2 score indicates that the dominant cycle in DM2 variability peaks at 1-2 and 4-8 years (Fig. 4.4 (b)). While the 1-2 year cycle exhibits intermittent significant power throughout the study period, the 2-8 year cycle only features a continuous significant power before 1970.

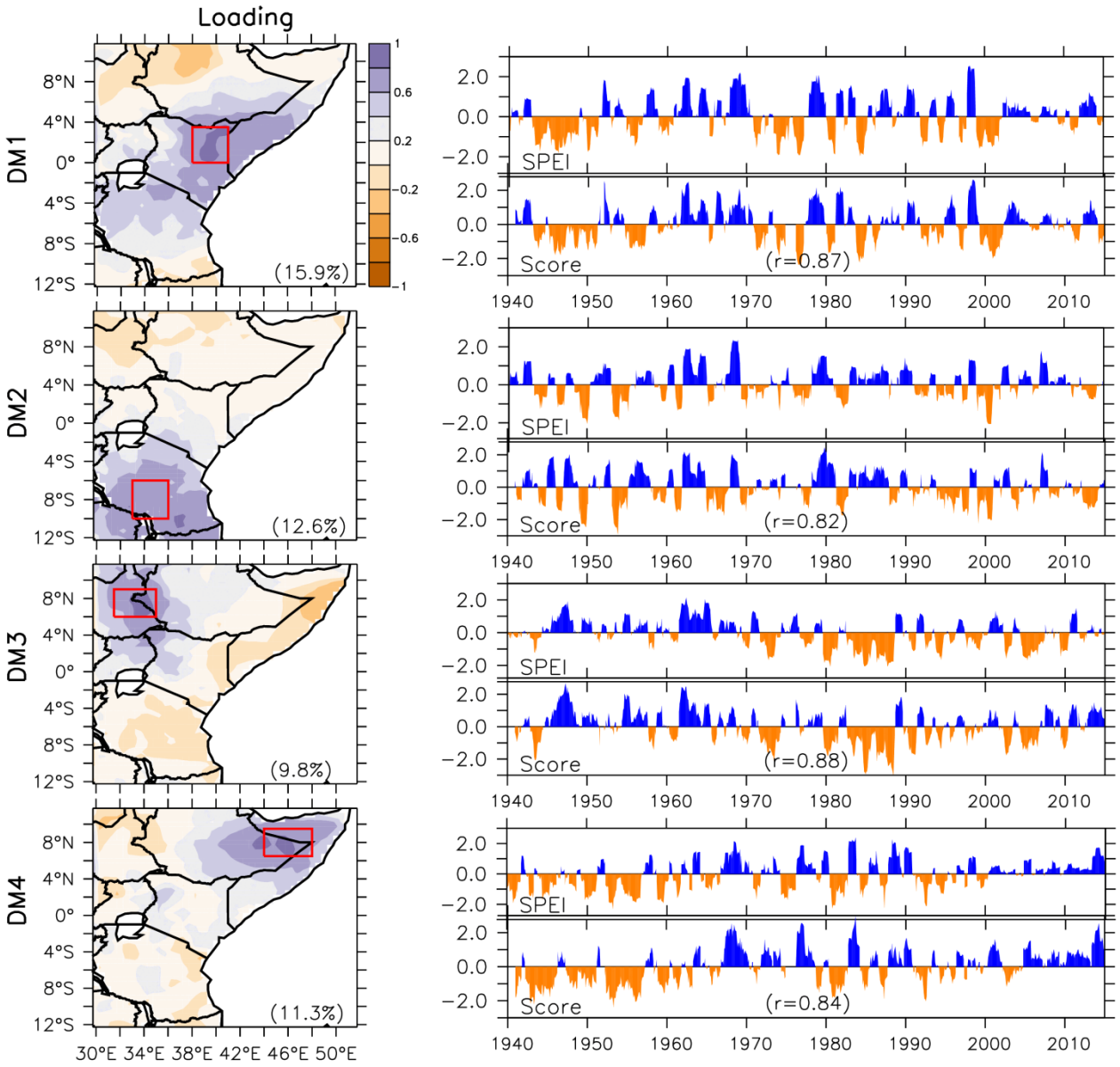

Figure 4.2: *As in Figure 4.1, but for SPEI drought intensity at the 12-month scale.*

***Table 4.1**: The coefficient of correlation between the drought modes over eastern Africa and climate indices*

Drought Modes	IOD ($5.31E^{-5}$)	Niño 3.4 ($1.87E^{-4}$*)	TADI ($6.02E^{-4}$**)	QBO ($8.05E^{-4}$)
DM1 ($2.5E^{-4}$*)	0.14**	0.24**	0.05	0.02
DM2 ($-1.7E^{-4}$)	0.13**	0.09*	-0.02	0.002
DM3 ($-3.3E^{-4}$**)	0.08*	-0.11*	0.09*	-0.005
DM4 ($8.9E^{-4}$**)	0.12**	0.14**	-0.02	0.03

The clarification of climate indices used is given in Table 3.2. All the variables were detrended before the correlation analysis, and the trend (unit per month) in each variable is indicated in brackets under the variable. Significant coefficients are indicated with * or **

*t significant at $p<0.05$

**t significant at $p<0.001$

The third drought mode (DM3) explains 11% (3-month SPEI) and 9.8% (12-month SPEI) of the SPEI variance and features the peak positive loadings (up to 0.8) in west-central Ethiopia and South Sudan (hereafter, DM3 region) with its negative loadings (≈ −0.2) along the coastal area. The correlation between the DM3 and SPEI over the DM3 region is more than 0.7. The SPEI time-series reveals that the DM3 region was dominated by wet conditions in 1945–1970, dry conditions in 1970–1990, and alternating wet and dry conditions in 1990–2010. Hence, in contrast to the DM1 score, the DM3 score features a negative trend over the study period (1940–2014), suggesting a dry condition in the DM3 mode (Table 4.1). At both 3- and 12-month scales, the DM3 drought (SPEI < -1) has a maximum decadal frequency in the 1980s followed by the 2000s (Fig. 4.3). This result agrees with Lyon (2014), who observed a rainfall deficit over the north-western part of eastern Africa in 1950–2010. Elagib and Elhag (2011) also found a decrease in precipitation under warmer conditions over most part of DM3 in the period of 1940–2008. The wavelet analysis of the DM3 scores (Fig. 4.4 (c)) shows that the dominant cycles in DM3 mode are at 1-4 years and 7-20 years. While the 1-4 year cycle features intermittent significant power throughout the study period (1940–2014), the 7-20 year cycle has weak but significant power in 1960–1990.

The fourth drought mode (DM4) accounts for 10.7% (3-month SPEI) and 11.3% (12-month SPEI) of the SPEI variability and features its highest loading over the Horn of Africa, i.e. over northern Somalia and eastern Ethiopia (hereafter, the DM4 region).

The DM4 score is also well correlated with SPEI over the DM4 region (r=0.8). The 12-month SPEI indicates that the DM4 region experienced more than three decades of persistent dry conditions in 1940–1965, followed by alternating wet and dry conditions in 1970–2000, and persistent wet conditions in 2004–2014. Hence, similar to DM1, DM4 has a generally positive trend (wet conditions) during the study period (Table 4.1). This result is similar to that of Damberg and Aghakouchak (2014), who found a positive trend in 6-month SPI over the Horn of Africa in 1980–2013. However, at both 3-month and 12-month scales, the DM4 drought has a maximum decadal frequency (about 32 months decade^{-1} and 63 months decade^{-1} respectively) in the 1950s, and features no drought in the 2000s (Fig. 4.3). The wavelet analysis (Fig. 4.4 (d)) indicates that the peak cycles in DM4 score are at the 1-12 years band, and that all the cycles feature significant power in 1950–2000.

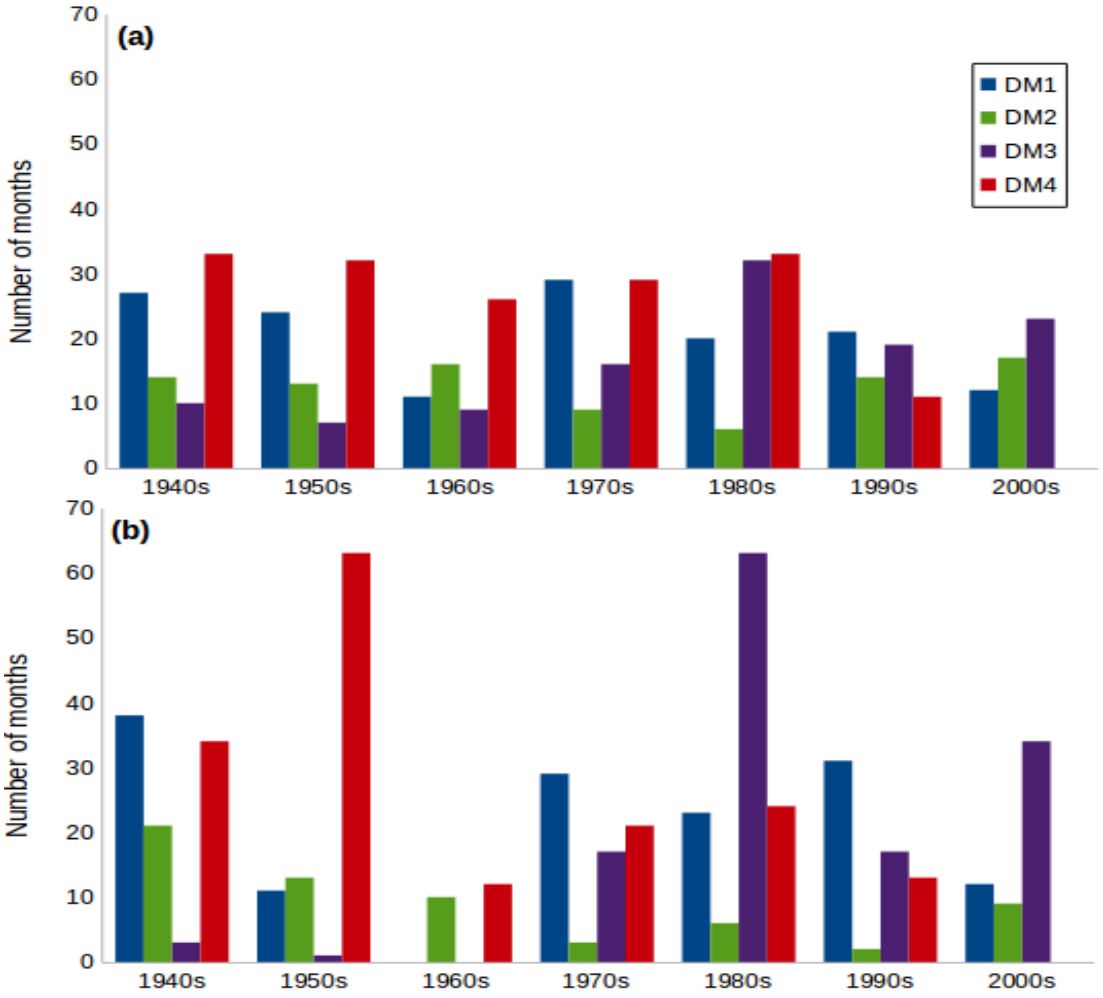

Figure 4.3: *Decadal variations of SPEI drought frequency at (a) 3- and (b) 12-month scale. The drought frequency is the representation of the DM regions over the red boxes in Figures 2 and 3 that have a drought intensity of less than -1.*

The differences in the spatial-temporal characteristics of these drought modes suggest that they have different drivers, which could be local or remote drivers, or both. Due to the difference in the spatial structure, a large-scale or synoptic scale driver could influence the drought model differently. In the next section, we explore the influence of four major atmospheric teleconnections on each drought mode.

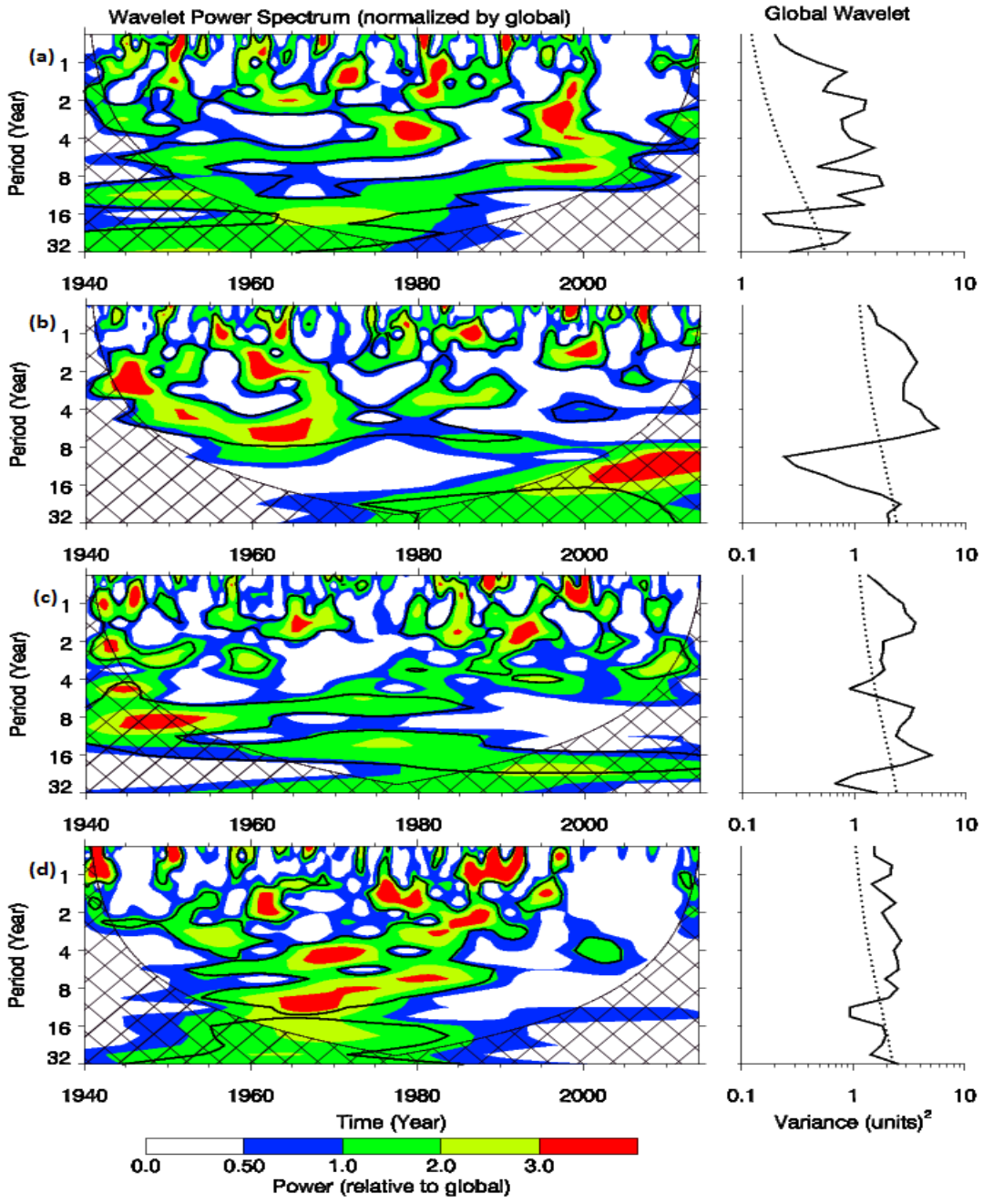

Figure 4.4: *The wavelet power spectrum and their associated global wavelet (the left and right panels respectively), derived using SPEI drought scores at 3-month scales for (a) DM1, (b) DM2, (c) DM3 and (d) DM4. The scaling of wavelet power has been done through the global wavelet spectrum. The cross-hatched region is the core of influence, where edge effects might influence the results or where zero padding has reduced the variance. The black contour is the 10% significance level, using the global wavelet as the background spectrum.*

4.2 Drivers of the drought modes

Table 4.1 presents the correlation between each drought mode and the four atmospheric teleconnections (ENSO, IOD, TADI and QBO), while Figs. 4.5-4.8 show the corresponding wavelet coherence. In general, Table 4.1 suggests a weak correlation ($r < 0.2$) between each drought mode and the teleconnections, but Figs. 4.5-4.8 reveal a strong intermittent coupling between them. However, the strength of the coupling varies with the drought modes, teleconnections, and cycle bands (Figs. 4.5-4.8).

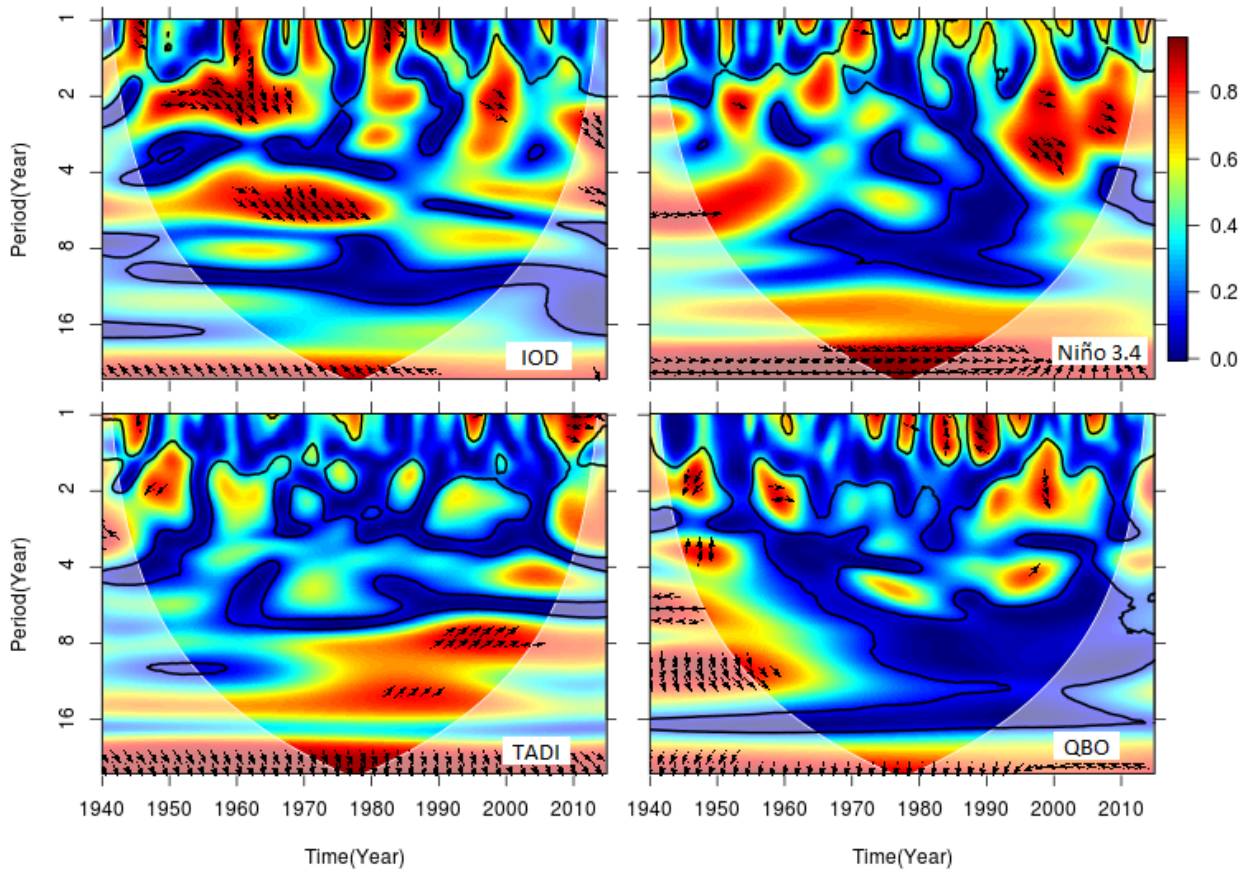

Figure 4.5: *Wavelet coherence of the SPEI drought score of the first drought mode (i.e. DM1) and the global teleconnections (i.e. IOD, Niño 3.4, TADI, and QBO). The 5% significance level*

against the red noise is shown as a black contour. The phases between the time series of the DM1 score and the teleconnections are shown as thick black arrows. Downward pointing arrows mean that the teleconnection leads DM1, and vice versa. Right pointing arrows mean that the teleconnection and DM1 are in phase, and vice versa.

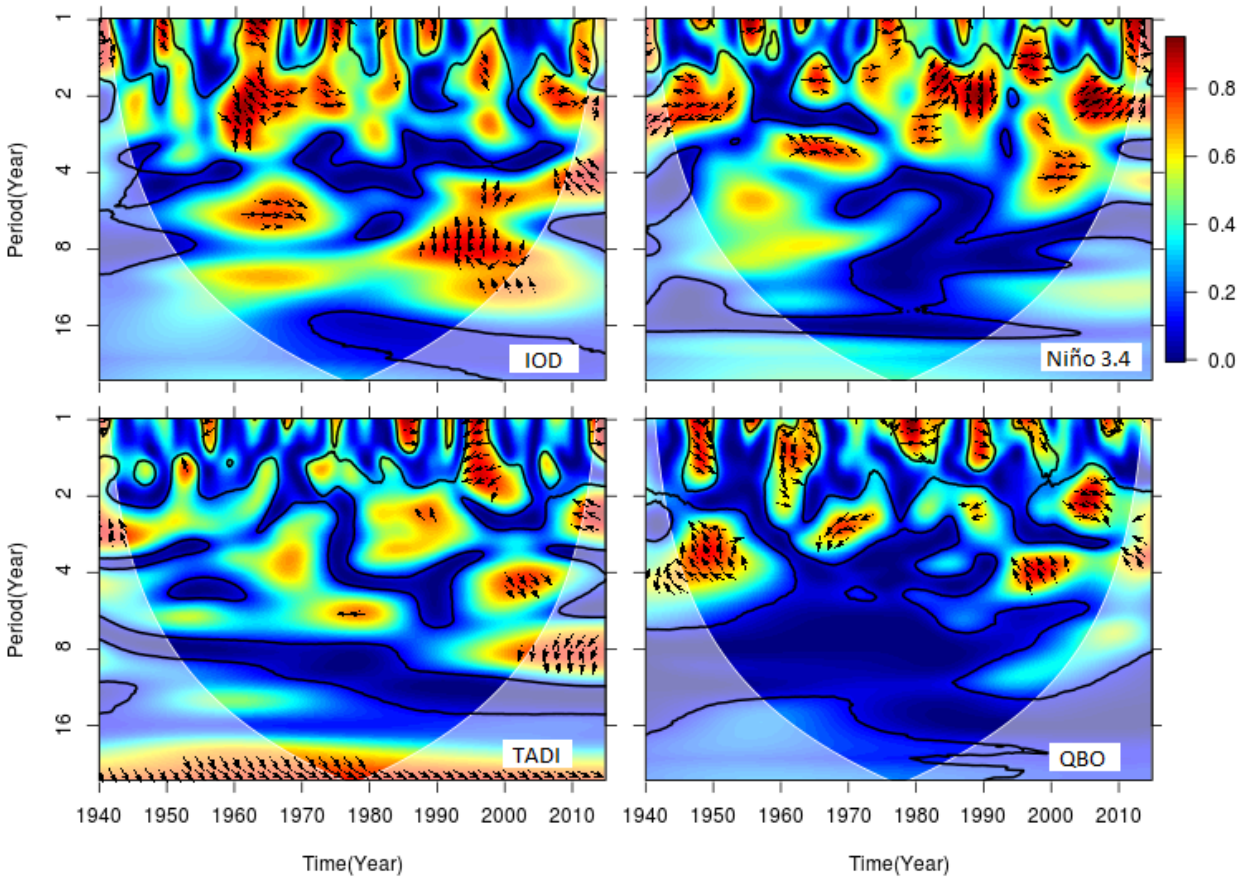

Figure 4.6: *As in Figure 4.5, but with drought mode DM2.*

The DM1 mode is coupled with the four climate indices but best linked with IOD and least associated with QBO. The significant coupling between DM1 and IOD persistently occurs at 1-3 year and 4-8 year cycles throughout the study period (1940–2014), although it is most prominent in 1940–1980 (Fig. 4.5). In contrast the coupling of DM1 with TADI is only significant at the 8-16 year cycles in 1980–2000, while the coupling of DM1 with ENSO only features at the 1-4 year band in 2000–2014. This suggests that the DM1 drought mode is generally coupled with IOD, but when this coupling is weak, its coupling with TADI (as in 1980–2000) or with ENSO (as in 2000–2014) becomes significant. Conversely, it could also be that an enhancement in the coupling of DM1 with TADI or ENSO weakens the coupling of DM1 with IOD.

However, this result agrees with Nicholson (1996), Lyon and DeWitt (2012), and Lyon (2014) who observed that the eastern Africa drought is primarily affected by the Indian Ocean (IOD), while ENSO (Niño3.4) and the Tropical Pacific Ocean (TADI) appear to have secondary effects. At the seasonal scale, the correlation between DM1 and SST over the Pacific Ocean and Indian Ocean is only strong during DJF and SON, and the pattern of the spatial correlation differs slightly in the seasons (Fig. 4.9). However, no correlation is found between DM1 and SST over the Southern Atlantic Ocean in all the seasons.

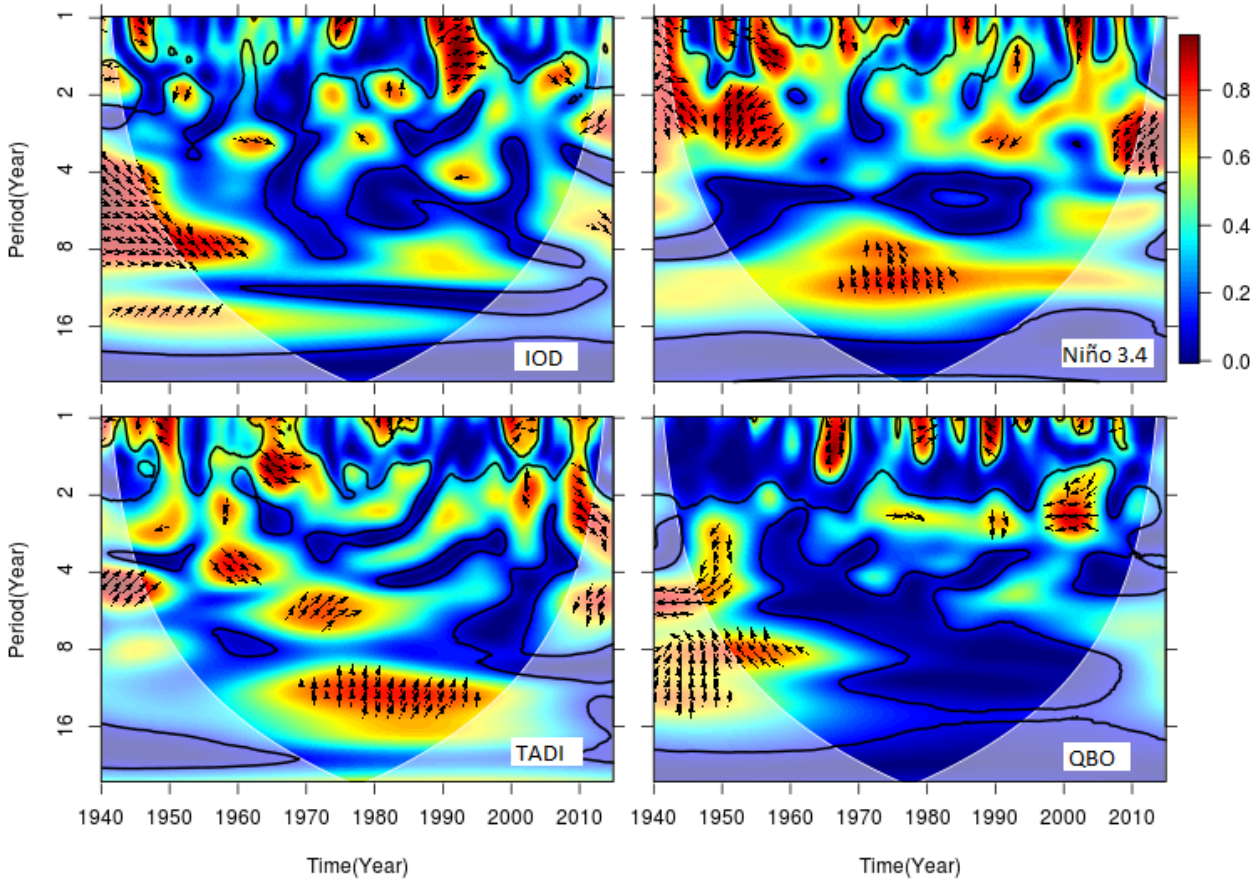

Figure 4.7: *As in Figure 4.5, but with drought mode DM3.*

The DM2 mode is better coupled with IOD and Niño3.4 than with TADI or QBO (Fig. 4.6). However, there are some differences in the coupling of DM2 with IOD and with Niño3.4. For example, while this drought mode is significantly coupled with Niño3.4 at the 1-6 year cycle throughout the study period, it is linked with IOD at a wider cycle band (1-12 years), and the link is only in 1950–1970 and 1980–2010. This

suggests that Niño3.4 may be the primary drivers of DM2, while IOD plays a secondary role. Nevertheless, the intensity and frequency of the DM2 drought in the 1960s and 1990s (Fig. 4.2 and Fig. 4.3) coincides with significant coupling between DM2 and IOD during this period (Fig. 4.6). At the seasonal scales, the coupling of DM2 with SST is moderately high (r > 0.51) over the Indian Ocean in SON. This is consistent with Endris et al. (2015) and Rowell (2013) who found that the DM2 region is more influenced by the Indian Ocean SST than by the Tropical Pacific Ocean SST.

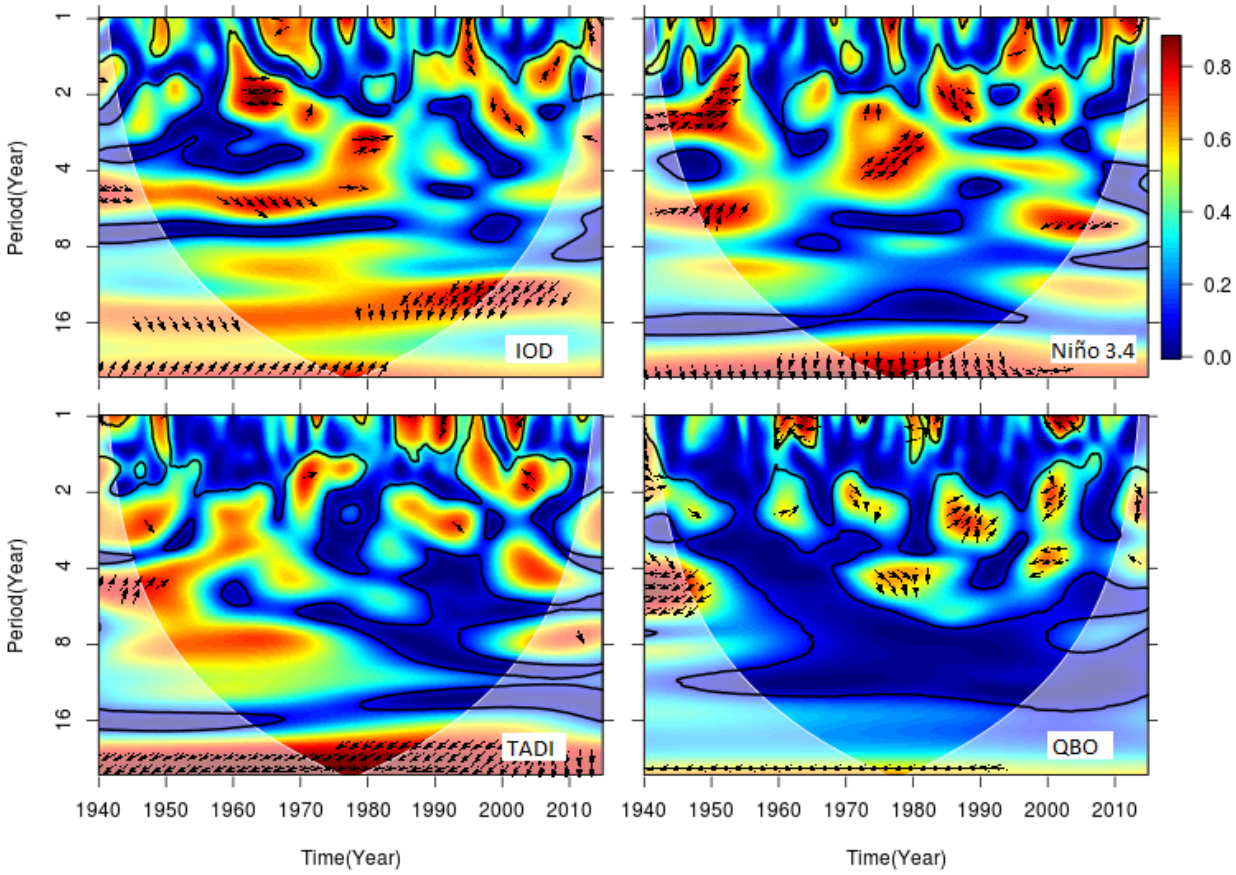

Figure 4.8: *As in Figure 4.5, but with drought mode DM4.*

The DM3 drought mode is better coupled with Niño3.4 and TADI than with IOD or QBO. The coupling of DM3 with Niño3.4 and TADI is significant at the 1-6 year and 8-16 year cycle but more persistent at the 8-16 year cycle, especially in the period of 1960–1990 (Fig. 4.7). This implies that the peaks in intensity and frequency of DM3 droughts in the 1980s may be attributed to the coupling of the mode with Niño3.4 and TADI at the 8-16 year cycle. This result agrees with previous studies (e.g. Korecha &

Barnston, 2007; Lyon, 2014; Segele et al., 2009) that the DM3 drought responds strongly to ENSO. However, some studies (e.g. Korecha & Barnston, 2007; Lyon, 2014) document a weak correlation between the DM3 region and Tropical Atlantic Ocean signals. Fig. 4.7 indicates that the coupling of the DM3 drought with IOD is weak throughout the study period, except at a 1-2 year cycle around 1990. Williams et al. (2012) also found a weak correlation between precipitation in the DM3 region and the southern tropical Indian Ocean, specifically during the intense drought years of the 1980s. At the seasonal scale, the correlation between DM3 and SST is generally weak in all the seasons; the highest correlation (about ±0.3) occurs over the North Atlantic Ocean and the Indian Ocean (in DJF) and over the Pacific Ocean (in SON).

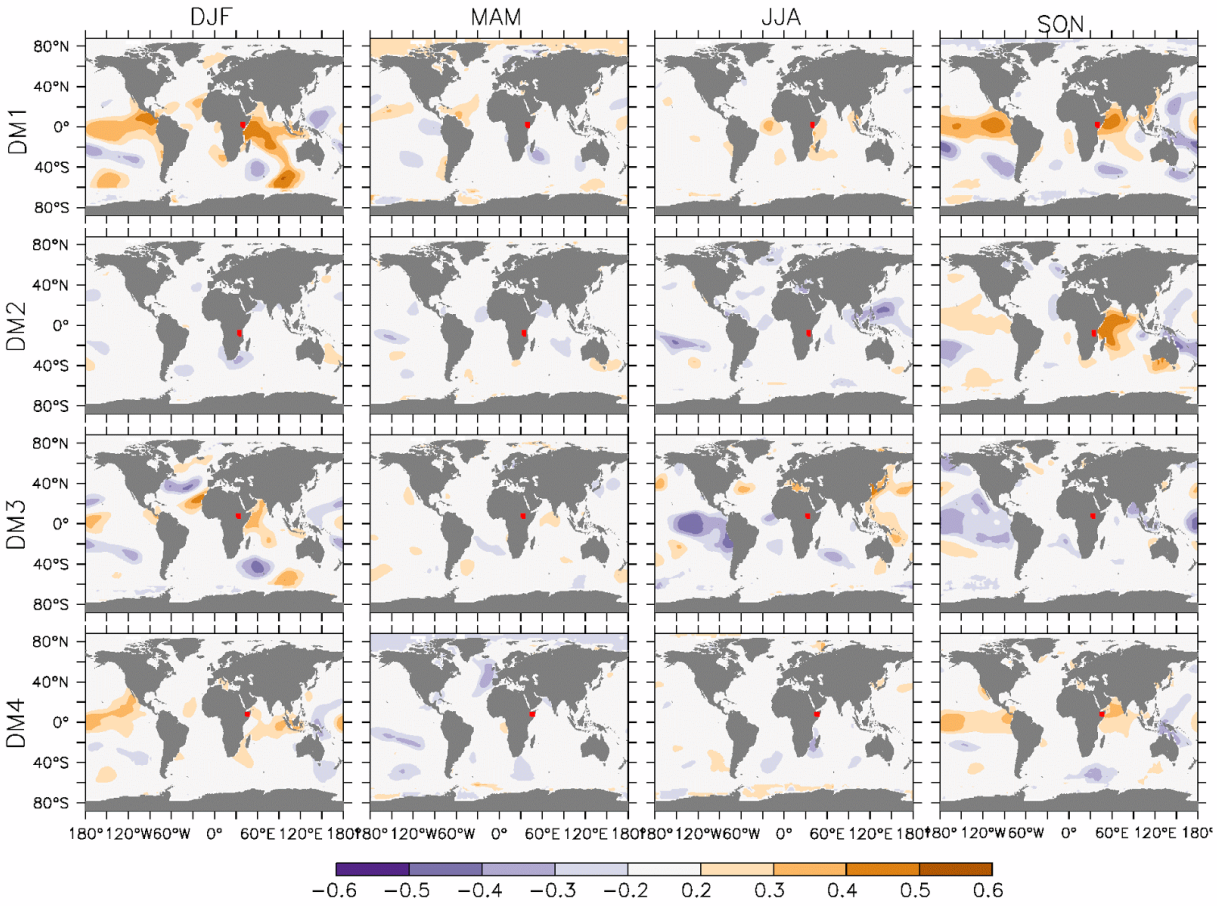

Figure 4.9: *The correlation between the scores of 3-month scale SPEI drought modes (DM1, DM2, DM3 and DM4) and the global SSTs in seasons DJF, MAM, JJA, and SON. The red boxes in the figure indicate where the DM regions are positioned.*

DM4 is also well coupled with the four teleconnections. However, this drought mode is better coupled with IOD and Niño3.4 than with QBO or TADI. The coupling of DM4 with IOD and Niño3.4 has a similar pattern in the 1-8 year band, suggesting that IOD and Niño3.4 jointly modulate the DM4 mode in this cycle band. However, IOD has additional significant modulation on this drought mode at the 16-year cycle. The continuous modulation, which persists throughout the study period, suggests that IOD may be the primary driver for quasi-decadal variability in this drought mode. TADI also makes a significant contribution to the quasi-decadal variability, but the contribution is not significant after 1970. However, the peaks in frequency and intensity of the DM4 drought (in the 1950s and 1990s) are well linked with the variability in IOD. This agrees with Bahaga et al. (2015) and Endris et al. (2015), who showed that the negative phase of IOD contributes to higher drought over the DM4 region compared to La Niña because the negative IOD additionally has a mechanism to reduce the moisture influx from the Congo basin to the DM4 region. At seasonal scales, the coupling of DM4 with SST is generally weak ($r < 0.4$) over all the ocean basins.

4.3 Atmospheric conditions associated with the drought modes

Figures 4.10-4.12 present the composites of SPEI and the corresponding wind and moisture transport anomalies during the three strongest 3-month droughts, in comparison with the climatology. Fig. 4.10 reveals that, while each drought mode can occur in any season, the associated drought intensity and area vary with the seasons. For example, DM1 and DM2 droughts, which are confined to their core regions in JJA, intensify and expand to almost the entire eastern Africa in other seasons. However, the seasonal variability is less pronounced in DM3 and DM4, whose drought areas hardly change with the seasons. The most intense drought over the DM1 and DM2 cores occurs in DJF and SON, while that over the DM3 and DM4 cores feature in MAM and SON. Nevertheless, all the drought mode cores experience their weakest drought intensity in JJA. Lyon (2014) showed that about 50% of the inter-annual variability of rainfall over the bimodal DM1, DM2 and DM4 regions can be attributed to variability of the short rain alone (OND maxima), and for location DM3, which has unimodal JJA rainfall, maxima are found with large inter-annual variations. Therefore, this might be the reason why SON is the most intense drought season in most parts of eastern Africa.

In all the seasons, there is a strong correlation between the composites of SPEI and SPI ($r > 0.8$), but there are some notable differences in the drought intensity produced by the two indices, especially at the core of the drought modes. In some cases (e.g. DM1 in SON), the SPEI drought intensity is higher than that of SPI (meaning that evapotranspiration enhances the drought intensity), while in other cases, the SPEI drought intensity is lower (e.g. DM1 in MAM, suggesting that a decrease in the evapotranspiration reduces the drought intensity). All the drought modes experience higher evapotranspiration during JJA (in this season SPEI drought intensity shows more negative values than SPI). Comparing to other drought mode core regions, DM4 seems to be mostly affected by drought because of low rainfall but higher evapotranspiration in all seasons.

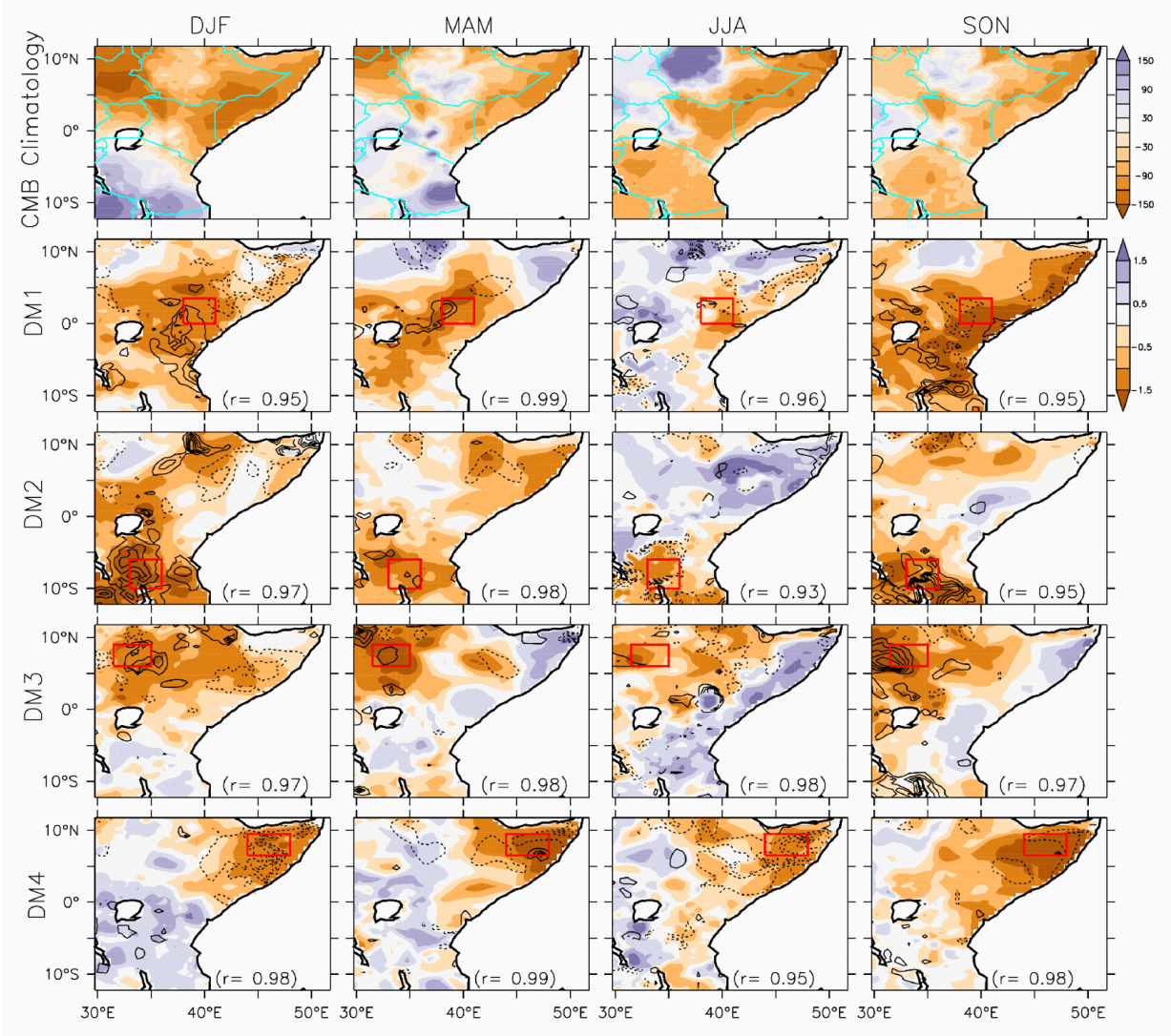

Figure 4.10: *The climatology of the moisture balance (CMB climatology) and the composite of 3-month scale SPEI drought intensity for the first four drought modes (i.e. DM1, DM2, DM3, and DM4) in the season DJF, MAM, JJA, and SON.*

Fig. 4.11 shows a net downward motion over each drought mode core and a net upward motion (i.e. enhanced convection) in the adjacent area (regions far from drought core). This suggests that the net downward motion that suppresses drought over the drought mode core is induced by the enhanced convection over the adjacent areas. However, the location of the adjacent convection varies with drought modes and with the seasons. For example, with DM1, the droughts are linked with enhanced convection over areas south of 20^{o}S in DJF, but over central Africa in SON. There is a net transport of moisture into the continent from the tropical Indian Ocean over the drought area, but the moisture seems to only enhance convection adjacent to the drought area (Fig. 4.12).

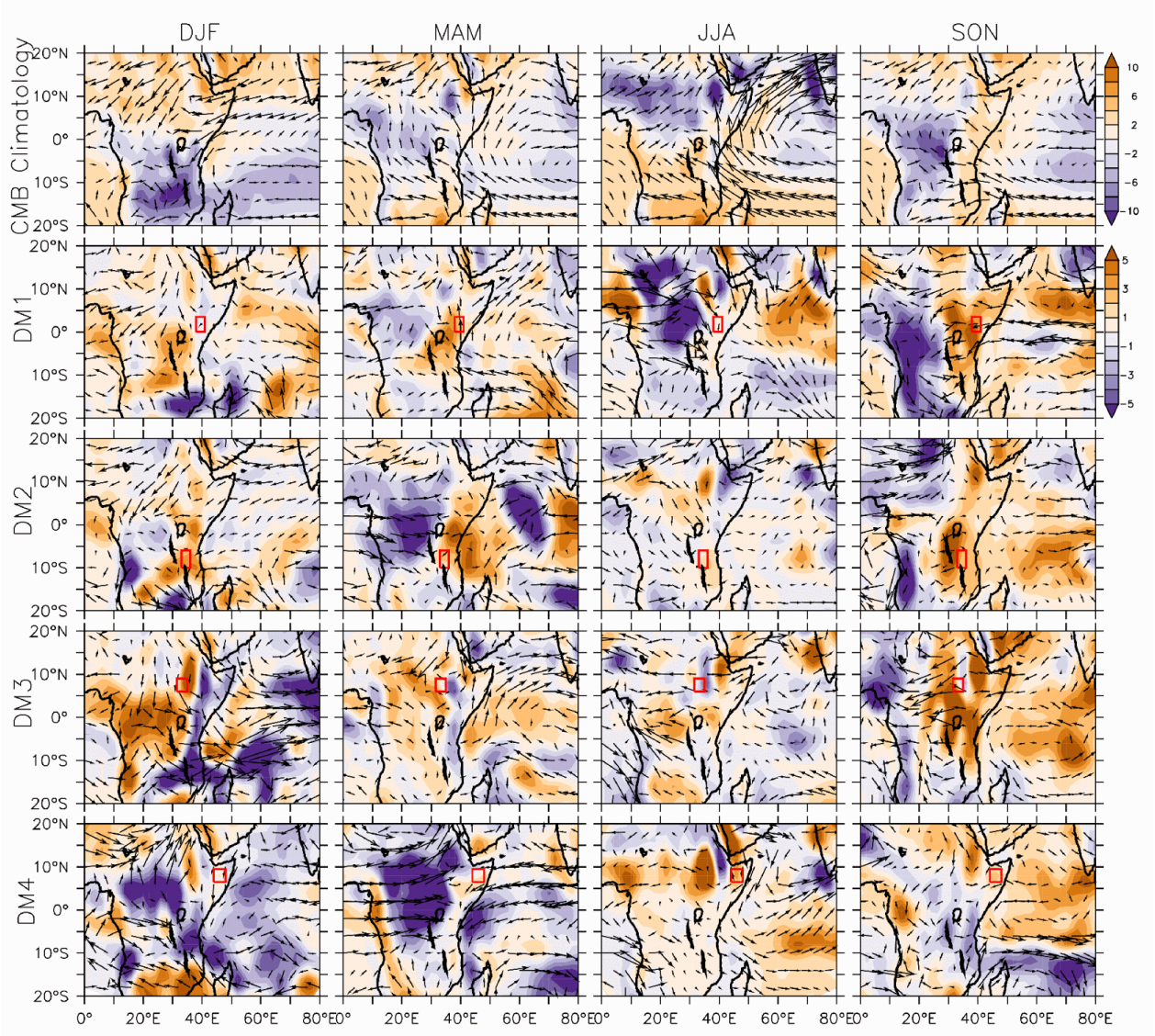

Figure 4.11: *The climatology of wind components (Climatology) and the composite of their anomalies for the SPEI drought intensity at 3-months scale for the drought modes DM1, DM2, DM3, and DM4 in the seasons DJF, MAM, JJA, and SON. The wind field found at 500mb level.*

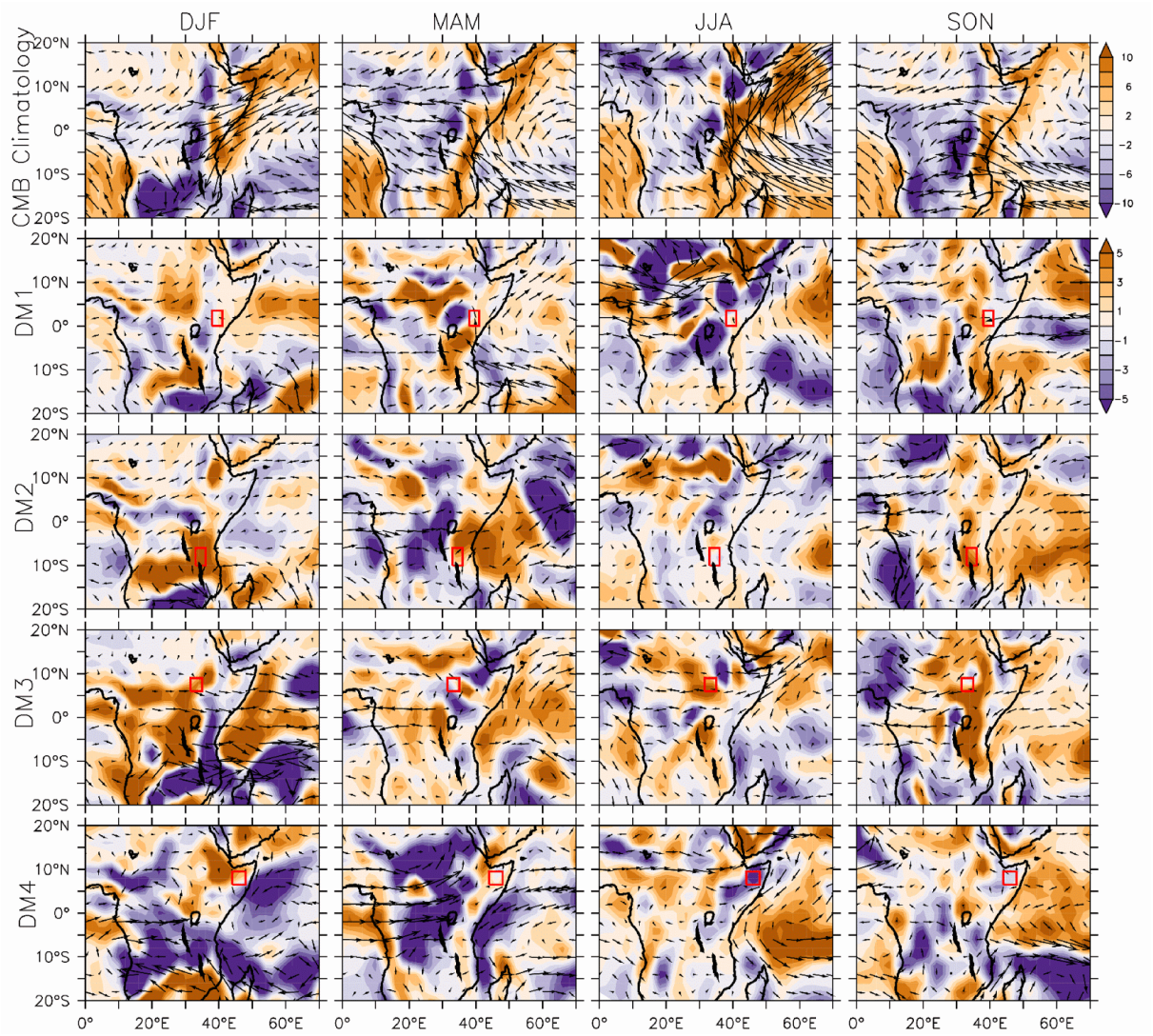

Figure 4.12: *The climatology of moisture transports (Climatology) and the composite of their anomalies for the SPEI drought intensity at 3-months scale for the drought modes DM1, DM2, DM3, and DM4 in the seasons DJF, MAM, JJA, and SON. The moisture transport level is 700mb*

4.4 Summary

This study has presented the temporal and spatial characteristics of drought modes over eastern Africa in the period 1940–2014, using a drought index (SPEI) in quantifying the droughts at two time-scales: 3-month and 12-month. The SPEI is a climate water balance, calculated from the CRU monthly precipitation and potential evapotranspiration (PET) dataset. We obtained the temporal and spatial structure of the four major drought modes over the region by applying PCA to extract the first four principal factors from the SPEI dataset. The temporal structures of the modes are

described by means of wavelet analysis. The influence of four climate indices (i.e. ENSO, IOD, TADI and QBO) and global SSTs on each drought mode was quantified, and the atmospheric condition associated with the drought modes was examined. Our findings can be summarised as follows:

- The four major drought modes (DM1, DM2, DM3 and DM4) account for more than 45% of SPEI variability over eastern Africa, and feature their cores over different areas of the region, namely: central eastern (DM1), southern and south-western (DM2), north-western (DM3) and far north-eastern (DM4).
- The drought modes have different temporal variation and produced their maximum drought frequency in different decades within the study period (1940–2014). In the wavelet spectrum, DM1 featured significant power at the 4-10 year cycle after 1980, DM2 at the 2-8 year cycle before 1970, DM3 at the 7-20 year cycle in 1960–1990, and DM4 at the 4-8 year cycle in 1960–1980.
- The coupling of the drought modes to the atmospheric teleconnections (i.e. ENSO, IOD, TADI and QBO) also differs. The DM1 mode is best coupled with IOD, DM2 with IOD and ENSO, DM3 with ENSO and TADI, and DM4 with IOD and ENSO.
- At the seasonal scale, there is a strong correlation between DM1 and SST over the Indian and Pacific Oceans in DJF and SON, and between DM2 and SST over the tropical Indian Ocean in SON.
- The composite of SPEI drought shows that each drought mode can occur in any season, but the difference lies in the associated drought intensity and area coverage at each season. The seasonal variability is, however, more pronounced for DM1 and DM2, and less seasonal changes are noted in DM3 and DM4.
- The analysis of the drought modes also suggests that the net downward motion that suppresses drought over the drought mode core area is induced by the enhanced convection over the adjacent areas. The location of the adjacent convection varies with drought modes and with the seasons.

Further work is done in the next chapters to understand the future impacts of climate change on eastern Africa droughts to assist in proper mitigation measures.

Chapter 5

Potential Impacts of 1.5°C and 2°C global warming levels on Drought Modes over Eastern Africa

This chapter discusses the impact of global warming at 1.5°C and 2.0°C levels on the characteristics of the four major drought modes discussed in the previous chapter. It starts by examining the capability of the CORDEX models in simulating the drought modes, and then describes the impacts of the two specified global warming levels on the major drought modes under two future climate forcing scenarios (RCP4.5 and RCP8.5).

5.1 Observed and simulated drought modes in the historical climate

To assess the credibility of CORDEX RCMs in simulating historical drought modes over eastern Africa, the characteristics of the simulated drought modes in the historical climate are compared with the observations (Fig. 5.1-5.3). The RCM ensemble replicates the spatial pattern of the observed drought modes well (Fig. 5.1). For all the drought modes, the correlation between the simulated and observed patterns is high ($r \geq 0.7$). The model ensemble mean features the core hotspot (i.e. the highest positive loadings) of the modes at the same locations as in the observations. The first drought regime (DM1) explains about 21% (CRU) and 13% (model ensembles mean) of the drought variability, and features its highest positive loadings (≈ 0.8) over northeastern Kenya and southern Somalia, and a negative loading (≈ 0.6) over northern Sudan and north-western Ethiopia. The second drought regime (DM2) explains 12% (CRU) and 14% (ensembles mean) of the SPEI variance, and features its highest positive loadings (≈ 0.6) over Tanzania. DM2 has the highest negative loadings (≈ 0.2) located far north of eastern Africa. The third drought regime (DM3) explains 11% and 16% of CRU and ensembles mean respectively of the SPEI variance, and shows its highest positive loadings (≈ 0.6) over the Horn of Africa (i.e. northern Somalia and eastern Ethiopia). The last drought mode (DM4) accounts for 11% (CRU) and 15% (ensembles mean) of the variability, and features its highest positive loading over most parts of South Sudan and some parts of west-central Ethiopia, while the negative loadings are found along the eastern Africa coastal area

In general, these drought modes correspond to different rainfall climate zones in eastern Africa (Cook & Vizy, 2012; Lyon, 2014; Yang et al., 2015). The DM1 area has a bimodal rainfall climatology with peaks during MAM (heavy rains) and OND (light rains). According to Yang et al. (2015), the DM4 area has a similar pattern of rainfall climatology as the DM1 area and therefore the differences can be on the large-scale systems (teleconnections) that influence their climate. For instance, the DM4 region is affected strongly by the Somali jet (Findlater, 1977; Segele et al., 2009) and the Asian monsoon (Camberlin, 1997; Vizy & Cook, 2003), and relatively no effect occurs in the DM1 region. Both DM2 and DM3 have a unimodal rainfall climatology, with similarities in their intensity ranges in the peak season but differing in terms of the time of the seasons. While DM2 peaks in DJFM, DM3 peaks in JJAS.

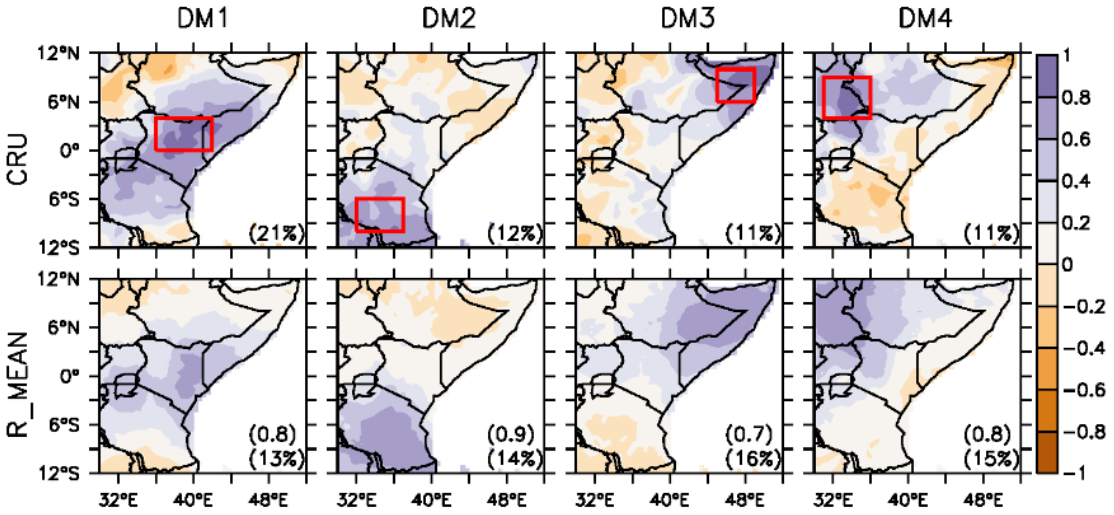

Figure 5.1: *The observed and simulated (ensembles mean) loadings of 12-month SPEI over eastern Africa for the period 1971-2000. The red boxes represent the core area of the four drought modes. The percentage of variance explained in terms of each mode (DM1, DM2, DM3 and DM4) of CRU and the ensemble is indicated at the right lower corner of each panel. The spatial correlation between the observed and simulated loadings for each mode is shown on top of each variance.*

The capability of RCMs to reproduce the spatial pattern of the drought modes varies among the simulations (Fig. 5.2). For all drought modes, the correlation between individual simulation and observation varies between 0.3 and 0.9. All the simulations show their best performance in simulating either DM1 ($r = 0.5 < r < 0.8$) or DM2 (0.6

< r < 0.9), and their worst performance in simulating DM3 (r = 0.3 < r < 0.8). The best performance of the model in simulating DM1 and DM2 may be because the modes are mostly controlled by the large-scale atmospheric circulation or teleconnections (e.g. ENSO and IOD), which are accurately reproduced by the simulations. Several studies have shown the DM2 hotspot to have a high correlation with the tropical Pacific Ocean and the western Indian Ocean (e.g. Dutra et al., 2013, Lott et al., 2013; Nicholson, 1996; Tierney et al., 2013; Trenberth et al., 2014).

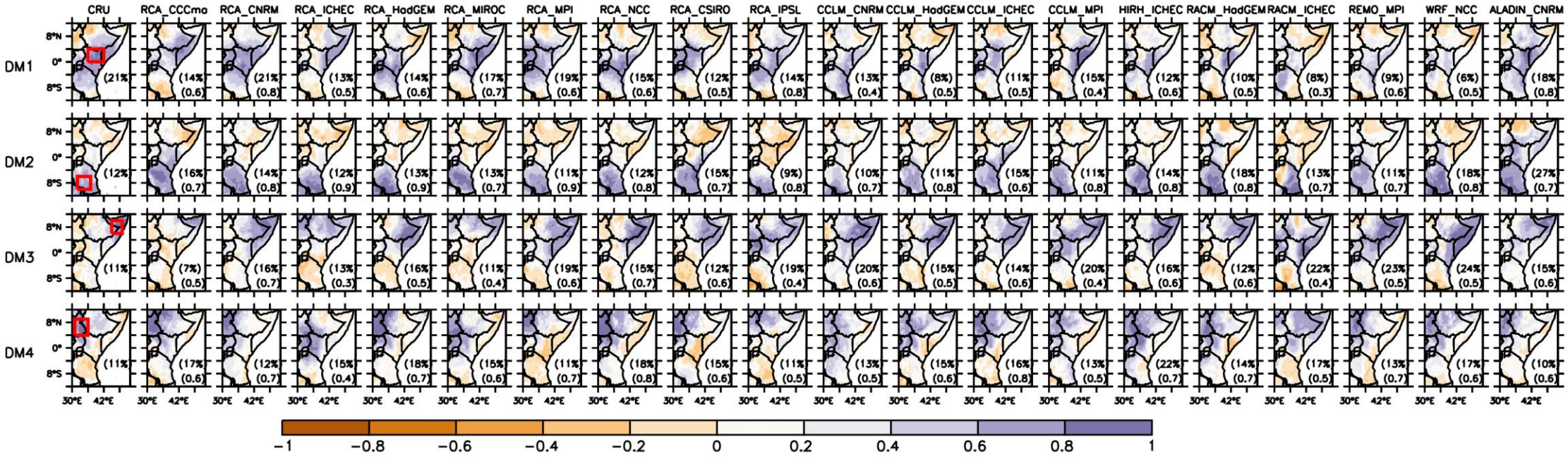

Figure 5.2: *The observed and simulated loadings of 12-month SPEI over eastern Africa for the period 1971-2000. The percentage of variance explained by the CRU and each RCM model for all drought modes is indicated at the right lower corner of each panel. The spatial correlation between observed and simulated is shown at the bottom of each variance.*

The RCMs give credible simulations of drought frequency over the core hotspots of the DM1, DM2, DM3 and DM4 (Fig. 5.3). For all the DMs, the observed drought frequency (in terms of both SPEI and SPI) falls within the simulations' spread. However, the performance of the simulations in reproducing the drought frequency is generally better with SPI than with SPEI. For instance, in DM1, more than 75% of the simulations overestimate the SPEI drought frequency, but less than 75% of them overestimate the SPI drought frequency. Also, in DM3 and DM4, while the observed SPI drought frequency falls within the 1st quartiles of the simulated values, the observed SPEI drought frequency is below the 1st quartile

The better performance of the RCMs in simulating SPI than SPEI suggests a larger bias in the simulated precipitation than in the simulated PET (which is calculated from Tmax and Tmin). Nevertheless, for all DMs, the observations and the simulations agree that the SPEI droughts are more frequent than the SPI droughts. The difference ranges from ~3 (CRU) and ~2 (RCM median) in DM1 to ~0.5 (CRU) and ~3 (RCM median) in DM4. This suggests that the inclusion of the PET enhances the intensity and frequency of droughts over the hotspots. The results agree with Vicente-Serrano et al. (2010a; 2012a) that SPI may underestimate drought severity and frequency.

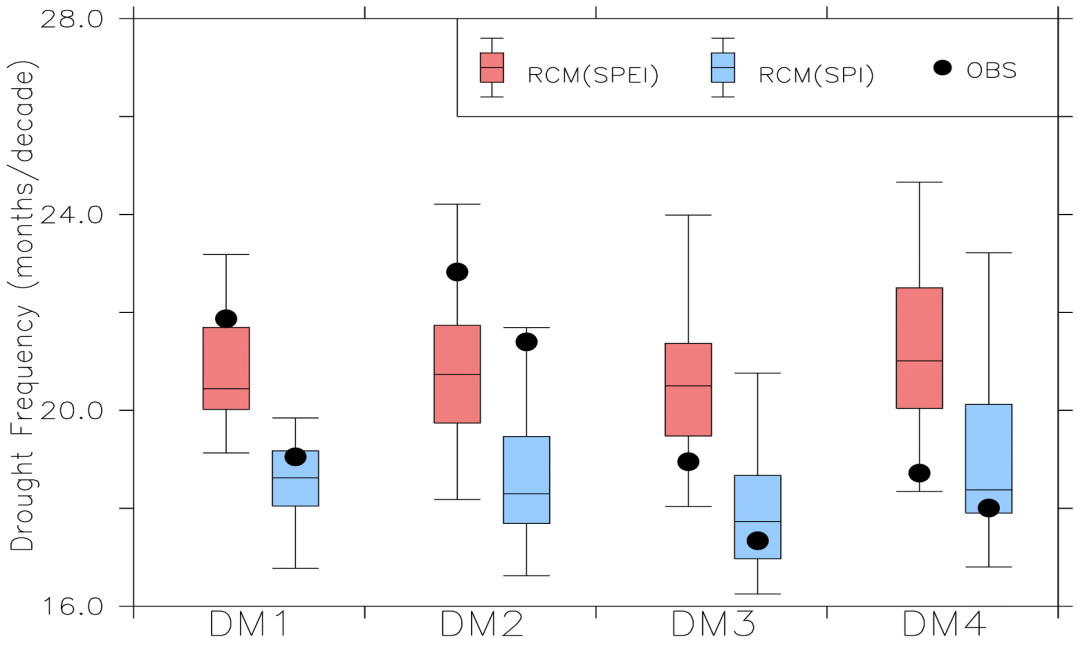

Figure 5.3: *The frequency of 12-month droughts (SPEI ≤ -1; SPI ≤ -1) over the core area of the four drought modes (DMs: DM1, DM2, DM3, and DM4) in the historical climate (1971-2000), as depicted by CRU observation and RCM simulations. The boxplot represents the interquartile model ensemble spread range: minimum, 1st quartile, median, 3rd quartile and maximum values.*

5.2 Impacts of 1.5ºC and 2ºC warming on drought modes under RCP4.5 scenarios

The simulation ensemble mean projects no changes in the spatial structures of the drought modes under both 1.5°C and 2.0°C global warming levels (Fig. 5.4). The correlation between the spatial distribution of the drought modes in past and future climates is very strong (r = ~ 1), the locations of the drought mode cores remain the same, and the changes in the percentage of variance explained by each drought mode are very small (< 2%). This suggests that the 1.5°C and 2.0°C global warming may not alter the location and structure of these major drought patterns. The weak sensitivity of the structure of the drought modes to 1.5°C and 2.0°C global warming may be because the locations of the large-scale drivers (e.g. ENSO, IOD) have been projected not to change with global warming. For example, Vecchi et al. (2010) found no clear evidence of ENSO activity to increase or decrease when considering future global warming trends and Stevenson et al. (2011) indicated insignificant weakening of ENSO variability with higher CO_2 concentrations. Cai et al. (2013) also documented a non-change of the IOD

mean frequency with global warming levels, and only a minor change in amplitude reduction between positive and negative dipole events.

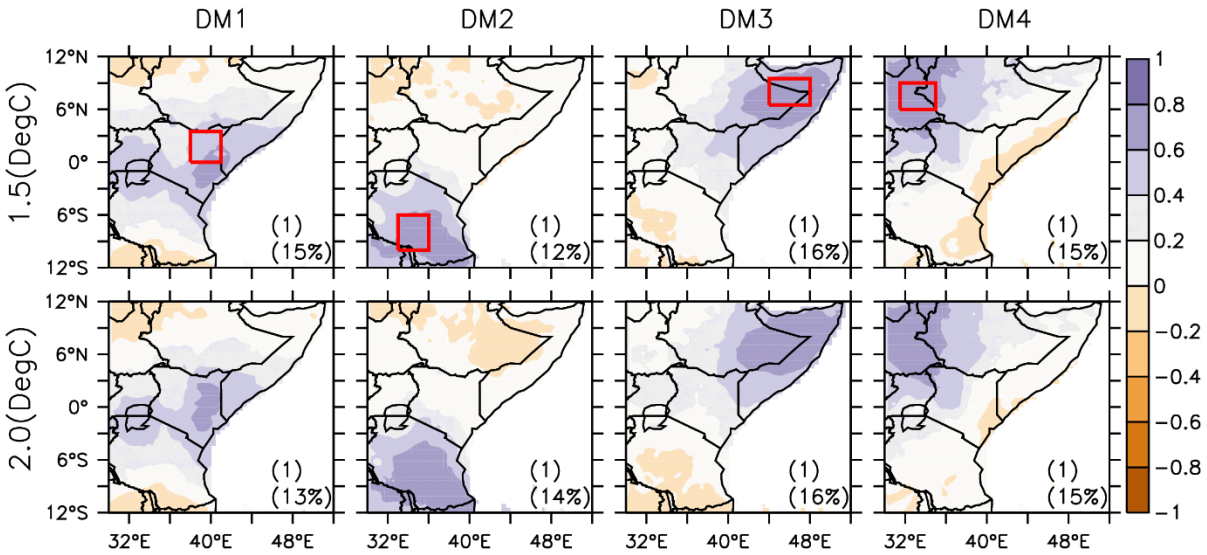

Figure 5.4: *The projected spatial structure of 12-month SPEI over eastern Africa in the future climate at 1.5°C and 2.0°C global warming levels under RCP4.5 scenarios. The percentage of variance explained by each drought mode is indicated in the lower right corner of each panel. The spatial correlation between historical and future simulation loadings for each mode is shown at the top of the variance.*

The RCMs project a substantial increase in the intensity and frequency of SPEI droughts over DM1, DM2, DM3 and DM4 hotspots under both 1.5^{o}C and 2^{o}C global warming levels (Fig. 5.5). The magnitude of the increase, which is generally higher under 2.0^{o}C than 1.5^{o}C warming, varies over the DM cores. The highest increase in SPEI drought intensity (i.e. reduced SPEI: -0.4 and -0.6 for 1.5^{o}C and 2^{o}C warming, respectively) and frequency (about 15 and 20 months per decade for 1.5^{o}C and 2^{o}C warming, respectively) occurs over the DM4 hotspot, while the smallest increase in the intensity (i.e. reduced SPEI: -0.1 and -0.3 for 1.5^{o}C and 2^{o}C warming respectively) and frequency (about 10 and 12 months per decade for 1.5^{o}C and 2^{o}C warming, respectively) occurs over the DM1 hotspot. The largest difference between the impacts of the two warming levels is over DM3. However, there are some discrepancies among the simulations as to the sign and magnitude of the projected changes. For example, in the 2^{o}C warming projection over the DM2 (Fig. 5.5 (a) and (c)), the projected changes in the drought intensity vary from -1.6 to +0.4 and the changes in drought frequency vary from -10 to

70 months decade^{-1}. Nevertheless, more than 75% of the simulations agree that both 1.5^{o}C and 2^{o}C warming will increase drought intensity and frequency over the four drought hotspots. This result agrees with those of previous studies that there is a projected decrease in precipitation and an increase in potential evapotranspiration over most parts of eastern Africa (e.g. Cook and Vizy 2012). However, the use of SPEI in the present study combines the projected changes in precipitation and evapotranspiration in accessing the impacts of the specific global warming levels on droughts in this region.

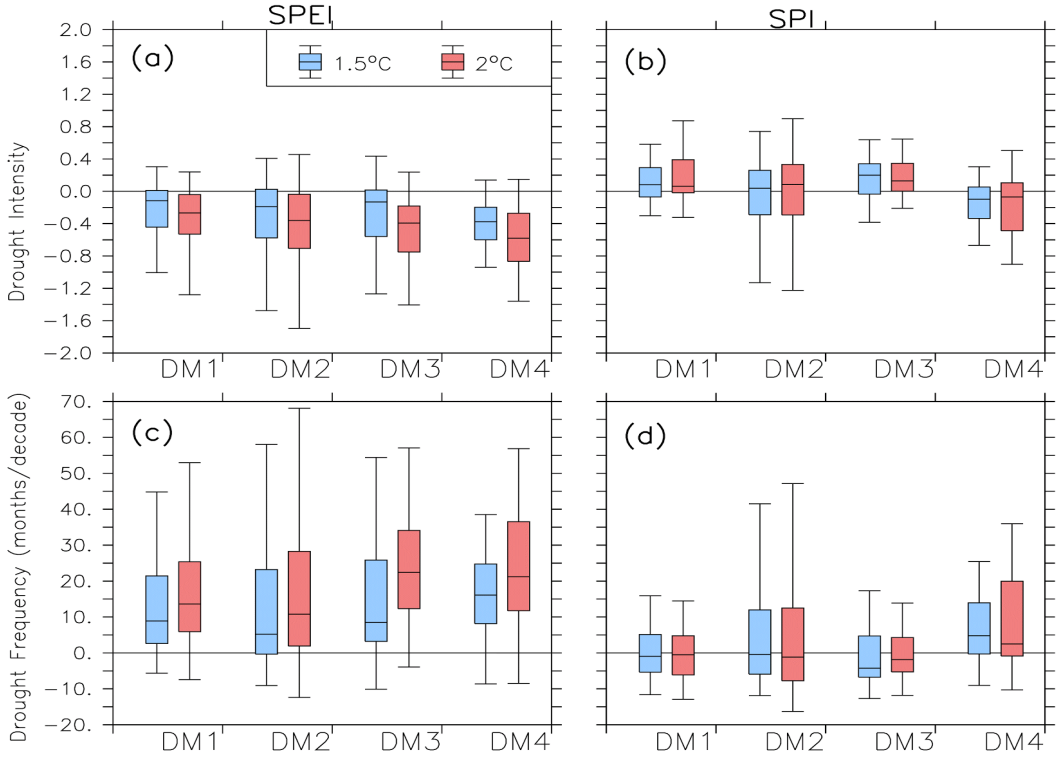

Figure 5.5: *Projected changes in intensity and frequency of 12-month droughts (SPEI < -1; 12-month SPI < -1) under future climates with 1.5°C and 2.0°C global warming levels under the RCP4.5 scenario. The changes are calculated with respect to the historical climate (1971-2000). The boxplot shows the interquartile of the simulation spread: minimum, 1st quartile, median, 3rd quartile and maximum values.*

The projected changes in SPI drought differ from those of SPEI in many aspects (Fig. 5.5). For example, over three of the DMs (DM1, DM2 and DM3), the projected changes (ensemble mean) in SPI drought characteristics have the opposite sign to that of SPEI. In contrast to the SPEI results, an increase in SPI (wet condition) and a decrease in SPI drought frequency are projected over the three DM hotspots (DM1, DM2 and DM3).

Under the 1.5ºC degree warming level, the maximum increase in SPI (about +0.2) and the maximum decrease in drought frequency (about -5 months/decade) occur over DM3. In addition, over the DM4 hotspot, where the signs of changes in SPI and SPEI drought are the same, the magnitude of the changes (for both drought intensity and frequency) is smaller in SPI than SPEI. Under 2ºC warming, the simulation ensemble projects a decrease of about -0.1 in SPI drought intensity (compared to about -0.6 in SPEI) with the simulations' spread ranging between -0.6 and +0.4 (compared to -1.4 and 0.2 in SPEI). The corresponding increase in SPI drought frequency (ensemble mean) is about 3 months decade^{-1} (compared to 20 months decade^{-1} in SPEI). Furthermore, the level of agreement among the simulations on the projections is weaker in SPI (less than 75% of the simulations agree) than in SPEI (more than 75% of the simulations agree). The differences in the SPI and SPEI projections are due to the influence of PET on droughts. While the SPEI projections account for this influence, the SPI projections do not. It is expected that global warming would enhance potential evapotranspiration, and thus induce a drier climate over eastern Africa. Hence, the difference between the SPEI and SPI projections stresses the need to include potential evapotranspiration in projecting the impact of global warming on droughts over the region.

5.3 Impacts of 1.5ºC and 2ºC warming on drought modes under RCP 8.5 scenarios

The RCP8.5 projection (Fig. 5.6, Fig. 5.7) features similar drought characteristics as the RCP4.5 projection (Fig. 5.4, Fig. 5.5). The spatial distribution of the drought modes is the same as those in historical and RCP4.5 patterns. This further suggests that the spatial structure distribution of major drought modes over the eastern Africa may be invariant to the global warming levels or climate forcing scenarios. While the changes in drought frequency and drought intensity are sensitive to the warming levels (1.5ºC and 2.0ºC), they do not vary much with the climate forcing scenarios (RCP4.5 and RCP8.5) (Fig. 5.7). For instance, with 2ºC warming, the difference between the RCP4.5 and RCP8.5 projections (i.e. ensemble mean) is small over DM4; with regard to drought intensity, it is less than 0.2, and with regard to drought frequency, it is less than 5 months decade^{-1}. The spread of the simulations among the two are also comparable, although the level of agreement is somehow weaker in the RCP8.5 projection, where less than 75% of the simulations agree on the projected changes over DM2. The discrepancy between the

SPEI and SPI results also features in the RCP8.5 projection, in that wetter conditions and less frequent SPI droughts are also projected over the DM hotspots, except over DM4. Hence, at a given warming level, there is no difference in the eastern African drought characteristics under RCP4.5 and RCP8.5. Some studies have reported a similar result for different variables over some regions (Shi et al., 2018; Karmalkar & Bradley, 2017). For example, Shi et al. (2018) found no significant difference in the projected mean temperature and temperature extremes over China under RCP4.5 and RCP8.5 at both 1.5^{o}C and 2.0^{o}C warming levels.

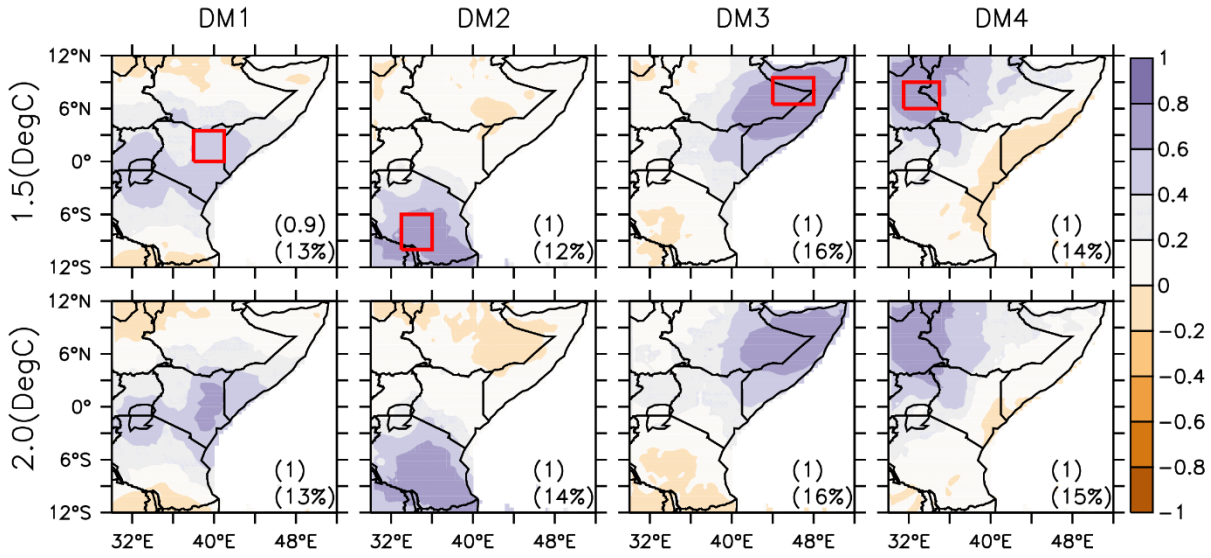

Figure 5.6: *The projected spatial structure of 12-month SPEI over eastern Africa in the future climate at 1.5°C and 2.0°C global warming levels under RCP8.5 scenarios. The percentage of variance explained by each drought mode is indicated in the lower right corner of each panel. The spatial correlation between historical and future simulation loadings for each mode is shown at the top of the variance.*

However, the most robust information from the RCP4.5 and RCP8.5 projections is that the spatial structure of the major drought modes in eastern Africa may not change with the global warming levels (1.5^{o}C and 2^{o}C), but that the intensity and frequency of SPEI drought over DM1, DM2, DM3 and DM4 hotspots may increase with the warming levels, although the projected change of SPI droughts may not change substantially. This suggests that the impact of global warming on future droughts may be stronger through increased potential evapotranspiration than through decreased precipitation. Hence, future drought mitigation options over the DM1, DM2, DM3 and DM4 hotspots should focus more on activities that minimise loss of moisture and surface runoff through

evaporation. Such activities could include planting of trees and shrubs to protect the land from direct evaporation and lower the strength of wind that accelerates the humidity loss above the surface of water reservoirs (Ritchie, 1983). Alvarez et al. (2006) recommended the use of shade structures, which reduce the energy available for evaporation and reduce the strength of wind blowing over the water surface specifically for small reserves. For a large dam, Craig et al. (2005) proposed the construction of deeper storages with smaller surface areas or dividing the dam into smaller sections to lower the wind flow.

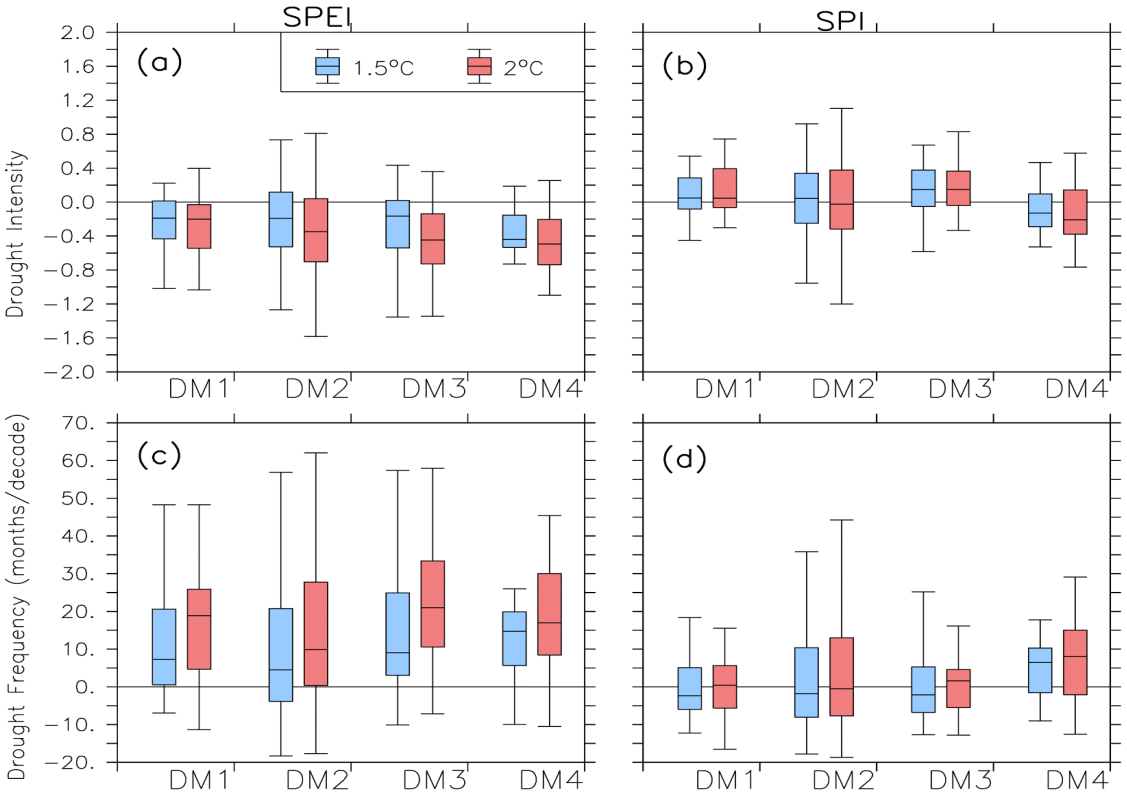

Figure 5.7: *Projected changes in intensity and frequency of 12-month droughts (SPEI < -1; 12-month SPI < -1) under future climates with 1.5°C and 2.0°C global warming levels under the RCP8.5 scenario. The changes are calculated with respect to the historical climate (1971-2000). The boxplot shows the interquartile of the simulation spread: minimum, 1st quartile, median, 3rd quartile and maximum values.*

5.4 Summary

This study has examined the potential impacts of ongoing global warming on the characteristics of major drought modes in eastern Africa at 1.5°C and 2°C warming levels under RCP4.5 and 8.5 scenarios. The CRU observation and 19 CORDEX RCM

simulation datasets were analysed for this study. The simulation datasets consist of rainfall and temperature (maximum and minimum) data for the historical climate (1971-2000) and for the future climate with 1.5^{o}C and 2^{o}C warming levels under RCP4.5 and 8.5 climate forcing scenarios. The SPEI (a drought index that is based on climate water balance) was used to quantify drought and the PCA was applied to the SPEI data to obtain the most dominant four drought modes over the region. The characteristics of drought modes that were considered include the spatial structure of such drought modes, as well as the intensity and frequency of drought over the hotspots. The capability of the CORDEX simulations to reproduce these characteristics was examined before analysing the simulations to investigate the impacts of global warming on the four drought modes. The results of the study can be summarised as follow:

- The RCM ensemble mean gives a realistic simulation of the characteristics of the four major drought modes over eastern Africa. The correlation between the simulated and observed spatial structures of the droughts is high ($r > 0.7$), and the observed drought frequency over the hotspots falls within the simulation spread.
- The simulations and CRU observations agree that using SPI (instead of SPEI) produced a lower drought frequency in the historical climate. However, the RCMs perform better at simulating SPEI than at reproducing SPI.
- The RCM ensemble project that the spatial structures of the drought modes are invariant to global warming levels (1.5°C and 2.0°C) and to changes in the RCP scenarios (RCP4.5 and RCP8.5). Nevertheless, the increases in the warming levels are projected to substantially increase the intensity and frequency of SPEI droughts over the core of the drought modes.
- The SPI projections (i.e. changes in drought intensity and frequency) give opposite results to those of SPEI over the first three drought modes, and the magnitude of the SPI changes is smaller than that of SPEI over the fourth drought mode.

Future work can improve the robustness of these results in many ways. For example, this present study has focused on meteorological droughts by using SPEI and SPI to quantify drought. Following Vicente-Serrano et al. (2010), the SPEI was calculated using potential evapotranspiration, which is only equal to actual evaporation when there is sufficient surface water supply. The SPEI might have overestimated the drought

intensity under the natural conditions, while the SPI might have underestimated it. Hence, using actual evaporation (which is not available for all CORDEX simulations) might improve the quality of the SPEI. Future studies can also extend the study to consider other impacts of global warming on agricultural, hydrological, and economic droughts by using appropriate drought indices to identify the agricultural, hydrological and economic drought regimes. These drought regimes might be the same or different from the meteorological drought regimes identified here, but understanding how the global warming might affect the hotspots of different types of drought will help policy makers to use the most appropriate options in mitigating the impacts. However, the present study has shown that, while the global warming may not alter the hotspot of the major drought modes over eastern Africa, it may indeed increase the intensity and frequency of drought over these hotspots.

Chapter 6

Projected changes in the characteristics of hydrological drought over East African basins

This chapter presents the projected future changes in hydrological drought over four river basins (i.e. Rufiji, Tana, Juba and Upper-Nile) in East Africa, as simulated by the CORDEX models. Before presenting the projections, the chapter discusses the capability of the climate simulations in representing the climatology over East Africa and over the basins. The projections, which are based on the RCP 8.5 future climate scenario, are discussed at four specific GWLs, namely, 1.5°C, 2.0°C, 2.5°C and 3.0°C, and for two drought indices (SPEI and SPI). The implications of both the similarity and the differences in the SPEI and SPI projections are also discussed.

6.1 Evaluation of climate simulation

The ensemble mean simulates the observed spatial heterogeneity in climate variables over East Africa well (Fig. 6.1 and Fig. 6.2). For all the variables, the correlation pattern between the ensemble mean and the observation is greater than 0.60. Like the observation, the simulations feature the highest temperatures (i.e. TMAX $\geq$ 30°C) over the north-western and eastern parts of East Africa (i.e. over South Sudan, northern Ethiopia, Somalia and northern Kenya), and the lowest temperatures (TMIN $\leq$ 3°C) over the mountains of Ethiopia, Kenya and Tanzania. The mean temperature pattern over the northern part of the region and Lake Victoria is well represented by the ensemble mean. The ensemble mean shows least bias for mean temperature over most of the region as compared to its bias on TMAX and TMIN.

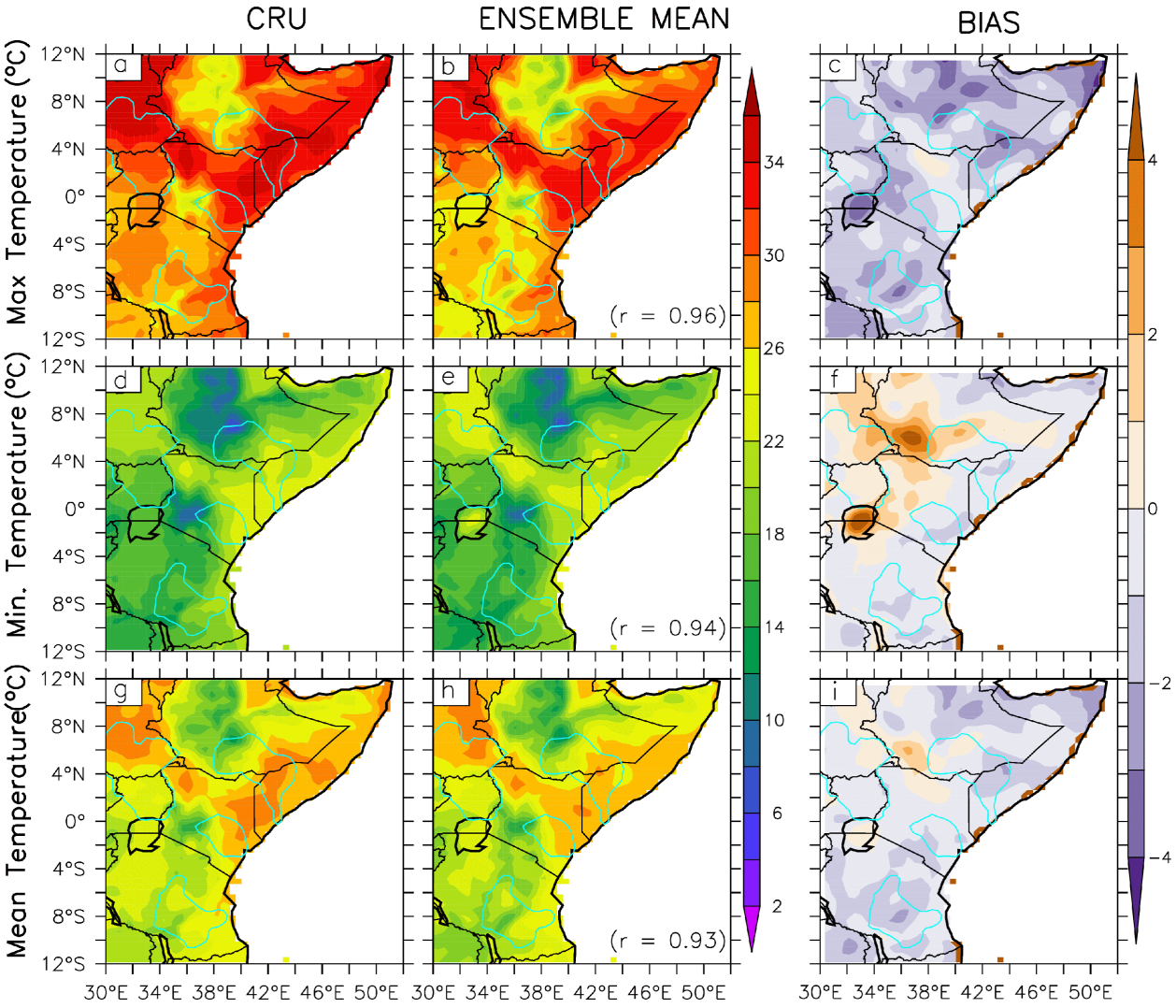

Figure 6.1: *The spatial distribution of climatology of maximum, minimum and mean temperatures over East Africa (1971 to 2000) as observed by CRU and depicted by the CORDEX RCMs ensemble. The evaluation of the climate simulation was done on an annual basis. The correlation between the observation and the simulation is shown in brackets in the lower right corner of the RCM panels. All the correlations are statistically significant (at 99% confidence level). The BIAS plots show the difference between RCMs and CRU (i.e. RCM minus CRU). The location of the basins is shown in light blue.*

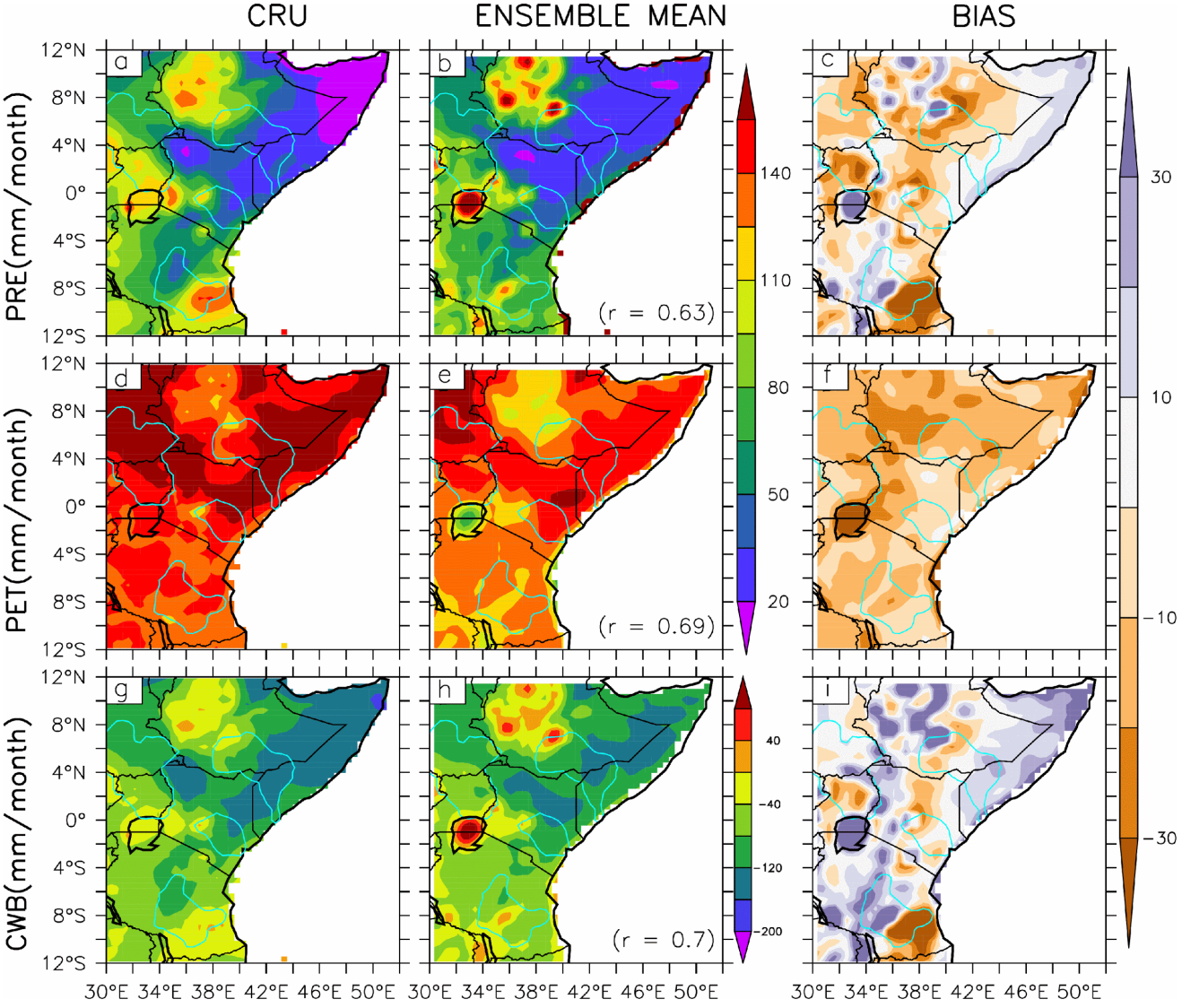

Figure 6.2: *Same as Figure 6.1, but for climatology of precipitation, potential evapotranspiration (PET) and climate water balance (CWB).*

The ensemble mean also captures the spatial variation of rainfall, even over the coast of Somalia and the highlands of Ethiopia, where substantial orographic rainfall occurs (Lyon, 2014). In addition, the model ensemble and the observations both show similar spatial changes with regard to PET and CWB in the northern parts of the region (Figs. 6.2 (d), (e), (g) and (h)). However, there are some biases in the simulation. For example, the simulation features a cold bias (about -4°C in TMAX) over the mountains in Ethiopia, and a warm bias (about 4°C in TMIN) over parts of Ethiopia, South Sudan and Lake Victoria (Fig. 6.1 (c)). The ensemble mean shows the least bias for the mean temperature over most part of the region, as compared to its bias on TMAX and TMIN.

Also, the simulation overestimates precipitation (by ~20 mm/month) over the Ethiopian highlands and Lake Victoria but underestimates it (by ~30mm/month) over south-eastern Tanzania (Fig. 6.2 (c)). The simulated PET is generally lower than the observed PET. Also, in most parts of East Africa, the PET bias is lower than the PRE bias, while the pattern of the CWB bias is similar to that of PRE (Fig. 6.2 (f)). For example, the maximum CWB bias (~10mm/month) is also located over southeastern Tanzania. Nevertheless, these biases are comparable to those reported by previous studies over East Africa (Anyah & Semazzi, 2007; Endris et al., 2015; Otieno & Anyah, 2013a; Riddle & Cook, 2008; Shongwe et al., 2011). For example, Riddle and Cook (2008) found a precipitation bias of about 4 mm/day over Lake Victoria between the CRU and the PSU/NCAR Mesoscale model (MM5) and attributed it to lake-induced local convection processes. Similarly, Thiery et al. (2015) document a double simulation of precipitation intensity by the COSMO-CLM model over the major lake surfaces of East Africa; however, there was a negligible effect on the air surfaces around the lake. Nikulin et al. (2012) document an underestimation of ~3 mm/day of the CORDEX RCM ensemble precipitation over most parts of southern Tanzania in comparison to the GPCP JFM precipitation. This underestimation might be due to the improper positioning of the ITCZ by the RCM ensemble over this area (Nikulin et al., 2012).

The model ensemble also gives a realistic annual cycle of the climate variables over the East African basins (Fig. 6.3). The models capture the annual cycle of TMAX and TMIN (Figs. 6.3 (a)– (c)), although they underestimate TMAX over all the basins and TMIN over the Rufiji and Tana River basins. The models' means also capture the different rainfall regimes that dominate each basin. Similar to CRU, the ensemble mean shows the bimodal (over Tana and Juba, see Figs. 6.3 (f) and 6.3 (g)) and unimodal (over Rufiji see Fig. 6.3 (e)) rainfall systems. The East African rainfall regimes are generally associated with the north-south migration of the ITCZ, which reaches its most northerly location during the JAS season and its most southerly location during JFM (Lyon, 2014; Nikulin et al., 2012). Therefore, the basins close to the equator experience the ITCZ peaks twice, while those distant from the equator have only one peak. As expected, the ensemble rainfall biases are diverse and vary across the individual basins. The large ensemble spread of rainfall is over the Upper-Nile basin, compared to the rest of the basins. The failure of the models to capture the transition rainfall changes may be because this basin has the largest area coverage and cuts across different climate

zones; consequently, some part have a unimodal rainfall pattern (further north), while others have a bimodal pattern (further south) (Camberlin, 2009). Or it could be due to the model resolution (0.44deg) is still too coarse to resolve the Upper-Nile/Lake Victoria Basin spatial-temporal distribution of rainfall. Additionally, the lake-induced precipitation over the upper Nile basin could also be a factor, which causes rainfall to be continuous throughout the year and not bimodal. It can be noted that the ensemble mean consistently underestimates and overestimates the MAM and OND precipitation peaks, respectively. The ensemble also transforms almost similar biases from TMAX to PET and from precipitation to CWB. Endris et al. (2013) documented that the CORDEX RCMs generally simulate the precipitation seasonal mean and annual cycle quite accurately, although the individual models can exhibit significant biases in some seasons and regions.

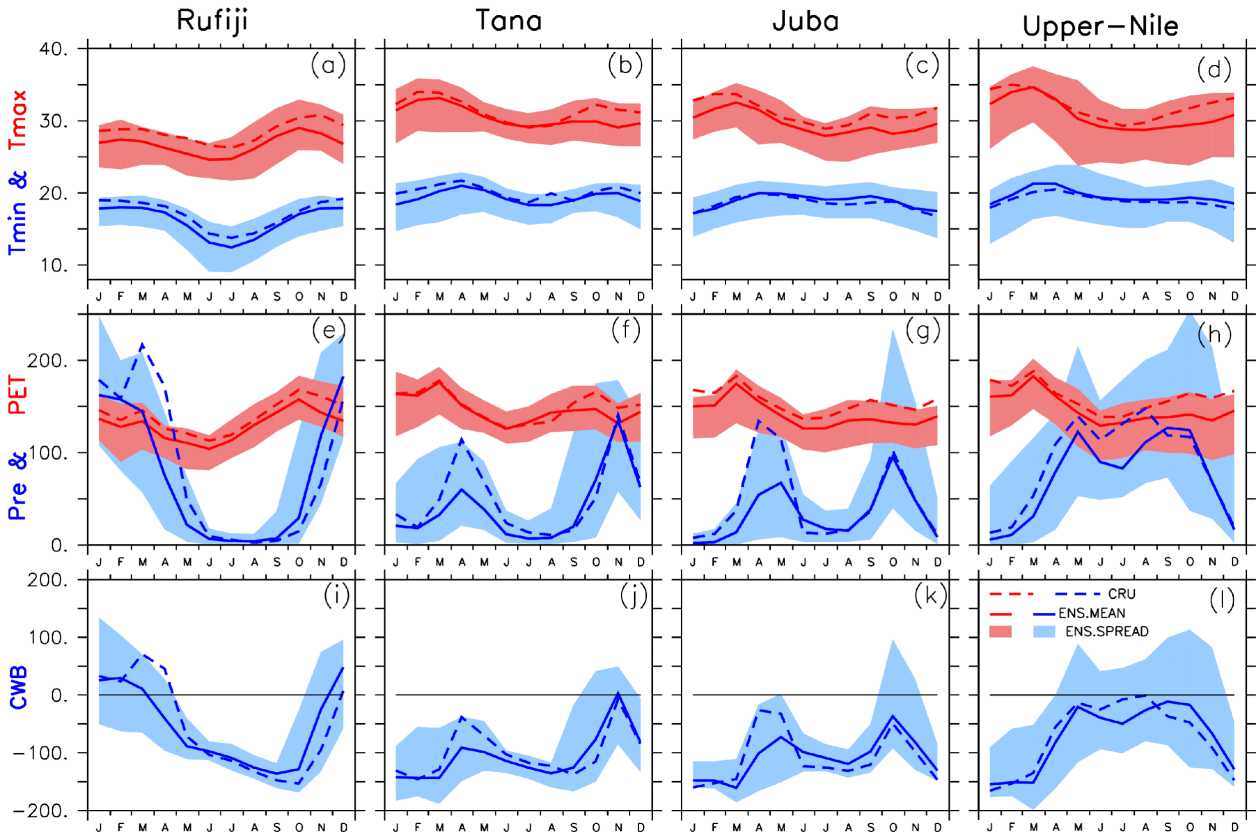

Figure 6.3: *The annual cycle of temperature (Tmax and Tmin(°C)), precipitation(mm/month), PET(mm/month) and CWB(mm/month) over the selected river basins (Rufiji, Tana, Juba and Upper-Nile basins) in the period 1971 to 2000, as depicted by CRU observation and CORDEX model ensemble. In the upper panes, the blue and red colours show TMIN and TMAX,*

respectively; but in the middle panels, they indicate PRE and PET, respectively. The CRU data is presented in a dashed line and the mean of the ensemble is shown by the thick line.

The ensemble mean simulates the extreme drought frequency at the range of the observation (Figs. 6.4 (a)–6.4 (b)) although its range is more confined. While the extreme frequency range of the ensemble simulation is between 0.4 and 0.8 events/decade, the range of the CRU exceeds 1.2 events/decade and goes below 0.4 events/decade (Fig. 6.4 (a)). The simulated narrow band of drought frequency can be due to the cancellation effects of the ensemble mean. In addition, the models overestimate the drought frequency (by > 0.2 events/decade) over Ethiopia, Kenya and central Tanzania and underestimate it (by < 0.2 events/decade) over the southern part of Lake Victoria and north-eastern Somalia. The performance of the models varies over the basins (Fig. 6.4 (g)). While more than 75% of the models overestimate the SPEI-based severe drought frequency over the Rufiji, Juba and Upper-Nile basins, all of them underestimate it over the Tana basin. The model performance also varies with the drought indices. Although the correlation between the spatial distribution of simulated and observed SPEI drought frequency is better for SPEI (r = 0.07) than for SPI (r = -0.003) (and the magnitude of the model biases is lower), the models generally perform better at the average value of the latter than the former over each basin. For instance, less than 75% of the models underestimate the observed SPI drought frequency over the Juba basin, while the median of the simulated values is almost the same as the observed values over the Rufiji and Upper-Nile basins. However, the spread of the drought frequency over each basin is higher for SPI than for SPEI. This is because SPEI incorporates the temperature factor, which the models capture more accurately, thus resulting in less biases as compared to the precipitation variable, which is the only parameter used in the SPI drought estimates. Moreover, Dosio and Panitz (2016) showed that the RCMs can have a better representation of temperature than of precipitation over East Africa, when compared to the corresponding observed data.

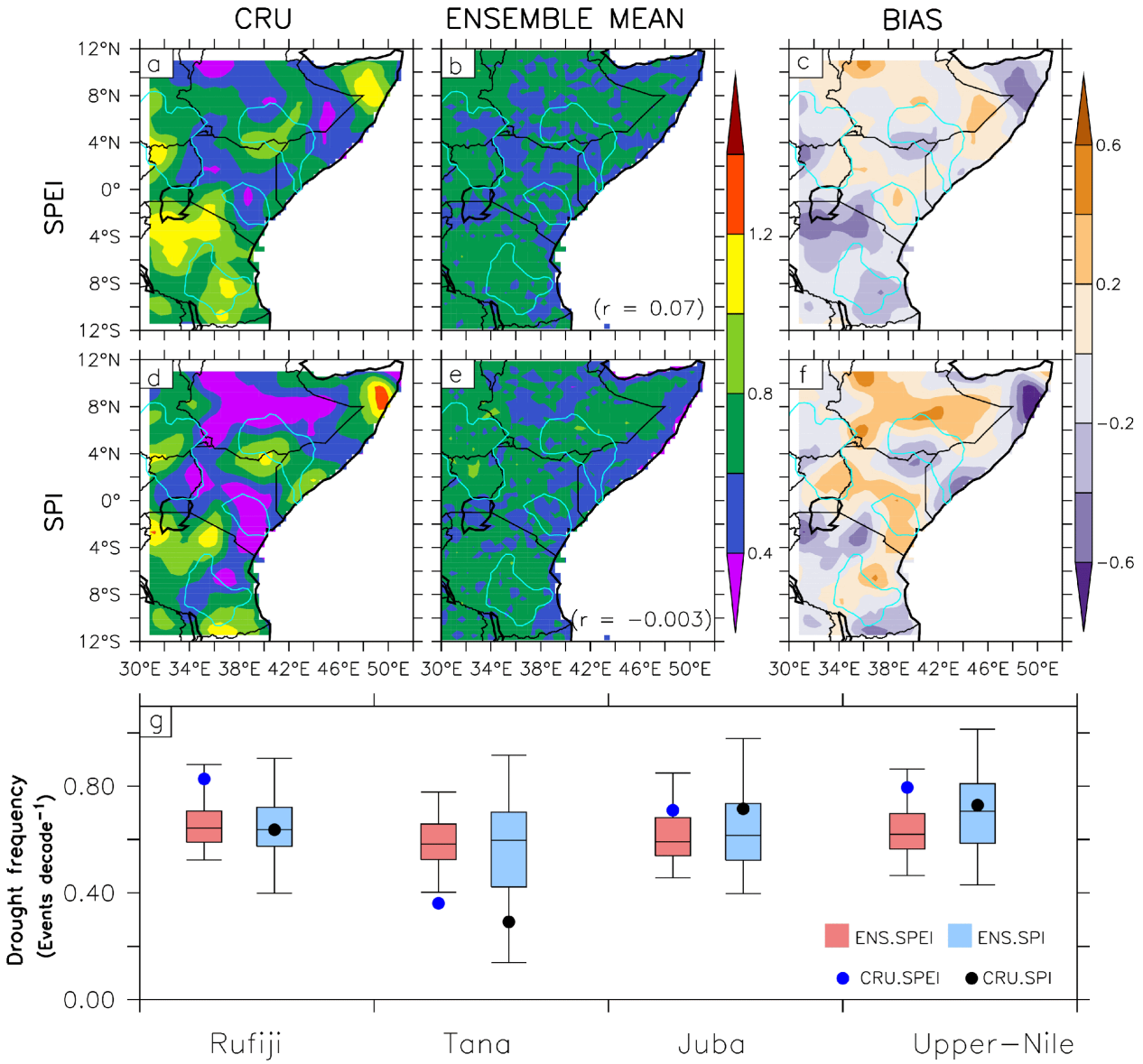

Figure 6.4: *The frequency of severe 12-month droughts (SPEI and SPI) over East Africa (panels (a) – (f)) and over the selected river basins (Rufiji, Tana, Juba, and Upper-Nile) (panel (g)), as depicted by drought frequency for CRU and CORDEX RCMs for the period 1970 to 2000. Panels (c) and (f) show the RCMs bias (RCMs - CRU). The boxplot shows the spread of the simulation ensemble. The location of the basins is shown in light blue.*

6.2 Drought projections

6.2.1 Spatial distribution of droughts over East Africa

The simulation ensemble mean projects an increase in SPEI drought intensity and severe drought frequency over the entire area of East Africa, but the magnitude of the projection varies across the region (Figs. 6.5 (a)–6.5 (d)). The SPEI drought intensity is projected to be more severe over South Sudan and Ethiopia than over the rest of the

region. For example, at GWL1.5, the increase in SPEI drought intensity is between -0.3 to -0.8 over South Sudan and Ethiopia, but between -0.1 and -0.3 over the rest of the region. The least increase in SPEI drought intensity is projected along the equatorial and coastal areas. The spatial pattern of the increase in the SPEI severe drought frequency (Figs. 6.5 (i)–6.5 (l)) is similar to that of SPEI drought intensity. More frequent severe droughts (up to 1.5 events/decade) are projected over the northern and southern interior regions of East Africa, but the increase is lower over the equatorial and coastal regions. Higher temperatures, which increase the PET rate, will increase SPEI drought severity. Hence, the increase in the severity and frequency of the SPEI droughts over East Africa grows with increasing GWLs (Fig. 6.5). For example, the increase in SPEI drought intensity over the northern and southern part of East Africa escalates from -0.3 at GWL1.5 to -1.0 at GWL3.0. And the increase in the severe drought frequency over these areas also jumps from 1 event/decade at GWL1.5 to more than 2 events/decade at GWL3.0. However, the rate of increase in the drought intensity and frequency with increasing GWL is minimal along the coast, possibly because of the cooling and moistening influence of ocean currents along the coast. These results are consistent with those presented by Ozturk et al. (2018), who projected stronger warming and drying over the northern parts of East Africa.

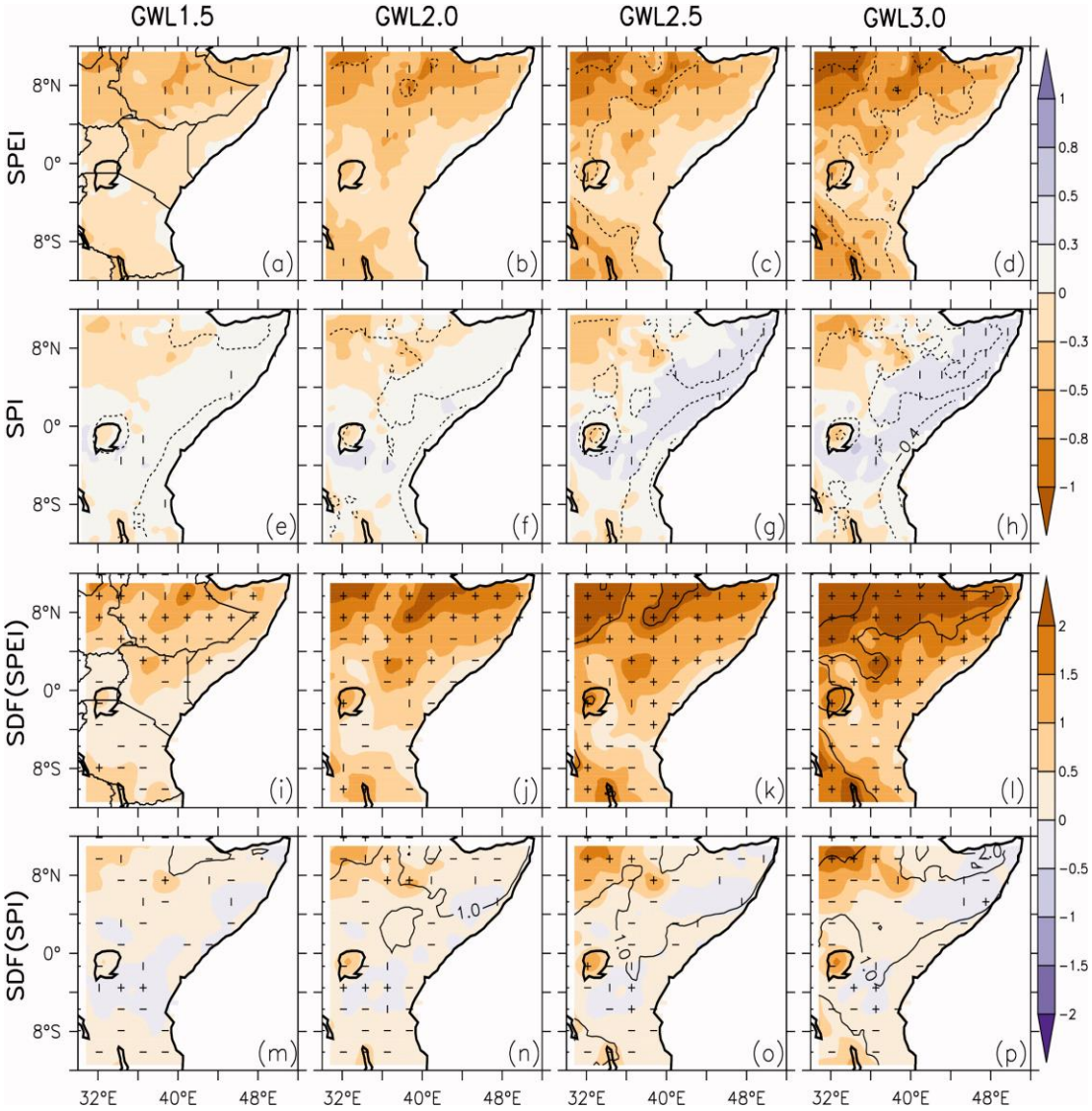

Figure 6.5: *Spatial distribution of the projected changes in 12-month SPEI and SPI drought intensity ((a)-(h)) and severe drought frequency (SDF) ((i)-(p)) over East Africa at different global warming levels (GWLs). The contours over SPEI represent the difference between other warming levels to GWL1.5 and those over SPI represent the difference between the SPEI minus SPI at the respective GWLs. The vertical stipple (|) indicates where at least 80% of the simulations agree on the sign of the changes, while the horizontal strip (–) indicates where at least 80% of the simulations agree that the projected change is statistically significant (at 99% confidence level). The cross (+) shows where both conditions are satisfied; hence the change is robust.*

In contrast to the findings using the SPEI, weak changes are projected for SPI droughts over the East African region (Figs. 6.5 (e)–(h), 6.5 (m)–(p)). For example, at GWL1.5, the projected changes in SPI drought over South Sudan and western Ethiopia range between 0 to -0.3 (compared to -0.3 to -0.8 in terms of the SPEI projections). Over the

same area, the projected increase in the SPI severe drought frequency is less than half of the SPEI projection. Also, the increase in GWL (i.e. from 1.5°C to 3.0°C) produces weaker changes in the SPI drought intensity than when using the SPEI. Furthermore, unlike the SPEI projection, the SPI projection indicates that the increase in GWL encourages drier conditions in some parts of East Africa and wetter conditions in other parts. For example, the increase in GWL from 1.5°C to 3.0°C changes the SPEI from 0 to 0.5 (i.e. inducing wetter conditions) over the coastal and equatorial areas.

A comparison of the SPEI and SPI drought projections clearly shows the contribution of PET to the projected changes in the drought characteristics over this region. For example, the increase in drought intensity (and frequency) over the north-western areas of East Africa can be attributed to both lower precipitation and higher PET. However, the magnitude of the increase in SPEI drought intensity and frequency is higher than that of the SPI, which suggests that the higher PET contributes more than the decrease in precipitation. In contrast, the increase in SPEI drought intensity (and frequency) over the coast and the equatorial region is due to the higher PET, because the changes in SPI suggest wetter conditions. The increase in PET thus plays a crucial role in the enhanced drought intensity (frequency) over the entire East African region, and the role becomes even more important as the GWLs increase. The SPEI and SPI drought intensity and frequency at 3-month scale for season DJF, MAM, JJA and SON are presented in supplementary material.

The SOM classification of the projected SPEI and SPI patterns (Fig. 6.6) reveals various patterns of projected changes in drought intensity from the simulations. According to the classification, the edge nodes (Nodes 1, 4, 9 and 12) show the most extreme four patterns, while the other nodes provide smooth transitions between the extreme nodes. Node 1 shows an increase in drought intensity (i.e. more negative drought index; > 1.4) over the entire East African region, with the least increase (about -0.2) along the coast. This pattern comes from the SPEI projections; the number of simulations that support the pattern increases with increasing GWLs. The pattern of Node 9 is similar to that of Node 1, except that Node 9 indicates there is no change in drought intensity near the equator (± 4° latitude) and along the coast. However, the Node 9 pattern is also from the SPEI projections, and more simulations agree on the occurrence of this pattern at GWL3.0 than at GWL1.5. In contrast to Node 1, Node 12 shows an increase in wet

conditions (i.e. more positive drought index; up to 1.4) over most parts of East Africa, except over a small area in the north-western part of the domain, where an increase in drought intensity (< 0.4) is projected. This pattern is from the SPI projections and its occurrence is more robust at GWL3.0 than at GWL1.5. The other extreme condition is illustrated by Node 4, which indicates a weak change to no change in drought intensity (< 0.2) over the entire East African region. While only one simulation (i.e. d4: RACMO forced by EC-EARTH-r1) suggest this pattern in the SPEI projection at all the warming levels, four simulations suggest it for the SPI projection. Hence, the SOM results provide additional information that was obscured in the ensemble mean projection, shown in Fig. 6.5. For instance, it reveals the possibility of wetter conditions near the equator in SPEI projections (Node 11) and shows the chance of having weak or no change in the drought intensity over most parts of East Africa (i.e. Nodes 3, 4, 7 and 8; accounting for 32% of the projections).

The results of the SOM distribution for drought frequency projection (Fig. 6.7) are similar to those relating to drought intensity (Fig. 6.6). For both drought intensity and frequency projections, most simulations clearly distinguish between SPEI and SPI projections (Figs. 6.6 (b) and 6.7(b)). There are only two cases where a simulation does not show the differences. The first case is for a drought intensity projection (Fig. 6.7 (b)), where a simulation (d4: RACMO forced by EC-EARTH-r1) features the same pattern (Node 4) for both SPEI and SPI at GWL2.5. The other case is for a drought frequency projection, where another simulation (d4: HIRLAM forced by EC-EARTH-r3) indicates the same pattern (Node 4) for both drought indices at all the GWLs. However, the level of the difference between the SPEI and SPI projections is depicted more accurately in SOM classifications than in the ensemble mean.

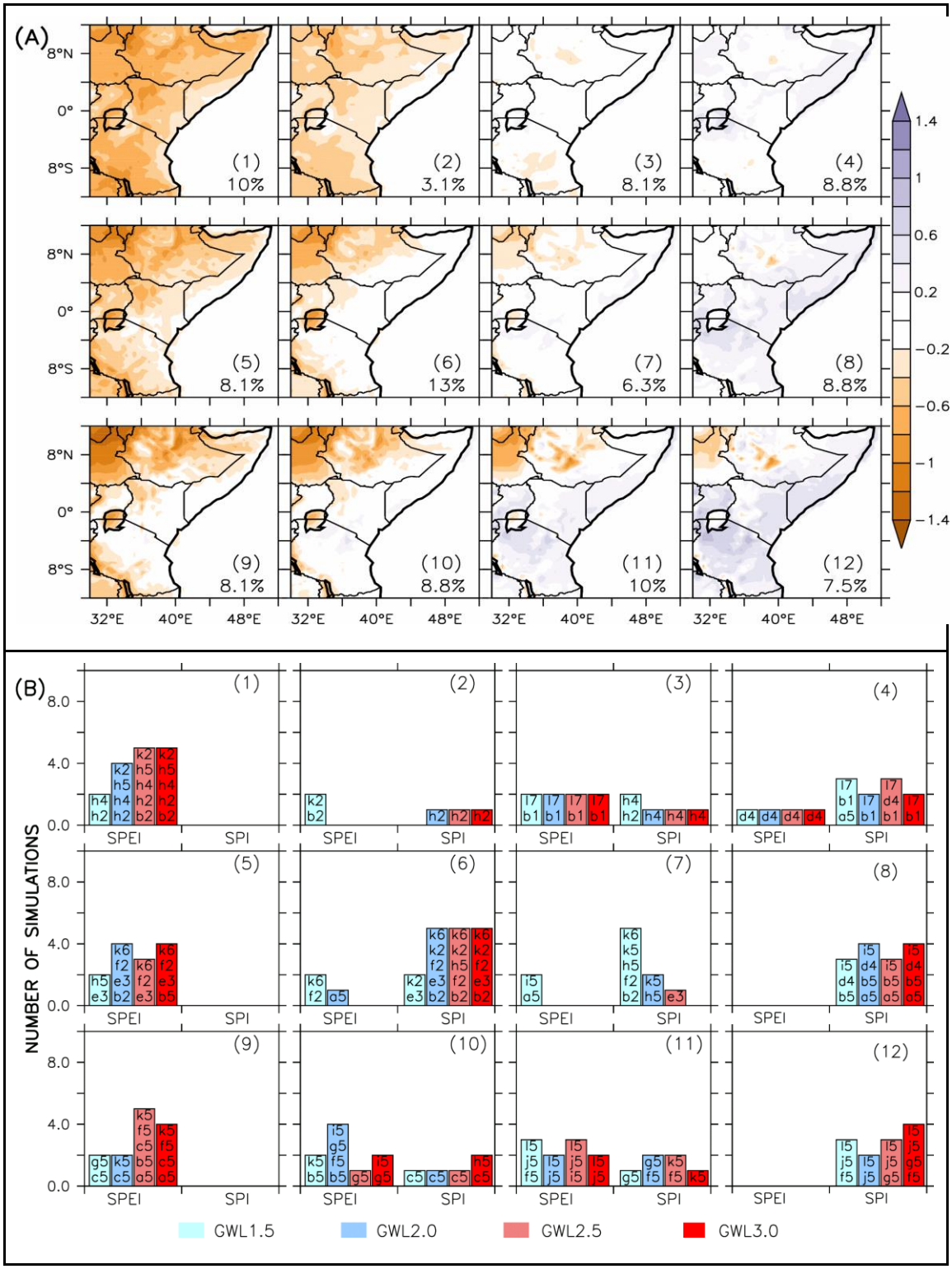

Figure 6.6: *Self Organizing Map (SOM) classification for (a) projected SPEI and SPI drought intensity at different warming levels (b) GCMs and RCMs responsible for the SOM nodes in panel (a) at each warming level. The first letter in the naming of the models represent the global model, while the second letter represents the regional model.*

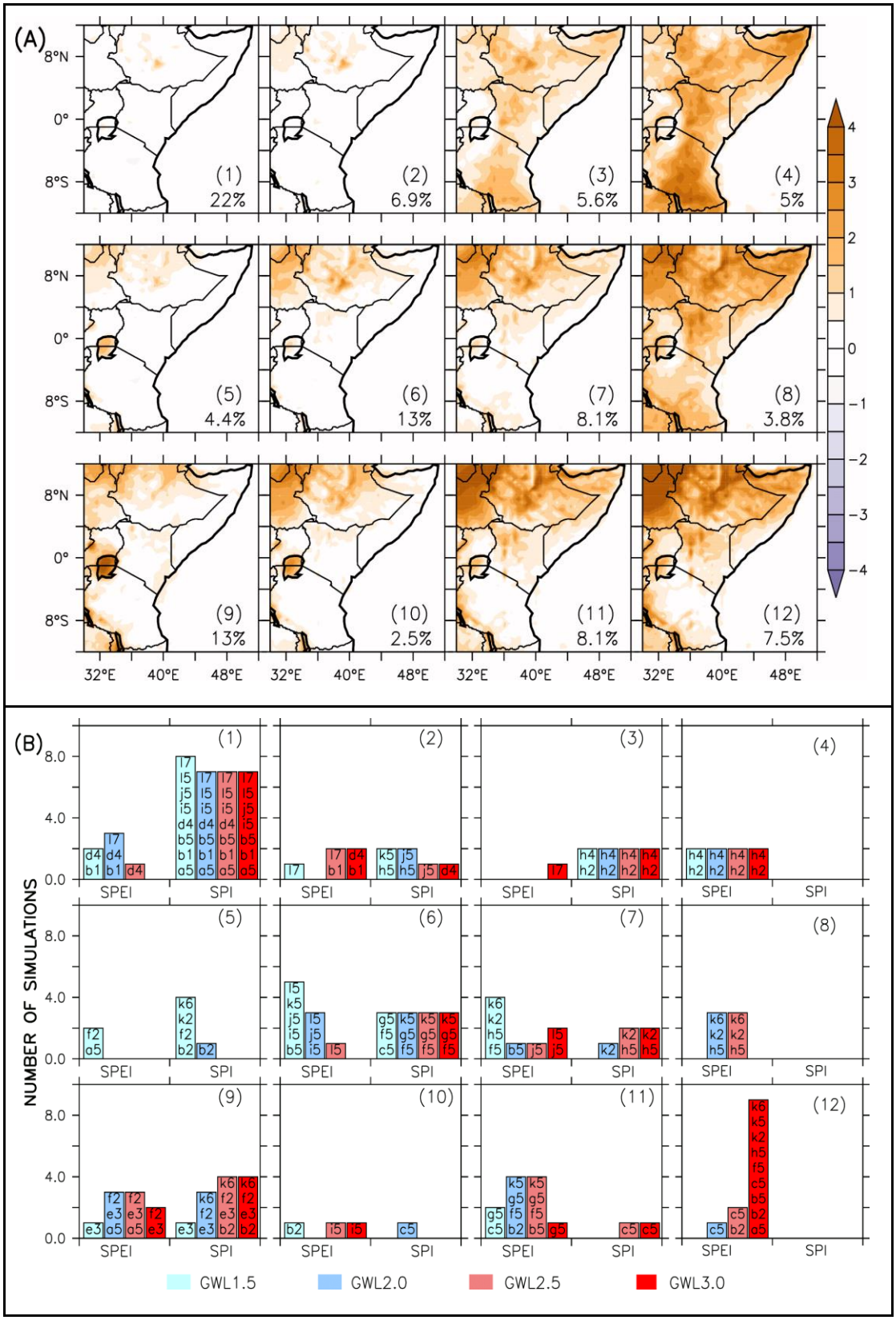

Figure 6.7: *The same as Figure 6.6 but for SPEI and SPI drought frequency.*

6.2.2 Projected changes in drought characteristics over the river basins

The magnitude and robustness (i.e. the agreement between the simulations) of the drought projections over the river basins depend on the drought indices and vary with increasing GWLs (Fig. 6.8). For example, over the Rufiji basin (Fig. 6.8 (a)), the simulation ensemble projects a decrease in SPEI (drying) but an increase in SPI (wetting). However, the magnitude and the robustness of the SPEI projection (i.e. agreement) increases with the GWLs, whereas those of the SPI projections do not vary with increasing GWLs. While less than 75% of the simulations agree on the decreased SPEI at GWL1.5, more than 75% agree on it at GWL3.0; in contrast, less than 75% of the simulations agree on the increase in SPI projection at all GWLs. The same is true for drought frequency (Fig. 6.8 (e)), for which the ensemble mean projects an increase in SPEI and a decrease in SPI. The drought projections over other basins are similar to that of Rufiji, but the magnitude and robustness of the projections are higher over some basins. For instance, the increase in SPEI drought severity and frequency are higher over the Juba and Upper-Nile basins, and more than 75% of the simulations agree on the increase at the various GWLs. In addition, the magnitude and robustness of the SPI projections are higher over the Tana and Juba basins than over Rufiji, especially at GWL2.0 and GWL2.5. Nevertheless, the distinction between the SPEI and SPI projections over all the basins is clear. Over all the basins, the magnitude and robustness of the SPEI drought projections are higher than those of the SPI, suggesting that the projected increase in PET due to global warming may enhance the severity and frequency of future droughts. Hence, using SPI alone to project the characteristics of droughts over these basins may underestimate their severity and frequency. The model simulations of RCP 4.5 show similar characteristics as that of RCP 8.5 at GWL1.5 and 2.0.

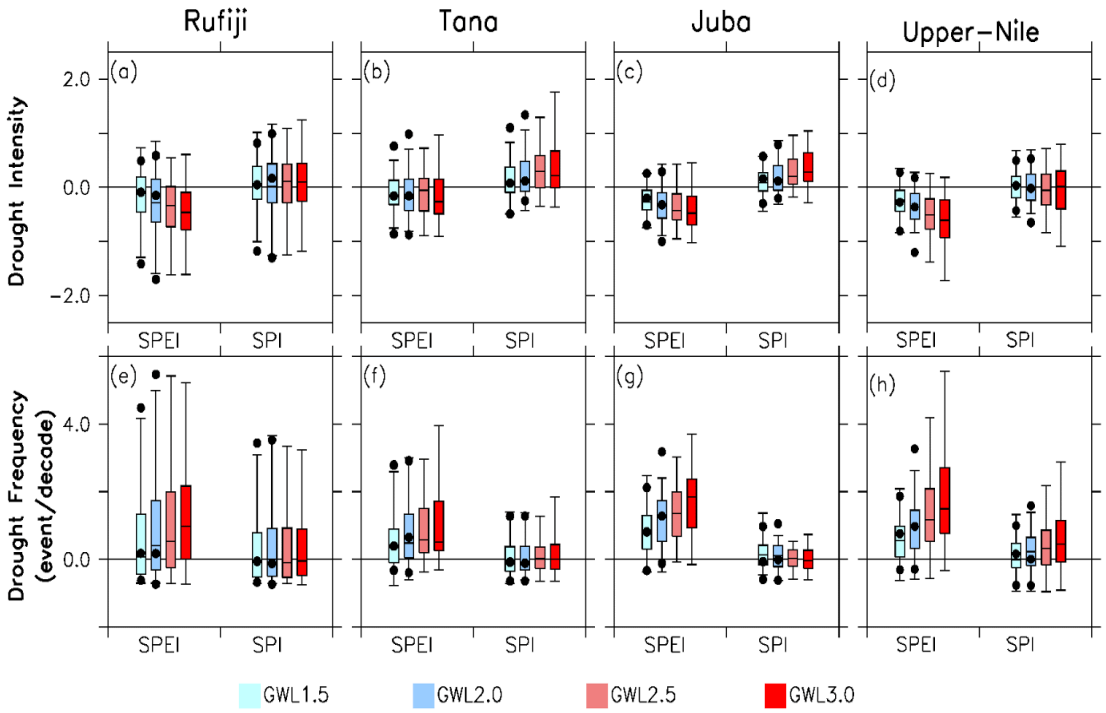

Figure 6.8: *Projected changes in SPEI and SPI drought intensity ((a)-(d)) and severe drought frequency ((e)-(h)) over East African river basins at different warming levels (GWL1.5, GWL2.0, GWL2.5 and GWL3.0) under the RCP8.5 scenario. The corresponding results for the RCP4.5 scenario are indicated with dots where the data are available.*

Based on the differences between the SPEI and SPI projections, two major suggestions can be made on combating future drought risks. Firstly, the greater robustness of the SPEI in characterising drought increases the evidence of future drought risks, but it also makes it possible to lower these impacts by considering some adaptation strategies. Secondly, the higher SPI drought projections over some of the basins suggest that the drought risks can hardly be avoided, because the mitigation measures to combat SPI drought risks are generally ineffective at the basin scale. In addition, when comparing the projections of the two drought indices, it is generally shown that increased evapotranspiration rather than reduced precipitation is the major reason for the higher future drought severity. It can be argued, therefore, that effective management practices to lower evapotranspiration intensities will be able to reduce future drought risks over the East African river basins. Effective management practices include well-organised land use and/or land cover changes that can reduce the amount of water loss through evaporation. Several researchers have proposed this method as the best practice to control drought severity, but it does require prior knowledge to understand what land use and/or land cover change would be the most suitable for the respective basins. For

example, the study of Githui et al. (2009) over the Nzoia catchment area in Kenya has shown decreasing evapotranspiration from the basin when changing the vegetation from tall trees to annual crops. Mango et al. (2011) documented the likelihood of decreasing dry season river flows and increasing peak flows when converting the natural forest to agriculture and grassland. Therefore, the drought projections above provide a solid basis for developing policy and strategy to reduce drought impacts over East African river basins in the future; it also calls for better preparations to be made to improve resilience and develop adaptive options to manage drought risks.

6.3 Summary

The study has examined the impacts of specific GWLs on the characteristics of future droughts in the East African region, with a focus on four river basins. To identify and quantify the role of PET on the drought projections, we used two drought indices (SPEI and SPI) to characterise droughts. Twenty RCM simulations using CORDEX were analysed at four GWLs: GWL1.5, GWL2.0, GWL2.5 and GWL3.0. The performance of the simulations in reproducing East African climate was evaluated by comparing the observed and simulated climate variables for the reference period (1971–2000). The projected changes induced by each GWL were quantified using the difference between the climatic condition for the GWL period and the reference period (i.e. GWL minus reference). Moreover, SOM analysis was employed to classify the projected changes in drought intensity and frequency into 12 groups based on their similarities. Our findings can be summarised below:

- The CORDEX simulation ensemble gives reliable simulations of climate variables over East Africa, although the models struggle to reproduce the observed spatial variations of severe drought frequency over the region. The ensemble mean reproduces the observed annual cycle of the climate variables over the basins but underestimates the temperatures (maximum and minimum) in all seasons. Similarly, while the simulations underestimate rainfall in some months (January–June), they overestimate it in other months (September–December).
- The simulation ensemble mean projects an increase in the intensity and frequency of SPEI droughts over most parts of East Africa, but with a smaller

increase near the equator and along the coast. The magnitude of the increase grows with increasing GWLs.

- Contrarily, at all GWLs, the ensemble mean projects weak changes in the intensity and frequency of SPI droughts over the entire East African region, featuring weak wetting near the equator and weak drying along the coast.
- The SOM classifications of the SPEI and SPI projections reveal that 90% of the simulations correctly distinguish between the SPEI and SPI projection patterns over East Africa. While some SOM nodes feature a substantial decrease in SPEI (drying) over the whole region, some nodes indicate an increase in SPI (wetting) over the entire region.
- The drought projections (intensity and frequency) over the basins are more robust with the SPEI than with the SPI. However, the magnitude and robustness of the SPEI projections are more pronounced over the Upper-Nile and Juba basins than over the Rufiji and Tana basins.

These results can be improved and applied to manage future drought risks throughout East Africa in many ways. Firstly, the quality of the projections can be improved with higher resolution (5–20 km) simulations that capture the interactions between the synoptic-scale features and the local-scale circulations better. This could reduce the model biases and improve the agreement among the models. Such high-resolution simulations are in fact the target of the second phase of CORDEX (Somot et al., 2018). Alternatively, the CORDEX simulations could be bias corrected by incorporating a relevant parameterisation scheme that can simulate more accurately the climate conditions of the region. Secondly, the climate drought projections can be translated to hydrological drought projections using hydrological models. Extending these projections to quantify the potential changes in hydrological water yields (e.g. streamflow, dam levels, soil moisture, and underground water levels) would give results that are more relevant for water resource management. Lastly, a series of land use change sensitivity experiments with hydrological models such as the Soil and Water Assessment Tool (SWAT) (Arnold et al., 2012) could help to identify the most appropriate land use change for mitigating future droughts by reducing the gaps between SPEI and SPI drought projections over the basins. The results of such sensitivity studies would be valuable to local and regional policymakers. However, the present study has also shown that using only rainfall to quantify future droughts in East

Africa may underestimate the severity of such droughts, and that the incorporation of PET may enhance the robustness of drought projections.

Chapter 7

Potential impacts of climate change and land cover change on hydrological droughts in Rufiji Basin, Tanzania

This chapter presents and discusses the results of the potential impacts of climate change and land use change on water availability in the Rufiji River basin in Tanzania, with an emphasis on hydrological droughts over the basin. The results are presented and discussed in four parts. The first part shows how well the GMFD reanalysis represents the annual cycles of climate variables over the Rufiji basin, using the available gauged records. The second section presents the results of the calibration and evaluation of the SWAT model using GMFD climate data as input to the SWAT model. The third section evaluates the performance of the CORDEX simulation dataset with reference to the GMFD reanalysis and shows how bias correction improves the simulation datasets. The fourth and final section shows the response of hydrological drought to LULC and climate changes. The projections, which are based on the RCP 8.5 future climate scenario, are discussed at four specific GWLs 1.5°C, 2.0°C, 2.5°C and 3.0°C.

7.1 A comparison of GMFD with station observations

There is a good agreement between the GMFD reanalysis and the station observation datasets (Fig. 7.1). Over most stations, the two datasets agree on the annual cycles of the climate variables (precipitation, temperature, and wind). For example, they agree that the annual cycle of rainfall is bimodal at Morogoromet (Fig. 7.1 (m)) and unimodal at other stations. The bimodal rainfall pattern at Morogoromet is caused by the passage of the ITCZ over the station twice (following the changes in hemispheric warming), while one long rainfall season over other stations (located further south of the basin) is because those stations fall within the area of the maximum southward position of the ITCZ (Kijazi & Reason, 2012; Nicholson, 1996; Fig. 1.6). Both datasets show that, at Morogoromet, the rainfall is about 6 mm/day^{-1} during the long rainfall season (MAM) and about 4 mm/day^{-1} during the short rainfall season (OND) and that, at the other stations, the rainfall season extends from November to April. They also agree that the Rufiji basin experiences the warmest conditions in DJF and the coldest conditions in

JJA. During OND, the Rufiji basin receives its maximum solar radiation, while during AMJ the insolation is weakest. Therefore, the hot and cold seasons are delayed for at least a month and they extend one extra month. The seasonal variation of wind is also well captured at Iringamet (Fig. 7.1 (s)). Despite such agreement, however, there are notable differences between the reanalysis and station observations (Fig. 7.1). For instance, while the reanalysis overestimates the rainfall at some stations (e.g. Mtandika (Fig. 7.1 (i)) and Mtera (Fig. 7.1 (j)), it underestimates it at other stations. The largest rainfall bias in the reanalysis occurs at Mtandika, where the reanalysis overestimates the rainfall by up to 4 mm per day in FMA. The least bias occurs over Morogoromet and Iringamet (Fig. 7.1 (d)), where the bias is less than 1 mm/day throughout the year. The reanalysis generally overestimates the temperature over the basin, but the magnitude of the bias is higher at Iringamet (Fig. 7.1 (p)) and Mbeyamet (Fig. 7.1 (q)) (up to 5^{o}C for Tmax) than at Morogoromet (Fig. 7.1 (r)). The temperature differences could be because Iringamet and Mbeyamet are located at a higher altitude, i.e. 1369 m and 1715 m above sea level respectively, as compared to Morogoromet (503 m); consequently, stations in colder climates experience large temperature deviation from the reanalysis dataset, while the stations in warm climates have relatively less deviation.

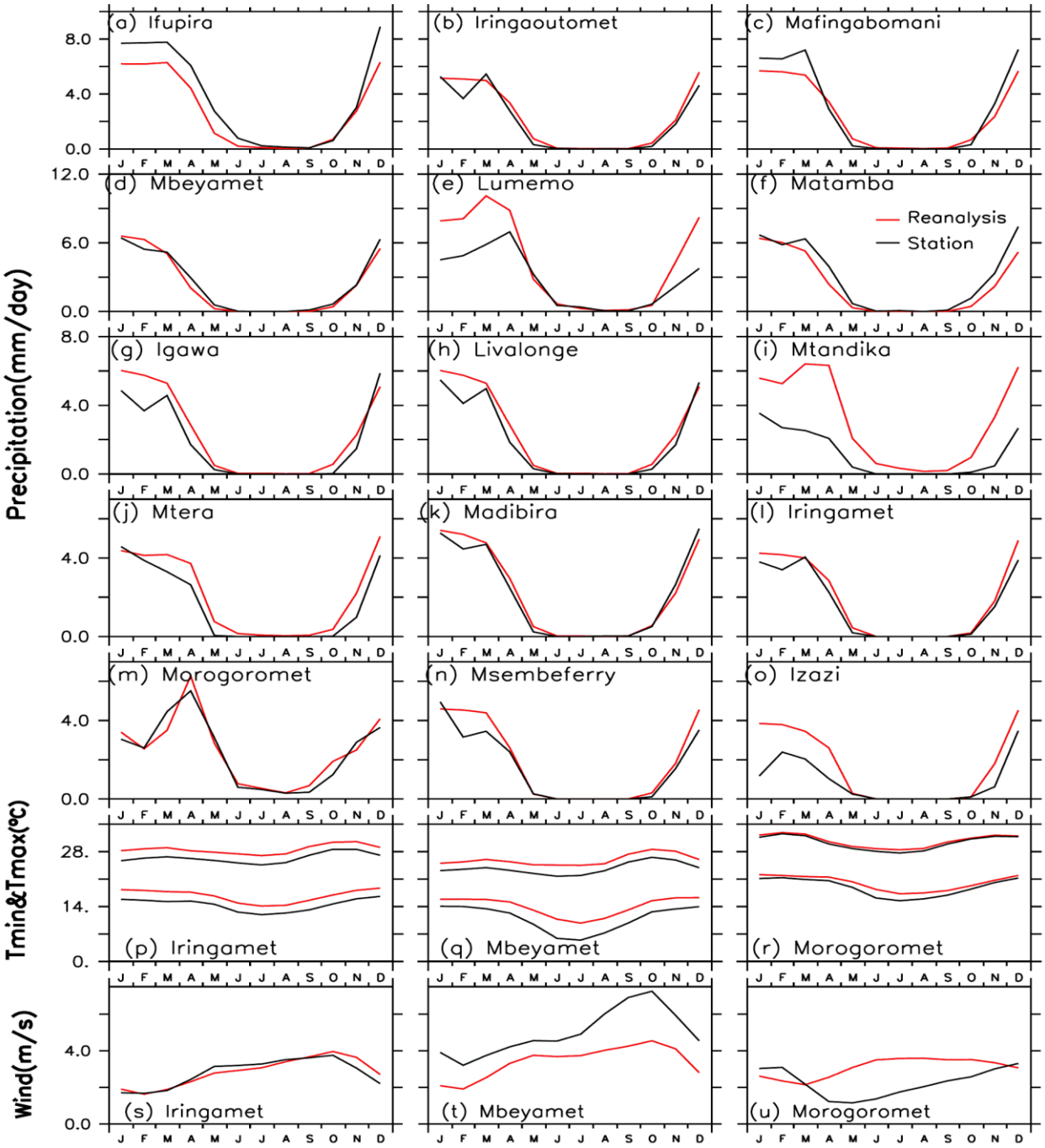

Figure 7.1: *A comparison of GMFD and the observed annual cycle of climate variables over some meteorological stations in the Rufiji River basin.*

7.2 Calibration and validation of SWAT model

The simulation setup of the SWAT model using the 2010 land use map and the GMFD climate data were used to calibrate and validate the streamflow in the Rufiji river basin. Fig. 7.2, which presents the simulated and observed streamflow during the SWAT

calibration period (1976–1980) and validation period (1995–1999), shows that the calibration improves the quality of the simulations. In 1976–1980, the calibration increases R^2 from 0.80 to 0.82 and NSE from 0.30 to 0.73, and, in 1995–1999, it increases R^2 from 0.49 to 0.61 and NSE from 0.14 to 0.31. According to Moriasi et al. (2007), our NSE and R^2 perform very well for the calibration period, but poorly during the validation period. The lower performance of the calibrated SWAT in 1995–1999 than in 1995–1999 could be due to the characteristics of the observed streamflow used for calibrating the model (in 1995–1999) differ from those of 1995–1999. Unlike the validation phase, where the observed streamflow is underestimated in some years (e.g. 1996) and overestimated in others (e.g. 1997), in the calibration period, the observed streamflow was underestimated during the peak months throughout the time period. The inconsistency between simulated and observed streamflow may thus be due to the limitation of the curve number method used in the SWAT model, as this considers the average daily rainfall depth instead of intensity and duration (Nie et al., 2011). Generally, however, the calibration processes added value to the model output, although we were unable to improve it further to the level where it would be much more precise, as observed in the validation period. The SWAT model thus simulated by using the calibrated parameters was applied to evaluate the hydrological drought projections to LULC and climate changes.

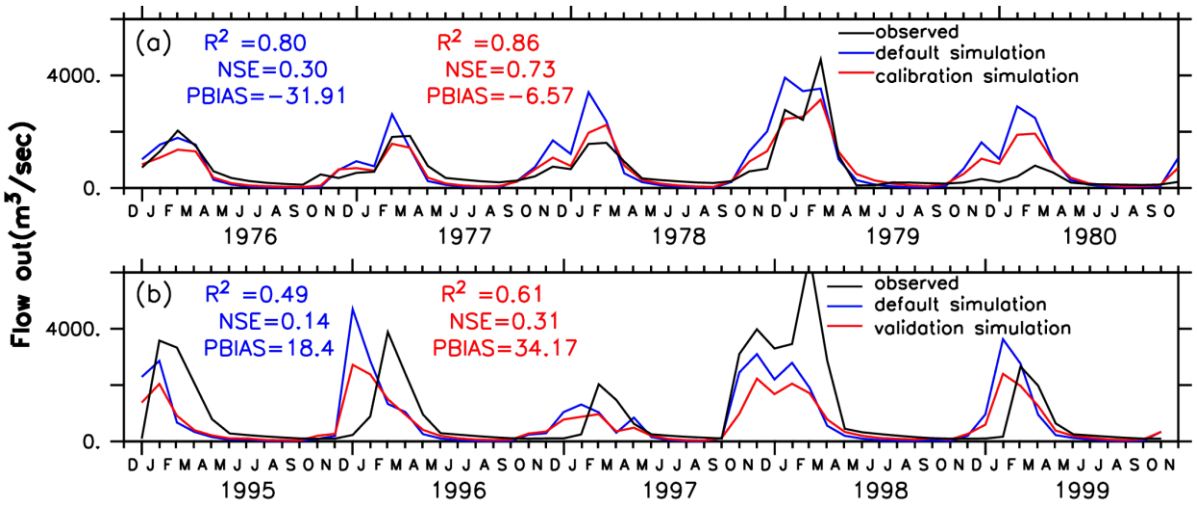

Figure 7.2: *A comparison of simulated and observed station stream flow during (a) calibration and (b) validation periods.*

7.3 Climate model evaluation and impacts of bias correction

In this section, we evaluate the ensemble model's performance by comparing the results with the reanalysis data over the Rufiji basin. The evaluation is done for 1971 to 2000, which is hereafter referred to as the reference period. The comparison between the raw ensemble and the bias corrected ensemble is also presented, so as to see the improvement of the ensemble after bias correction. The variables considered for evaluation are grouped into two sections: (a) Climate parameters that are the input to the SWAT model (e.g. solar radiation, temperature, and precipitation), and (b) Hydrological parameters that are the output from the SWAT (e.g. potential evapotranspiration (PET), evapotranspiration (ET), soil water (SW), percolation (PER), surface runoff (SF), water yield (WYLD), and flow out (FLOWOUT

The original CORDEX simulations with their ensemble mean reproduce well the seasonality of climate variables over the Rufiji basin (Fig. 7.3 (a)-(e)). In good agreement with the reanalysis, the ensemble simulation reproduces the dry, wet, cold and hot seasons over this region. It simulated the minimum solar radiation in MAM and the maximum in SO (Fig. 7.3 (a)). The coldest season of June-July and the warmest season of NDJF are also well presented (Fig. 7.3 (b), (c), (d)). With regard to precipitation, the ensemble shows a peak in the rainy months of NDJFM and the driest months in JJASO (Fig. 7.3 (e)). This shows that the ensemble captures the larger scale systems such as the ITCZ that control the major precipitation season over this region. Nevertheless, there are notable biases in the ensemble in representing the season's climate parameters. For example, the ensemble temperature (min, max and average temperatures) are shown to be lower than the reanalysis by ~2^{o}C through the seasons. The ensemble underestimation of temperature could also affect the projections by delaying the time at which the GWL increases. The solar insolation is overestimated by ~ 10-30MJM-2D-1. As was the case with regard to the precipitation, the ensemble generally underestimates the rainfall in JFMAM (~ 30mm/day) and overestimates it in ND (~10mm/day). The seasonality of the hydrological variables is also well captured by the ensembles (Fig. 7.3 (f)- (q)), especially for variables PET, ET, SF, and WYLD. However, the ensemble underestimates SW during March-September and overestimates it in November-February. With regard to the stream flow, the ensemble

generally overestimates the intensity throughout the year, in particular during November-March, which is the season of high rainfall.

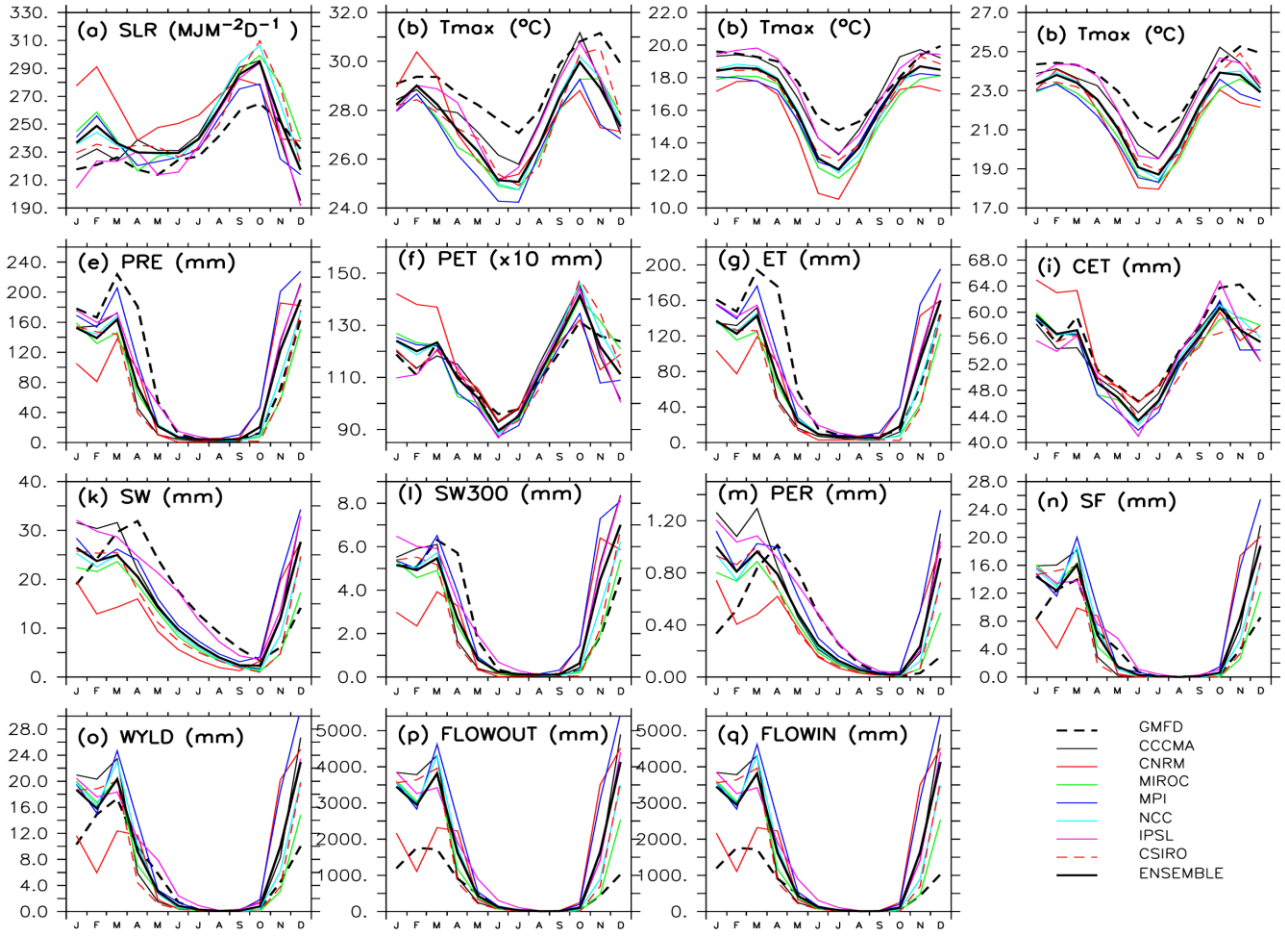

Figure 7.3: *A comparison of SWAT variables climatology (1971-2000) for Reanalysis (GMFD) and non-biased corrected CORDEX models averaged over the entire Rufiji basin.*

The ensemble mean captures some parts of the complex spatial structure of the climatology of both climate and hydrological variables over the basin (Figs. 7.5 – 7.8 of GMFD and CONTROL). For example, the variables SW, PER and WYLD are well represented, especially in the northern parts of the basin. Biases are however noticeable for most parts of the basin and for almost all parameters involved. While some variables are underestimated, e.g. solar radiation, others are overestimated, e.g. temperature. The ensembles moreover overestimate the spatial climatology mostly in the southern part of the basin, while underestimating it in the central part of the basin.

The results from this analysis indicate that the bias correction method QDM decreases the bias of the climate models for all the climate and hydrological variables. The bias ensemble clearly shows improvement in presenting the seasonal intensity (Fig. 7.4) as well as spatial climatology (Figs. 7.5-7.8 of GFMD and QDM) over the Rufiji basin. For example, the bias in temperature has clearly removed for both seasonal (Fig. 7.4 (b), (c), (d)) and spatial (Fig. 7.5 (j), (o), (t)) estimates. However, the bias method in some cases slightly underestimates the parameters (e.g. Fig. 7.4 (a), (o), (p), and (q)), while overestimating it in other cases (Fig. 7.5 (e), Fig. 7.6 (j)). And in some instances, the difference between the bias and control ensembles is negligible. For example, the seasonal climatology of precipitation (Fig. 7.4 (e)) and evapotranspiration (Fig 7.4 (g)) do not show improvement from the bias correction process.

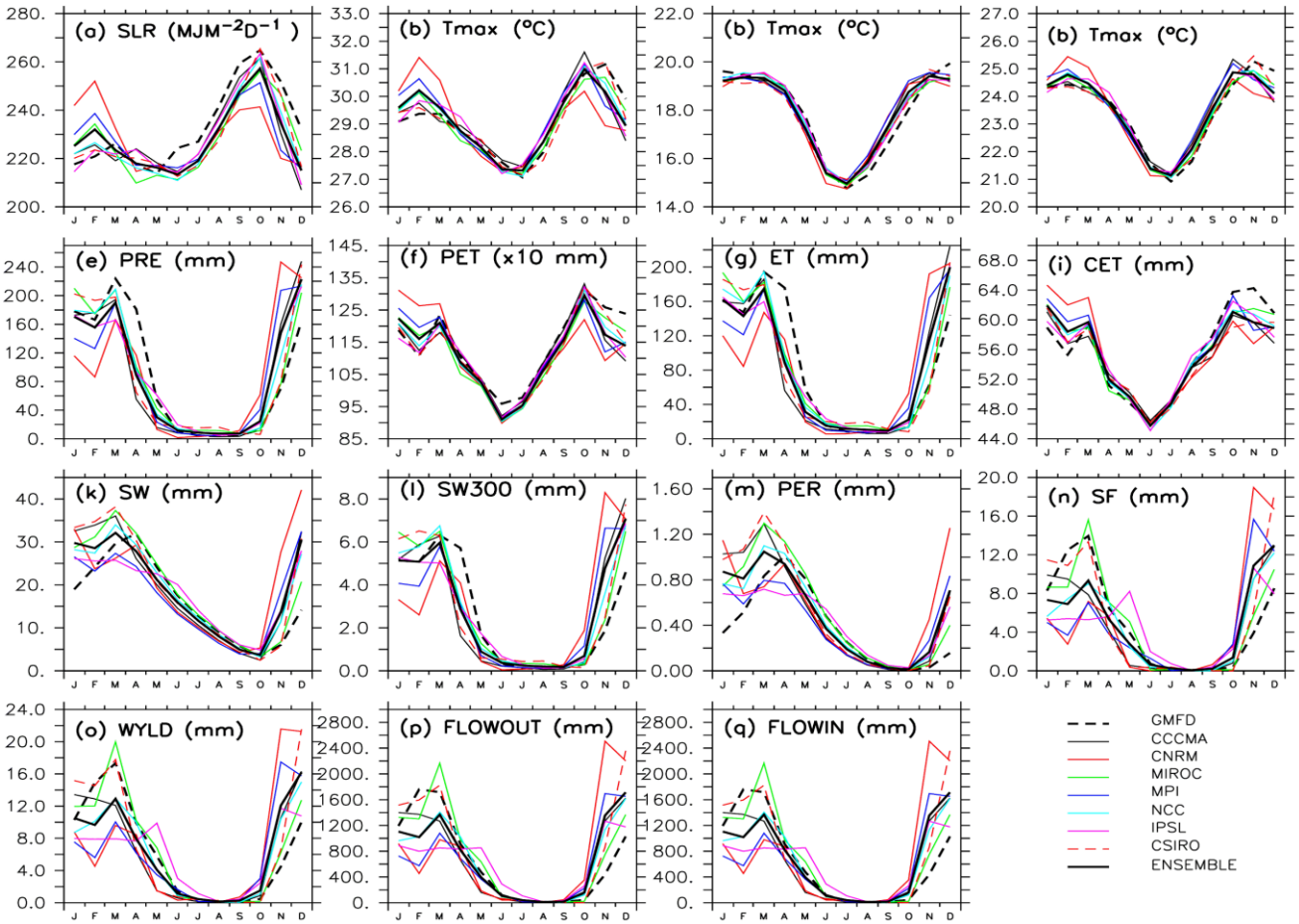

Figure 7.4: *The same as Fig. 7.3 but for GMFD and bias corrected CORDEX models.*

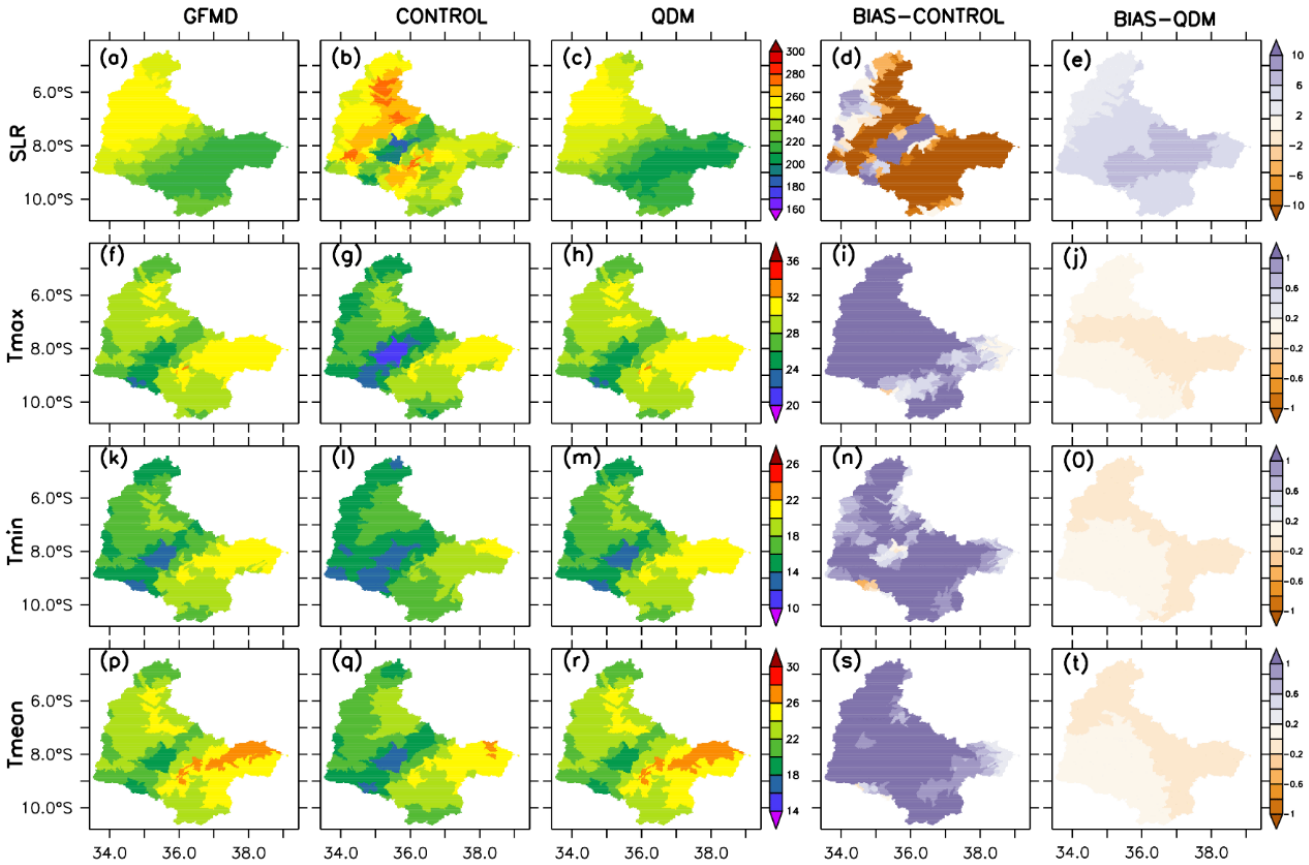

Figure 7.5: *Climate variables (i. e solar radiation: SLR; temperature: Tmax, Tmin and Tmean) comparison between reanalysis (GMFD), unbiased corrected ensemble (CONTROL), and biased corrected ensemble (QDM) over the Rufiji basin for 1971-2000. BIAS-CONTROL and BIAS-QDM correspond to the difference between CONTROL minus GMFD and QDM minus GMFD respectively.*

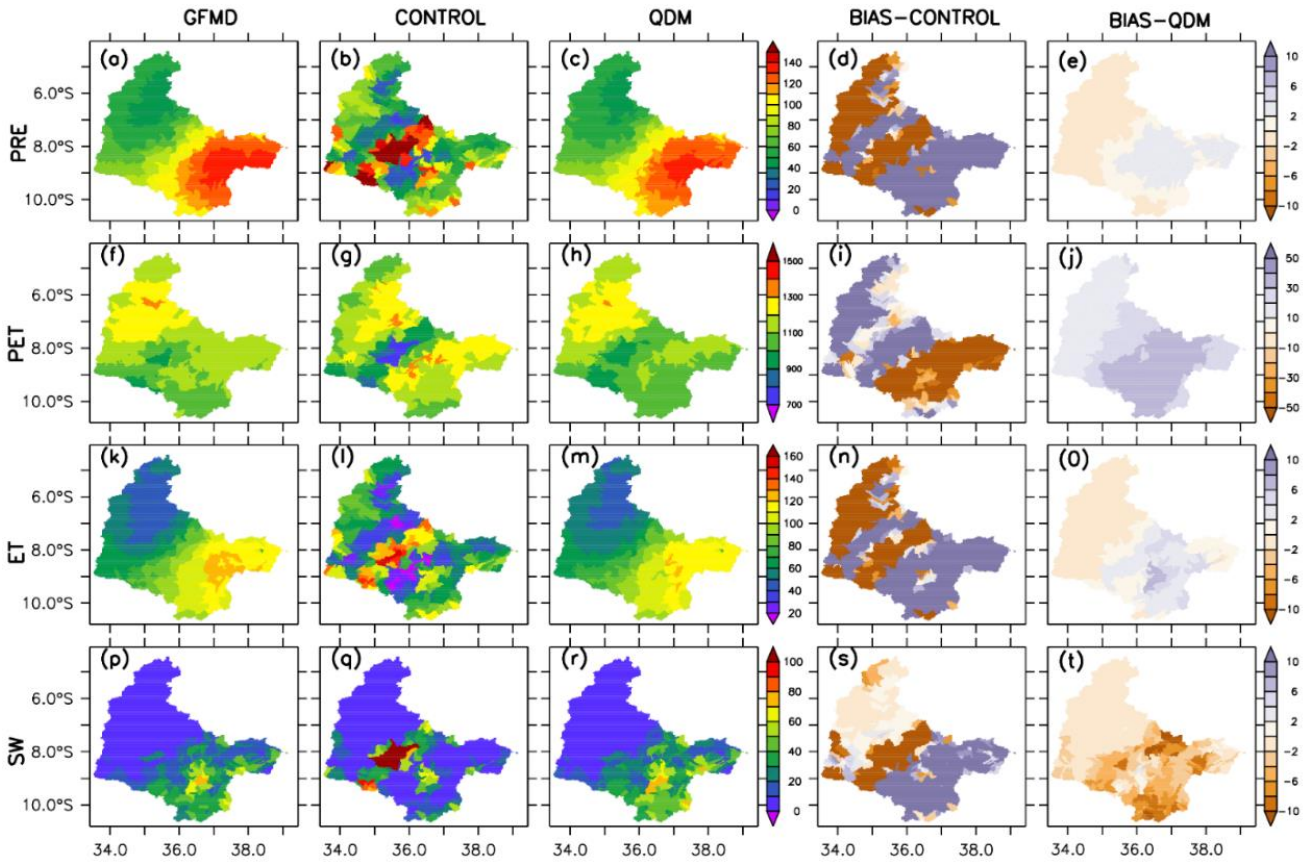

Figure 7.6: *The same as Fig. 7.5 but for precipitation (PRE), potential evapotranspiration (PET), evapotranspiration (ET) and soil water (SW).*

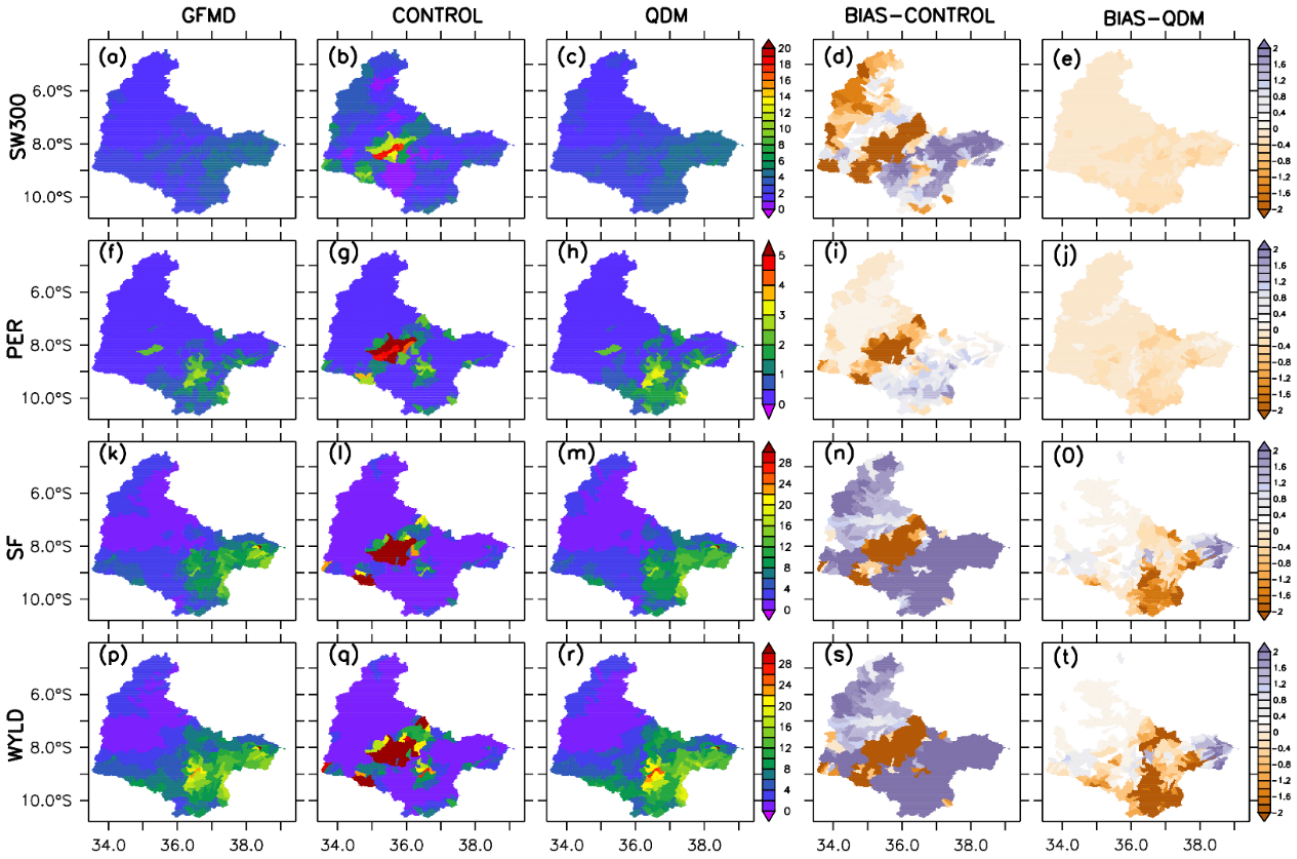

Figure 7.7: *The same as Fig. 7.5 but for soil water at 300 (SW300), percolation (PER), surface runoff (SF) and water yield (WYLD).*

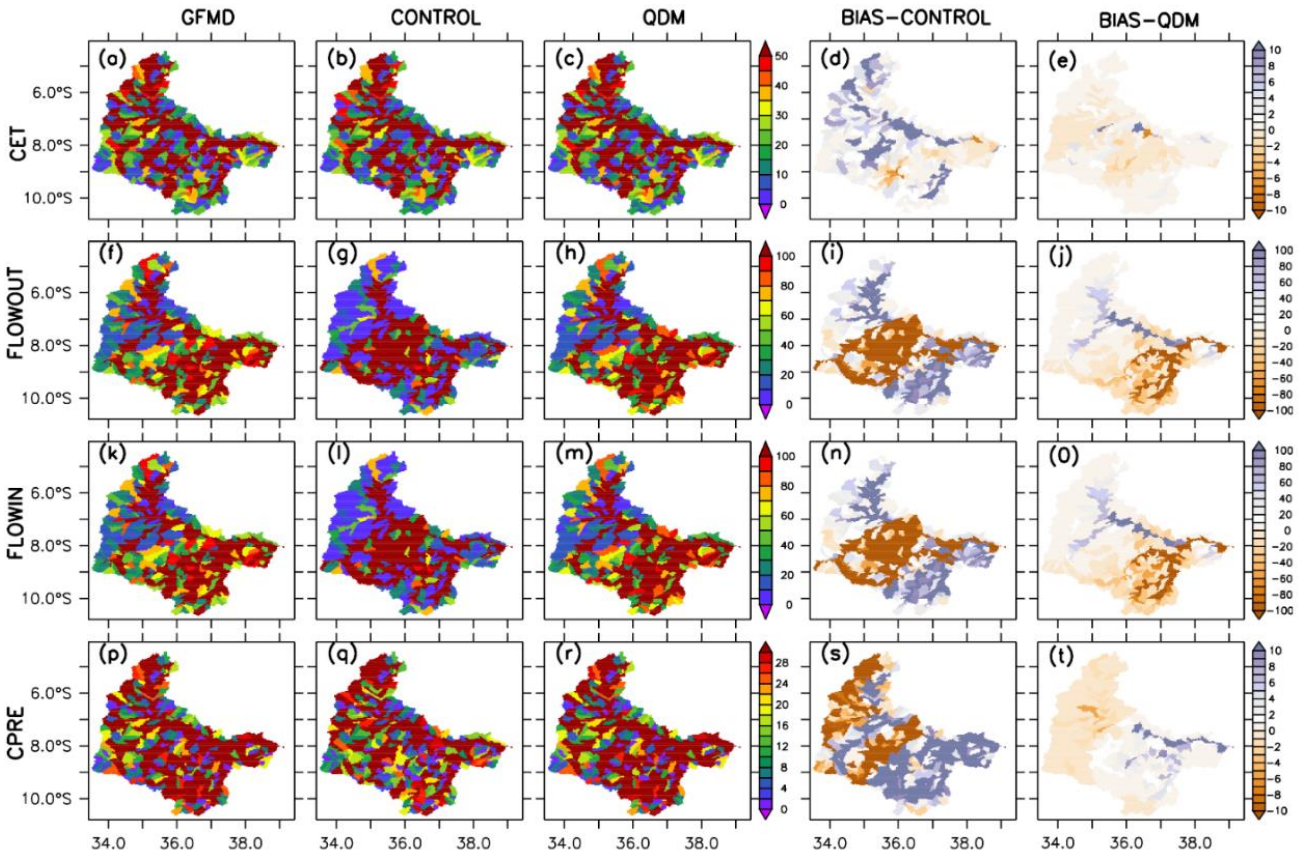

Figure 7.8: *The same as Fig. 7.5 but for channel evapotranspiration (CET), flowout, flowin and channel precipitation (CPRE).*

7.4 Impact of global warming increase on hydrological variables and hydrological drought

Figs. 7.9, 7.10, and 7.11 show the effect of global warming level increases in RRB for selected climate and hydrological variables under the LULC of 2010. The ensemble mean shows an increase in the mean temperature ranging from 1^{o}C at GWL1.5 to ~3^{o}C at GWL3.0; in the western parts of the basin, it increases by more than 3^{o}C. The projected increase in PET ranges from ~1mm to greater than 6mm at GWL3.0. For variable solar radiation, the change is towards increasing only in the central and southern parts of the basin, although in the rest of the basin, solar radiation is projected to decrease from ~ -2 to -5. Precipitation is also projected to increase in most parts of the basin by approximately 1mm between GWL1.5 to 2.0, but not much changes from GWL2.0 to 3.0. The ensemble mean projected an increase in evapotranspiration throughout the basin, although it is more pronounced in the northern part of the basin

than in the southern part. In the north, ET increases by ~4mm at GWL3.0. The changes in the soil water are not homogeneous either: in the north, the ensemble projects no changes in soil water with increasing GWL, but over the central part, there is a decrease in soil water, especially from GWL1.5 to 2.0, and no changes at GWL2.5 and 3.0. As for percolation and surface runoff, no changes are projected at different GWLs in the basin; for water yield and flow out, the decreasing condition is projected only in the central part of the basin and no noticeable differences occur elsewhere. Therefore, in RRB, the impact of an increase in global warming appears not to have much effect on the hydrology system, except for evapotranspiration, which is mostly controlled by temperature. However, the changes can mostly be projected on the climate parameters.

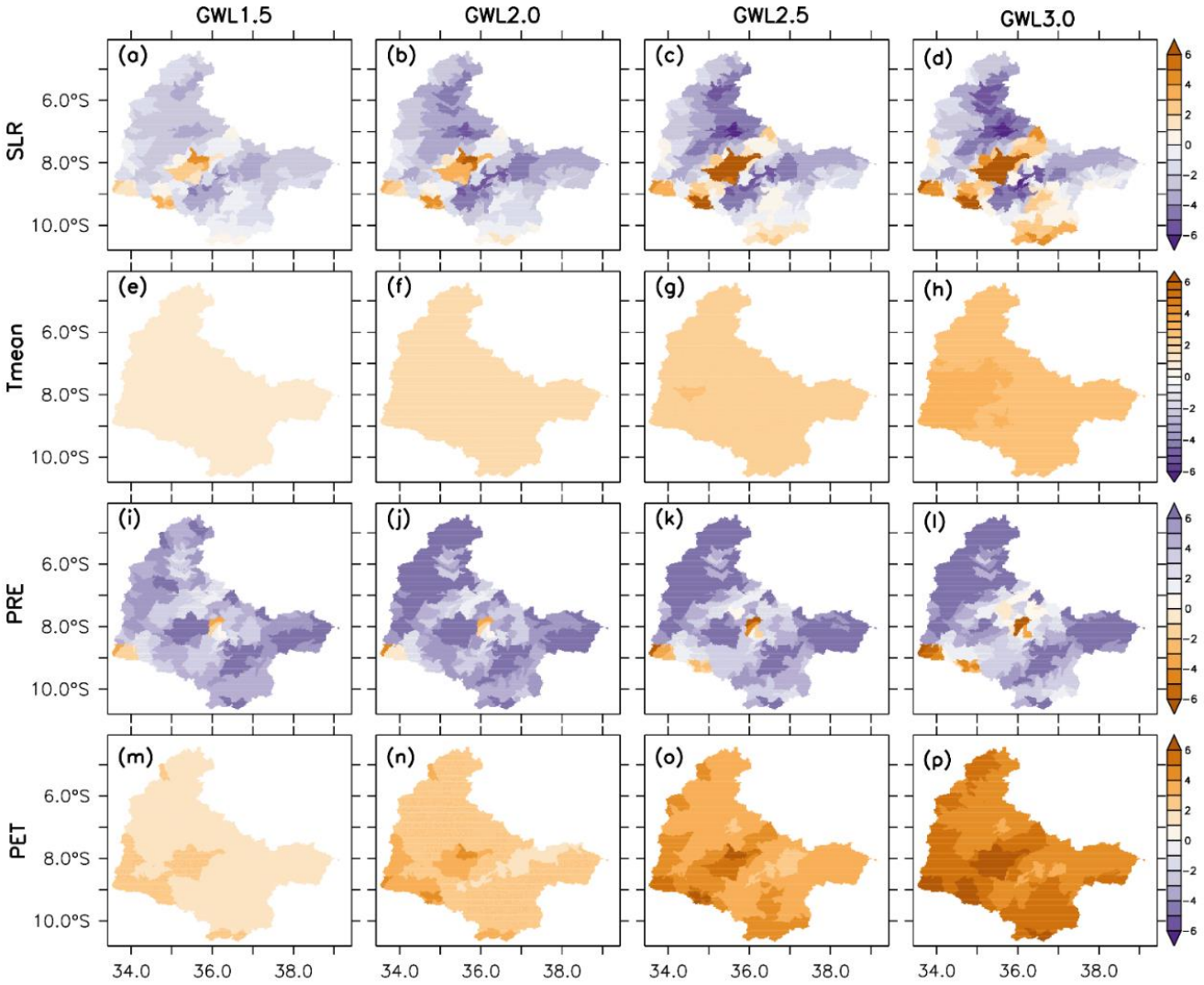

Figure 7.9: *Climate variables (i.e. solar radiation: SLR; temperature: Tmean; precipitation: PRE; potential evapotranspiration: PET) for bias corrected ensemble at different global warming levels (GWL1.5, GWL2.0, GWL2.5,GWL3.0) over the Rufiji basin.*

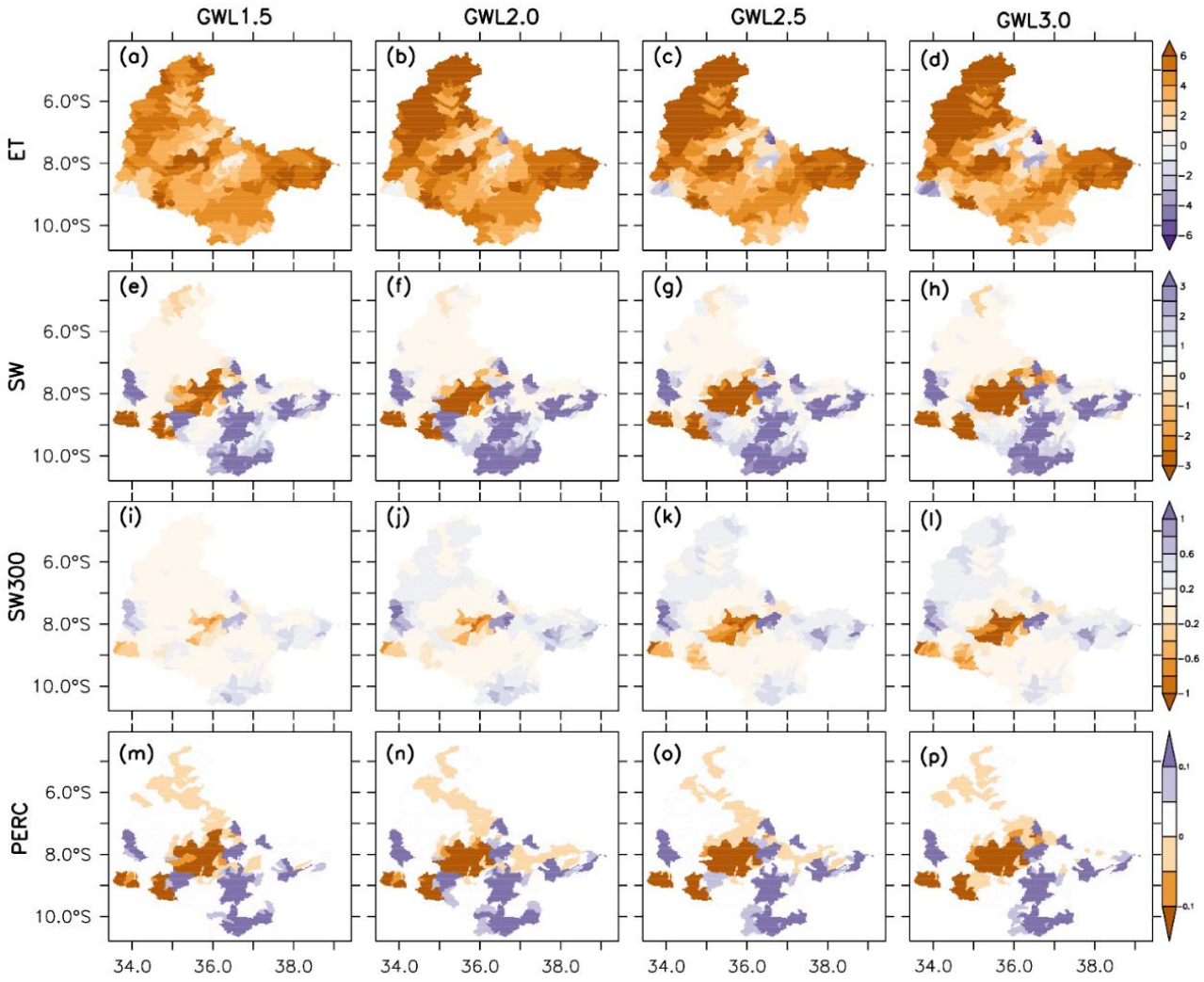

Figure 7.10: *The same as Fig.7.9 but for evapotranspiration (ET), soil water (SW), soil water at 300 (SW300), and percolation (PERC).*

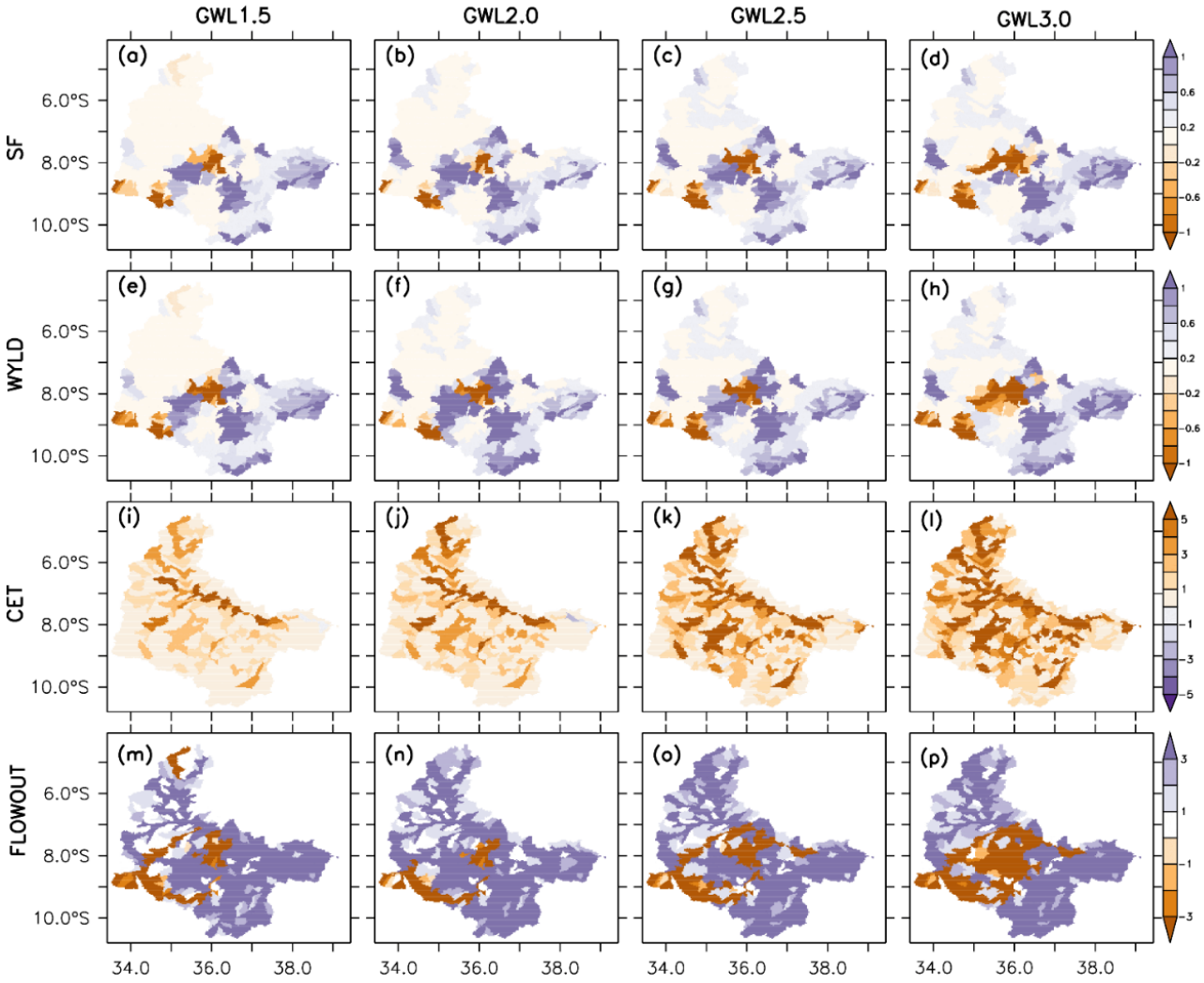

Figure 7.11: *The same as Fig.7.9 but for surface runoff (SF), water yield (WYLD), channel evapotranspiration (CET), flow out, flow in and channel precipitation (CPRE).*

Fig. 7.12 shows the effect of the various global warming levels on hydro meteorological drought indices (SPEI and SPI), soil water index (SWI), surface runoff index (RFI), water yield index (WYI) and channel flowout index (SFI) in RRB (under the LULC of 2010). The ensemble mean shows an increase of SPEI drought intensity from 0.3 to 0.8 for GWL1.5 and 3.0, respectively. But for SPI, the drought intensity change with increasing GWLs is unnoticeable. With regard to drought frequency, SPEI also shows an increase as the GWLs increase, whereas the SPI projections show no changes in drought frequency. This result is similar to that of Nguvava et al. (2019), reported in the previous chapter. Over the RRB the drought intensity and frequency are projected to increase at higher warming levels under SPEI, but no changes are projected over the

basin under SPI. While the ensemble mean does project an increase in evapotranspiration, which intensifies the SPEI drought intensity and frequency, the ensemble mean also projects some wetter conditions in most parts of the basin and therefore no changes in SPI drought intensity and frequency, because SPI is the product of precipitation alone (Fig. 7.9).

With regard to the hydrological drought index SWI, the drought intensity and frequency show no changes, as the ensemble mean at different GWL remains at zero. This means that the projection of SWI intensity and frequency over the RRB does not show any changes at increasing GWLs. The ensemble mean projection of RFI shows some increase in drought intensity, especially from GWL1.5 (intensity ~0.1) to GWL2.5 (intensity ~ 0.3), but a slight decrease at GWL3.0 (intensity ~0.2). RFI drought frequency is however projected to decrease with increasing GWLs. At GWL1.5 the RFI frequency is ~20 events/decade but at GWL3.0 the frequency is ~8events/decade. In the RFI, the intensification of drought intensity corresponds to a reduction in drought frequency. Similar projections as RFI are also shown for index SFI, although the intensity and frequency of SFI is less than that of RFI. As for WYI, the ensemble mean projects a decrease in both drought frequency and intensity as GWL increases. For example, at GWL1.5 WYI drought intensity is ~0.1 but at GWL3.0 it is ~0; its frequency is ~ 8 events/decade at GWL1.5 and less than 0 events/decade at GWL3.0.

Therefore, over RRB, while the projected increases in GWL may intensify SPEI drought (i.e. leading to higher intensity and frequency) and river flow drought (RFI and SFI), it may reduce the intensity of SPI, SWI and WYI drought. Increasing SPEI intensity and frequency could be because of higher PET rates projected in RRB (Fig. 7.9 (m)-(p)). Likewise, with regard to river flow drought, Fig. 7.11 (i)-(l) shows higher channel evapotranspiration projected with increasing GWL, which may contribute to increasing drought intensity and frequency for these variables. The decreasing drought projections for SPI, SWI and WYI could be because these drought variables are mostly affected by the precipitation factor, which is projected to increase with GWL in some parts of the RRB (Fig. 7.9 (i)-(l)).

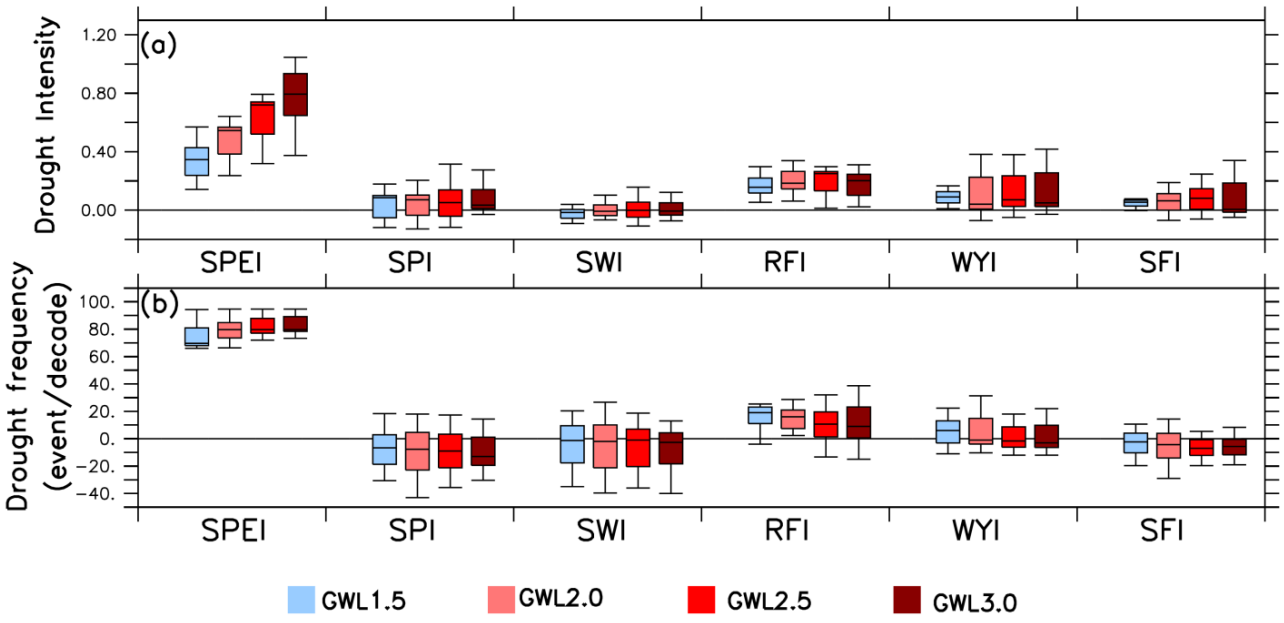

Figure 7.12: *Projected changes in hydro meteorological (i.e. SPEI; SPI; soil water index: SWI; surface runoff index: RFI; water yield index: WYI; channel flowout index: SFI) drought intensity (a) and severe drought frequency (b) over the Rufiji River basin at different warming levels (GWL1.5, GWL2.0, GWL2.5 and GWL3.0) under the RCP8.5 scenario using 2010 land use cover maps.*

7.5 Response of hydrological variables and hydrological drought to LULC

Figs. 7.13 and 7.14 show the variations of different hydrological variables, i.e. evapotranspiration, soil water, percolation, surface runoff, water yield and flow out on the spatial scale between the different land use scenarios. Among the four land uses proposed, the projection of all hydrological variables is more pronounced (for both increase and decrease intensity) with increased forestry land use but for other land uses, the changes were minimal and sometimes no changes were observed. Under forestry, evapotranspiration increases in the northern half of the basin and decreases in the southern half. This could be caused by the higher PET demand shown in the northern part as compared to the southern part of the basin (Fig. 7.6 (h); forestry increases the transportation of deep water to the atmosphere from the deep roots of woody plants and ensures that the demand of the atmosphere is achieved. For other land uses evapotranspiration does show changes but the magnitude of these changes is lower than forestry. With soil water, forestry shows an increasing capability of the land to retain water by more than 0.5mm but agriculture, cropland grassland and shrubland generally

show a decreasing condition, especially in the south-central part of the basin. Forests retain surface soil moisture because woody plants, unlike shrubs and small vegetation, do not use surface water for evaporation because of their deep roots; in contrast, small plants do use surface water because of their shallow roots and because there is not enough shade to avoid direct soil water loss by evaporation. This is also confirmed by Fig. 7.13 (j), where deep soil water (i.e. SW300) is shown to decrease under forestry, although there is no change shown for agriculture, cropland grassland and shrub. The change in percolation is also noticeable with forestry land use: percolation increases by ~0.3mm with increasing forestry, mostly in the southern part of the basin. In contrast, surface runoff and water yield generally decrease with forestry cover, by ~0.5mm. Other land uses do not show any changes on surface runoff and water yield. Those areas that do show decreasing water yield also show a decrease in flow out, especially under forestry.

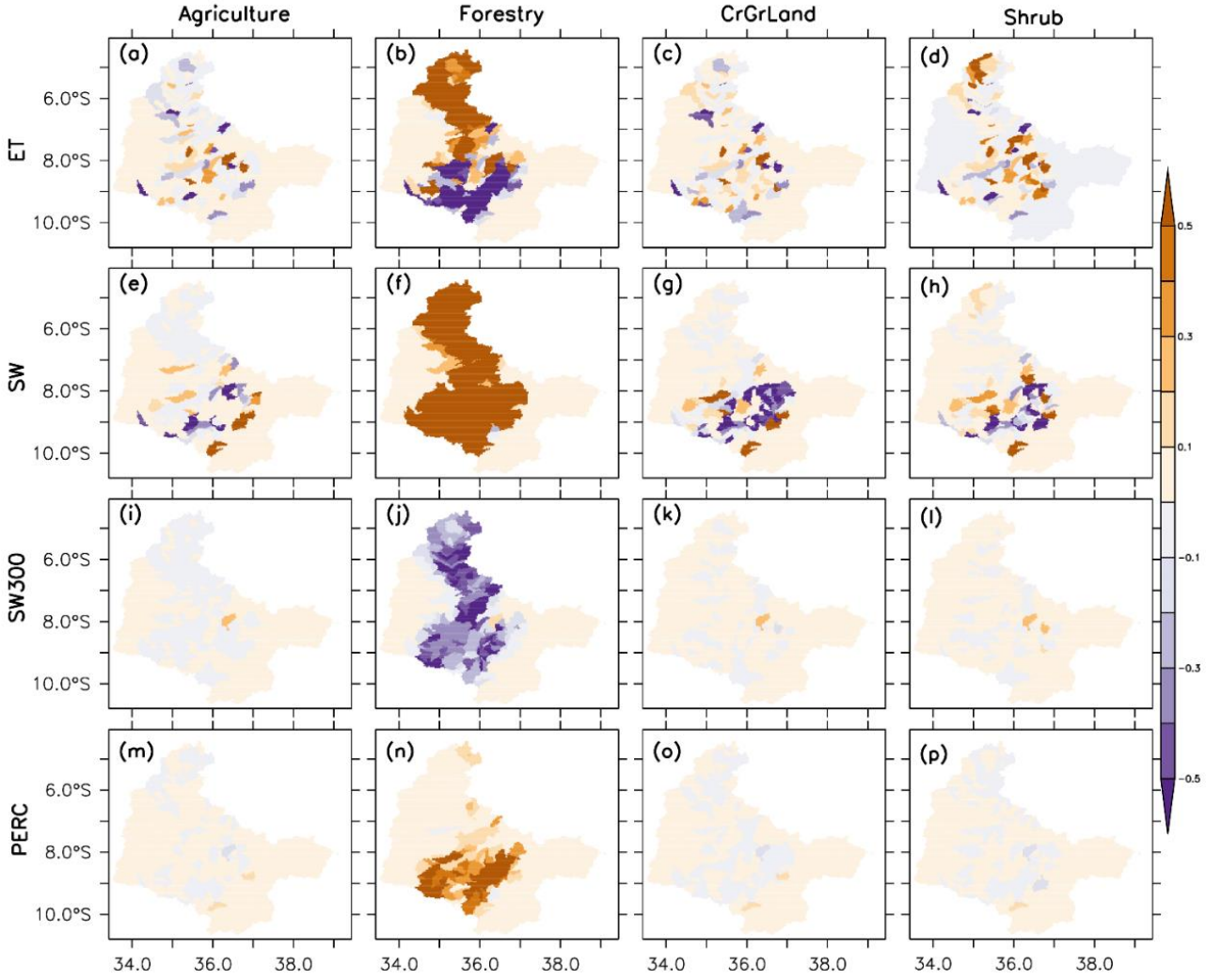

Figure 7.13: *Hydrological variables (i.e. evapotranspiration: ET; soil water: SW; soil water at 300 m: SW300; percolation: PERC) for land uses agriculture, forestry, cropland grassland and shrub using bias corrected ensemble at GWL3.0 over the Rufiji basin.*

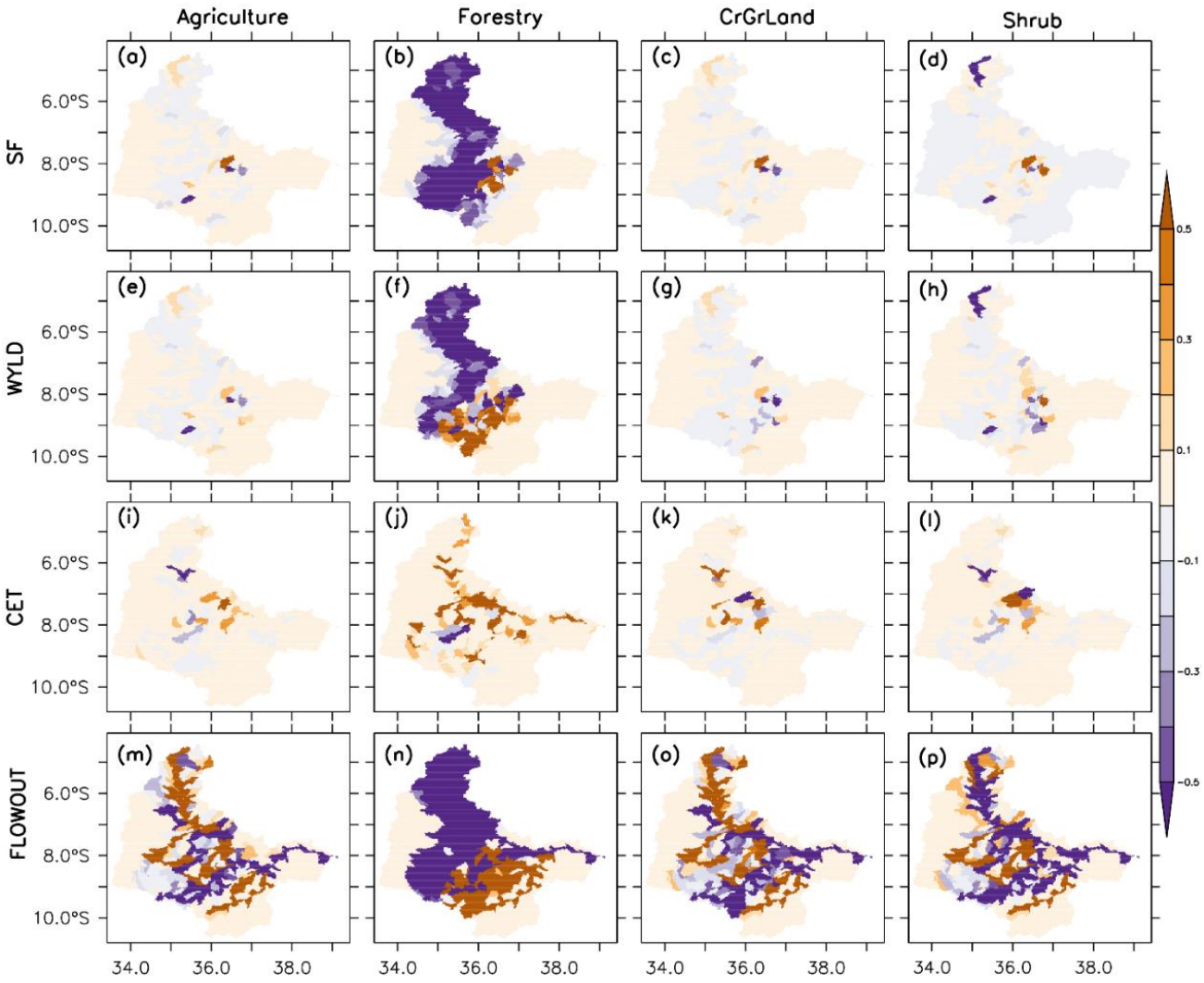

Figure 7.14: *The same as Fig. 7.12 but for surface runoff (SF), water yield (WYLD), channel evapotranspiration (CET) and flowout (FLOWOUT).*

The contribution of higher surface runoff, high water yield, high soil water and flow out from the basin throughout the year is important for the ecosystem, which relies on the good functioning of the river basin, such as plants, wildlife and humans. However, the large expansion of agricultural activities alone might not improve the hydrological system of the RRB, nor will they be sustainable. This is similar to what is projected to happen when shrubs and cropland grassland expand. In the RRB, afforestation should

also be considered with caution, as it may have both positive and negative consequences. For example, afforestation increases soil moisture in all parts of the basin, which is a good outcome for the ecosystem. It also increases percolation, which then may insure the contribution of groundwater fluxes for longer periods of the year. Nevertheless, afforestation decreases evapotranspiration only in some parts of the basin, while increasing it in other parts. It also decreases the existence of deep soil water because the roots of trees are able to penetrate deeper into the soil, thus increasing evapotranspiration. In this scenario, the species of trees to be planted should be carefully considered, as they may not consume too much of the deep water systems. Also, afforestation decreases surface runoff and water yields in some parts of the basin, while increasing it in other places. In other words, the south-eastern part of the basin shows a much clearer benefit of increasing forest plantations than the northern part of the basin, and thus afforestation should be site specific and not implemented throughout the whole basin.

A comparison of the impact of different land uses at GWL2.0 on hydrological drought shows that changing the land use of the RRB to forestry and shrub rather than to agriculture and cropland grassland will have a significant impact (Fig. 7.15 (a), (b)). Some land uses show a great impact on both the intensity and frequency of the hydrological drought indices. For example, the results show that afforestation of the RRB increases SWI intensity to ~0.2 and frequency to ~50 events/decade. This could mean that forestry increases evapotranspiration at higher warming levels because the moisture atmospheric demand over this region also increases at higher temperatures (Fig. 7.9 (m)-(p)). Greater evapotranspiration means more depletion of soil water in the basin, thus leading to a higher soil water drought intensity and frequency at higher GWLs. There is evidence that the soil water projection in the RRB will decrease more with increasing warming levels, when looking at the deep soil layer (Fig.7.10(i)-(l)) than when looking only at the surface layer (Fig. 7.10(e)-(h)). It could also affect RFI, WYI and SFI drought indices, although the effects are less than that of SWI. Such higher impacts in terms of the SWI might be due to the weak horizontal movement of soil water as compared to river flow and water yield. Therefore, vegetation has a higher chance to utilise soil water for evaporation than do non-stationary sources, i.e. river flow and water yield. For the land uses of agriculture and cropland grassland, no changes in drought intensity and frequency were simulated for both indices SWI and

RFI. Both agriculture (in this case seasonal crops) and cropland grassland are characterised by biodiversity of small vegetation with little or no woody properties and with shallow roots. This can be further described as vegetation with little evapotranspiration capabilities for both soil and runoff water, as shown in Fig. 7.13 (a) and (c). Given that precipitation is projected to increase in the future, these types of vegetation therefore balance the supply and demand of water and ensure that SWI and SFI will not change in the future. Converting the RRB land uses to shrubland will mostly affect RFI, where the intensity will be ~0.1 and the frequency ~50events/decade. Shrublands are short and woody plants with many branches, and usually with many stems and medium roots (longer roots than seasonal plants but shorter roots than forest trees). Therefore, such plants will have more access to extract streamflow water than agriculture and cropland grassland vegetation (Fig. 7.13 (a), (c), (d)), and will increase river flow drought intensity and frequency in the future. For WYI and SFI, shrubland shows a greater impact to drought frequency than intensity. This could be because shrublands do not have a direct impact on water yield and channel flow out, but by increasing the drought frequency of the river flow it would also decrease total water yield and channel flow.

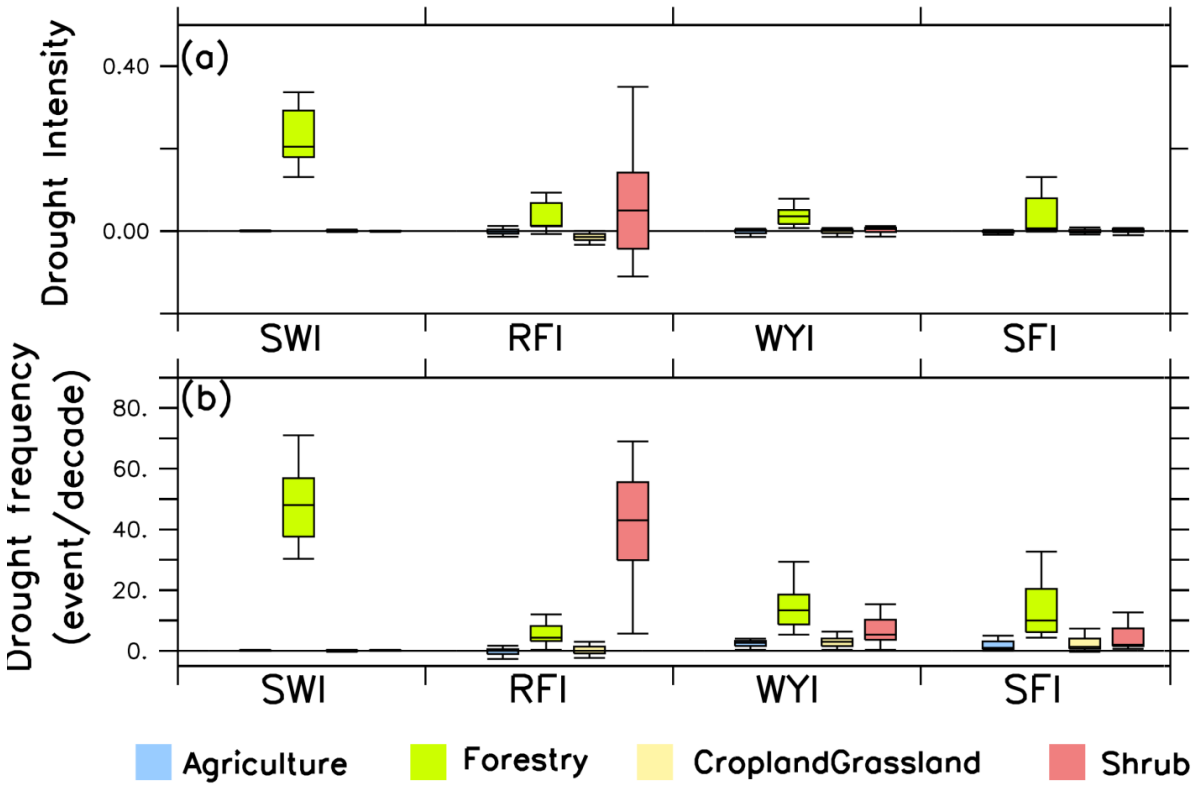

Figure 7.15: *Projected changes in hydrological (i.e. soil water index: SWI; surface runoff index: RFI; water yield index: WYI; channel flowout index: SFI) drought intensity (a) and severe drought frequency (b) over the Rufiji river basin under different land uses (Agriculture, Forestry, Cropland Grassland and shrub) at GWL2.0 under the RCP8.5 scenario.*

The drought intensity and frequency of hydrological drought increases at higher GWL3.0 (Fig. 7.16 (a), (b)) but mostly for the land uses that show an impact at GWL2.0. For example, with land use forestry, SWI intensity increased by ~0.05, but its frequency does not show much difference between GWL2.0 and GWL3.0. With regard to the RFI, forestry does not show any differences between the two warming levels, but for WYI and SFI, the frequency seems to increase slightly at higher GWL, while its intensity does not change. As for shrub, the changes are noticeable for RFI and WYI, but there are no changes at higher GWLs for SWI and for SFI.

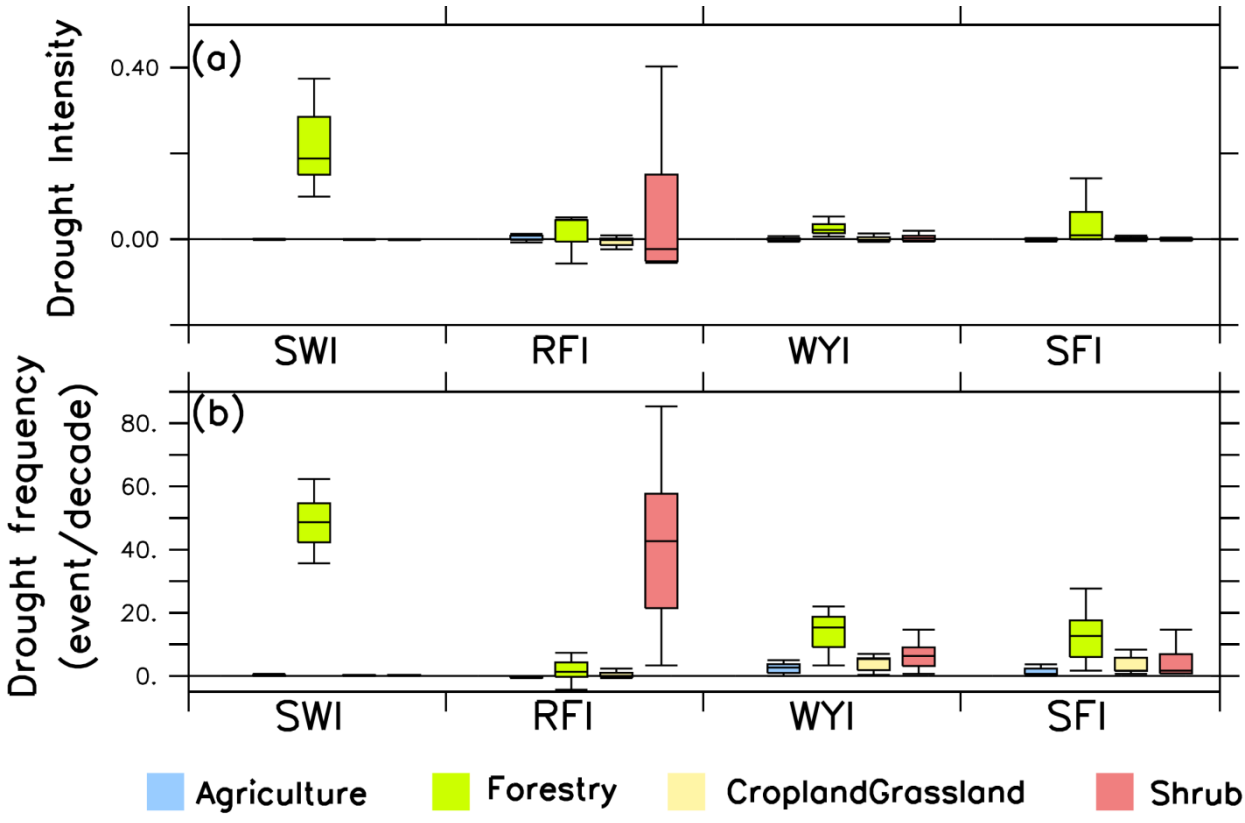

Figure 7.16: *The same as Fig. 7.15 but for GWL3.0*

Based on the drought projections over the RRB, different suggestions can be made with regard to the future of the basin. Firstly, future drought conditions are mostly evidenced

by SPEI meteorological drought whereas hydrological drought does not pose a robust threat over this basin. Under higher warming levels, even at GWL3.0, the hydrological droughts considered in this study do not appear to be influenced significantly. This could be because the hydrological droughts over the RRB are mostly affected by changes in rainfall, of which the ensemble mean is projected to increase in most parts of the basin. Therefore, the likelihood of higher precipitation in the RRB also poses no threat to hydrological drought at higher GWL. Secondly, hydrological drought over the RRB is only affected by certain land uses and land cover changes. Having higher projections of hydrological drought intensity and frequency under the forestry land use shows that, over the RRB, hydrological drought mitigation should be considered with caution, especially when considering planting trees as a measure to combat drought. Also, planting shrubs in the basin can also pose some threats, although not as significant as forestry land cover. Finally, we can also make some suggestions when considering changing the land cover to agriculture and cropland grassland. Although these land uses are projected to pose no threat to the basin in terms of hydrological drought, it is always important to investigate further before using these as drought mitigation measures, because, for example, the type of agriculture practice can create some drawbacks under the drought conditions of the basin.

7.6 Summary

This study has examined the impacts of climate change and land use land cover changes on future hydrological droughts in the Rufiji River Basin. The SWAT hydrological model was used to generate the relevant hydrological variables, namely, PET, ET, SW, PER, SF, WYLD and FLOWOUT. The impacts of climate change were analysed at four GWLs: GWL1.5, GWL2.0, GWL2.5 and GWL3.0, and four different land uses were considered: agriculture, forestry, cropland grassland and shrubs. Our analysis also considered four types of hydrological drought indices: soil water index (SWI), surface runoff index (RFI), water yield index (WYI), and channel flowout index (SFI). However, we have also incorporated meteorological drought indexes SPEI and SPI to enable us to make comparisons with the hydrological droughts. To quantify the hydrological drought projections, we used seven RCM simulations from CORDEX. The comparison between the raw ensemble and the bias corrected ensemble was also presented so as to see how the ensemble was improved after bias correction. The

performance of the simulations in reproducing RRB climate was evaluated by comparing the observed and simulated climate and hydrological variables for the reference period (1971–2000) with the land use map of 2010. The projected changes induced by each GWL were quantified using the difference between the climatic and hydrological conditions for the GWL period and the reference period (i.e. GWL minus reference) with land use map of 2010. Moreover, boxplot analysis was employed to quantify the projected changes in hydrological drought intensity and frequency at different GWLs (using the land use map of 2010) as well as different land uses (using GWL2.0 and GWL3.0). Our findings can be summarised below:

- There is a good agreement between the reanalysis dataset used (GMFD) and the station observation datasets over most stations considered in the study. The reanalysis dataset GMFD is therefore a reasonable dataset to be used to represent the observed data in RRB.
- The SWAT calibration and validation process shows that the calibration improves the quality of the simulations. Using the statistical tool NSE and the correlation between the observed stream flow and the simulated stream flow, their values were found to improve after calibration.
- The CORDEX simulation ensemble gives reliable simulations of climate and hydrological variables over the Rufiji River Basin. The ensemble mean reproduces the observed annual cycles and spatial patterns of the climate and hydrological variables over the RRB. However, some biases are noticeable for most part of the basin and for almost all the parameters involved. While some variables are underestimated, e.g. solar radiation, others are overestimated, e.g. temperature. The performance of the ensembles improves when considering the bias corrected models.
- The simulation ensemble mean projects an increase in mean temperature, PET, ET, and precipitation over most parts of the basin with increasing GWL. However, the ensemble simulation projects inhomogeneous changes of hydrological variables, with some variables showing an increase, while others show a decrease with GWL.
- The simulation ensemble mean projects an increase in the intensity and frequency of SPEI droughts with increased GWL over RRB but no changes with SPI. And for hydrological drought indices, the ensemble mean projects and

increase in RFI and SFI drought intensity but no changes for SWI and WYI with increasing GWL. As for drought frequency all the hydrological drought indices considered projected generally no change in frequency at all GWL.

- Among the four land uses proposed, the projection of all hydrological variables (i.e. evapotranspiration, soil water, percolation, surface runoff, water yield and flow out) appears to be more pronounced (in terms of both increase and decrease intensity) with increased forestry land use, but for other land uses, the changes are minimal and sometimes no changes are observed at all.
- The analysis of hydrological drought using different land uses shows that the ensemble projects a generally higher drought intensity and frequency for the land use of forestry, and to a lesser degree shrubs, but no changes are projected with land uses of agriculture and cropland grassland.

Chapter 8

Conclusion

This chapter summarises the findings of all the analyses performed in the study. It also presents the concluding remarks and provides some recommendations on how the study could be improved in the future and on the way forward.

8.1 Summary

This study has been motivated by the need to understand the characteristics of drought in Eastern Africa under past and future climates, because droughts pose such a serious threat to the lives and development of the people in the region. Whether it is meteorological drought, agricultural or hydrological drought, Eastern Africa is highly at risk. This study has thus used the recent drought index, i.e. the Standardized Precipitation-Evapotranspiration Index (SPEI), computed using rainfall and temperature data, to identify 3-month as well as 12- month drought over Eastern Africa. It firstly presented the temporal and spatial characteristics of the various drought modes over the region, and then examined the potential impacts of ongoing global warming on the characteristics of the major drought modes in eastern Africa. It also zoomed in to provide details of how climate change might affect four major river basins (Rufiji, Tana, Upper-Nile and Juba) at different warming levels, i.e. GWL1.5, GWL2.0, GWL2.5 and GWL3.0 under RCP4.5 and 8.5 scenarios. Lastly, the study examined the impacts of climate change and land use or land cover changes on future hydrological droughts in the Rufiji River Basin using the SWAT hydrology model. Four different land uses were considered in this regard: agriculture, forestry, cropland grassland and shrubs.

To understand the capability of the model in capturing the climate as well as the drought of the region, a comparison was made of the observed and simulated climate and drought patterns. The observation data were obtained from different sources, i.e., the Climate Research Unit (CRU), station datasets from the Tanzania Meteorological Agency (TMA) and the Wami/Ruvu Basin Water Office (WRBWO), and the Global

Meteorological Forcing Dataset (GMFD). The simulation data came from 19 RCMs that participated in the Coordinated Regional Climate Downscaling Experiment (CORDEX) project. We also used SST, 20th Century Reanalysis, and GIS data. The major drought modes were extracted from the SPEI and SPI data by applying a PCA tool. The temporal structures of the modes were described by means of wavelet analysis. We used the wavelet coherence and correlation analysis to investigate the link between four climate indices (i.e. ENSO, IOD, TADI and QBO) and global SSTs in relation to each drought mode. The Self Organizing Map (SOM) algorithm was used to classify drought patterns into 12 most important patterns. Moreover, boxplot analysis was employed to quantify the projected changes in drought intensity and frequency at different GWLs, as well as under different land uses. Our study used the 1940-2014 period to identify the major drought patterns in the observations. In order to evaluate the RCMs, the 1971-2000 period was used. The projected changes induced by each GWL were quantified using the difference between the climatic condition for the GWL period and the reference period (i.e. GWL minus reference).

The findings of this thesis are divided into two main categories; a) results that extended previous studies and b) results that uniquely adding new dimensions in the characterization of droughts over eastern Africa. In both categories, the application of combining empirical methods (Wavelet Analysis, Wavelet Coherence, SOM, and SPEI/SPI) as well as numerical modeling (an ensemble of CORDEX regional climate and SWAT model simulations) ensures the robustness of the results and conclusions. The summary for each category is presented below:

(a)

- Four major drought modes (DM1, DM2, DM3 and DM4) account for more than 46% of SPEI variability over eastern Africa and feature their cores over different areas of the region, namely: central eastern (DM1), southern and south-western (DM2), north-western (DM3) and far north-eastern (DM4). These drought modes have different temporal variations and produced their maximum drought frequency in different decades within the study period (1940–2014).
- The coupling of the drought modes to the atmospheric teleconnections (i.e. ENSO, IOD, TADI and QBO) also differ. DM1 mode is best coupled with IOD, DM2 with IOD and ENSO, DM3 with ENSO and TADI, and DM4 with IOD and ENSO. At the seasonal scale, there is a strong correlation between DM1

and SST over the Indian and Pacific Oceans in DJF and SON, and between DM2 and SST over the tropical Indian Ocean in SON.

- The CORDEX simulation ensemble gives reliable simulations of climate variables as well as the characteristics of the four major drought modes over eastern Africa, although the models struggle to reproduce the observed spatial variations of severe drought frequency over the region. The simulations and the CRU observations agree that using SPI (instead of SPEI) produced a lower drought frequency in the historical climate. However, the RCMs perform better at simulating SPEI than at reproducing SPI.
- The simulation ensemble mean projects a substantial increase in the intensity and frequency of SPEI drought over the core of the drought modes and an increase in the intensity and frequency of SPEI droughts over most parts of East Africa, but with a smaller increase near the equator and along the coast. The magnitude of the increase grows with increasing GWLs. The SPI projections give opposite results to the SPEI over the drought modes and the entire eastern African region, in that the magnitude of the SPI changes is smaller than that of SPEI.
- The drought projections (intensity and frequency) over the basins are more robust with the SPEI than with the SPI. However, the magnitude and robustness of the SPEI projections are more pronounced over the Upper-Nile and Juba basins than over the Rufiji and Tana basins. And with regard to the hydrological drought indices, the ensemble mean projects an increase in RFI and SFI drought intensity, but no changes for SWI and WYI with increasing GWL. As for drought frequency, all the hydrological drought indices considered projected generally no change in frequency at any of the GWLs.
- The SOM classifications of the SPEI and SPI projections reveal that 90% of the simulations correctly distinguish between the SPEI and SPI projection patterns over East Africa. While some SOM nodes feature a substantial decrease in SPEI (drying) over the whole region, some nodes indicate an increase in SPI (wetting) over the entire region.

(b)

- The composite of SPEI drought shows that each drought mode can occur in any season, but the difference is in the associated drought intensity and area coverage during each season. The seasonal variability is more pronounced for

DM1 and DM2, with less seasonal changes noted in DM3 and DM4. The analysis of the drought modes also suggests that the net downward motion that suppresses drought over the drought mode core area is induced by the enhanced convection over the adjacent areas. The location of the adjacent convection varies with drought modes and with the seasons.

- Among the four land uses proposed, the projection of all hydrological variables (i.e. evapotranspiration, soil water, percolation, surface runoff, water yield and flow out) appears to be more pronounced (in terms of both increase and decrease intensity) with increased forestry land use, but for other land uses, the changes are minimal and sometimes no changes are observed at all.
- The analysis of hydrological drought using different land uses shows that the ensemble projects a generally higher drought intensity and frequency for the land use of forestry, and to a lesser degree shrubs, but no changes are projected with land uses of agriculture and cropland grassland.

Therefore, over the RRB, hydrological drought mitigation should be considered with caution, especially when considering planting trees as a measure to combat drought. Also, planting shrubs in the basin can also pose some threats, although not as significant as forestry land cover. Although land uses agriculture and cropland grassland projected with positivity, it is always important to investigate further before using these as drought mitigation measures, because, for example, the type of agriculture practice can create some drawbacks under the drought conditions of the basin.

8.2 Recommendations for future work

Future work can improve the robustness of these results in many ways. For example, this present study has focused on using meteorological and hydrological drought indices to quantify drought. However, extending these projections to quantify the potential changes in drought using other types of drought indices may improve the knowledge gaps about droughts in eastern Africa. Also, more long-term droughts, like 24-months and 48-months, should be considered in order to have a longer term of drought evolution in eastern Africa. More work is also needed to improve the observation datasets at the local to regional level. High resolution observation datasets for climate as well as hydrology would add value for better representation of the region. The

consistency of the climate models in reproducing observed relevant climatic feature over eastern Africa is a key indicator of their potential use for future climate change projections. In this thesis, CORDEX ensemble demonstrated good skill in capturing drought over this region, although some inconsistencies still exist. Therefore, the quality of the projections can be improved by using higher resolution (5–20 km) simulations that better capture the interactions between the synoptic-scale features and the local-scale circulation. This could reduce the model biases and improve agreement among the models. Such high-resolution simulations are in fact the target of the second phase of CORDEX (Somot et al., 2018).

References

Abramopoulos, F., Rosenzweig, C. and Choudhury, B., 1988. Improved ground hydrology calculations for global climate models (GCMs): Soil water movement and evapotranspiration. *Journal of Climate*, 1(9), pp.921–941.

ACTED, 2011. Horn of Africa. Drought Predictable and Predicted. Agency for Technical Cooperation and Development, Paris, France. https://reliefweb.int/report/somalia/horn-africa-drought-predictable-and-predicted. Accessed 1st November 2016

Adhikari, U., Nejadhashemi, A.P., Herman, M.R. and Messina, J.P., 2017. Multiscale assessment of the impacts of climate change on water resources in Tanzania. *Journal of Hydrologic Engineering*, *22*(2), p.05016034.

Adhikari, U., Nejadhashemi, A.P. and Woznicki, S.A., 2015. Climate change and eastern Africa: A review of impact on major crops. *Food and Energy Security*, 4(2), pp.110–132.

AghaKouchak, A., 2015. A multivariate approach for persistence-based drought prediction: Application to the 2010–2011 East African drought. *Journal of Hydrology*, 526, pp.127–135.

Allen, R.G., 1986. A Penman for all seasons. *Journal of Irrigation and Drainage Engineering*, *112*(4), pp.348-368.

Alvarez, V.M., Baille, A., Martínez, J.M. and González-Real, M.M., 2006. Efficiency of shading materials in reducing evaporation from free water surfaces. *Agricultural Water Management*, *84*(3), pp.229-239.

American Meteorological Society, 1997. Meteorological drought-policy statement. *Bulletin of the American Meteorological Society*, *78*, pp.847-849.

Andréassian, V., 2004. Waters and forests: from historical controversy to scientific debate. *Journal of hydrology*, *291*(1-2), pp.1-27.

Annamalai, H., Murtugudde, R., Potemra, J., Xie, S.P., Liu, P. and Wang, B., 2003. Coupled dynamics over the Indian Ocean: Spring initiation of the zonal mode. *Deep Sea Research Part II: Topical Studies in Oceanography*, *50*(12-13), pp.2305-2330.

Anyah, R.O. and Qiu, W., 2012. Characteristic 20th and 21st century precipitation and temperature patterns and changes over the Greater Horn of Africa. *International Journal of Climatology*, *32*(3), pp.347-363.

Anyah, R.O. and Semazzi, F.H., 2007. Variability of East African rainfall based on multiyear RegCM3 simulations. *International Journal of Climatology*, 27(3), pp.357–371.

Anyamba, A., Tucker, C.J. and Mahoney, R., 2002. From El Niño to La Niña: Vegetation response patterns over east and southern Africa during the 1997–2000 period. *Journal of climate*, *15*(21), pp.3096-3103.

Arnold, J.G., Moriasi, D.N., Gassman, P.W., Abbaspour, K.C., White, M.J., Srinivasan, R., Santhi, C., Harmel, R.D., Van Griensven, A., Van Liew, M.W. and Kannan, N., 2012. SWAT: Model use, calibration, and validation. *Transactions of the ASABE*, *55*(4), pp.1491–1508.

Arnold, J.G., Srinivasan, R., Muttiah, R.S, and Williams, J.R., 1998. Large area hydrologic modeling and assessment part I: model development 1. *JAWRA Journal of the American Water Resources Association*, *34*(1), pp.73-89.

Artan, G., Gadain, H., Muthusi, F., Muchiri, P., 2007. Improving flood forecasting and early warning in Somalia; Feasibility study. FAO-SWALIM (GCP/SOM/EC045) Project Publication N ◦ W-10, Nairobi, Kenya.

Bahaga, T.K., Mengistu Tsidu, G., Kucharski, F. and Diro, G.T., 2015. Potential predictability of the sea-surface temperature forced equatorial East African short rains interannual variability in the 20th century. *Quarterly Journal of the Royal Meteorological Society*, *141*(686), pp.16-26.

Bärring, L., 1988a. Reginalization of daily rainfall in Kenya by means of common factor analysis. *Journal of climatology*, *8*(4), pp.371-389.

Bärring, L., 1987b. Spatial patterns of daily rainfall in central Kenya: application of principal component analysis, common factor analysis and spatial correlation. *Journal of climatology*, *7*(3), pp.267-289.

Baker, T.J. and Miller, S.N., 2013. Using the Soil and Water Assessment Tool (SWAT) to assess land use impact on water resources in an East African watershed. *Journal of hydrology*, *486*, pp.100-111.

Basnyat, D.B., 2007. *Water Resources of Somalia*. Nairobi, Kenya: FAO-SWALIM (GCP/SOM/EC045) project, Technical Report no. W–11.

Beguería, S., Vicente-Serrano, S.M., Reig, F. and Latorre, B., 2014. Standardized precipitation evapotranspiration index (SPEI) revisited: Parameter fitting, evapotranspiration models, tools, datasets and drought monitoring. *International Journal of Climatology*, 34(10), pp.3001–3023. http://hdl.handle.net/10261/128892

Behera, S.K., Luo, J.J., Masson, S., Delecluse, P., Gualdi, S., Navarra, A. and Yamagata, T., 2005. Paramount impact of the Indian Ocean dipole on the East African short rains: A CGCM study. *Journal of Climate*, *18*(21), pp.4514-4530.

Behera, S.K., Luo, J.J., Masson, S., Rao, S.A., Sakuma, H. and Yamagata, T., 2006. A CGCM study on the interaction between IOD and ENSO. *Journal of Climate*, *19*(9), pp.1688-1705.

Belayneh, A., Adamowski, J., Khalil, B. and Ozga-Zielinski, B., 2014. Long-term SPI drought forecasting in the Awash River Basin in Ethiopia using wavelet neural network and wavelet support vector regression models. *Journal of Hydrology*, 508, pp.418–429.

Bennun, L.A. and Njoroge, P., 1999. *Important bird areas in Kenya*. Nature Kenya, East Africa Natural History Society.

Bernard, B., Vincent, K., Frank, M. and Anthony, E., 2013. Comparison of extreme weather events and streamflow from drought indices and a hydrological model in River Malaba, Eastern Uganda. *International Journal of Environmental Studies*, 70(6), pp.940–951.

Bernacsek, G.M. and Kapetsky, J.M., 1981. Freshwater fisheries and industry in the Rufiji River basin, Tanzania: the prospects for coexistence.

Bessems, I., Verschuren, D., Russell, J.M., Hus, J., Mees, F. and Cumming, B.F., 2008. Palaeolimnological evidence for widespread late 18th century drought across equatorial East Africa. *Palaeogeography, Palaeoclimatology, Palaeoecology*, *259*(2-3), pp.107-120.

Bhalme, H.N. and Mooley, D.A., 1979. On the performance of modified Palmer index. *Archiv für Meteorologie, Geophysik und Bioklimatologie, Serie B*, *27*(4), pp.281-295.

Bieger, K., Arnold, J.G., Rathjens, H., White, M.J., Bosch, D.D., Allen, P.M., Volk, M. and Srinivasan, R., 2017. Introduction to SWAT+, a completely restructured version of the soil and water assessment tool. *JAWRA Journal of the American Water Resources Association*, *53*(1), pp.115-130.

Black, E., 2005. The relationship between Indian Ocean sea–surface temperature and East African rainfall. *Philosophical Transactions of the Royal Society A: Mathematical, Physical and Engineering Sciences*, *363*(1826), pp.43-47.

Black, E., Slingo, J. and Sperber, K.R., 2003. An observational study of the relationship between excessively strong short rains in coastal East Africa and Indian Ocean SST. *Monthly Weather Review*, *131*(1), pp.74-94.

Bosch, J.M. and Hewlett, J.D., 1982. A review of catchment experiments to determine the effect of vegetation changes on water yield and evapotranspiration. *Journal of hydrology*, *55*(1-4), pp.3-23.

Brown, A.E., Zhang, L., McMahon, T.A., Western, A.W. and Vertessy, R.A., 2005. A review of paired catchment studies for determining changes in water yield resulting from alterations in vegetation. *Journal of hydrology*, *310*(1-4), pp.28-61.

Burghof, S., Gabiri, G., Stumpp, C., Chesnaux, R. and Reichert, B., 2018. Development of a hydrogeological conceptual wetland model in the data-scarce north-eastern region of Kilombero Valley, Tanzania. *Hydrogeology journal*, *26*(1), pp.267-284.

Burke, E.J., Brown, S.J. and Christidis, N., 2006. Modeling the recent evolution of global drought and projections for the twenty-first century with the Hadley Centre climate model. *Journal of Hydrometeorology*, *7*(5), pp.1113-1125.

Cai, W. and Cowan, T., 2013. Why is the amplitude of the Indian Ocean Dipole overly large in CMIP3 and CMIP5 climate models?. *Geophysical Research Letters*, *40*(6), pp.1200-1205.

Cai, W., Zheng, X.T., Weller, E., Collins, M., Cowan, T., Lengaigne, M., Yu, W. and Yamagata, T., 2013. Projected response of the Indian Ocean Dipole to greenhouse warming. *Nature geoscience*, *6*(12), pp.999-1007.

Camberlin, P., 1997. Rainfall anomalies in the source region of the Nile and their connection with the Indian summer monsoon. *Journal of Climate*, *10*(6), pp.1380-1392..

Camberlin, P., 2009. Nile basin climates. In *The Nile* (pp. 307-333). Springer, Dordrecht.

Cannon, A.J., Sobie, S.R. and Murdock, T.Q., 2015. Bias correction of GCM precipitation by quantile mapping: how well do methods preserve changes in quantiles and extremes?. *Journal of Climate*, *28*(17), pp.6938-6959.

Cao, W., Bowden, W.B., Davie, T. and Fenemor, A., 2009. Modelling impacts of land cover change on critical water resources in the Motueka River catchment, New Zealand. *Water Resources Management*, *23*(1), pp.137-151.

Chang, F.J., Chang, L.C. and Wang, Y.S., 2007. Enforced self-organizing map neural networks for river flood forecasting. *Hydrological Processes: An International Journal*, 21(6), pp.741–749.

Chretien, J.P., Anyamba, A., Bedno, S.A., Breiman, R.F., Sang, R., Sergon, K., Powers, A.M., Onyango, C.O., Small, J., Tucker, C.J. and Linthicum, K.J., 2007. Drought-associated chikungunya emergence along coastal East Africa. *The American journal of tropical medicine and hygiene*, *76*(3), pp.405-407.

Christy, J.R., Norris, W.B. and McNider, R.T., 2009. Surface temperature variations in East Africa and possible causes. *Journal of Climate*, *22*(12), pp.3342-3356.

Clark, C.O., Webster, P.J. and Cole, J.E., 2003. Interdecadal variability of the relationship between the Indian Ocean zonal mode and East African coastal rainfall anomalies. *Journal of Climate*, *16*(3), pp.548-554.

Compo, G.P., Whitaker, J.S., Sardeshmukh, P.D., Matsui, N., Allan, R.J., Yin, X., Gleason, B.E., Vose, R.S., Rutledge, G., Bessemoulin, P. and Brönnimann, S., 2011. The twentieth century reanalysis project. *Quarterly Journal of the Royal Meteorological Society*, *137*(654), pp.1-28.

Conway, D. and Schipper, E.L.F., 2011. Adaptation to climate change in Africa: Challenges and opportunities identified from Ethiopia. *Global Environmental Change*, 21(1), pp.227–237.

Conway, D., Persechino, A. and Syroka, J., 2007: Reducing vulnerability in Ethiopia: addressing the implications of climate change. Drought risk financing in Ethiopia: technical assessment of indicators used for contingency financing mechanisms. University of East Angelia, Overseas Development Group, 39 p

Cook, K.H. and Vizy, E.K., 2013. Projected changes in East African rainy seasons. *Journal of Climate*, *26*(16), pp.5931-5948.

Cook, K.H. and Vizy, E.K., 2012. Impact of climate change on mid-twenty-first century growing seasons in Africa. *Climate Dynamics*, *39*(12), pp.2937-2955.

Craig, I., Green, A., Scobie, M. and Schmidt, E., 2005. Controlling evaporation loss from water storages. NCEA Publication No 1000580/1.

Croke, B.F.W., Merritt, W.S. and Jakeman, A.J., 2004. A dynamic model for predicting hydrologic response to land cover changes in gauged and ungauged catchments. *Journal of Hydrology*, *291*(1-2), pp.115-131.

Dai, A., 2011. Drought under global warming: a review. *Wiley Interdisciplinary Reviews: Climate Change*, *2*(1), pp.45-65.

Dai, A., 2013. Increasing drought under global warming in observations and models. *Nature climate change*, *3*(1), pp.52-58.

Damberg, L. and AghaKouchak, A., 2014. Global trends and patterns of drought from space. *Theoretical and applied climatology*, *117*(3-4), pp.441-448.

Daron, J.D., 2014. Regional Climate Messages: East Africa. Scientific report from the CARIAA Adaptation at Scale in Semi-Arid Regions (ASSAR) Project.

Degefu, W., 1987. Some aspects of meteorological drought in Ethiopia (pp. 23–36). Cambridge University Press.

Degefu, M.A. and Bewket, W., 2015. Trends and spatial patterns of drought incidence in the omo-ghibe river basin, ethiopia. *Geografiska Annaler: Series A, Physical Geography*, *97*(2), pp.395-414.

Degefu, M.A. and Bewket, W., 2014. Variability and trends in rainfall amount and extreme event indices in the Omo-Ghibe River Basin, Ethiopia. *Regional environmental change*, *14*(2), pp.799-810.

Déqué, M., Calmanti, S., Christensen, O.B., Aquila, A.D., Maule, C.F., Haensler, A., Nikulin, G. and Teichmann, C., 2017. A multi-model climate response over tropical Africa at+ 2 C. *Climate Services*, *7*, pp.87-95.

Dessu, S.B. and Melesse, A.M., 2012. Modelling the rainfall–runoff process of the Mara River basin using the Soil and Water Assessment Tool. *Hydrological Processes*, *26*(26), pp.4038-4049.

Diasso, U. and Abiodun, B.J., 2017. Drought modes in West Africa and how well CORDEX RCMs simulate them. *Theoretical and applied climatology*, *128*(1-2), pp.223-240.

Di Baldassarre, G., Elshamy, M., van Griensven, A., Soliman, E., Kigobe, M., Ndomba, P., Mutemi, J., Mutua, F., Moges, S., Xuan, Y. and Solomatine, D., 2011. Future hydrology and climate in the River Nile basin: A review. *Hydrological Sciences Journal – Journal des Sciences Hydrologiques*, 56(2), pp.199–211.

Dosio, A. and Panitz, H.J., 2016. Climate change projections for CORDEX-Africa with COSMO-CLM regional climate model and differences with the driving global climate models. *Climate Dynamics*, 46(5–6), pp.1599–1625.

Dommenget, D., 2018. An Introduction to Climate Dynamics. Monash Univerity, School of Earth, Atmosphere and Environment, Clayton, Victoria 3800, Australia. http://users.monash.edu.au/~dietmard/teaching/dommenget.climate.dynamics.lecture.notes.pdf. Accessed 13th February 2019

Dutra, E., Magnusson, L., Wetterhall, F., Cloke, H.L., Balsamo, G., Boussetta, S. and Pappenberger, F., 2013. The 2010–2011 drought in the Horn of Africa in ECMWF reanalysis and seasonal forecast products. *International Journal of Climatology*, 33(7), pp.1720–1729.

EARTH OBSERVATORY**,** 2011: Severe Drought Causes Famine in East Africa**.** The Earth Observatory report is part of the EOS Project Science Office located at NASA Goddard Space Flight Center**.** http://earthobservatory.nasa.gov/NaturalHazards/view.php?id=51411**.** Accessed 7th November 2016

Elagib, N.A., 2013. Meteorological drought and crop yield in Sub-Saharan Sudan. *International Journal of Water Resources and Arid Environments*, 3, pp.164–171.

Elagib, N.A. and Elhag, M.M., 2011. Major climate indicators of ongoing drought in Sudan. *Journal of Hydrology*, *409*(3-4), pp.612-625.

Edossa, D.C., Babel, M.S. and Gupta, A.D., 2010. Drought analysis in the Awash river basin, Ethiopia. *Water resources management*, 24(7), pp.1441–1460.

Elagib, N.A. and Elhag, M.M., 2011. Major climate indicators of ongoing drought in Sudan. *Journal of Hydrology*, 409(3-4), pp.612–625.

El-Fadel, M., El-Sayegh, Y., El-Fadl, K. and Khorbotly, D., 2003. The Nile River Basin: A case study in surface water conflict resolution. *Journal of Natural Resources and Life Sciences Education*, *32*, pp.107-117.

Elkollaly, M., Khadr, M. and Zeidan, B., 2017. Drought analysis in the Eastern Nile basin using the standardized precipitation index. *Environmental Science and Pollution Research*, 25(31), pp.30772-30786.

EMBRAPA - Empresa Brasileira de Pesquisa Agropecuária 1979. In: Reunião de Levantamento de Solos. Rio de Janeiro, EMBRAPA.

Endris, H.S., Omondi, P., Jain, S., Lennard, C., Hewitson, B., Chang'a, L., Awange, J.L., Dosio, A., Ketiem, P., Nikulin, G. and Panitz, H.J., 2013. Assessment of the performance of CORDEX regional climate models in simulating East African rainfall. *Journal of Climate*, 26(21), pp.8453–8475.

Endris, H.S., Lennard, C., Hewitson, B., Dosio, A., Nikulin, G. and Panitz, H.J., 2015. Teleconnection responses in multi-GCM driven CORDEX RCMs over Eastern Africa. *Climate Dynamics*, 46(9-10), pp.2821–2846.

FAO, 1983. World Food Security: A Reappraisal of the Concepts and Approaches. Director General's Report.

Fereday, D.R., Knight, J.R., Scaife, A.A., Folland, C.K. and Philipp, A., 2008. Cluster analysis of North Atlantic–European circulation types and links with tropical Pacific sea surface temperatures. *Journal of Climate*, 21(15), pp.3687–3703.

Findlater, J., 1977. Observational aspects of the low-level cross-equatorial jet stream of the western Indian Ocean. In *Monsoon Dynamics* (pp. 1251-1262). Birkhäuser, Basel.

Fjelde, H. and Von Uexkull, N., 2012. Climate triggers: Rainfall anomalies, vulnerability and communal conflict in sub-Saharan Africa. *Political Geography*, 31(7), pp.444–453.

Franczyk, J. and Chang, H., 2009. The effects of climate change and urbanization on the runoff of the Rock Creek basin in the Portland metropolitan area, Oregon, USA. *Hydrological Processes: An International Journal*, *23*(6), pp.805-815.

Funk, C., 2011. We thought trouble was coming: Chris Funk explains how his group last year forecast the drought in Somalia that is now turning into famine – and how that warning wasn't enough. *Nature*, 476(7358), pp.7–8.

Funk, C., Hoell, A., Shukla, S., Blade, I., Liebmann, B., Roberts, J.B., Robertson, F.R. and Husak, G., 2014. Predicting East African spring droughts using Pacific and Indian Ocean sea surface temperature indices. *Hydrology and Earth System Sciences*, *18*(12), pp.4965-4978.

Gassman, P.W., Reyes, M.R., Green, C.H. and Arnold, J.G., 2007. The soil and water assessment tool: historical development, applications, and future research directions. *Transactions of the ASABE*, *50*(4), pp.1211-1250.

General, U.S., 1994. United Nations convention to combat drought and desertification in countries experiencing serious droughts and/or desertification, particularly in Africa. *Particularly in Africa*.

Georgakakos, A.P., 2007. Decision support systems for integrated water resources management with an application to the Nile basin (pp. 99-116). Elsevier: Amsterdam, The Netherlands.

Giannini, A., Saravanan, R. and Chang, P., 2003. Oceanic forcing of Sahel rainfall on interannual to interdecadal time scales. *Science*, *302*(5647), pp.1027-1030.

Giorgi, F. and Mearns, L.O., 1999. Introduction to special section: Regional climate modeling revisited. *Journal of Geophysical Research: Atmospheres*, *104*(D6), pp.6335-6352.

Giorgi, F., Jones, C. and Asrar, G.R., 2009. Addressing climate information needs at the regional level: the CORDEX framework. *World Meteorological Organization (WMO) Bulletin*, *58*(3), p.175.

Githui, F.W., 2009. Assessing the impacts of environmental change on the hydrology of the Nzoia catchment, in the Lake Victoria (Doctoral dissertation, PhD thesis, Vrije Universiteit Brussel, Brussels, Belgium).

Goddard, L. and Graham, N.E., 1999. Importance of the Indian Ocean for simulating rainfall anomalies over eastern and southern Africa. *Journal of Geophysical Research: Atmospheres*, *104*(D16), pp.19099-19116.

Guo, F., Liu, Q., Sun, S. and Yang, J., 2015. Three types of Indian Ocean dipoles. *Journal of Climate*, *28*(8), pp.3073-3092.

Guo, H., Hu, Q. and Jiang, T., 2008. Annual and seasonal streamflow responses to climate and land-cover changes in the Poyang Lake basin, China. *Journal of Hydrology*, *355*(1-4), pp.106-122.

Gupta, H.V., Sorooshian, S. and Yapo, P.O., 1999. Status of automatic calibration for hydrologic models: Comparison with multilevel expert calibration. *Journal of Hydrologic Engineering*, *4*(2), pp.135-143.

Hamerlynck, O., Luke, Q., Nyange, T.M., Duvail, S. and Leauthaud, C., 2012. Range extension, imminent threats and conservation options for two endangered primates: the Tana River Red Colobus Procolobus rufomitratus rufomitratus (Peters, 1879) and the Tana River Mangabey Cercocebus galeritus (Peters, 1879) in the Lower Tana Floodplain and Delta, Kenya.

Hargreaves, G.H. and Samani, Z.A., 1985. Reference crop evapotranspiration from temperature. *Applied Engineering in Agriculture*, 1(2), pp.96–99.

Harris, I.P.D.J., Jones, P.D., Osborn, T.J. and Lister, D.H., 2014. Updated high-resolution grids of monthly climatic observations–the CRU TS3. 10 Dataset. *International journal of climatology*, *34*(3), pp.623-642. http://badc.nerc.ac.uk/data/cru/

Hassanein, M.K., Khalil, A.A. and Essa, Y.H., 2013. Assessment of drought impact in Africa using standard precipitation evapotranspiration index. *Nat. Sci*, *11*, pp.75-81.

Hastenrath, S., 2001. Variations of East African climate during the past two centuries. *Climatic change*, *50*(1-2), pp.209-217.

Hastenrath, S., Nicklis, A. and Greischar, L., 1993. Atmospheric-hydrospheric mechanisms of climate anomalies in the western equatorial Indian Ocean. *Journal of Geophysical Research: Oceans*, *98*(C11), pp.20219-20235.

Hastenrath, S., Polzin, D. and Mutai, C., 2007. Diagnosing the 2005 drought in equatorial East Africa. *Journal of Climate*, *20*(18), pp.4628-4637.

Hayes, M., Svoboda, M., Wall, N. and Widhalm, M., 2011. The Lincoln declaration on drought indices: universal meteorological drought index recommended. *Bulletin of the American Meteorological Society*, *92*(4), pp.485-488.

Heim Jr, R.R., 2002. A review of twentieth-century drought indices used in the United States. *Bulletin of the American Meteorological Society*, *83*(8), pp.1149-1166.

Herrmann, S.M. and Mohr, K.I., 2011. A continental-scale classification of rainfall seasonality regimes in Africa based on gridded precipitation and land surface temperature products. *Journal of Applied Meteorology and Climatology*, *50*(12), pp.2504-2513.

Hewitson, B.C. and Crane, R.G., 2002. Self-organizing maps: applications to synoptic climatology. *Climate Research*, *22*(1), pp.13-26.

Hirabayashi, Y., Kanae, S., Motoya, K., Masuda, K. and Döll, P., 2008. A 59-year (1948-2006) global meteorological forcing data set for land surface models. Part II: Global snowfall estimation. *Hydrological Research Letters*, *2*, pp.65-69.

Hoerling, M., Hurrell, J., Eischeid, J. and Phillips, A., 2006. Detection and attribution of twentieth-century northern and southern African rainfall change. *Journal of climate*, *19*(16), pp.3989-4008.

Houghton-Carr, H.A., Print, C.R., Fry, M.J., Gadain, H. and Muchiri, P., 2011. An assessment of the surface water resources of the Juba-Shabelle basin in southern Somalia. *Hydrological sciences journal*, *56*(5), pp.759-774.

Huang, B., Banzon, V.F., Freeman, E., Lawrimore, J., Liu, W., Peterson, T.C., Smith, T.M., Thorne, P.W., Woodruff, S.D. and Zhang, H.M., 2015. Extended reconstructed sea surface temperature version 4 (ERSST. v4). Part I: Upgrades and intercomparisons. *Journal of climate*, *28*(3), pp.911-930.

Huffman, G.J., Adler, R.F., Morrissey, M.M., Bolvin, D.T., Curtis, S., Joyce, R., McGavock, B. and Susskind, J., 2001. Global precipitation at one-degree daily resolution from multisatellite observations. *Journal of hydrometeorology*, *2*(1), pp.36-50.

Huffman, G.J., Bolvin, D.T., Nelkin, E.J., Wolff, D.B., Adler, R.F., Gu, G., Hong, Y., Bowman, K.P. and Stocker, E.F., 2007. The TRMM multisatellite precipitation analysis (TMPA): Quasi-global, multiyear, combined-sensor precipitation estimates at fine scales. *Journal of hydrometeorology*, *8*(1), pp.38-55.

Hurkmans, R.T.W.L., Terink, W., Uijlenhoet, R., Moors, E.J., Troch, P.A. and Verburg, P.H., 2009. Effects of land use changes on streamflow generation in the Rhine basin. *Water resources research*, *45*(6).

Ide, T., Schilling, J., Link, J.S., Scheffran, J., Ngaruiya, G. and Weinzierl, T., 2014. On exposure, vulnerability and violence: Spatial distribution of risk factors for climate change and violent conflict across Kenya and Uganda. *Political Geography*, 43, pp.68–81.

Indeje, M. and Semazzi, F.H.M., 2000. Relationships between QBO in the lower equatorial stratospheric zonal winds and East African seasonal rainfall. Meteorology and Atmospheric Physics, 73(3), pp.227-244.

Indeje, M., Semazzi, F.H. and Ogallo, L.J., 2000. ENSO signals in East African rainfall seasons. *International Journal of Climatology*, 20(1), pp.19–46.

IPCC 2014. "Africa" Climate change 2014: Impacts, Adaptation, and Vulnerability. Part B: Regional Aspects. Contribution of Working Group II to the 5th Assessment Rep. of the Intergovernmental Panel on Climate Change, Cambridge University Press, Cambridge, 1199–1265.

IPCC 2007. Climate change 2007 (Intergovernmental Panel on Climate Change) In: Solomon S, Qin D, Manning M, Chen Z, Marquis MC, Averyt KB, Tignor M, Miller HL (eds) The physical science basis. Cambridge University Press, Cambridge

Jolliffe, I.T., 2003. Principal component analysis. *Technometrics*, *45*(3), p.276.

Jolliffe, I.T., Trendafilov, N.T. and Uddin, M., 2003. A modified principal component technique based on the LASSO. *Journal of computational and Graphical Statistics*, *12*(3), pp.531-547.

Jung, D., Choi, Y.H. and Kim, J.H., 2017. Multiobjective automatic parameter calibration of a hydrological model. *Water*, *9*(3), p.187.

Jury, M.R., Mc Queen, C. and Levey, K., 1994. SOI and QBO signals in the African region. *Theoretical and Applied Climatology*, *50*(1-2), pp.103-115.

Kalnay, E., Kanamitsu, M., Kistler, R., Collins, W., Deaven, D., Gandin, L., Iredell, M., Saha, S., White, G., Woollen, J. and Zhu, Y., 1996. The NCEP/NCAR 40-year reanalysis project. *Bulletin of the American meteorological Society*, *77*(3), pp.437-472.

Kameer, D., 1989. *Brief description of major drainage basins affecting Somalia with reference to surface water resources*. Mogadishu, Somalia: FAO.

Karmalkar, A.V. and Bradley, R.S., 2017. Consequences of global warming of 1.5 C and 2 C for regional temperature and precipitation changes in the contiguous United States. *PloS one*, *12*(1).

Kashaigili, J.J., 2008. Impacts of land-use and land-cover changes on flow regimes of the Usangu wetland and the Great Ruaha River, Tanzania. *Physics and Chemistry of the Earth, Parts A/B/C*, *33*(8-13), pp.640-647.

Kaunda, C.S. and Mtalo, F., 2013. Impacts of environmental degradation and climate change on electricity generation in Malawi. *International Journal of Energy & Environment*, 4(3).

Khadr, M., 2016. Forecasting of meteorological drought using hidden Markov model (Case study: The upper Blue Nile river basin, Ethiopia). *Ain Shams Engineering Journal*, 7(1), pp.47–56.

Kichonge, B., Mkilaha, I.S., John, G.R. and Hameer, S., 2016. The Economics of Renewable Energy Sources into Electricity Generation in Tanzania. *Journal of Energy*, *2016*.

Kijazi, A.L. and Reason, C.J.C., 2012. Intra-seasonal variability over the northeastern highlands of Tanzania. *International Journal of Climatology*, *32*(6), pp.874-887.

Kijazi, A. L., and Reason, C. J. C., 2009: Analysis of the 1998 to 2005 drought over the northeastern highlands of Tanzania. Climate Research, 38, 209-223

King, A.D., Karoly, D.J. and Henley, B.J., 2017. Australian climate extremes at 1.5 C and 2 C of global warming. *Nature Climate Change*, *7*(6), pp.412-416.

Kingston, D.G. and Taylor, R.G., 2010. Sources of uncertainty in climate change impacts on river discharge and groundwater in a headwater catchment of the Upper Nile Basin, Uganda. *Hydrology and Earth System Sciences*, *14*(7), pp.1297-1308.

Kinuthia, J. H., 1992: Horizontal and vertical structure of the Lake Turkana jet. J. Appl. Meteor., 31, 1248–1274

Kitheka, J.U., Obiero, M. and Nthenge, P., 2005. River discharge, sediment transport and exchange in the Tana Estuary, Kenya. *Estuarine, Coastal and Shelf Science*, 63(3), pp.455–468.

Klutse, N.A.B., Ajayi, V.O., Gbobaniyi, E.O., Egbebiyi, T.S., Kouadio, K., Nkrumah, F., Quagraine, K.A., Olusegun, C., Diasso, U., Abiodun, B.J. and Lawal, K., 2018. Potential impact of 1.5° C and 2° C global warming on consecutive dry and wet days over West Africa. *Environmental Research Letters*, 13(5), p.055013.

Kohonen, T., 1990. The self-organizing map. *Proceedings of the IEEE*, 78(9), pp.1464–1480.

Kohonen, T., 1999. Comparison of SOM point densities based on different criteria. *Neural Computation*, 11(8), pp.2081–2095.

Kohonen, T., 2013. Essentials of the self-organizing map. *Neural Networks*, 37, pp.52–65.

Korecha, D. and Barnston, A.G., 2007. Predictability of june–september rainfall in Ethiopia. *Monthly weather review*, *135*(2), pp.628-650.

Krause, P., 2002. Quantifying the impact of land use changes on the water balance of large catchments using the J2000 model. *Physics and Chemistry of the Earth, Parts A/B/C*, *27*(9-10), pp.663-673.

Latif, M., Dommenget, D., Dima, M., and Grötzner, A., 1999: The role of Indian Ocean sea surface temperature in forcing east African rainfall anomalies during December-January 1997/98. Journal of Climate, 12(12), 3497-3504

Lau, K.M. and Weng, H., 1995. Climate signal detection using wavelet transform: How to make a time series sing. *Bulletin of the American meteorological society*, *76*(12), pp.2391-2402.

Leauthaud, C., Belaud, G., Duvail, S., Moussa, R., Grunberger, O. and Albergel, J., 2013. Characterizing floods in the poorly gauged wetlands of the Tana River Delta, Kenya, using a water balance model and satellite data. *Hydrology and Earth System Sciences*, *17*(8), pp.p-3059.

Legesse, D., Vallet-Coulomb, C. and Gasse, F., 2003. Hydrological response of a catchment to climate and land use changes in Tropical Africa: case study South Central Ethiopia. *Journal of hydrology*, *275*(1-2), pp.67-85.

Leloup, J.A., Lachkar, Z., Boulanger, J.P. and Thiria, S., 2007. Detecting decadal changes in ENSO using neural networks. *Climate Dynamics*, 28(2-3), pp.147–162.

Liu, W., Huang, B., Thorne, P.W., Banzon, V.F., Zhang, H.M., Freeman, E., Lawrimore, J., Peterson, T.C., Smith, T.M. and Woodruff, S.D., 2014. Extended reconstructed sea surface temperature version 4 (ERSST. v4): Part II. Parametric and structural uncertainty estimations. *Journal of Climate*, *28*(3), pp.931-951.

Liu, Y., Weisberg, R.H. and Mooers, C.N., 2006. Performance evaluation of the self-organizing map for feature extraction. *Journal of Geophysical Research: Oceans*, 111(C5).

Li, Z., Liu, W.Z., Zhang, X.C. and Zheng, F.L., 2009. Impacts of land use change and climate variability on hydrology in an agricultural catchment on the Loess Plateau of China. *Journal of hydrology*, *377*(1-2), pp.35-42.

Lørup, J.K., Refsgaard, J.C. and Mazvimavi, D., 1998. Assessing the effect of land use change on catchment runoff by combined use of statistical tests and hydrological modelling: case studies from Zimbabwe. *Journal of hydrology*, *205*(3-4), pp.147-163.

Lott, F.C., Christidis, N. and Stott, P.A., 2013. Can the 2011 East African drought be attributed to human-induced climate change?. *Geophysical Research Letters*, *40*(6), pp.1177-1181.

Luke, Q., Hatfield, R. and Cunneyworth, P., 2005. Rehabilitation of the Tana Delta Irrigation Project, Kenya. An environmental assessment. *Unpublished Report to the Critical Ecosystem Partnership Fund. www. cepf. net/Documents/Final. TDIP_Environmental_Assessment. pdf*

Lyon, B., 2014. Seasonal drought in the Greater Horn of Africa and its recent increase during the March–May long rains. *Journal of Climate*, *27*(21), pp.7953-7975.

Lyon, B. and DeWitt, D.G., 2012. A recent and abrupt decline in the East African long rains. *Geophysical Research Letters*, *39*(2).

Maingi, J.K. and Marsh, S.E., 2002. Quantifying hydrologic impacts following dam construction along the Tana River, Kenya. *Journal of Arid Environments*, 50(1), pp.53–79.

Malmgren, B.A. and Winter, A., 1999. Climate zonation in Puerto Rico based on principal components analysis and an artificial neural network. *Journal of Climate*, 12(4), pp.977–985.

Manatsa, D. and Matarira, C.H., 2009. Changing dependence of Zimbabwean rainfall variability on ENSO and the Indian Ocean dipole/zonal mode. *Theoretical and applied climatology*, *98*(3-4), pp.375-396.

Mango, L.M., Melesse, A.M., McClain, M.E., Gann, D. and Setegn, S.G., 2011. Land use and climate change impacts on the hydrology of the upper Mara River Basin, Kenya: results of a modeling study to support better resource management. *Hydrology and Earth System Sciences*, 15(7), p.2245.

Masih, I., Maskey, S., Mussá, F.E.F. and Trambauer, P., 2014. A review of droughts on the African continent: a geospatial and long-term perspective. *Hydrology and Earth System Sciences*, *18*(9), p.3635.

Máure, G., Pinto, I., Ndebele-Murisa, M., Muthige, M., Lennard, C.J., Nikulin, G., Dosio, A., and Meque, A., 2018. The southern African climate under 1.5°C and 2°C of global warming as

simulated by CORDEX regional climate models. Environmental Research Letters, 13(6), p. 065002.

Marshall, M., Funk, C. and Michaelsen, J., 2012. Examining evapotranspiration trends in Africa. *Climate dynamics*, *38*(9-10), pp.1849-1865.

Mbaga, D.P., 2015. *Impact of Hydro-meteorological Drivers on the Streamflow of the Usangu Catchment*. University of Twente, Faculty of Geo-Information and Earth Observation (ITC).

McCartney, M.P., Kashaigili, J.J., Lankford, B.A. and Mahoo, H.F., 2008. Hydrological modelling to assist water management in the Usangu wetlands, Tanzania. *International Journal of River Basin Management*, 6(1), pp.51–61.

McGregor, G.R. and Nieuwolt, S., 1998. *Tropical climatology: an introduction to the climates of the low latitudes* (No. Ed. 2). John Wiley & Sons Ltd.

McHugh, M.J. and Rogers, J.C., 2001. North Atlantic oscillation influence on precipitation variability around the southeast African convergence zone. *Journal of Climate*, *14*(17), pp.3631-3642.

McKee, T. B., Doesken, N. J., and Kleist J., 1993: The relation of drought frequency and duration to time scales, in: Eighth Conference on Applied Climatology, edited by: Department of Atmospheric Science and C. S. University, Anaheim, California

Meehl, G.A., Stocker, T.F., Collins, W.D., Friedlingstein, P.I.E.R.R.E., Gaye, A.T., Gregory, J.M., Kitoh, A.K.I.O., Knutti, R.E.T.O., Murphy, J.M., Noda, A.K.I.R.A. and Raper, S.C., 2007. Global climate projections. Climate change 2007: the physical science basis. Contribution of Working Group I to the Fourth Assessment Report of the Intergovernmental Panel on Climate Change.

Meyers, G., 1996. Variation of Indonesian throughflow and the El Niño-Southern Oscillation. *Journal of Geophysical Research: Oceans*, *101*(C5), pp.12255-12263.

Meque, A. and Abiodun, B.J., 2015. Simulating the link between ENSO and summer drought in Southern Africa using regional climate models. *Climate Dynamics*, *44*(7-8), pp.1881-1900.

Meyers, G., McIntosh, P., Pigot, L. and Pook, M., 2007. The years of El Niño, La Niña, and interactions with the tropical Indian Ocean. *Journal of Climate*, *20*(13), pp.2872-2880.

Michaelides, S.C., Pattichis, C.S. and Kleovoulou, G., 2001. Classification of rainfall variability by using artificial neural networks. *International Journal of Climatology: A Journal of the Royal Meteorological Society*, 21(11), pp.1401–1414.

Mishra, A.K. and Singh, V.P., 2010. A review of drought concepts. *Journal of hydrology*, *391*(1-2), pp.202-216.

Mishra, A.K. and Singh, V.P., 2009. Analysis of drought severity-area-frequency curves using a general circulation model and scenario uncertainty. *Journal of Geophysical Research: Atmospheres*, *114*(D6).

Mitchell, T.D. and Jones, P.D., 2005. An improved method of constructing a database of monthly climate observations and associated high-resolution grids. *International Journal of Climatology: A Journal of the Royal Meteorological Society*, *25*(6), pp.693-712.

Mombo, F., Speelman, S., Huylenbroeck, G.V., Hella, J. and Pantaleo, M., 2011. Ratification of the Ramsar convention and sustainable wetlands management: Situation analysis of the Kilombero Valley wetlands in Tanzania.

Mombo, F., Lusambo, L., Speelman, S., Buysse, J., Munishi, P. and Van Huylenbroeck, G., 2014. Scope for introducing payments for ecosystem services as a strategy to reduce deforestation in the Kilombero wetlands catchment area. *Forest Policy and Economics*, *38*, pp.81-89.

Moriasi, D.N., Arnold, J.G., Van Liew, M.W., Bingner, R.L., Harmel, R.D. and Veith, T.L., 2007. Model evaluation guidelines for systematic quantification of accuracy in watershed simulations. *Transactions of the ASABE*, *50*(3), pp.885-900.

Mtalo, F., Mulungu, D., Mwanuzi, F., Mkhandi, S., Kimaro, T. and Valimba, P., 2005. *Hydrological Analysis for the Eastern Arc Mountain Forests. Conservation and Management of the Eastern Arc Mountain Forests*. Forestry and Beekeeping Division, Dar es Salam.

Mulungu, D.M. and Munishi, S.E., 2007. Simiyu River catchment parameterization using SWAT model. *Physics and Chemistry of the Earth, Parts A/B/C*, *32*(15-18), pp.1032-1039.

Mutemi, J.N., 2003. *Climate anomalies over eastern Africa associated with various ENSO evolution phases* (Doctoral dissertation, PhD thesis, University of Nairobi, Kenya).

Mutua, F. and Balint, Z., 2011. *Analysis of the general climatic conditions to support drought monitoring in Somalia*. Technical Report W-14. Nairobi, Kenya: FAO and Somalia Water and Land Information Management (SWALIM).

Mwakalila, S., 2011. Vulnerability of people's livelihoods to water resources availability in semi-arid areas of Tanzania. *Journal of Water Resource and Protection*, pp. 3(9), 678-685.

Mwalyosi, R.B., 1990. Resource potentials of the Rufiji River basin, Tanzania. *Ambio*, 19(1), pp. 16-20.

Mwangi, E., Wetterhall, F., Dutra, E., Di Giuseppe, F. and Pappenberger, F., 2014. Forecasting droughts in East Africa. *Hydrology and Earth System Sciences*, *18*(2), p.611.

Näschen, K., Diekkrüger, B., Leemhuis, C., Steinbach, S., Seregina, L.S., Thonfeld, F. and Van der Linden, R., 2018. Hydrological modeling in data-scarce catchments: The Kilombero floodplain in Tanzania. *Water*, *10*(5), p.599.

Natkhin, M., Dietrich, O., Schäfer, M.P. and Lischeid, G., 2015. The effects of climate and changing land use on the discharge regime of a small catchment in Tanzania. *Regional Environmental Change*, *15*(7), pp.1269-1280.

Naumann, G., Dutra, E., Barbosa, P., Pappenberger, F., Wetterhall, F. and Vogt, J.V., 2014. Comparison of drought indicators derived from multiple data sets over Africa. *Hydrology and Earth System Sciences*, *18*(5), pp.1625-1640.

Ndomba, P.M., Mtalo, F.W. and Killingtveit, Å., 2008. A guided SWAT model application on sediment yield modeling in Pangani river basin: lessons learnt. *Journal of Urban and Environmental Engineering*, *2*(2), pp.53-62.

Neitsch, S.L., Arnold, J.G., Kiniry, J.R., Williams, J.R. and King, K.W., 2005. Soil and water assessment tool theoretical documentation version 2005. Grassland. *Soil and Water Research Laboratory, Blackland Research Center, Temple, Texas*.

Ng'ongolo, H.K. and Smyshlyaev, S.P., 2010. The statistical prediction of East African rainfalls using quasi-biennial oscillation phases information. *Natural Science*, *2*(12), p.1407.

Nguvava, M., Abiodun, B.J. and Otieno, F., 2019. Projecting drought characteristics over East African basins at specific global warming levels. *Atmospheric Research*, *228*, pp.41-54.

Niang, I., Ruppel, O.C., Abdrabo, M.A., Essel, A., Lennard, C., Padgham, J. and Urquhart, P., 2014. Africa Climate Change 2014: Impacts, Adaptation, and Vulnerability. Part B: Regional Aspects. Contribution of Working Group II to the Fifth Assessment Report of the Intergovernmental Panel on Climate Change ed VR Barros et al.

Nicholson, S.E., 1996: A review of climate dynamics and climate variability in Eastern Africa. In The Limnology, Climatology and Paleoclimatology of the East African Lakes. Johnson TC, Odata E (eds), Gordon and Breach Publishers, The Netherlands, 25-56

Nicholson, S.E., 2017. Climate and climatic variability of rainfall over Eastern Africa. Review of Geophysics. https ://doi.org/10.1002/2016R G0005 44

Nicholson, S.E. and Kim, J., 1997. The relationship of the El Niño–Southern oscillation to African rainfall. *International Journal of Climatology*, 17(2), pp.117–135.

Nie, W., Yuan, Y., Kepner, W., Nash, M.S., Jackson, M. and Erickson, C., 2011. Assessing impacts of Landuse and Landcover changes on hydrology for the upper San Pedro watershed. *Journal of Hydrology*, *407*(1-4), pp.105-114.

Nikulin, G., Jones, C., Giorgi, F., Asrar, G., Büchner, M., Cerezo-Mota, R., Christensen, O.B., Déqué, M., Fernandez, J., Hänsler, A. and van Meijgaard, E., 2012. Precipitation climatology in an ensemble of CORDEX-Africa regional climate simulations. *Journal of Climate*, *25*(18), pp.6057-6078.

Nikulin, G., Lennard, C., Dosio, A., Kjellström, E., Chen, Y., Hänsler, A., Kupiainen, M., Laprise, R., Mariotti, L., Maule, C.F. and Van Meijgaard, E., 2018. The effects of 1.5 and 2 degrees of global warming on Africa in the CORDEX ensemble. *Environmental Research Letters*, 13(6), p.065003.

Ntale, H.K. and Gan, T.Y., 2003. Drought indices and their application to East Africa. *International Journal of Climatology: A Journal of the Royal Meteorological Society*, *23*(11), pp.1335-1357.

Nyakwada, W., Ogallo, L.A. and Okoola, R.E., 2009. The Atlantic-Indian Ocean dipole and its influence on East African seasonal rainfall. *Journal of Meteorology and Related Sciences*, 3, pp.21–35.

Nyingi, D.W., Bart, H., Hamerlynck, O., Gichuki, N., Gathua, J., Ndiwa, T. and Duvail, S., 2011, November. Species composition and diversity of fishes of the upper and lower Tana river. In *Communication to the third biennial scientific conference of the National Museums of Kenya* (Vol. 9).

Ogallo, L.J., 1989. The spatial and temporal patterns of the East African seasonal rainfall derived from principal component analysis. *International Journal of Climatology*, *9*(2), pp.145-167.

Oja, M., Somervuo, P., Kaski, S. and Kohonen, T., 2003, September. Clustering of human endogenous retrovirus sequences with median self-organizing map. In *Proc. WSOM* (Vol. 3).

Osima, S., Indasi, V.S., Zaroug, M., Endris, H.S., Gudoshava, M., Misiani, H.O., Nimusiima, A., Anyah, R.O., Otieno, G., Ogwang, B.A. and Jain, S., 2018. Projected climate over the Greater Horn of Africa under 1.5° C and 2° C global warming. *Environmental Research Letters*, 13(6), p. 065004.

Otieno, V. O., and Anyah, R. O., 2013a: CMIP5 simulated climate conditions of the Greater Horn of Africa (GHA). Part 1: contemporary climate. *Climate dynamics*, 41(7-8), 2081-2097

Otieno, V. O., and Anyah, R. O., 2013b: CMIP5 simulated climate conditions of the Greater Horn of Africa (GHA). Part II: projected climate. *Climate dynamics*, 41(7-8), 2099-2113

Ozturk, T., Turp, M.T., Türkeş, M. and Kurnaz, M.L., 2018. Future projections of temperature and precipitation climatology for CORDEX-MENA domain using RegCM4. 4. *Atmospheric Research*, *206*, pp.87-107.

Palamuleni, L.G., Ndomba, P.M. and Annegarn, H.J., 2011. Evaluating land cover change and its impact on hydrological regime in Upper Shire river catchment, Malawi. *Regional Environmental Change*, *11*(4), pp.845-855.

Palmer, W.C., 1965. *Meteorological drought* (Vol. 30). US Department of Commerce, Weather Bureau.

Patricola, C.M. and Cook, K.H., 2011. Sub-Saharan Northern African climate at the end of the twenty-first century: forcing factors and climate change processes. *Climate dynamics*, *37*(5-6), pp.1165-1188.

Paulo, A.A., Rosa, R.D. and Pereira, L.S., 2012. Climate trends and behaviour of drought indices based on precipitation and evapotranspiration in Portugal. *Natural Hazards and Earth System Sciences*, 12(5), pp.1481–1491.

Pinto, I., Jack, C. and Hewitson, B., 2018. Process-based model evaluation and projections over southern Africa from coordinated regional climate downscaling experiment and coupled model intercomparison project phase 5 models. *International Journal of Climatology*, *38*(11), pp.4251-4261.

Ramsar Bulletin Board, 2002. Tanzania designates rich new Ramsar site < https://www.ramsar.org/wetland/united-republic-of-tanzania> (accessed 06.04.2019).

Rao, S.A., Behera, S.K., Masumoto, Y. and Yamagata, T., 2002. Interannual subsurface variability in the tropical Indian Ocean with a special emphasis on the Indian Ocean dipole. *Deep Sea Research Part II: Topical Studies in Oceanography*, *49*(7-8), pp.1549-1572.

Ren, L., Liu, X., Yuan, F., Xu, J. and Liu, W., 2012. Quantitative analysis of runoff reduction in the Laohahe basin. *Hydrology Research*, *43*(1-2), pp.38-47.

Reusch, D.B., Alley, R.B. and Hewitson, B.C., 2007. North Atlantic climate variability from a self-organizing map perspective. *Journal of Geophysical Research: Atmospheres*, 112(D2).

Richman, M.B., 1986. Rotation of principal components. *Journal of climatology*, *6*(3), pp.293-335.

Riddle, E.E. and Cook, K.H., 2008. Abrupt rainfall transitions over the Greater Horn of Africa: Observations and regional model simulations. *Journal of Geophysical Research: Atmospheres*, 113(D15).

Ritchie, J.T., 1983. Efficient water use in crop production: discussion on the generality of relations between biomass production and evapotranspiration. *Limitations to efficient water use in crop production*, pp.29-44.

Rowell, D.P., 2013. Simulating SST teleconnections to Africa: What is the state of the art?. *Journal of Climate*, *26*(15), pp.5397-5418.

Russell, J.M. and Johnson, T.C., 2007. Little Ice Age drought in equatorial Africa: intertropical convergence zone migrations and El Niño–Southern Oscillation variability. *Geology*, *35*(1), pp.21-24.

Rummukainen, M., 2010. State-of-the-art with regional climate models. *Wiley Interdisciplinary Reviews: Climate Change*, *1*(1), pp.82-96.

Sajikumar, N. and Remya, R.S., 2015. Impact of land cover and land use change on runoff characteristics. *Journal of Environmental Management*, *161*, pp.460-468.

Saji, N.H. and Yamagata, T., 2003. Possible impacts of Indian Ocean dipole mode events on global climate. *Climate Research*, *25*(2), pp.151-169.

Saji, N.H., Goswami, B.N., Vinayachandran, P.N. and Yamagata, T., 1999. A dipole mode in the tropical Indian Ocean. *Nature*, *401*(6751), pp.360-363.

Samuelsson, P., Jones, C.G., Will´ En, U., Ullerstig, A., Gollvik, S., Hansson, U.L.F., Jansson, E., Kjellstro¨ M, C., Nikulin, G. and Wyser, K., 2011. The Rossby Centre Regional Climate model RCA3: model description and performance. *Tellus A: Dynamic Meteorology and Oceanography*, *63*(1), pp.4-23.

Santhi, C., Arnold, J.G., Williams, J.R., Hauck, L.M. and Dugas, W.A., 2001. Application of a watershed model to evaluate management effects on point and nonpoint source pollution. *Transactions of the ASAE*, *44*(6), p.1559.

Santos, J.F., Pulido-Calvo, I. and Portela, M.M., 2010. Spatial and temporal variability of droughts in Portugal. *Water Resources Research*, *46*(3).

Schneider, S. H. (ed.) 1996. Encyclopaedia of Climate and Weather, New York: Oxford University Press.

Schubert, S., Gutzler, D., Wang, H., Dai, A., Delworth, T., Deser, C., Findell, K., Fu, R., Higgins, W., Hoerling, M. and Kirtman, B., 2009. A US CLIVAR project to assess and compare the responses of global climate models to drought-related SST forcing patterns: overview and results. *Journal of Climate*, *22*(19), pp.5251-5272.

Schulze, R.E., 2000. Modelling hydrological responses to land use and climate change: a southern African perspective. *Ambio*, pp.12-22.

Seegers, L., De Vos, L. and Okeyo, D.O., 2003. Annotated checklist of the freshwater fishes of Kenya (excluding the lacustrine haplochromines from Lake Victoria). *Journal of East African Natural History*, *92*(1), pp.11-47.

Segele, Z.T., Lamb, P.J. and Leslie, L.M., 2009. Seasonal-to-interannual variability of Ethiopia/horn of Africa monsoon. Part I: associations of wavelet-filtered large-scale atmospheric circulation and global sea surface temperature. *Journal of Climate*, *22*(12), pp.3396-3421.

Setegn, S.G., Dargahi, B., Srinivasan, R. and Melesse, A.M., 2010. Modeling of Sediment Yield From Anjeni-Gauged Watershed, Ethiopia Using SWAT Model 1. *JAWRA Journal of the American Water Resources Association*, *46*(3), pp.514-526.

Sheffield, J., Wood, E.F. and Roderick, M.L., 2012. Little change in global drought over the past 60 years. *Nature*, *491*(7424), pp.435-438.

Shi, C., Jiang, Z.H., Chen, W.L. and Li, L., 2018. Changes in temperature extremes over China under 1.5 C and 2 C global warming targets. *Advances in Climate Change Research*, *9*(2), pp.120-129.

Shongwe, M.E., van Oldenborgh, G.J., van den Hurk, B. and van Aalst, M., 2011. Projected changes in mean and extreme precipitation in Africa under global warming. Part II: East Africa. *Journal of climate*, *24*(14), pp.3718-3733.

Solomon, S., Manning, M., Marquis, M. and Qin, D., 2007. *Climate change 2007-the physical science basis: Working group I contribution to the fourth assessment report of the IPCC* (Vol. 4). Cambridge university press.

Somot, S., Ruti, P., Ahrens, B., Coppola, E., Jordà, G., Sannino, G. and Solmon, F., 2018. Editorial for the Med-CORDEX special issue.

Souverijns, N., Thiery, W., Demuzere, M. and Van Lipzig, N.P., 2016. Drivers of future changes in East African precipitation. *Environmental Research Letters*, *11*(11), p.114011.

Stackhouse, P., Whitlock, C., Chandler, W., Hoell, J. and Zhang, T., 2004, July. Solar renewable energy data sets from NASA satellites and research. In *Proceedings of the solar conference* (pp. 279-284). AMERICAN SOLAR ENERGY SOCIETY; AMERICAN INSTITUTE OF ARCHITECTS.

Stevenson, S., Fox-Kemper, B., Jochum, M., Neale, R., Deser, C. and Meehl, G., 2012. Will there be a significant change to El Niño in the twenty-first century?. *Journal of Climate*, *25*(6), pp.2129-2145.

Strauch, M. and Volk, M., 2013. SWAT plant growth modification for improved modeling of perennial vegetation in the tropics. *Ecological Modelling*, *269*, pp.98-112.

Su, B., Jian, D., Li, X., Wang, Y., Wang, A., Wen, S., Tao, H. and Hartmann, H., 2017. Projection of actual evapotranspiration using the COSMO-CLM regional climate model under global warming scenarios of 1.5° C and 2.0° C in the Tarim River Basin, China. *Atmospheric Research*, *196*, pp.119-128.

Suliman, A.H.A., Jajarmizadeh, M., Harun, S. and Darus, I.Z.M., 2015. Comparison of semi-distributed, GIS-based hydrological models for the prediction of streamflow in a large catchment. *Water resources management*, *29*(9), pp.3095-3110.

Tadele, K. and Förch, G., 2007. Impact of land use/cover change on streamflow: the case of Hare River Watershed, Ethiopia. In *Catchment and lake research, proceedings 2nd Lake Abaya research symposium (LARS), Arba Minch, Ethiopia*.

Taylor, K.E., Stouffer, R.J. and Meehl, G.A., 2012. An overview of CMIP5 and the experiment design. *Bulletin of the American Meteorological Society*, *93*(4), pp.485-498.

Temple, P.H. and Sundborg, Å., 1972. The Rufiji River, Tanzania hydrology and sediment transport. *Geografiska Annaler: Series A, Physical Geography*, *54*(3-4), pp.345-368.

Thiery, W., Davin, E.L., Panitz, H.J., Demuzere, M., Lhermitte, S. and Van Lipzig, N., 2015. The impact of the African Great Lakes on the regional climate. *Journal of Climate*, *28*(10), pp.4061-4085.

Thiery, W., Panitz, H.J., Davin, E. and Van Lipzig, N., 2014, May. The impact of the African Great Lakes on the regional climate in a dynamically downscaled CORDEX simulation. In *EGU General Assembly Conference Abstracts* (Vol. 16).

Tierney, J.E., Smerdon, J.E., Anchukaitis, K.J. and Seager, R., 2013. Multidecadal variability in East African hydroclimate controlled by the Indian Ocean. *Nature*, *493*(7432), pp.389-392.

Torrence, C. and Compo, G.P., 1998. A practical guide to wavelet analysis. *Bulletin of the American Meteorological society*, *79*(1), pp.61-78.

Trenberth, K.E., 1997. The definition of El Nino. *Bulletin of the American Meteorological Society*, *78*(12), pp.2771-2778.

Trenberth, K.E., Dai, A., Van Der Schrier, G., Jones, P.D., Barichivich, J., Briffa, K.R. and Sheffield, J., 2014. Global warming and changes in drought. *Nature Climate Change*, *4*(1), pp.17-22.

Ujeneza, E.L. and Abiodun, B.J., 2015. Drought regimes in Southern Africa and how well GCMs simulate them. *Climate Dynamics*, *44*(5-6), pp.1595-1609.

Ummenhofer, C.C., Sen Gupta, A., England, M.H. and Reason, C.J., 2009. Contributions of Indian Ocean sea surface temperatures to enhanced East African rainfall. *Journal of Climate*, *22*(4), pp.993-1013.

UNDP (United Nations Development Programme), 2008: UNDP climate change country profile: Ethiopia. UNDP

UNFCCC., 2015. *Report on the Structured Expert Dialogue (SED) on the 2013–2015 Review*, FCCC/SB/2015/INF.1

United Republic of Tanzania (URT) 2003. Initial National Communication under the United Nations Framework Convention on Climate Change, (UNFCCC). Vice-President's Office (VPO). Government printers, Dar es Salaam.

Vautard, R., Gobiet, A., Sobolowski, S., Kjellström, E., Stegehuis, A., Watkiss, P., Mendlik, T., Landgren, O., Nikulin, G., Teichmann, C. and Jacob, D., 2014. The European climate under a 2 C global warming. *Environmental Research Letters*, *9*(3), p.034006.

Vecchi, G.A. and Wittenberg, A.T., 2010. El Niño and our future climate: where do we stand?. *Wiley Interdisciplinary Reviews: Climate Change*, *1*(2), pp.260-270.

Verschuren, D., Laird, K.R. and Cumming, B.F., 2000. Rainfall and drought in equatorial east Africa during the past 1,100 years. *Nature*, *403*(6768), pp.410-414.

Vicente-Serrano, S.M., Beguería, S. and López-Moreno, J.I., 2010a. A multiscalar drought index sensitive to global warming: The standardized precipitation evapotranspiration index. *Journal of Climate*, 23(7), pp.1696–1718.

Vicente-Serrano, S.M., Beguería, S., López-Moreno, J.I., Angulo, M. and El Kenawy, A., 2010b. A new global 0.5 gridded dataset (1901–2006) of a multiscalar drought index: comparison with current drought index datasets based on the Palmer Drought Severity Index. *Journal of Hydrometeorology*, *11*(4), pp.1033-1043.

Vicente-Serrano, S.M., Beguería, S., Gimeno, L., Eklundh, L., Giuliani, G., Weston, D., El Kenawy, A., López-Moreno, J.I., Nieto, R., Ayenew, T. and Konte, D., 2012a. Challenges for drought mitigation in Africa: The potential use of geospatial data and drought information systems. *Applied Geography*, *34*, pp.471-486.

Vicente-Serrano, S.M., Beguería, S., Lorenzo-Lacruz, J., Camarero, J.J., López-Moreno, J.I., Azorin-Molina, C., Revuelto, J., Morán-Tejeda, E. and Sanchez-Lorenzo, A., 2012b. Performance of drought indices for ecological, agricultural, and hydrological applications. *Earth Interactions*, 16(10), pp.1–27.

Viste, E., Korecha, D. and Sorteberg, A., 2013. Recent drought and precipitation tendencies in Ethiopia. *Theoretical and Applied Climatology*, 112(3–4), pp.535–551.

Vizy, E.K. and Cook, K.H., 2003. Connections between the summer East African and Indian rainfall regimes. *Journal of Geophysical Research: Atmospheres*, *108*(D16).

von Storch, H., 1995. Inconsistencies at the interface of climate impact studies and global climate research. *Meteorologische Zeitschrift*, pp.72-80.

Wang, D., Hejazi, M., Cai, X. and Valocchi, A.J., 2011. Climate change impact on meteorological, agricultural, and hydrological drought in central Illinois. *Water Resources Research*, *47*(9).

Wang, G., Xia, J. and Chen, J., 2009. Quantification of effects of climate variations and human activities on runoff by a monthly water balance model: a case study of the Chaobai River basin in northern China. *Water resources research*, *45*(7).

Wang, Y., Leung, L.R., McGREGOR, J.L., Lee, D.K., Wang, W.C., Ding, Y. and Kimura, F., 2004. Regional climate modeling: progress, challenges, and prospects. *Journal of the Meteorological Society of Japan. Ser. II*, *82*(6), pp.1599-1628.

Webster, P.J., Moore, A.M., Loschnigg, J.P. and Leben, R.R., 1999. Coupled ocean–atmosphere dynamics in the Indian Ocean during 1997–98. *Nature*, *401*(6751), pp.356-360.

Weng, H. and Lau, K.M., 1994. Wavelets, period doubling, and time–frequency localization with application to organization of convection over the tropical western Pacific. *Journal of the atmospheric sciences*, *51*(17), pp.2523-2541.

Wilby, R.L. and Wigley, T.M.L., 1997. Downscaling general circulation model output: a review of methods and limitations. *Progress in physical geography*, *21*(4), pp.530-548.

Wilhite, D.A., 2005. *Drought and water crises: science, technology, and management issues*. Crc Press.

Wilhite, D.A., 2000: Drought as a natural hazard: Concepts and definitions. In: Wilhite, D.A. (Ed.), Drought: A Global Assessment, vol. 1. Routledge, New York, pp. 1–18

Wilhite, D.A. and Glantz, M.H., 1985. Understanding: the drought phenomenon: the role of definitions. *Water international*, *10*(3), pp.111-120.

Williams, A.P., Funk, C., Michaelsen, J., Rauscher, S.A., Robertson, I., Wils, T.H., Koprowski, M., Eshetu, Z. and Loader, N.J., 2012. Recent summer precipitation trends in the Greater Horn of Africa and the emerging role of Indian Ocean sea surface temperature. *Climate Dynamics*, *39*(9-10), pp.2307-2328.

World Meteorological Organization, 1986. Report on drought and countries affected by drought during 1974–1985. *WMO, Geneva*, p.118.

Yamagata, T., Behera, S.K., Luo, J.J., Masson, S., Jury, M.R. and Rao, S.A., 2004. Coupled ocean-atmosphere variability in the tropical Indian Ocean. *Earth's Climate: The Ocean–Atmosphere Interaction, Geophys. Monogr*, *147*, pp.189-212.

Yang, P., Ames, D.P., Fonseca, A., Anderson, D., Shrestha, R., Glenn, N.F. and Cao, Y., 2014. What is the effect of LiDAR-derived DEM resolution on large-scale watershed model results?. *Environmental modelling & software*, *58*, pp.48-57.

Yanda, P.Z. and Munishi, P.K.T., 2007. Hydrologic and land use/cover change analysis for the Ruvu River (Uluguru) and Sigi River (East Usambara) watersheds. repository.udsm.ac.tz

Yang, W., Seager, R., Cane, M.A. and Lyon, B., 2015. The annual cycle of East African precipitation. *Journal of Climate*, *28*(6), pp.2385-2404.

Yang, X.L., Ren, L.L., Jiang, S.H., Yuan, S.S. and Shi, L., 2012. Analysis of trend and influencing factors of runoff variation in headwater basin of West Liaohe River. *Journal of Hohai University: Natural Sciences*, *40*(1), pp.37-41.

Yates, D.N. and Strzepek, K.M., 1998a. Modeling the Nile Basin under climatic change. *Journal of Hydrologic Engineering*, *3*(2), pp.98-108.

Yates, D.N. and Strzepek, K.M., 1998b. An assessment of integrated climate change impacts on the agricultural economy of Egypt. *Climatic Change*, *38*(3), pp.261-287.

Yevjevich, V.M., 1967. Objective approach to definitions and investigations of continental hydrologic droughts, An. *Hydrology papers (Colorado State University); no. 23*.

Ying, X., Bo-Tao, Z., Jie, W., Zhen-Yu, H., Yong-Xiang, Z. and Jia, W., 2017. Asian climate change under 1.5–4° C warming targets. *Advances in Climate Change Research*, *8*(2), pp.99-107.

Yuan, X., Wood, E.F., Chaney, N.W., Sheffield, J., Kam, J., Liang, M. and Guan, K., 2013. Probabilistic seasonal forecasting of African drought by dynamical models. *Journal of Hydrometeorology*, *14*(6), pp.1706-1720.

Yu, M., Li, Q., Hayes, M.J., Svoboda, M.D. and Heim, R.R., 2014. Are droughts becoming more frequent or severe in China based on the standardized precipitation evapotranspiration index: 1951–2010?. *International Journal of Climatology*, *34*(3), pp.545-558